Universitat de les
Illes Balears

Doctoral Thesis

Athermal and isothermal characteristics in diffusionless martensitic transformations

by
Daniel Salas Mula

Supervisors:
Prof. Sergey Kustov
Prof. Eduard Cesari Aliberch

2014

Universitat de les
Illes Balears

Doctoral Thesis

Athermal and isothermal characteristics in diffusionless martensitic transformations

by
Daniel Salas Mula

2014
Doctoral Programme of Physics

Supervisors:
Prof. Sergey Kustov
Prof. Eduard Cesari Aliberch

Doctor by the Universitat de les Illes Balears of the Doctorate of Physics

Resum

Les transformacions martensítiques (TM) constitueixen una important classe de transicions sòlid-sòlid, famoses per les especials propietats que confereixen als materials, tals com l'efecte memòria de forma, la superelasticitat o l'efecte magnetocalòric.

Una de les questions fonamentals relacionades amb la natura de les TMs és el rol de les fluctuacions tèrmiques. Des d'aquest punt de vista, les TMs són generalment classificades com atèrmiques (les fluctuacions tèrmiques no estan involucrades en la TM i la fracció de martensita nomes depèn de la força motriu: temperatura/esforç/camp magnètic) o com isotèrmiques (les fluctuacions tèrmiques estan involucrades i la TM depèn també del temps). Aquestes característiques són font de debat i controvèrsies encara que són conegudes des de fa dècades.

Recentment, el interès en la natura atèrmica/isotèrmica de les transformacions isotèrmiques ha augmentat degut al descobriment de la natura isotèrmica dels nous aliatges metamagnètics Ni–Mn–X, X=In,Sn,Sb,Al.

Els aliatges metamagnètics són sistemes multiferroics que exhibeixen tant l'ordenament macroscòpic de les deformacions de la xarxa atòmica (aparició del dominis elàstics martensítics) com dels moments magnètics de la fase d'alta temperatura (es formen dominis ferromagnètics). Llavors, les TMs en els aliatges metamagnètics són transicions magnetoestructurals. A més, no se coneix en profunditat el rol de la interacció entre els subsistemes elàstic i magnètic sobre la natura atèrmica/isotèrmica de la TM. D'altre banda, els efectes isotèrmics no són exclusius dels aliatges metamagnètics, pel que també s'han investigat els aliatges convencionals no magnètics Ni–Ti–X, X=Fe,Cu. Aquesta família d'aliatges és especialment important donat que és la més estesa en aplicacions comercials.

En aquest treball, els efectes isotèrmics en els aliatges convencionals Ni–Ti–X (X=Fe, Cu) i metamagnètics Ni–Mn–In–Co han estat estudiats extensivament mitjançant mesures de resistivitat i, en menor mesura, de anelasticitat, obtenint els següents resultats i conclusions.

La doctrina convencional atribueix les transformacions isotèrmiques a processos difusius. En aquest treball mostrarem que la natura de les TM isotèrmiques en inherent a les transformacions sense difusió. Altre creença habitual és que la natura isotèrmica de les TMs es deguda al procés de nucleació, mentre que el creixement de les variants martensítiques és atèrmic. En aquest treball proposem el cas contrari i afirmem que, dintre del materials estudiats i condicions experimentals, el moviment tèrmicament activat de les interfícies martensítiques és responsable de la natura isotèrmica de les TMs.

S'ha posat en evidència una sèrie de regularitats fenomenològiques, com

la cinètica isotèrmica logarítmica, la correlació entre la quantitat d'austenita que transforma anisotèrmicament i la intensitat dels efectes isotèrmics, la diferència entre la intensitat dels efectes isotèrmics durant les TMs directes i inverses i l'efecte de la temperatura en aquesta intensitat.

A partir del model de Néel de l'efecte retardat de fluctuacions magnètiques i tenint en compta les principals regularitats fenomenològiques observades experimentalment, s'ha proposat un model fenomenològic per descriure les TMs isotèrmiques. Aquest model reflexa les principals característiques de les TMs isotèrmiques: la cinètica isotèrmica logarítmica, la correlació entre la quantitat d'austenita que transforma anisotèrmicament i la intensitat dels efectes isotèrmics i l'existència de la saturació i el temps d'incubació de les MTs isotèrmiques.

Finalment, els experiments inicials realitzats amb els aliatges metamagnètics Ni–Mn–In–Co durant les TM completes i "arrestades" són analitzats en termes del nostre model. Mentre que les TM completes en Ni–Mn–In–Co segueixen les mateixes regularitats que els aliatges no magnètics Ni–Ti, el comportament isotèrmic de les TM parcialment "arrestades" resulta ser molt més complicat. Alguns dels trets d'aquest complicat comportament, com l'aparició de llargs temps d'incubació, han estat atribuïts a que la força motriu de les TMs "arrestades" és petita; altres aspectes romanen sense interpretació i definiran la direcció de futures investigacions.

Resumen

Las transformaciones martensíticas (TM) constituyen una importante clase de transiciones sólido-sólido, famosas por las propiedades especiales que confiere a los materiales, tales como el efecto memoria de forma, la superelasticidad o el efecto magnetocalórico.

Una de las cuestiones fundamentales relacionadas con la naturaleza de las TMs es el rol de las fluctuaciones térmicas. Desde este punto de vista, las TMs son generalmente clasificadas como atérmicas (las fluctuaciones térmicas no están involucradas en la TM y la fracción de martensita sólo depende de la fuerza motriz: temperatura/esfuerzo/campo magnético) o como isotérmicas (las fluctuaciones térmicas están involucradas y la TM depende también del tiempo). Estas características siguen siendo fuente de debate y controversias a pesar de ser conocidas desde hace décadas.

Recientemente, el interés en la naturaleza atérmica/isotérmica de las transformaciones isotérmicas ha aumentado a causa del descubrimiento de la naturaleza isotérmica de las nuevas aleaciones metamagnéticas Ni–Mn–X, X=In,Sn,Sb,Al.

Las aleaciones metamagnéticas son sistemas multiferroicos que exhiben tanto el ordenamiento macroscópico de las deformaciones de la red atómica (aparición de los dominios elásticos martensíticos) como de los momentos magnéticos en la fase de alta temperatura (se forman dominios ferromagnéticos). Así pues, las TMs en las aleaciones metamagnéticas son transiciones magnetoestructurales. Además, no se conoce en profundidad el rol de la interacción entre los subsistemas elástico y magnético sobre la naturaleza atérmica/isotérmica de la TM. Por otro lado, los efectos isotérmicos no son exclusivos de las aleaciones metamagnéticas, por lo que también han sido investigadas las aleaciones convencionales no magnéticas Ni–Ti–X, X=Fe,Cu. Esta familia de aleaciones es especialmente importante ya que es la más extendida en aplicaciones comerciales.

En este trabado, los efectos isotérmicos en las aleaciones convencionales Ni–Ti–X (X=Fe, Cu) y metamagnéticas Ni–Mn–In–Co han sido estudiados extensivamente mediante medidas de resistividad y, en menor caso, de anelasticidad, obteniendo los siguientes resultados y conclusiones.

La doctrina convencional atribuye las transformaciones isotérmicas a procesos difusivos. En este trabajo mostramos que la naturaleza de las TM isotérmicas es inherente en las transformaciones sin difusión. Otra creencia habitual es que la naturaleza isotérmica de las TMs es debida al proceso de nucleación, mientras que el crecimiento de las variantes martensíticas es atérmico. En este trabajo proponemos el caso contrario y afirmamos que, dentro de los materiales estudiados y condiciones experimentales, el movimiento

térmicamente activado de las interfaces martensíticas es responsable de la naturaleza isotérmica de las TMs.

Se han puesto en evidencia una serie de regularidades fenomenológicas, como la cinética isotérmica logarítmica, la correlación entre la histéresis y la naturaleza isotérmica de las TMs en Ni–Ti–X, la proporcionalidad entre la cantidad de austenita que transforma anisotérmicamente y la intensidad de los efectos isotérmicos, la diferencia entre la intensidad de efectos isotérmicos durante las TMs directas e inversas y el efecto de la temperatura en esta intensidad.

A partir del modelo de Néel del efecto tardío de fluctuaciones magnéticas y teniendo en cuenta las principales regularidades fenomenológicas observadas experimentalmente, se ha propuesto un modelo fenomenológico para describir las TMs isotérmicas. Este modelo refleja las principales características de las TMs isotérmicas: la cinética logarítmica, la proporcionalidad entre la cantidad de austenita que transforma anisotérmicamente y la intensidad de los efectos isotérmicos y la existencia de la saturación y el tiempo de incubación de las MTs isotérmicas.

Finalmente, los experimentos iniciales realizados con las aleaciones metamagnéticas Ni–Mn–In–Co durante las TM completas y “arrestadas” son analizados en términos de nuestro modelo. Mientras las TM completas en Ni–Mn–In–Co siguen las mismas regularidades que las aleaciones no magnéticas Ni–Ti, el comportamiento isotérmico de las TM parcialmente “arrestadas” resulta ser mucho más complicado. Algunos de los rasgos de este complicado comportamiento, como la aparición de largos tiempos de incubación, han sido atribuidos a que la fuerza motriz de las TMs “arrestadas” es pequeña; otros aspectos permanecen sin interpretación y definirán la dirección de futuras investigaciones.

Abstract

Martensitic transformations (MT) constitute an important class of solid-solid transitions, famous for special properties which they give to materials, like shape memory effect, superelasticity or magnetocaloric effect.

One of the fundamental issues related to the nature of the MTs is the role of thermal fluctuations during the transformation. From this point of view, the MTs are usually classified as athermal (thermal fluctuations are not involved into the MT and the fraction of martensite is a function of only the driving force like temperature/stress/magnetic field) or isothermal ones (thermal fluctuations are involved and the MT becomes time-dependent). Although this problem is known for decades, it remains a matter of controversies and intense discussions.

A new interest to this long-standing problem the athermal/isothermal nature of the martensitic transformations has emerged due to a discovery of the isothermal nature of the novel metamagnetic Ni–Mn–X, X=In,Sn,Sb,Al alloys.

Metamagnetic alloys are multiferroic systems which exhibit macroscopic ordering of the lattice strains (appearance of the elastic martensitic variants) and of the magnetic moments in the high-temperature phase (ferromagnetic domains are formed). Therefore, the MTs in metamagnetic alloys become magnetostructural transitions and a clear understanding of the role of the interaction between the magnetic and elastic subsystems with respect to the athermal/isothermal nature of the MT does not exist. On the other hand, the isothermal effects are not exclusive properties of metamagnetic alloys, so that conventional non-magnetic Ni–Ti–X, X=Fe,Cu alloys have been investigated. This alloys system is especially important since it has found the majority of commercial applications.

In the present work an extensive experimental study of the isothermal effects in non-magnetic Ni–Ti–X (X=Fe, Cu) and metamagnetic Ni–Mn–In–Co alloys has been performed by means of the resistance and, to a less extent, anelasticity studies, resulting in the following main results and conclusions.

The standard doctrine ascribes isothermal transformations to diffusive processes. In the present work we show that the isothermal MTs are inherent in some diffusionless transformations. Another common belief is that the isothermal nature of MTs is due to the nucleation process, whereas the growth of the martensitic variants is athermal. In the present work we draw an inverse picture and claim that, within our laboratory observation window and in the materials studied, the thermally activated motion of the martensitic interfaces is responsible for the isothermal nature of MTs.

A number of phenomenological regularities have been put into evidence,

like logarithmic isothermal MT kinetics, correlation between the MT hysteresis and isothermal nature of the MTs in Ni–Ti–X, proportionality between the amount of anisothermally transforming austenite and the intensity of isothermal effects, difference between the intensity of isothermal effects during direct and reverse MTs and effect of temperature on this intensity.

Based on the most important experimentally observed phenomenological regularities and taking as a starting point the Néel model of thermal fluctuation magnetic aftereffect, a phenomenological description of the isothermal effects is suggested. This model reflects the most important regularities of the isothermal MTs like logarithmic kinetics, proportionality between the amount of anisothermally transforming martensite and the intensity of isothermal effects and existence of saturation and incubation time of the isothermal MT.

Finally, the initial experiments performed for the metamagnetic multiferroic Ni–Mn–In–Co alloy during the complete and “arrested” MT are analyzed in terms of the developed description. Whereas the complete MT in Ni–Mn–In–Co follows the same regularities as non-magnetic Ni–Ti alloys, the isothermal behavior of the partial “arrested” MT turns out to be much more complicated. Certain features of this complicated behavior, like emergence of the incubation time, have been attributed to the low driving force of the MT in the “arrested” state, other aspects still pending interpretation, delineate the prospects for future research.

List of abbreviations

AC - Alternate current
ADIF - Amplitude-dependent internal friction
AIIF - Amplitude-independent internal friction
AGC unit - Automatic gain control unit
BCC - Body centered cubic
DC - Direct current
DSC - Differential scanning calorimetry
FCC - Face centered cubic
FSMA - Ferromagnetic shape memory alloy
HPIB - Hewlett-Packard instrument bus
IF - Internal friction
IMT - Isothermal martensitic transformation
KK - Kurdjumov-Kakeshita approach
LRO - Long-range order
MFIS - Magnetic field-induced strain
MMSMA - Metamagnetic shape memory alloy
MT - Martensitic transformation
OR - Otsuka-Ren approach
PC - Personal Computer
PCI - Peripheral component interconnect
PSD - Power spectral density
PUCOT - Piezoelectric ultrasonic composite oscillator technique
RMS - Root mean square
SE - Superelasticity
SMA - Shape memory alloy
SME - Shape memory effect
TAM - Thermally activated martensite
TFMA - Thermal fluctuation magnetic aftereffect
TTL - Transistor-transistor logic
TTT diagram - Temperature time transformation diagram

List of publications

The following publications have a close relation with the topic of the thesis. Results of these publications are included in the thesis.

- S. Kustov, D. Salas, R. Santamarta, E. Cesari, and J. Van Humbeeck. Isothermal and athermal martensitic transformations in the B2–R–B19' sequence in NiTi shape memory alloys. *Scripta Materialia*, 63(12):1240-1243, 2010.
- E. Cesari, D. Salas, and S. Kustov. Entropy changes in ferromagnetic shape memory alloys. *Materials Science Forum*, 684:49-60, May 2011.
- S. Kustov, D. Salas, E. Cesari, R. Santamarta, and J. Van Humbeeck. Isothermal and athermal martensitic transformations in Ni–Ti shape memory alloys. *Acta Materialia*, 60(6-7):2578-2592, 2012.
- D. Salas, E. Cesari, I. Golovin, and S. Kustov. Magnetomechanical and structural internal friction in Ni–Mn–In–Co metamagnetic shape memory alloy. *Solid State Phenomena*, 184:372-377, January 2012.
- S. Kustov, D. Salas, E. Cesari, R. Santamarta, D. Mari, and J. Van Humbeeck. Structural anelasticity, elasticity and broken ergodicity in Ni–Ti shape memory alloys. *Acta Materialia*, 73:275-286, July 2014.
- D. Salas, E. Cesari, J. Van Humbeeck, and S. Kustov. Isothermal B2–B19' martensitic transformation in Ti-rich Ni–Ti shape memory alloy. *Scripta Materialia*, 74:64-67, March 2014.

Other publications related to the topic of the thesis and/or carried out during the doctorate term.

- S. Kustov, R. Santamarta, D. Salas, E. Cesari, K. Sapozhnikov, and J. Van Humbeeck. Hyperstabilization of martensites. *Functional Materials Letters*, 05(01):1250005, March 2012.
- J. I. Pérez-Landazábal, V. Recarte, V. Sánchez-Alarcos, S. Kustov, D. Salas, and E. Cesari. Effect of magnetic field on the isothermal transformation of a Ni–Mn–In–Co magnetic shape memory alloy. *Intermetallics*, 28:144-148, September 2012.
- J. M. Barandiaran, V. A. Chernenko, E. Cesari, D. Salas, P. Lazpita, J. Gutierrez, and I. Orue. Magnetic influence on the martensitic transformation entropy in Ni–Mn–In metamagnetic alloy. *Applied Physics Letters*, 102(7):071904, February 2013.

- J. M. Barandiaran, V. A. Chernenko, E. Cesari, D. Salas, J. Gutierrez, and P. Lazpita. Magnetic field and atomic order effect on the martensitic transformation of a metamagnetic alloy. *Journal of Physics: Condensed Matter*, 25(48):484005, December 2013.
- S. Kustov, D. Salas, E. Cesari, R. Santamarta, D. Mari, and J. Van Humbeeck. Strain-glass revisited. *Materials Science Forum*, 738-739: 274-275, January 2013.

Contents

Chapter 1

Introduction

1.1 The Martensitic Transformation

1.1.1 Historical background

The word “martensite” has its origin in a phase appearing in steels. This phase was named “martensite” in honor of the German metallurgist Adolf Martens (1850-1914). He was the first person that studied the morphology of the new phase and explained its properties. This phase is produced by quenching a face-centered cubic (F.C.C.) iron doped with carbon to give a supersaturated body-centered cubic (B.C.C.) phase. On quenching, the material is cooled very quickly to a temperature well below the ordering temperature; this avoids the atomic diffusion of carbon and keeps the disorder level and high carbon concentration of the high temperature state. The high temperature phase is called austenite.

Martensitic phase proved to have an improved hardness. Due the general interest in steels which had become a main industrial and construction material, this solid-solid phase transition received a large amount of attention. Then, numerous works on martensites in iron-based alloys were made and the transformation between austenite and martensite was called Martensitic Transformation (MT).

However, this kind of transformation had shown to be a more general transformation type. As early as in 1930, the existence of the MT was found in several non-iron-based alloy systems. It was in these materials that some of its more characteristics properties were revealed. These properties are the Thermoelasticity, the Super Elasticity (SE) and the Shape Memory Effect (SME). Two last properties are closely linked to the MT, but not all materials that exhibit a MT will present SE and SME.

These two properties are very interesting from the point of view of their applications and the materials are named depending on whether they have a certain property, for example, the alloys that show SME are known as Shape Memory Alloys (SMA).

Among the SMA, the Ni-Ti alloy system is the most used for commercial, industrial and medical applications. This alloy was developed in the 1960's by Buehler at al. [1], who discovered that the equiatomic $Ni_{50}Ti_{50}$ alloy exhibit a MT. This alloy is often named Nitinol, name formed by Ni (Nickel), ti (Titanium) and nol (acronym of the laboratory in which was developed: Naval Ordnance Laboratory). This name is very common especially in commercial uses.

1.1.2 What is a Martensitic Transformation?

Originally, the notion "martensitic transformation" was only used to name the transition typical of the steels, but nowadays its meaning is much wider. By MT we are referring to one of the main solid phase transitions that appear in a wide variety of materials under different conditions. This produces a large set of different manifestations of MTs which can vary in many aspects. There are two features that are fundamental and common to all the MTs, as stated by Kurdjumov [2]. These features are:

- The MTs are diffusionless transformations: there is no any compositional change between the initial and product phases.

- The MTs are displacive transformations: the transformation occurs by means of a collective and ordered movement of the atoms in the lattice. The atomic displacements cannot be larger than the interatomic distance.

In addition, the MT usually presents several thermodynamic, kinetic and morphologic secondary features. However, none of these secondary features is an "if and only if" condition for the transition to be a MT. This is because on one hand, some of these features may not be generic or be vague or arguable, and on the other hand, some of these features are shared with other solid-solid transformation. These features were enumerated by A. L. Roitburd and G. V. Kurdjumov [3]:

1. The structural element that results from a MT usually has plate-like morphology. The thickness of the plates is usually small as compared to their dimensions in two other spatial directions.

2. The plane separating the two phases (habit plane) has a defined orientation with respect to the crystallographic axes of the initial and product phases. Therefore, there is a relationship between the crystallographic orientation of the initial and product lattices.

3. The transformation proceeds with a shape change in the transformed region. This change produces a macroscopic deformation, which is revealed as a surface relief of an initially flat sample. This deformation is uniform and is due to the combination of shear and compression. The parameters of this deformation are constant for each transformation.

4. There is a tendency to the formation of an ordered distribution of the plates during the formation of the structure of the new phase.

5. The MT takes place only when there is a deviation from the thermodynamic equilibrium between the parent and martensitic phases.

6. If the transformation is kept under constant external conditions, the initial phase will not be completely consumed during the MT. The new phase grows with the increase of the deviation from the condition of equilibrium.

7. The growth rate of the martensite crystals is high, of the order of $10^4 - 10^5$ cm·s^{-1}, even at low temperatures. This rate does not show a noticeable temperature dependence and is much higher in the direction parallel to the habit plane than in the direction perpendicular to the same plane [4].

8. The MT can be described as athermal or isothermal. In the former case, the transformation will not proceed under isothermal conditions, being time-independent; it will only proceed with the increase of the deviation from the equilibrium condition (see point 6). By contrast, in the isothermal transformations, the transformation will proceed with time although the external macroscopic conditions are kept constant (temperature, applied stress, applied magnetic field,etc.). That is, when its deviation from the equilibrium condition is constant too.

9. The MT can be subdivided into thermoelastic and non-thermoelastic transformations. In the first case, the available driving force during the transformation, expressed as a difference of Gibbs free energies of the parent $G^{(p)}$ and the martensitic $G^{(m)}$ phases, $G^{(p)} - G^{(m)}$, is small, the interphase between the austenite and martensite phases is very mobile and the transformation is fully reversible: the reverse transformation

> proceeds along the same sequence of events as during the direct transformation, but in the reverse order as a backwards movement of the interfaces. In the second case, the driving force is large; the transformation interphase becomes immobile when the new phase grains reach a critical size. The reverse transformation requires renucleation of the austenite to proceed. This means that, in the last case, the sequence of configurations during the direct and reverse MTs is not reversible.

1.1.3 Transformation temperatures

There is a set of characteristic transformation temperatures in a MT induced by temperature change under hydrostatic conditions: M_S (Martensite Start) marks the temperature, on cooling, at which the transformation from austenite to martensite starts to proceed; M_F (Martensite Finish) is the temperate when the direct transformation is considered finished; A_S (Austenite Start), analogously to M_S, is the temperature at which the reverse transformation from martensite to austenite starts; A_F (Austenite Finish) marks the temperature for which the reverse transformation ends. Finally, T_0 is the temperature at which the austenite and martensite are in thermodynamic equilibrium, in other words, the Gibbs free energies of both phases become equal and, therefore, the driving force is zero.

The MT always presents a hysteresis, which is a characteristic of the first order transformations. The following relations between the transformation temperatures are always true: $M_S < A_F$ and $M_F < A_S$. The width of the transformation hysteresis varies strongly for different MTs; from quite small hysteresis, nearly inexistent, for thermoelastic transformations in high quality crystals, to very wide hysteresis in non-thermoelastic MTs. This variation may depend, in general, on the alloy composition, the macro- and microstructure of the transforming phases.

The four characteristic transformation temperatures, M_S, M_F, A_S and A_F, must be determined experimentally. This can be done by different methods, for example, from the electrical resistance, Figure 1.1, or from the calorimetric signals, Figure 1.2. However, these are approximate methods, the exact temperatures at which the transformation physically starts or ends are hardly possible to known. By contrast with the previous four transformation temperatures, it is difficult to estimate experimentally the thermodynamic equilibrium temperature, T_0. In addition, the relation between T_0 and the characteristic temperatures, M_S, M_F, A_S and A_F is not trivial and it needs the concepts of frictional work and stored elastic energy to be explained.

The frictional work is the work done during the movement of the inter-

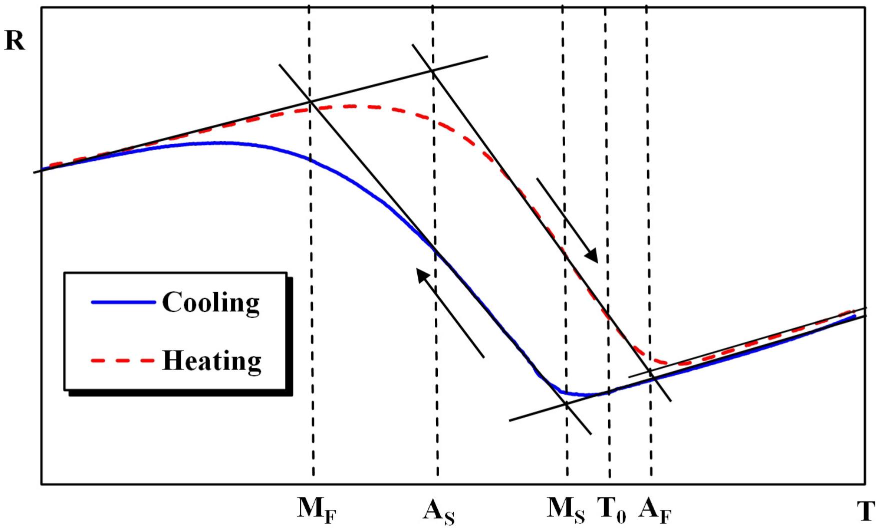

Figure 1.1: Example of deriving the characteristic transformation temperatures, M_S, M_F, A_S, A_F and T_0, from the temperature dependence of the real part of the impedance, R, for a polycrystalline sample of $\mathrm{Ni_{45}Mn_{36.7}Co_5In_{13.3}}$ quenched in water from 770 K.

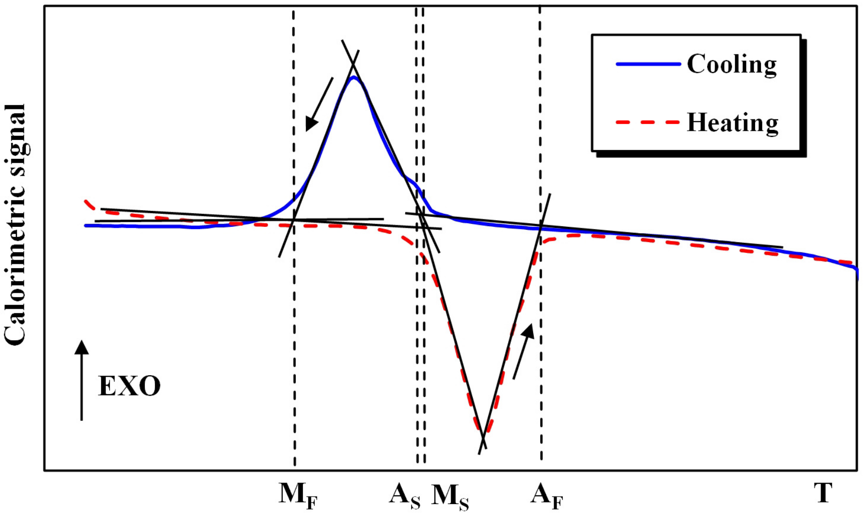

Figure 1.2: Example of deriving the characteristic transformation temperatures, M_S, M_F, A_S and A_F, from the calorimetric signal for a polycrystalline sample of $\mathrm{Ni_{50.2}Ti_{49.8}}$ quenched from 1070 K.

phase between the austenite and martensite. This work is not converted into stored elastic energy, but is dissipated when the interphase interacts with/overcomes obstacles impeding its movement. In addition, thermodynamically, frictional work is a source of irreversibility.

The stored elastic energy is related with the shape and volume changes during the transformation. The elastic energy is stored during the direct transformation and released during the reverse transformation. The storage of elastic energy and the subsequent release are mechanically reversible, but they may be not reversible from a thermodynamic point of view (due to possible relaxation of elastic energy and since there is frictional work).

In the case of a single-crystal single interface MT, Salzbrenner and Cohen [5] observed that during the direct transformation under constant cooling rate, the temperature of the interphase between both phases is constant, with a value Tg. The same was true for the reverse transformation, where the temperature of the interphase is Tr.

Neither Tg nor Tr are equal to the equilibrium temperature T_0. This means that the transformation needs certain overcooling/overheating to proceed. The origin of this difference is the frictional work produced by the interphase. The overcooling, $T_0 - Tg$, and the overheating, $Tr - T_0$, have identical absolute values if the frictional work is equal for the direct and reverse transformation. Then, within this assumption, the equilibrium temperature can be calculated as:

$$T_0 = \frac{Tg + Tr}{2} \tag{1.1}$$

Salzbrenner and Cohen [5] demonstrated that the temperatures Tg and Tr are equal, within the experimental precision, to the temperatures M_S and A_F respectively. Therefore, T_0 can be estimated from M_S and A_F, temperatures that are easily experimentally obtained:

$$T_0 = \frac{M_S + A_F}{2} \tag{1.2}$$

If the stored elastic energy is not taken into consideration, the start and finish transformation temperature are equal and the hysteresis will, schematically, have the shape shown in Figure 1.3.

However, due to the elastic energy (including the increase of interfacial energy), the MT may not start and finish at the same temperature, rather it transforms as the driving force is increased until the MT is completed or it gets arrested. So the effect of the storage of elastic energy during the MT

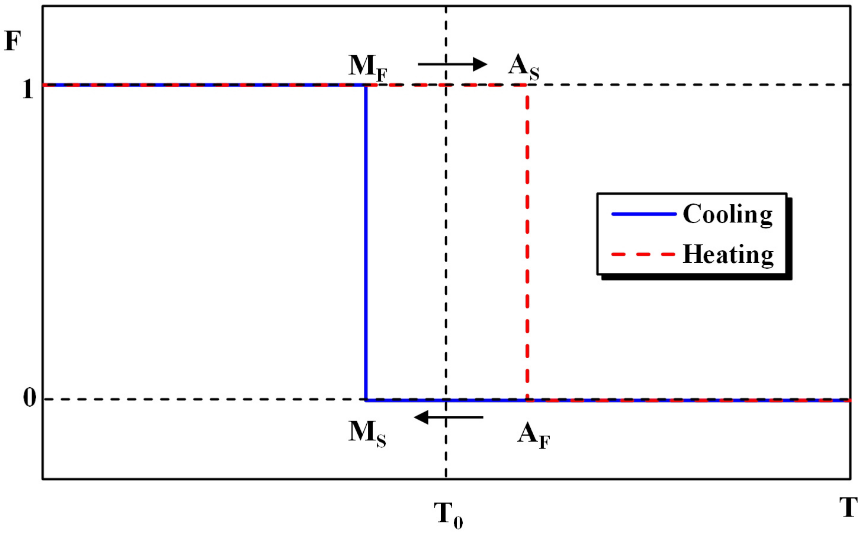

Figure 1.3: Simplified diagram of the martensite volume fraction F in a martensitic transformation without stored elastic energy. The frictional work is considered as independent on the fraction of transformed phase.

is seen in Figure 1.4. Therefore, the sum of both contributions is observed in Figure 1.5. One can compare Figure 1.1 and Figure 1.5 and observe that the real case is quite close to the simplified diagram. In fact, the difference is mainly due to the contributions to the real part of the impedance that are not shown in Figure 1.5. These contributions are not related to the MT (but to the material's phase) and are the defects and phonon contributions. Another difference between the diagram and the real case is T_0. Although it can still be approximated and drawn using the equation (1.2), it has a more complex relation with the transformation temperatures. Therefore, the approximated value of T_0 from the impedance data may not be accurate.

The previous analysis is true for a system under constant hydrostatic pressure where the transformation is temperature induced. However, there are other external fields that contribute to the Gibbs free energy and can affect the phase stability and induce the MT. Therefore, the transformation temperatures depend on such external fields. The most typical external parameter is the mechanical stress; since both austenite and martensite lattices have different symmetries, martensite can be induced by increasing the external applied stress, which increases T_0. Similarly, in the magnetic materials, an external magnetic field will affect the transformations temperatures. The effect of magnetic field is the strongest in alloys wherein the magnetization of both phases is markedly different, for example, in the metamagnetic SMA

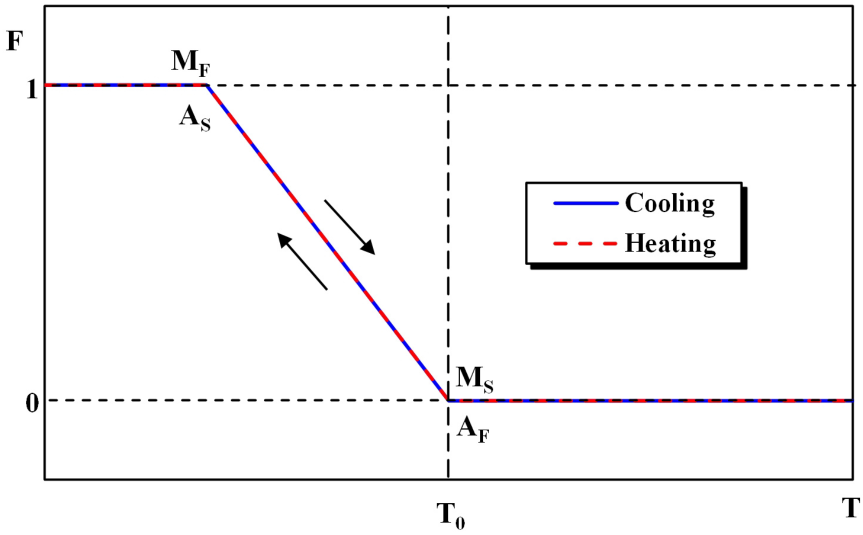

Figure 1.4: Simplified diagram of the martensite volume fraction F in a martensitic transformation without frictional work, but with stored elastic energy.

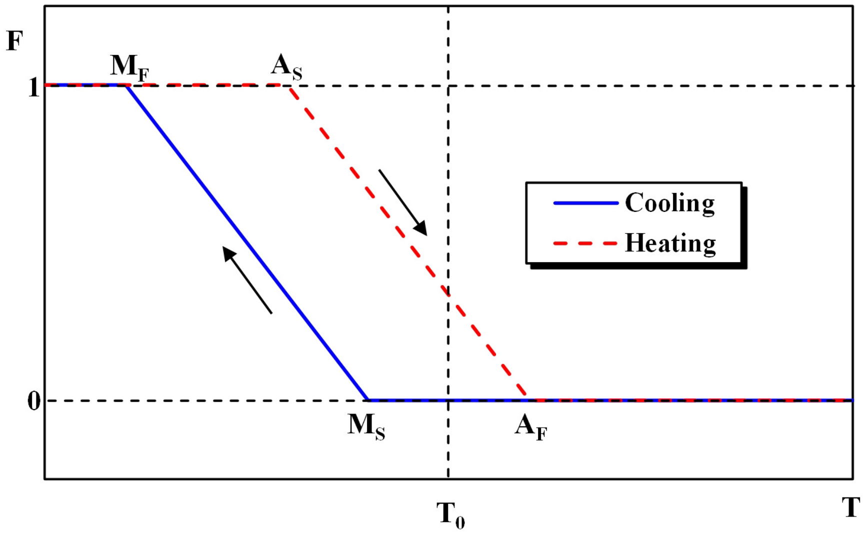

Figure 1.5: Simplified diagram of the martensite volume fraction F in a martensitic transformation with the combination of the effects of frictional work and the storage of elastic energy.

where austenite is ferromagnetic and martensite para- o antiferromagnetic.

A detailed analysis of the concepts dealt with in this paragraph is given by [6].

1.1.4 Shape memory effect

The Shame Memory Effect (SME) is a behavior closely related to the martensitic transformation, and is one of the key points in the high interest raised by these materials.

The crystallographic phases that take part in a MT have different lattice symmetries: the high temperature phase (austenite) possesses the higher symmetry. In shape memory alloys, usually, it is a cubic phase. In its turn, the low temperature phase (martensite) has a lower symmetry and may belong to tetragonal, trigonal, orthorhombic, monoclinic or triclinic crystallographic systems.

This difference in symmetry of the parent and product phases results in the formation of martensite variants. When an element of the high symmetry phase (austenite) transforms into the low symmetry phase (martensite), it can adopt different orientations that correspond to the same orientation of the parent phase because the martensitic phase is degenerate, i.e. there is a certain number of atomic configurations which are energetically equivalent but with different crystallographic orientation. Each one of these possible orientations in martensite is a martensitic domain or variant.

Since the unit cell of the martensite has different shape and volume than that of the austenite, local stresses between both phases are generated during the formation of a nucleus during the direct transformation. To reduce (accommodate) these stresses, the new phase grows from different nuclei with different crystallographic orientations, forming finally different variants of martensite that accommodate the shape and volume change during the MT. Such polyvariant structure eliminates also the possible macroscopic deformation of the sample. Nevertheless, if a single crystal of austenite transforms into a single variant of martensite, a large macroscopic deformation is produced which is easily observable.

The number of possible martensite variants depends on the crystallographic structure of both phases, as shown on Table 1.1 [7].

Martensite variants play a crucial role in the SME. On one hand, martensite variants can change their orientation under the effect of an external applied stress. This reorientation is owing to the fact that one of the variants will accommodate the external stress better than the other, in other words, will become energetically more favorable. One could say that this variant has been “chosen” by the external applied stress. On the other hand,

Crystal system of the parent phase	Crystal system of the product phase	Number of martensite variants
Cubic	Tetragonal	3
	Trigonal	4
	Orthorhombic	6
	Monoclinic	12
	Triclinic	24
Tetragonal	Orthorhombic	2
	Monoclinic	4
	Triclinic	8
Trigonal	Monoclinic	3
	Triclinic	6
Orthorhombic	Monoclinic	2
	Triclinic	4
Monoclinic	Triclinic	2

Table 1.1: Total number of martensitic variants depending on symmetry of the parent and product phases

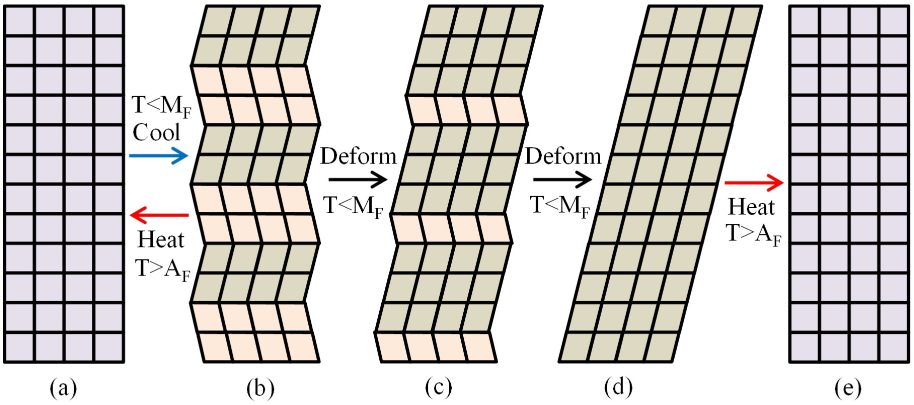

Figure 1.6: Simplified diagram of the shape memory effect: (a)↔(b) martensitic transformation between the austenitic structure (a) and the martensitic structure (b), martensite is in an auto-accommodate form, with two twinned variants; (b)→(d) martensite is deformed by reorienting its variants; (d)→(e) during the reverse transformation the original shape in the austenite is recovered [8].

since all martensite variant orientations correspond to the same orientation in the austenitic phase, all martensite variants will converge during the reverse transformation. Taking into account these two points, one can transform the sample to polyvariant martensite and deform it, not by classical plastic deformation but by reorienting its martensites variants, then, one can retransform the sample back to austenite eliminating the deformation produced by the martensite variant reorientation. This behavior is shown in Figure 1.6 [8].

From a macroscopic point of view, a sample with SME seems to be able to recover a permanent deformation upon increasing its temperature; it looks like as if the sample remembers or memorizes its original shape prior to the deformation in martensite. That is why this effect is called shape memory effect and the alloys which present it are called shape memory alloys and classified as smart materials.

A more detailed description of this subject can be found in [9] and references cited therein.

1.1.5 Superelasticity

The SuperElasticity (SE) is a behavior related with the MT induced by an external stress and, as the SME, with the existence of martensitic variants. This feature also generates a large interest thanks to the possibility of obtaining very large recoverable strains, up to 9% [10], which is much larger than the conventional deformations recovered on normal elastic deformation in metals (≈0.2%).

As mentioned in section 1.1.3, the MT can be induced by an external applied stress: a martensitic variant with a certain orientation will be stable (more favorable energetically than the austenite) under a high enough external stress. In addition, such a transformation will generate a large strain because only one of the possible martensitic variants is selected by the external stress.

From a macroscopic point of view, in a stress-strain essay, this critical value of the applied stress necessary to induce the MT will be followed by a plateau because the growth of the nucleated selected martensitic variant requires only a small increase of the applied stress, see for example Figure 1.7 [11]. This plateau looks similar to the one produced by plastic deformation, but this deformation may be recovered by removing the stress (due to the reverse MT). The SE is also called pseudo-elasticity, since the produced strain is reversible, like the elastic strain, but the physical origins of both deformations are different.

Two different phenomena can occur depending on the temperature range where the material is stressed:

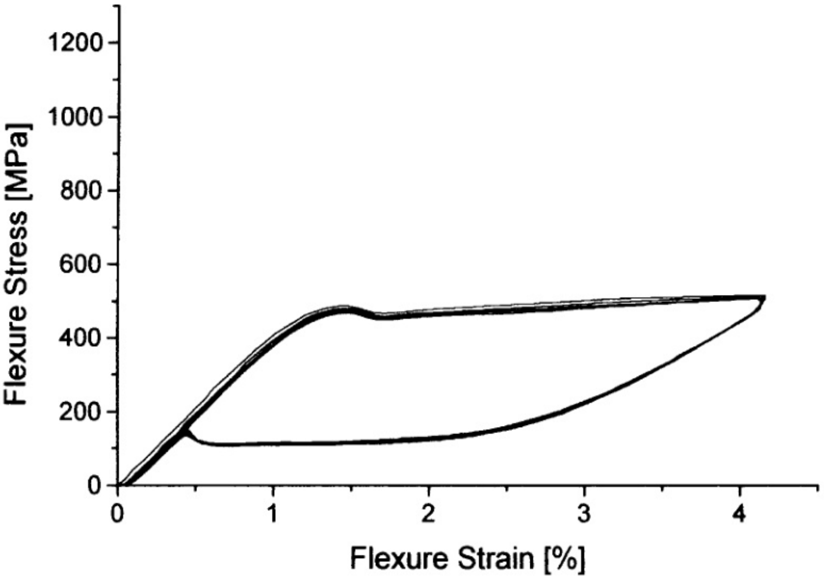

Figure 1.7: Several stress-strain cycles performed above A_F (T=310 K) for a sample of $Ni_{52.5}Ti_{47.5}$ made by Es-Souni et al. [11], the plateau is observed at the critical stress needed for the direct MT, in addition, almost all strain is recovered on unload.

- loading at a temperature between M_S and A_F.
- loading at a temperature higher than A_F.

The difference between both cases lays in the stability of the stress-induced martensite.

For temperatures between M_S and A_F, a fraction or all the martensite will be stable without the need for an external applied stress. Then, if the MT is induced between M_S and A_F, some or all of the material will remain in the martensitic phase after removing the external applied stress. One needs to heat the material above A_F to retransform it to its original state (austenite). This situation is similar to the one explained in section 1.1.4 and it constitutes another kind of SME. Summarizing, the SME can be obtained both by reorientation of the martensitic variants, below M_S, or by transforming the austenite directly to the selected martensitic variant, between M_S and A_F. In both cases the sample should be heated above A_F to recover completely its initial shape.

By contrast, for temperatures above A_F, the martensite will only be stable as long as the stress is applied, and then, once it is removed, the reverse MT will take place and the deformation will be completely recovered. This case corresponds to the above mentioned SE or pseudo-elasticity.

Superelastic stress-strain cycles may be reversible mechanically, but not thermodynamically because of the frictional work done during the transformation. In addition, the external stress would also move the crystallographic defects, like dislocations, generating crystallographical irreversibility. Furthermore, with the increase of temperature above A_F, the critical stress to induce the transformation σ_0 also increases, which raises the possibility of defect generation and displacement in austenite, and, eventually, the plastic deformation of the parent phase prior to the stress-induced MT.

1.1.6 Relation between the transformation temperatures and the applied stress

Similar to the transformation temperatures in the case of a temperature induced transformation, the critical stress needed to induce the transformation should be introduced. However, as is clear from all commented above, one cannot treat the temperature-induced and stress-induced transformations as separate phenomena. The transformation temperatures and the critical stress will affect each other since both, temperature and applied stress, alter the phase stability.

The equation which describes this relation is the Clausius-Clapeyron one. The form of this equation depends on the type of the system (pure hydrostatic, magnetic,…). Most of the MTs can be treated as a non-magnetic system subjected to an uniaxial applied stress σ which suffers a strain ϵ. In this case, the work per unit volume is $\partial w = -\sigma \partial \epsilon$. To deduce the Clausius-Clapeyron equation for this system, one needs the first and the second principles of the thermodynamics

$$\partial u = \delta q - \delta w \tag{1.3}$$

$$\partial s \geq \frac{\delta q}{T} \tag{1.4}$$

where u is the internal energy, q is the exchanged heat and s is the entropy, all of them are normalized per unit volume. The Gibbs free energy per unit volume is defined as function of the previous thermodynamic variables as

$$g = h - Ts = u - \sigma\epsilon - Ts \tag{1.5}$$

where h is the enthalpy per unit volume. Therefore, using equations (1.3), (1.4) and (1.5), one gets that the dependence on the temperature and the applied stress of the Gibbs free energy per unit volume in a reversible process is

$$\partial g = -s\partial T - \epsilon\partial\sigma \tag{1.6}$$

The system will be in thermodynamic equilibrium at a certain temperature T_0 and applied stress σ_0 for which the difference of the Gibbs free energies of both phases is zero, i.e. there is not driving force, $g_M - g_A = 0$. For a new equilibrium condition at $T_0 + dT$, $\sigma_0 + d\sigma$, one has

$$(\epsilon_M - \epsilon_A)\partial\sigma + (s_M - s_A)\partial T = 0 \tag{1.7}$$

where indices M and A stand for martensite and austenite respectively. Reordering the equation (1.7) one gets the Clausius-Clapeyron relation which shows how the stress needed to induce the transformation changes with temperature or how the transformation temperatures vary for different applied stresses.

$$\frac{\partial\sigma}{\partial T} = -\frac{\Delta s}{\Delta\epsilon} \tag{1.8}$$

In addition, if the process is under a constant applied stress, the relation can be written as function of the enthalpy change

$$\frac{\partial\sigma}{\partial T} = -\frac{\Delta h}{\Delta\epsilon T} \tag{1.9}$$

which, in some cases, could be easier to determine than the entropy change [12].

1.2 Applications of shape memory alloys

1.2.1 Non-medical applications

Actuators

The main application fields for the SMAs are the sensors and actuators; or a combination of both. The ability to sense and to react to temperature changes is a unique property of the SMAs which is missing in other conventional actuators as electromagnetic solenoids, hydraulic or pneumatic devices or electric engines. The shape memory element can thus be classified as a thermal actuator. In addition, SMA actuators are able to do more work than the ceramic actuators. The mechanism is simple, the alloy changes its shape when transforms, this deformation produces an expansion in a certain direction, expansion that can proceed against an external force which, for example, is applied to an object situated in the expansion direction. Then, an output work is done by the alloy over the object. This mechanism is limited by the magnitude of the external force, if the force is too high, comparable to the critical stress σ_0 needed to induce the transformation, the alloy will not transform.

The SMA actuators are classified into two different types by Ohkata and Suzuki [13] depending on how they are heated. Those that are of the first kind feel the temperature, and when a certain level is achieved, they carry out its MT giving a corrective force and a certain displacement to the system. The actuators of the other type are heated by a fluid, liquid or gas (air), or by an electric current (Joule-effect), and they give the output work on demand. Therefore, the first kind acts depending on the ambient conditions and the second kind acts when they are asked to do it.

When the SMA actuator acts as a sensor and as an actuator, it usually forms part of a mechanism composed by a SMA spring and an adjustable spring. This set can form more reliable and less expensive systems than more conventional electronic control systems; in addition, the SMA spring system do not need power supply. The thermostatic mixing valves are good examples [13] of this kind of actuators. In these valves, the mixing between cold and hot water is regulated by a SMA spring in contact with the hit water. This way, the SMA spring reacts to the actual temperature of the hot water and stabilizes the temperature of the final mix. This operation mode evidences that the first kind of actuators requires higher critical tuning of the transformation temperatures than the ones activated on demand.

Following Van Humbeeck [14], the second type of actuators is especially interesting for robotic applications. Usually in these applications, the shape memory element works by linear deformation, so it is a round or strip wire and is heated by an electric current. The biggest problems of this mechanism are the precise control of the position, since it needs extra devices and the cool down of the element, because is less controllable and slower than the heating.

Other applications

Apart from the actuators, Van Humbeeck [14] did a classification of the applications based not on the specific functional properties the SMA which permits the application but on the topic.

- Fashion, decoration and gadgets: applications which uses the pseudoelastic behavior or the SME of the SMAs to obtain innovative features. As an examples, there are wires which reinforce clothes or shoes which are able to recover its original shape after a heat treatment [15]. There are also pure decorative applications, like dynamic sculptures.

- Couplings and fasteners: applications that make use of the force created by a deformed SMA element during constrained recovery. A common example of these kind of applications is the first large scale application of SMA, a Ni–Ti–Fe coupling to connect titanium hydraulic tubing in the Grumman F-14 aircraft, developed by Raychem as early as in 1971 [16]. Apart from the classic Ni–Ti alloy system, used for most applications, other alloys systems are being successfully used for couplings and fasteners, like the Ni–Ti–Nb [17] and the Fe–Mn–Si [18].

- High damping materials: diverse applications are based on the high damping of the SMAs. There were some innovations that not became successfully because of the relatively elevated cost for the SMAs for these kinds of applications, as some applications to reduce the noise: tennis rackets and saw blades. For military purposes, there are SMAs used to reinforce bullet proofs and to improve the shock wave absorption of armored materials. There are also important civil engineering applications for protection of civil constructions, such as buildings and bridges, against earth quake vibration damage [19, 20].

1.2.2 Medical applications

The requirements that a material needs to be optimal for medical applications, like biomaterials, are numerous. These requirements can be subdivided into two groups: the general requirements and the specialized ones. The general properties that any biomaterial should possess are a good corrosion resistance and biocompatibility. In addition, depending on its function, the material should meet other requirements, for example, a material for a bone transplant needs to have a Young's modulus value close to the one of the human bone. In view of numerous restrictions, only a few metals are accepted for medical applications, the classical examples being the Fe–Cr–Ni, Co–Cr and Ti–Al–V alloy systems.

Recently, SMAs have been introduced in many medical applications because of their unique functional properties: the SME, the SE and a high damping capacity. Apart from the material properties, other circumstances were crucial for the development of medical applications. Following Duerig et al. [21], the industry had an increasing tendency to less invasive procedures. This created a demand of devices for new medical devices which cannot be made with conventional materials. In addition, other crucial circumstances were the availability of micro-tubing and the ability to laser cut tubing with very high precision.

The most used SMA in medical applications is the Ni–Ti, which possesses good mechanical and all the above mentioned functional properties. However, there exists controversy about the biocompatibility of the Ni–Ti alloys. This is because nickel ions could eventually diffuse from the alloy to the organic tissue and, since pure nickel is toxic, this is dangerous for hyper sensible patients [22]. Therefore, on one hand, Ni-free SMAs, which can avoid this biocompatibility problem, have been developed. The main Ni-free SMA system developed for medical applications is the Ti–Nb alloy system [23, 24]. On the other hand, many literature reviews indicate that Ni–Ti alloys have extremely good biocompatibility, due to the formation of a passive titanium-oxide layer (TiO_2) [25,26]. However, following Morgan [27], the thick oxide layers tend to result in short crack incubation periods due to crack initiation in the comparatively brittle oxide layer. Furthermore, cracks in the oxide layer will expose fresh surfaces of the underlying bulk material which may then accelerate corrosion. Therefore, the formation of thick oxide layer reduces the fatigue life and the biocompatibility, thus the performance of the alloy for many medical applications become worse. Despite of the controversy, the Ni–Ti alloys have demonstrated a similar biocompatibility than other implantable alloys [28–30], but it may not be suitable for any medical application [27].

In orthopedic surgery, Ni–Ti applications include the bone compression used in osteotomy and fixation of fractures, Ni–Ti rods for the correction of the scoliosis, screws for the surgery of small bones and for the fixation of sutures of tissues by means of minimally invasive techniques.

An example of the use of Ni–Ti as a functional biomaterial is the implants into deformed bones, Figure 1.8 [31]. The implant applies a continuous stress to the bone due to the SME: the implant is introduced in martensite, and then its temperature is increased to reach the body temperature and the reverse transformation is induced. Therefore, the implant attempts to transform and recover its original shape in austenite but the deformed bone is opposing this movement; as a consequence, the implant continuously applies a stress directly to the bone. This stress may gradually deform the bone because it has the capacity to react to external mechanical forces adapting its external geometry and its internal structure [31].

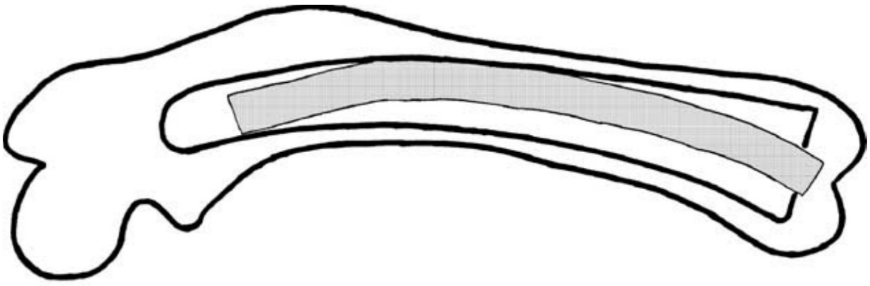

Figure 1.8: Diagram of an intramedullary nail made by Kujala et al [31]

The SMAs are also used as orthodontic wires, because of the SE [32]. For example, a Ni–Ti wire can be stretched inducing the martensitic transformation and then adjusted to the patient dentition. The advantage over other alloys is that the stress produced by the reverse transformation will be constant during the transformation and equal to the critical stress of the reverse transformation. Therefore, SMA-based dental treatment requires less frequent periodical maintenance [32]. In addition, the constant and prolonged stress allows the tooth to move without causing physical discomfort in the patient or damage the gum tissues.

Other important medical applications are the stents [33,34], where a SMA wire forms a cylindrical lattice without basis. The radius of the cylinder depends on whether the material is in austenite or martensite. The stent is introduced intravenously in its martensitic state. When it is heated to the body temperatures it transforms to austenite and increases its radius. This opens the vein and helps the blood circulation of the patient. Following Duerig et al. [21], the stents made of 316L stainless steel are the main competitor of the Ni-Ti stents. The principal advantage of the shape memory device, apart from being self-expanding, is due to the SE, which gives to the Ni–Ti alloy a flexibility about 10–20 times greater than stainless steel. In some superficial stent applications, the vessels may be subject to outside pressures that would cause conventional stents to crush. This fact and other aspects of the SE points to the selection of the Ni–Ti alloys for the stents applications.

1.3 Athermal and isothermal martensitic transformations

1.3.1 On the classification of martensitic transformations as athermal/isothermal

Usually, martensitic transformations can be classified as athermal or isothermal ones depending on its transformation kinetics. From an experimental point of view, a MT is isothermal when the volume fraction of martensite is increasing/decreasing (direct/reverse MT) with time without any change of the transformation driving force. In other words, the transformation will progress despite the temperature and other external fields (mainly, applied stress or applied magnetic field) remain constant. In contrast, a MT is athermal when it needs an increase of the transformation driving force to progress, at least, within our experimental time-scale window [35]. However, even the terminology involved in the description of thermal/isothermal MT remains unsettled if the physical mechanisms are considered.

A closer look shows that the lexeme “thermal” has two different meanings in both key words: athermal and isothermal. On one hand, for the isothermal transformations, the word “isothermal” makes reference to a transformation at constant temperature, and then the lexeme “thermal” is a synonym of “temperature”. In the other hand, for the athermal transformations, the word “athermal” indicates a transformation without any thermally activated process. So, in this case the lexeme “thermal” is a synonym of “thermally activated”.

Due to this difference, recently Massalski [36] and Laughlin et al. [37] revisited the fundamental features of isothermal MT and suggested a classification closer to the nature of physical phenomena involved in the MT. They insisted on distinguishing between thermally activated (rather than isothermal) martensite and non-thermally activated (athermal). Therefore, martensites with a thermally activated transformation should be named as Thermally Activated Martensite (TAM). In terms of characteristics of the MT, it is suggested that the TAM can be formed by thermally activated processes during isothermal holding (isothermal MT) as well as during continuous cooling (anisothermal MT). Then, TAM is a broader term than isothermal MT.

However, to define an isothermal MT as a thermally activated process is not an unequivocal classification. One can distinguish between transformations which are “pure” isothermal and others which may be considered as anisothermal. The former transformations unavoidably need time to proceed, will strongly depend on the cooling rate and then can be arrested by quenching. One example of this kind are the transformations controlled by atomic diffusion. By contrast, the anisothermal transformations are thermally activated too, but cannot be suppressed by rapid quenching, they will proceed both on rapid cooling/heating and under isothermal conditions. The last seems to be the case for the diffusionless thermally activated martensitic transformations.

1.3.2 Basic approaches to the athermal/isothermal nature of the martensitic transformations

Less clear is the situation with specific microscopic mechanisms responsible for the thermally activated nature of isothermal/anisothermal MT and non-thermally activated athermal MT. On a phenomenological level one can distinguish two basic approaches.

Kurdjumov-Kakeshita approach

As early as 1948 Kurdjumov compared the “mechanical” and “thermal” origins of MT. Following Kurdjumov [38], thermally activated processes are involved in all martensitic transformations, i. e., all martensites are TAM. Then, both nucleation and growth rates are controlled by the Boltzmann factor e^{-U/k_BT}, where k_B is the Boltzmann constant ($k_B = 1.38 \cdot 10^{-23}$ J/K), T is the temperature and U is the activation energy. In all cases, nucleation and growth processes imply thermally activated overcoming of effective activation barrier of height U. According to modern interpretations (see, for example, Lobodyuk and Estrin [4,39], Ghosh and Olson [40] and Guimarães and Rios [41]), this effective activation barrier for MT has a certain critical value.

Therefore, according to Kurdjumov point of view, to classify the MTs as athermal makes sense only from an experimental point of view. The occurrence of athermal/isothermal MT depends on the value of the chemical driving force with respect to the critical value of the activation barrier. In the “athermal” MTs the value of the effective activation energy U is low compared to chemical driving force, and then the transformation proceeds too quickly to observe its isothermal kinetics experimentally. Since, following Kurdjumov, the athermal MTs has a low activation energy value for the nucleation and growth of martensite, the necessary condition to have a low U is the same as to have an athermal MT. Kurdjumov formulated these necessary requisites to have a rapid growth of the martensite (athermal martensitic kinetics):

- A good coherence between the parent and product phase at the interface. In particular, the material needs a high yield stress to avoid plastic strain at the interface because the plastic deformation eliminates the coherence in the interface.

- Transformation temperatures for the MT should be low to avoid diffusional (recrystallization) growth since it is time-dependent.

In the opposite case, if the effective activation energy U is high in comparison to chemical driving force, the transformation will need the assistance of thermal fluctuations to overcome the activation barrier and to proceed. The MT becomes time-dependent within our experimental observation time window and, hence, shows anisothermal and/or isothermal behavior. The transformation chemical driving force can be increased by changing the system temperature of by applying an external field (stress or magnetic field in the case of magnetic materials). Then, a MT which shows isothermal kinetics will proceed athermally if the temperature scan rate is high enough or if an external field is applied.

A similar approach has been used by Kakeshita et al. in their phenomenological model explaining both athermal and isothermal MT in Fe–Ni–Mn alloys [42]. Their universal model was stimulated by the observed transition of MT in a Fe–Ni–Mn system from isothermal to athermal under the action of magnetic field pulses [43]. This model was applied to the isothermal transformations in the Fe–Ni and Fe–Ni–Cr alloys systems [44] giving a good approximation to the behavior of incubation time as function of the difference between the holding temperature and M_S.

In what follows we will call this approach the Kurdjumov-Kakeshita approach (KK).

Otsuka-Ren approach

The second approach is suggested by Otsuka and Ren [45]. Following Otsuka et al. nucleation and growth processes of the thermoelastic (displacive and diffusionless) MT are non-thermally activated processes and then all MT are athermal in essence. The MTs that show isothermal behavior are special cases in which the nucleation and growth processes require a certain type of atomic diffusion. Therefore, an isothermal MT necessarily implies the occurrence of atom migration/diffusion on the spatial scale exceeding the interatomic distances.

According to the authors, the athermal character of the MTs emerges naturally if the MT is interpreted as a result of a time-independent phonon condensation process. This version explains why the majority of diffusionless thermoelastic MT are athermal whereas only a few demonstrate time-dependent MT, and also, why MT can take place at very low temperatures. This is the main criticism by Otsuka et al. of the KK approach: if all MTs are thermally activated processes, how some rapid (athermal) MT can take place near 0 K where the thermal energy is very low?

As a support for their analysis Otsuka et al. used experiments [45] (basically reproducing the ones by Kakeshita et al. [46] for $\beta \leftrightarrow$2H MT in single and polycrystalline Cu–Al–Ni samples) performed with an equiatomic NiTi alloy exhibiting the B2→B19’ MT. The authors studied the effect of isothermal holding the samples slightly (within 2 K) above the direct MT start temperature MS. In contrast to the results of Kakeshita et al. [46], Otsuka et al. did not find any isothermal effect during isothermal holding. In addition, they cooled down the sample after isothermal holding to check if B19’ martensite nuclei were formed during the isothermal holding. If nucleation process was isothermal and growth was not, then some nuclei would be formed isothermally and when the cooling is resumed they all would start to grow producing a jump in the resistance. Otsuka et al. did not observe any evidence of isothermal nucleation. Therefore, they concluded that the MT itself and the nucleation of martensite in Ni–Ti is perfectly athermal, likely due to the absence of diffusion in Ni–Ti at moderate temperatures covering the MT range.

Low temperature isothermal $\beta \leftrightarrow$2H MT in Cu–Al–Ni reported by Kakeshita et al. [46] has been interpreted by Otsuka et al. as possibly due to the ordering of quenched Cu–Al–Ni samples, which shifts the MT temperatures [45].

However, the fact that isothermal MT in Cu–Al–Ni has been observed at rather low temperatures (around 180-200 K), i.e. 400 K lower than the ordering temperature for CuAlNi [47], casts the interpretation [45] into doubt. Thus a fundamental question concerning the possible role of diffusion in isothermal MT in SMA remains a matter of controversy. From now on we will call this approach the Otsuka-Ren approach (OR).

Other studies

Apart from the above mentioned studies, isothermal MT in SMA has been dealt with in a number of publications. Attempts to investigate the athermal/isothermal nature of the B2↔R↔B19’ transformation sequence have been undertaken recently by Chandni et al. [48]. The authors used a “fluctuation-based technique” to characterize films of an equiatomic NiTi alloy and commercial NiTi wires. The authors intended to draw conclusions on the role of thermal fluctuations in MT based on the studies of the power spectral density (PSD) of the resistance fluctuations as a function of the cooling/heating rate. They claim that during cooling of a bulk sample, just at the onset of the R→B19’ transformation, there is no $\dot{T}$ effect on the PSD, pointing to an athermal nature of this direct MT. Based on some minor differences in the temperature spectra of the PSD during cooling and heating the authors conclude that the “reverse MT to the R phase is slightly athermal in nature”, but the direct MT has a “much stronger athermal nature”. However, experimental data reported in Chandni et al. [48] are far from being convincing. Firstly, the temperature spectra of fluctuations were insensitive to any of the MT. Secondly, the strongest effects of cooling/heating rate were detected in the B19’ and austenitic phases, rather than during MT. These facts, in addition to the high scatter of data, throw into doubt the applicability of the method in its present form to study the properties of MT.

Planes et al. studied the acoustic emission during MT in Cu–Zn–Al and Cu–Al–Ni alloys [49] and concluded that $\beta \leftrightarrow$18R MT in the former alloy is athermal, whereas the $\beta \leftrightarrow$2H transformation in Cu–Al–Ni probably demonstrates variations in the M_S temperature with cooling rate, in line with the results of Kakeshita et al. [46]. Lipe and Morris [50], as well as later on Meng et al. [51], reported a substantial effect of heating/cooling rate during calorimetry tests in Cu–Al–Ni–Mn and nearly equiatomic Ni–Ti alloys, respectively. This observation essentially implies a notable effect of thermal fluctuations on MT in SMA. However, the use of calorimetry experiments in this kind of study has been criticized by Van Humbeeck and Planes [52]. They argued that extreme care should be taken in both the technical aspects (determination of the temperature-dependent time constants of the equipment) and the treatment of the experimental results using the Arrhenius rate equation.

There are many other works about the time-dependent MTs in non-magnetic alloys, like in In–Tl [53] and Ni–Al–Pt [54] alloy systems, which demonstrates the large interest awaken by this topic. In its turn, the isothermal MT is also present in ferromagnetic alloys. Hürrich et al. [55] investigated the saturation magnetization as a function of time and temperature of a $Ni_{50}Mn_{29}Ga_{21}$ alloy, in which both martensite and austenite are ferromagnetic. They found that both direct and reverse MT are affected by isothermal dwelling.

Recently a strong effect of the magnetic field on MT in metamagnetic SMA belonging to the Ni–Mn–X (X = In, Sb or Sn) system has been reported (see, for example, Kainuma et al. [56] and Umetsu et al. [57]). The austenite in those SMA possesses ferromagnetic ordering, while the martensite is non-magnetic (para/antiferromagnetic). Therefore, application of a magnetic field stabilizes the austenitic phase and can partially or completely inhibit direct MT, an effect referred to as the arrest of MT. The recent interest in isothermal MT in SMA has been stimulated by observations of low temperature relaxation phenomena revealed by electrical resistance measurements in a ternary Ni–Mn–In alloy [58] and magnetization in Ni–Mn–Sn [59] during direct MT under an applied magnetic field, as well as by time-dependent completion, upon removal of the magnetic field, of arrested MT in a Ni–Mn–In–Co alloy [60, 61]. However, it has been shown that the arrested state is not a prerequisite for time-dependent direct MT in metamagnetic SMA and that an isothermal nature is inherent in the direct MT of metamagnetic SMA [62]. Therefore, the application of magnetic field does not change the character of the MT in metamagnetic alloys. Recently Kakeshita et al. [63] tried to reconstruct a TTT diagram considering MT in a Ni–Co–Mn–In alloy as isothermal. On the other hand, it is instructive to mention that MT in metamagnetic alloys usually occurs at around and well below room temperature, and that isothermal MT upon removal of the magnetic field is observed well below 100 K [64], i.e. over the temperature range wherein no diffusion is expected to occur.

Thus, despite the accumulation of experimental data pointing to the isothermal character of the MT in a continuously increasing number of SMA, the fundamental problem related to the role of diffusion in isothermal (diffusionless) MT, or the controversy between the Kurdjumov-Kakeshita and Otsuka et al. approaches, remains unsolved.

——Add: Cite [65], Isothermal transformation in Ni–Mn–In–Co, they demonstrate the behavior of the C-Curve. Incubation time Ms and Ms'.

"The application of the magnetic field affects the incu- bation time of martensitic transformation as described in a previous paper"

1.3.3 Nucleation and growth processes

The martensitic transformations are first order transitions, so that the phase change is heterogeneous; it is produced by the creation of nuclei of the new phase in the most favorable places of the lattice, and, afterwards, these nuclei grow consuming the initial phase. The stages of nuclei incubation and plate growth are distinguishable and can play different roles in the athermal/isothermal nature of the transformation. Normally, martensite is not generated from a few initial nuclei, but from numerous nuclei that are forming continuously during the transformation until the transformation is completed. [4].

Therefore, it is important to know whether or not these two basic processes are thermally activated or related to thermally activated processes. Often, it is assumed that TAMs are a consequence of a thermally activated nucleation stage. By contrast, the plates growth occurs rapidly and without the need for thermally activation unless it is controlled by some time-dependent phenomena like atomic diffusion (for reviews see, for example, Massalski [36], Laughlin et al. [37] and Lobodyuk and Estrin [4, 39]).

However, this problem deserves a closer look. For instance, Kakeshita et al. [43] directly observed the isothermal growth of martensitic plates in a Fe–24.9Ni–3.9Mn [wt.%] alloy. In addition, in a subsequent work [42] on Cu–Al–Ni alloy system, they found crucial evidence of isothermal reverse MT; this experimental fact has not received adequate attention. Since the reverse MT in Cu–Al–Ni proceeds without the need for nucleation, its isothermal behavior cannot be attributed to the nucleation process. Then, the data [42] show that it is erroneous to assume in general that only the nucleation stage can be thermally activated: on several occasions clear evidence exists that the growth stage is isothermal. Therefore, this is a clear indication that, in particular, the motion of interfaces may well be responsible for the isothermal character of MT, even if the MT is diffusionless.

Although the isothermal growth of martensite/austenite is an experimental fact observed in several important studies, the possibility of isothermal growth of martensite/austenite remains essentially unexplored theoretically. Even Kakeshita et al., authors of the abovementioned experimental studies, use a model in which the nucleation is the only thermally activated process. Recently Laughlin et al. mentioned the possibility of the thermally activated growth of martensite [37], but again related its isothermal nature to atomic diffusion. Such a transformation has been classified as MT in which nucleation is athermal but growth is controlled by diffusion (line 4 of Table 1 in Laughlin et al. [37]), and thus as an isothermal transformation. Therefore, Laughlin and Massalski concept supports the approach of Otsuka et al. [45] by assigning the potential isothermal character of martensite/austenite growth to the atomic diffusion.

Concerning Otsuka et al. results, new experimental data on Ni–Ti–X alloy system [62, 66] evidences the isothermal accumulation of martensite as detected by electrical impedance in various MT developed by this system, in particular, in the B2→B19' MT. This is the same transformation that Otsuka et al. [45] classified as athermal. These two conclusions seem to be opposite, but in fact are perfectly compatible. The experiments by Otsuka et al and Kustov et al were performed over different range of temperatures. In the experimental results [45] the isothermal holding took place slightly above M_S temperature, whereas in experiments made by Kustov et al [66] the isothermal holding experiments were performed over a wide range of temperatures, inside and outside the transformation range. Otsuka et al. show that the nucleation stage is athermal and concluded that B2→B19' MT is athermal since they assumed, as usually, that only the nucleation stage can be responsible for the isothermal nature of the MT. Data by Kustov et al. confirm that the nucleation stage is athermal, but show, contrary to the conventional point of view, that the stage of martensite growth is isothermal.

1.3.4 Formulation of the problem and of a new theoretical approach/concept

In conclusion, the two fundamental issues remain controversial. First, assuming that the isothermal MT is necessarily related to the atomic diffusion, one cannot account for the isothermal MTs which occur at low temperatures and in alloys which are supposed to demonstrate the diffusionless MT (Cu–Al–Ni, Ni–Ti). Second, if one assumes, as usually, that only the nucleation stage is responsible for the isothermal nature of MTs, how to explain the isothermal reverse MT? Both these problems cannot be resolved based on the classical interpretation of isothermal MTs. Therefore, a new mechanism should be suggested to explain the isothermal nature of both direct and reverse diffusionless MTs.

The resolution of the above mentioned problems requires a new approach to the interpretation of the isothermal nature of the MTs. As a first idea we suggest to reconsider relative roles of nucleation and growth in isothermal MTs.

First, it should be mentioned that, according to the performed analysis of previous experiments and results, the growth of the martensite can be the origin of the isothermal nature of difussionless MTs, rather than the nucleation stage. Second, the existence and importance of different friction forces opposing the motion of interphase boundaries during first order phase transitions (and, of course, during diffusionless MT) is well established, see e.g. [67]. These friction forces are at the origin of energy dissipation during MT and contribute to its thermal hysteresis. Then, an obvious solution to the above mentioned controversies would be to admit that the obstacles to the motion of interphase boundaries can also be overcome with the assistance of thermal activation, without involving atomic diffusion.

The advantages of this interpretation are:

1. it admits the existence of isothermal growth of martensitic plates independently of atomic diffusion, so it would explain the appearance of isothermal growth at temperatures well below the material ordering temperatures;

2. it admits the existence of TAM independently of the athermal/isothermal nature of the nucleation stage, then it would explain the existence of the isothermal reverse MT, for example in $\beta \leftrightarrow$2H MT in Cu-Al-Ni alloy system.

1.4 Aim and general working plan

The present work has emerged after the very first results confirming the isothermal nature of the transformation in Ni–Mn–In–Co system alloy were obtained. The goal of this work was to get a deeper insight in the nature of isothermal martensitic transformations not only in metamagnetic, but also in conventional, widely used alloys. This work was motivated by the disparity between the main approaches to the problem of athermal/isothermal MTs and the failure of these approaches to describe some cases, like the reverse isothermal MT in Cu-Al-Ni. Inside the large theoretical framework of the isothermal and diffusionless MT, this work was aimed at answering two main questions:

- Whether or not diffusion is the only possible source of the time dependence during thermoelastic MT in SMA;
- Whether or not it is the incubation stage which is subjected to the effect of thermal activation

To be able to answer these questions, one needs to study the behavior of different alloy systems which fulfill some requirements. Firstly, these systems should exhibit a MT at sufficiently low temperature to avoid atomic diffusion, that is, its MT must be isothermal for which the origin of time-dependence cannot be explained as a result of an interaction between the transformation and the atomic diffusion. And secondly, to track the generic features of IMTs, these systems should have a broad variety of types of MT, between different crystallographic systems and with different magnetic behaviors.

Following the above criteria, two alloys systems were selected for the present study: the conventional SMA Ni–Ti alloy system and the metamagnetic shape memory alloy (MMSMA) Ni–Mn–In alloy system. On one hand, Ni–Ti system is optimal for this work because it is a conventional system which develops different MT depending on its composition, thermal history and doping elements, some of these MT are shown to have an isothermal behavior. In addition, Ni–Ti is a common SMA system widely used in commercial applications. On the other hand, Ni–Mn–In alloy system was introduced more recently. The MT exhibited by this material has an additional degree of freedom due to the magnetic subsystem: the parent and product phases have different magnetic behavior, and then, the MT is a magnetostructural transformation.

The standard experimental procedure used for each alloy type and composition normally includes the following steps:

- The high purity elements with the desired nominal composition were melted several times in an electric arc furnace to obtain an ingot.
- The ingot was homogenized. Despite of it may vary between alloys, an annealing at 1170 K during 24 hours was the most common heat treatment in this step.
- The samples of the needed size were cut from this ingot by means of a diamond saw or a spark cutter.
- The samples were heat treated. Different kinds of heat treatments were selected depending on the material and its desired properties. One can choose the temperature and time of the heat treatment, to treat the sample in air or encapsulated under a low pressure argon atmosphere, and finally, to quench it in water or to slow cool it at room temperature.

For every sample and MT, its athermal/isothermal nature was investigated by means of the electrical resistance or the real part of the electrical impedance. This parameter was obtained as function of temperature and time. In addition, in the case of the magnetostructural MT, the effect of the magnetic subsystem was taken into consideration by performing the experiments with or without applied magnetic field. These measures were complemented with calorimetric measurements made in a commercial DSC.

Afterward, experimental data were treated in order to:

1. Determine whether the method is suitable for analyze qualitatively and quantitatively the possible time-dependence of the MT. This was applied to both the direct and reverse transformation.
2. Conclude whether or not the studied MT were isothermal.
3. Quantify the intensity of the isothermal effects.
4. Find the possible relations between the isothermal evolution and other characteristics of the MT and of the material in general.

All this information was interpreted in an attempt to answer the above mentioned main questions of this work.

1.5 Material selection

Different materials were selected to achieve the goals of this work. We focused on two alloy system, the conventional SMA and popular Ni-Ti-X alloy system and the novel metamagnetic SMA Ni-Mn-In-X alloy system.

1.5.1 Conventional SMA: Ni–Ti–X alloy system

The alloys of the Ni–Ti–X alloy system (with X = Fe, Cu) show the SME and SE effect due to the thermoelastic MT when its composition is near equiatomic, $Ni_{50}Ti_{50}$.

A detailed description of this alloy system is given by Saburi [8] and Otsuka and Ren [68] and references therein.

The Ni-Ti alloy system exists in several different phases and shows transitions between them depending on composition, microstructure and additions of dopants (usually, Fe or Cu).

Most common MT in the Ni-Ti alloy system is between a high temperature phase B2 (cubic, austenite) to a low temperature phase B19' (monoclinic, martensite). This transformation can proceed following different paths: in a single-step B2↔B19' transformation or in a two-step transformation with an intermediate R phase (trigonal, martensite). In the latter case, the entire transformation sequence B2↔R↔B19' is split in two stages, the B2↔R (thermoelastic MT) and the R↔B19' transitions (intermartensitic transformation). The two-step B2↔R↔B19' transformation is also present in the alloy doped with iron when its atomic percentage is lower than 3%.

On the other hand, the alloys doped with copper could show a two-step transformation with an intermediate B19 phase (orthorhombic, martensite) and then they exhibit also a two-stage B2↔B19↔B19' transformation.

In addition, these alloys do not exhibit one or all of the above mentioned transformations when the composition is far from the equiatomic $Ni_{50}Ti_{50}$. If the nickel content of the binary Ni-Ti is increased, first, the intermartensitic R↔B19' transformation will disappear and the MT will be a single-step B2↔R. If nickel content is further increased, the B2↔R MT will disappear too. Similarly, in the Ni-Ti-Cu alloys, the B19↔B19' intermartensitic transformation will vanish for concentrations of copper beyond 15 %.

Other phases would appear in the Ni-Ti system when the composition is far from the equiatomic NiTi. These phases normally appear as precipitates which are rich in nickel or in titanium. The capacity of the equiatomic B2 phase to absorb an excess of nickel or titanium without precipitate increases with temperature. It has its maximum at about 1390 K when is stable inside the range of Ni content between 49% and 58%. Then is reduced until reach the melting temperature (1580 K). For temperatures below 900 K, this range is reduced between 50% and 50.5%. Therefore, for compositions outside this range, the B2 phase is metastable and it will decompose into a equiatomic NiTi matrix and Ni-rich or Ti-rich precipitates.

The precipitates or second phases of the binary Ni-Ti alloy are the phases rich in titanium: Ti_2Ni, $Ti_4Ni_2O_X$ (with $0<X<1$) and the phases rich in nickel: Ni_4Ti_3, Ni_3Ti_2, Ni_3Ti and pure nickel.

Following Saburi [8], Ni_4Ti_3 and Ni_3Ti_2 phases are metastable. Therefore, these phases can appear during the decomposition of the equiatomic phase, but they will not appear in the final result of the decomposition. However, Ni_4Ti_3 has appeared as a final product after heat treatments at low temperatures. Following Srivastava et al. [69], it appears after a long time annealing of 5 hours at 770 K. On the other hand, the Ti_4Ni_2O oxide is easily formed and appears often in this alloy system. It has been sometimes confused with Ti_2Ni since both have nearly the same structure [70].

Following Somsen et al. [71], the martensitic transformation depends strongly on precipitates. Ni_4Ti_3 precipitates becomes unstable above 900 K and decompose. Below this point, the Ni–Ti alloy will have Ni_4Ti_3 precipitates and exhibits a two stage transformation with the occurrence of the R phase. With a heat treatment at temperatures between 900 and 1300 K, the Ni_3Ti_2 precipitates are metastable, the Ni_3Ti ones are stable and the one stage B2↔B19' transformation will take place. The strong influence of the Ni_4Ti_3 precipitates is corroborated by Zel'dovich et al [72] in $Ni_{51}Ti_{49}$ and $Ni_{52}Ti_{48}$ alloys. They found that the Ni_4Ti_3 precipitates serve as nucleation sites for the formation of the R phase or the B19' phase depending on their size. The Ni_4Ti_3 precipitates which are larger than a critical size lose their coherence with the matrix and promote the B19' phase. Then, for these alloys, the Ni_4Ti_3 precipitates with a size from 100 nm to 1-2 μm promotes the two stage B2→R→B19' transformation, whereas the single stage B2→B19' MT is observed outside this range.

The phase diagram of the Ni–Ti system is shown in Figure 1.9 [73]. This diagram has been involved in controversy until 1980's because the effects produced by some of the above mentioned precipitations were not understood, and the trigonal R phase was considered as a premartensitic effect. These difficulties usually occur simultaneously, making the whole problem much more difficult to resolve.

The most common doping elements are Fe and Cu, substituting Ni, but there are other possible doping elements like Co, Cr, Mn, Al, Pd and Au. Fe and Cu were the dopants of our interest used in the present work.

The Ni-Ti-Fe alloy system is characterized by the two-step transformation B2↔R↔B19' and by a reduction of the transformation temperatures

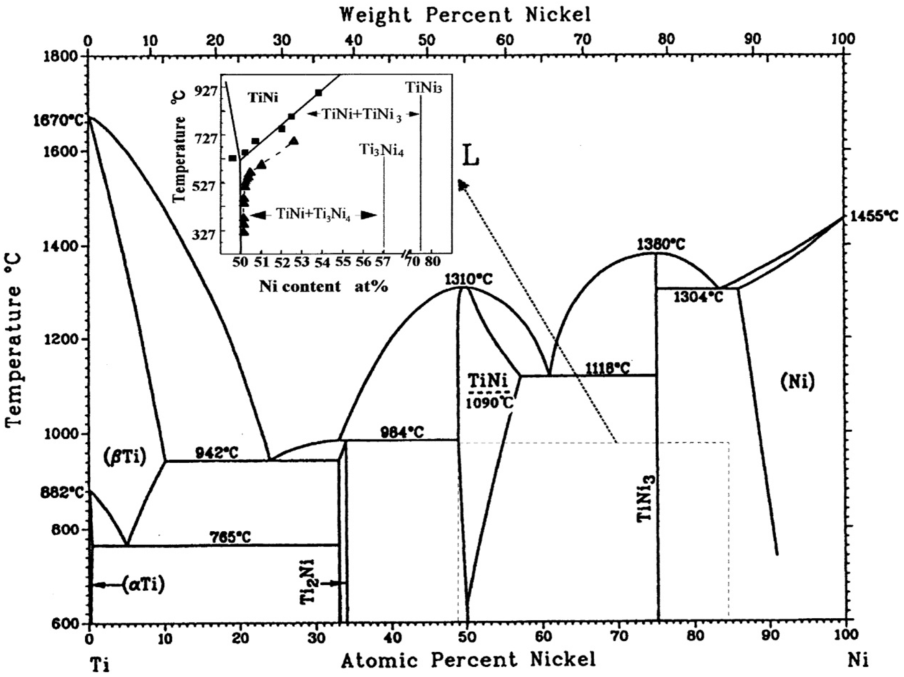

Figure 1.9: Phase diagram of a binary Ni-Ti alloy after Massalski [73]. The inset shows the composition range close to the equiatomic B2 austenite for high temperatures.

of these transitions with respect to the Ni-Ti. Partially annealed samples of the Ni-Ti alloy can also exhibit the B2↔R↔B19' two-step MT, but the MT and the intermartensitic transformation may be overlapped, especially during the reversal transformation. The addition of Fe not only reduces the transformation temperature, but increases the difference between the transformation temperatures of B2↔R and R↔B19', for both, direct and reverse MTs. Therefore, these steps usually are well decoupled in this alloy system.

The Ni–Ti–Cu alloy system demonstrates a B2↔B19↔B19' two-step martensitic transformation when the copper composition is between 5 and 16 at%. Its advantages over the binary alloy are the reduction of the total hysteresis of transformation and the improvement of its mechanical properties. In addition, it has somewhat lower transformation temperatures. The B2→B19 and B19→B19' transformation are overlapped for Cu content between 5 and 8.5 at%.

1.5.2 Metamagnetic SMA: Ni–Mn–In–X alloy system

The ferromagnetic shape memory alloys (FSMAs) are alloys in which one or both of the austenite and martensite are ferromagnetic. Due to the magnetic behavior, the martensitic variants orientation can be affected by an external magnetic field and/or the MT can be magnetically induced. This opens the possibility of magnetically controlled actuators, which may be advantageous with respect to classical SMA actuators driven by a change of temperature or an external applied stress.

The main possible advantage of the magnetic actuators is their working frequency. In actuators made of classical SMAs, the operation frequency, i.e. the speed of a heating-cooling cycle, is quite limited. Following Bertacchini and Lagoudas [74], to heat the actuator is relatively quick but it takes some time to cool it, so its working frequency is around 0.1 Hz.

The strain induced by a magnetic field is called Magnetic Field-Induced Strain (MFIS) and can be produced by two different mechanisms. First, in a magnetically induced MT; in this case, an external applied field will affect the phase stability since it contributes differently to the Gibbs free energy of two phases. However, in the major part of the FSMAs, both austenite and martensite are ferromagnetic, and then the magnetization change during the MT is small. Therefore, the change of the transformation temperatures by means of an external applied field is small as well. Second, MFIS can also be produced by a martensitic variant reorientation. This is, in fact, a special kind of magnetostriction that can produce MFIS up to 10% [75, 76].

Most studied alloys from the FSMA family are based on Ni_2MnGa Heusler alloy [76].

The MetaMagnetic SMAs (MMSMAs) is a subtype of the FSMAs. These alloys have the peculiarity that above its transformation the high temperature phase is ferromagnetic, but below the MT its low temperature phase is non-magnetic (paramagnetic or magnetically frustrated). In other words, the Curie temperature of austenite T_{CA} is above T_0 but the Curie temperature of martensite T_{CM} is not above T_0, like in convencional FSMAs, but below. This adds an additional degree of freedom to the MT which becomes a magnetostructural transformation of the first order.

MMSMA have attracted considerable attention since Kainuma et al. [56] showed that these alloys are able to demonstrate martensitic transformation induced by an applied magnetic field. In particular, the reverse MT can be magnetically induced since the magnetic field stabilizes the ferromagnetic austenite. The stress than these actuators can provides is potentially much larger than in conventional FSMA, where the MFIS is generated by the magnetically induced rearrangement of martensite variants. For example, under an applied magnetic field of 70 kOe, a Ni-Co-Mn-In alloy was found to show stress levels which are approximately 50 times larger than in conventional FSMA [77]. Then, they are very promising materials for magnetic controlled actuator applications.

In addition, several interesting phenomena such us large magnetocaloric effect [78,79], kinetic arrest [80], magnetic superelasticity [81] and large magnetoresistance [78,82] have also been found and investigated in these alloys.

The alloys which are classified as MMSMA are the Heusler Ni_2-Mn_{1+X}-Z_{1-X} alloys with Z=In, Sn, Sb and, more recently, Al. These alloys are often doped with Co, which substitutes Ni, to increase its magnetization, and, this way, to increase the effect of the applied magnetic field over the transformation temperatures. The peculiar magnetic character of the Ni-Mn-Z MSMAs is due to, first and mainly, the ferromagnetic coupling between the Mn atoms located in the Mn sublattice and, second, the antiferromagnetic coupling between Mn atoms in the Mn sublattice and Mn atoms in the Z sublattice [83,84].

Chapter 2

Experimental methods and procedures

2.1 Calorimetry

Acquisition of the heat flux which is generated or absorbed by the sample during the MT is a common tool used to study any type of first order phase transition.

In a DSC (Differential Scanning Calorimeter) two samples of different materials are placed inside a furnace with controlled atmosphere, of N_2 gas in the present work, and heated/cooled to investigate its heat flux behavior. One sample represents the material under investigation while the second sample should be any material that is inert and has a well-defined heat capacity over the temperature range of interest. Then, we will refer to the first material as sample and to the second as reference. In our case a copper reference was used. The sample and reference are kept at an approximately the same temperature while cooling/heating. To do this, sample and reference will require different amounts of heat to change their temperatures. This difference is because of the different heat capacity and the possible exothermic/endothermic processes that may occur in the sample. Therefore, the DSC detects those processes by means of the different thermal behavior of the sample and the reference.

However, the DSC does not measure directly the heat flux absorbed/emitted by the sample. Instead of that, the DSC used in the present work, DSC822^e FRS5, obtains the furnace temperature T_F by means of a sensor composed of 56 Au/AuPd thermocouples and the voltage U at the sensor. The voltage U is the original measured signal of the DSC, which is proportional to the difference between the sample temperature T_S and the reference temperature T_R, $\Delta T = T_S - T_R$. The relation between U and ΔT is a factor defined as the sensitivity of the sensor S. S and T_R are not measured but calculated from the equipment calibration as function of the furnace temperature T_F. Then,

$$\Delta T = \frac{U}{S(T_F)} \tag{2.1}$$

$$T_S = \Delta T + T_R(T_F) \tag{2.2}$$

In addition, the final signal given by the DSC is a heat flux ϕ calculated by the thermal equivalent of Ohms Law

$$\phi = \frac{\Delta T}{R_{th}} \tag{2.3}$$

where R_{th} is the thermal resistance of the disc on which sample and reference are placed. R_{th} is also obtained by the calibration of the DSC as function of T_F. Therefore, the relation between the resulting signal and the original measured data is

$$\phi = \frac{U}{S(T_F) \cdot R_{th}(T_F)} \tag{2.4}$$

However, the heat flux absorbed/emitted by an active sample ϕ_r is not equivalent to the heat flux given by the DSC ϕ. They are related in a complex way [85].

In general, if the sample and the reference are on a support that is called furnace, there is a heat flux exchanged between the sample and the support ϕ_{FS} because of the difference in their temperatures. This flux is

$$\phi_{FS} = \kappa_S A \frac{T_F - T_S}{\Delta l} \tag{2.5}$$

where A is the cross section of the heat conductor between furnace and the sample (reference), Δl is the distance between the temperature measurement point and the furnace and κ_S is the thermal conductivity between the furnace and the sample. In a similar way, the flux exchanged between the support (furnace) and the reference ϕ_{FR} is

$$\phi_{FR} = \kappa_R A \frac{T_F - T_R}{\Delta l} \tag{2.6}$$

Here one can recover the concept of thermal resistance and write the equations (2.5) and (2.6) as

$$\phi_{Fi} = \frac{T_F - T_i}{R_{th\ i}}; i = S, R \tag{2.7}$$

where equation 2.7 represents ϕ_{FS} or ϕ_{FR} depending on the subscript i.

The sample and reference temperatures are different from the furnace temperature because they need some heat to vary their temperatures. This produces a delay between T_F, that changes linearly with time, and $T_i(i = S, R)$, that follows the set temperature. The heat flux absorbed by the sample/reference in changing its temperature is

$$\phi_i = C_i \frac{\partial T_i}{\partial t}; i = S, R \tag{2.8}$$

where $C_i(i = S, R)$ is the heat capacity of the sample/reference and is proportional to the mass m of the sample/reference. In addition, when the sample is not inert, it exchanges a heat flux ϕ_r due to the transformation. This flux can be expressed by an energy balance as

$$\phi_r = (\phi_{FS} - \phi_S) - (\phi_{FR} - \phi_R) \tag{2.9}$$

where $\phi_{Fi} - \phi_i(i = S, R)$ is the amount of flux between the sample (reference) and the furnace which is not used to warm/cool the sample (reference). By using the equations (2.7) and (2.8), one can write the energy balance of (2.9) as

$$\phi_r = \frac{T_R}{R_{th\ R}} - \frac{T_S}{R_{th\ S}} - (C_S - C_R)\frac{\partial T_R}{\partial t} - C_S \frac{\partial (T_S - T_R)}{\partial t} \tag{2.10}$$

The time derivative of the reference temperature will be constant and equal to the T-scan rate β. If thermal resistances for both sample and reference are equal and considering that $\Delta T = T_S - T_R$, then equation (2.10) is

$$\phi_r = -\frac{\Delta T}{R_{th}} - \beta(C_S - C_R) - C_S\frac{\partial \Delta T}{\partial t} \tag{2.11}$$

Therefore, following the equations (2.3) and (2.11), the different contributions to the heat flux given by the DSC are

$$\phi = \frac{\Delta T}{R_{th}} = -\phi_r - \beta(C_S - C_R) - C_S\frac{\partial \Delta T}{\partial t} \tag{2.12}$$

The sign of the equation (2.3), and then of the equation (2.12) too, is arbitrary and should be chosen depending on the sign criteria. As ϕ_r is defined, it is positive for endothermic processes and negative for exothermic ones. On the contrary, the heat flux calculated by the DSC following equations (2.3) and (2.12) is positive when the transformation is exothermic. The latter is the sign criteria used along the present work.

Therefore, there are three main contributions to the calorimetric signal given by the DSC

- ϕ_r contains the thermal information of the transformation under study. It is null when the sample is inert (outside the transformation range) and would describe a peak versus time or temperature when the transformation takes place.

- $\beta(C_S - C_R)$ is the baseline of the calorimetric signal. Since the heat capacity of the sample and the reference are usually different, this term contributes to the signal inside and outside of the transformation range. It changes its sign between cooling and heating because it depends on the T-scan rate β. This baseline should be subtracted from the calorimetric signal inside the transformation range to identify the transformation heat. To do this, the baseline is commonly approximated by a straight line between the sides of the transformation as it is not possible to distinguish between the contributions of the peak and the baseline inside the transformation range. This is a good approximation if the transformation range is small enough. However, in general, the temperature dependence of the baseline is not lineal and C_S may depend strongly on the sample's phase.

- $C_S\frac{\partial \Delta T}{\partial t}$ is the main responsible of the non-equivalency between the measured ϕ and the transformation's heat flux ϕ_r. The measured signal is delayed with time and distorted. The value of this term outside the transformation range depends on the temperature dependence of the heat capacities of sample and reference and of the thermal resistance of the furnace. If the temperature dependence of C_S, C_R and R_{th} is weak, then $T_F - T_S$, $T_F - T_R$ and $T_S - T_R$ will be approximately constant and $C_S \frac{\partial \Delta T}{\partial t}$ will be negligible. If not, it will contribute to the baseline. Similarly, the temperature dependence of C_S, C_R and R_{th} also affects the contribution of this term to the peak. Since T_S is always going to change due to the thermal effect of the transformation, $C_S \frac{\partial \Delta T}{\partial t}$ is never zero nor negligible inside the transformation range. However, if the temperature dependence of the baseline is weak, the contribution of this third term to the peak will vanish when the peak is integrated over time or temperature. In other words, under some conditions, this term delays and distorts the signal, but does not contribute to the calculation of the total exchanged heat of the transformation.

Finally, the heat flux given by the DSC is modified in order to compare between different samples and materials. Since these measurements will be affected by the temperature scan rate β used in the experiment and the mass m of the sample, the heat flux ϕ is divided by these two values, β and m, obtaining a calorimetric signal in J/(g·K)(Note: the temperature scan rate might affect the transformation temperatures in case of an isothermal transformation).

As have been introduced in Section 1.3.2 (page 23), some authors have utilized the calorimeter to study the kinetics of the transformations [50, 51, 86]. However, Van Humbeeck and Planes [52] criticized these kind of studies and show that the DSC is disadvantageous to study the transformation kinetics since it needs to know with high accuracy the time constant of the apparatus. Consequently, in the present work, DSC does not have been used to discern the athermal/isothermal nature of the transformations. Instead, it have been only used to characterize the martensitic transformation/s exhibited by the different studied alloys by means of continuous thermal cycles.

In addition to the difficulties of the method, it is worthy to mention an important misconception committed by Zheng et al. in references [86, 87]. They observed the variation of the transformation temperatures with the temperature scan rate of the experiment. They assumed this as part of the behavior of the transformation and argued that M_S actually increases during the isothermal dwell. However, such dependence of the calorimetric signal with the T-scan rate is the normal and may not be related with the transformation. As have been previously discussed and is shown by the third term of the equation (2.12), the measured signal is delayed with time and distorted as compared with the original heat exchanged between the sample and reference. As long as this effect is time-dependent, it depends strongly on the T-scan rate β of the experiment, in other words, the higher is $\beta = \frac{\partial T_R}{\partial t}$, the higher is also $\frac{\partial T_S}{\partial t}$, and consequently, $\frac{\partial \Delta T}{\partial t}$ too. Therefore, there is a temperature shift between the transformation temperatures measured under isothermal conditions and under a thermal cycle with constant $\dot{T}$. This fact was exhaustively studied by Chang and Wu [88]. They investigated the dependence of M_S on the T-scan rate of the experiment calculated from heat measurements in a DSC and from the internal friction spectrum obtained with a DMA. They found a linear dependence of M_S with the cooling rate for both, DSC and DMA experiments, being this dependence stronger for the DMA. They explain this difference by the different specimen and furnace sizes inherently designed into the DSC and DMA experiments. Despite the different cooling rate dependence, M_S calculated by both systems tends to the same limit value as the cooling rate approaches zero. In addition, the dependence of M_S on β also depends on the mass of the specimen which reflects the greater temperature gradient from the center to the surface when the sample is cooled/heated at constant rate. The last cannot be extracted from equation (2.12) since the temperature distribution along the sample and reference was not considered in the previous analysis. In conclusion, the dependencies observed by Zheng et al. have more plausible origins different from the isothermal variation of M_S.

2.2 DC resistance and AC impedance

The experimental setup permits to measure both DC resistance and AC impedance. In the former case, the system holds a constant intensity of the current in the sample and acquires the voltage drop across it, which is proportional to the DC resistance of the sample (Ohm's law). In addition, both the voltage drop and the DC resistance are proportional to the electrical resistivity ρ. Assuming the sample to be cylindrical, the DC resistance R_{DC} depends on the length l and the radius a

$$R_{DC} = \frac{l}{\pi a^2}\rho \tag{2.13}$$

The sample impedance Z, its real (R) and imaginary parts (X) are obtained from AC experiments. The impedance in terms of the real (resistive, R) and the imaginary (inductive, X) parts is given by

$$Z = R + iX \tag{2.14}$$

From Maxwell equations, the relationship between the AC impedance and the DC resistance for a cylindrical sample with radius a is given by [89]

$$Z = R_{DC} ka \frac{J_0(ka)}{2J_1(ka)} \tag{2.15}$$

where J_n are the Bessel functions of the first kind, $k = \frac{1+i}{\delta}$ and δ is the skin depth

$$\delta = \sqrt{\frac{2\rho}{\omega\mu}} \tag{2.16}$$

with ω the angular frequency of the flowing electric current and μ the effective transverse magnetic permeability. Expanding the Bessel functions in equation (2.15) and comparing with equation (2.14) one obtains

$$R = R_{DC}\left[1 + \frac{1}{48}\left(\frac{a}{\delta}\right)^4 + \ldots\right] \tag{2.17}$$

$$X = R_{DC}\left[\frac{1}{4}\left(\frac{a}{\delta}\right)^2 - \frac{1}{384}\left(\frac{a}{\delta}\right)^6 + \ldots\right] \tag{2.18}$$

The angular frequency ω was always selected in experiments in such a way as to maintain the factor $\frac{a}{\delta}$ small. Then, the series can be restricted to the quadratic terms and equations (2.17) and (2.18) take the form

$$R \approx R_{DC} = \frac{l}{\pi a^2}\rho \tag{2.19}$$

$$X \approx \frac{a^2\omega\mu}{8\rho} R_{DC} = \frac{l\omega}{8\pi}\mu \tag{2.20}$$

Therefore, under these conditions the value of DC resistance and the real part of AC impedance will coincide. In addition, AC impedance measurements yield information on the magnetic state of the sample through the effective transverse magnetic permeability μ. Then, the selection of the angular frequency ω is a compromise between being low enough to maintain $\frac{a}{\delta}$ small and being high enough to obtain a value of X high enough to increase the signal-to-noise ratio.

2.3 Estimating the volume fraction of martensite

The martensite fraction F is the volume of sample which is in the martensitic phase over the total one. If the isothermal MT proceeds, the martensite fraction will change with time being a key tool to evaluate the isothermal nature of the MT in different materials. Unfortunately, F and, hence, its kinetics are difficult to obtain from direct observations. That is why F is derived in the present work from the real part of the impedance.

In general, the real part of the impedance R for each phase is different, both in absolute value and in its dependence with temperature. Therefore, a change in F could produce certain change in real part of the impedance that can be detected experimentally.

In some materials, the change of real part of the impedance during the MT is monotonic; accordingly, a direct relation between the martensite fraction and the real part of the impedance can be established. It is assumed that a change ∂F will produce a proportional change ∂R ($\partial R \propto \partial F$). The resistance values, between which the resistance varies during the MT, can be denoted as R_{MIN} and R_{MAX}. The fraction which corresponds to the start transformation temperature has value $F = 0$ and the one which corresponds to the finish transformation temperature is $F = 1$. So, one has

$$F \approx \frac{R - R_{MIN}}{R_{MAX} - R_{MIN}} \tag{2.21}$$

The dependence of R with T is assumed to be only caused by the MT in the above equation (2.21). This means that the change of R due to the change with T of the contribution of scattering by phonons is neglected. This approximation will be good if the transformation range ($M_S - M_F$) is narrow and the total resistance change ($R_{MAX} - R_{MIN}$) is high, and thus, if the dependence with temperature due to the MT is much larger than the effects of phonon scattering. In the present work this approximation was applicable in most cases.

If cooling/heating scan is interrupted within the MT range and the temperature is kept constant, Figure 2.1, the variation of martensite fraction ΔF accumulated with time during isothermal holding is given by

$$\Delta F(t) \approx \frac{R(t) - R_0}{R_{MAX} - R_{MIN}} \tag{2.22}$$

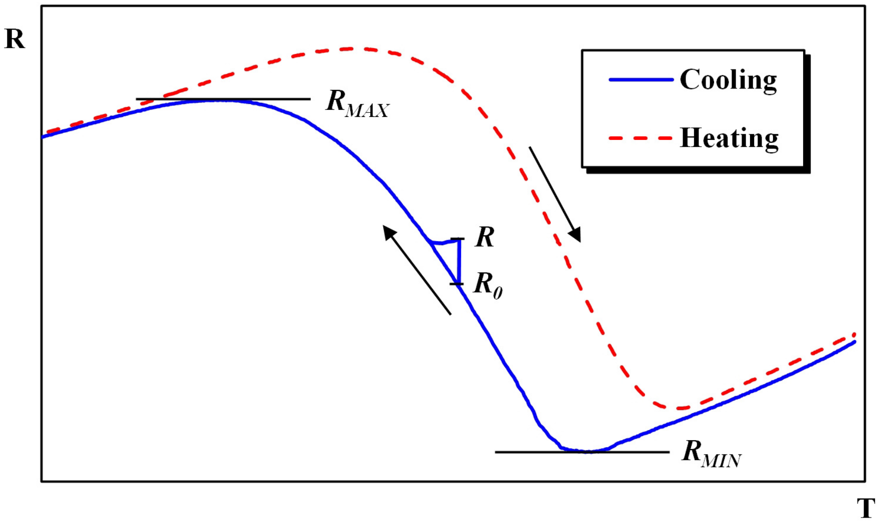

Figure 2.1: Diagram of the sample resistance in a temperature cycle where the typical effect of an isothermal holding experiment over the resistance is shown. R and R_0 are the actual resistance and the initial resistance during an isothermal holding experiment respectively; R_{MIN} and R_{MAX} are the minimum and maximum resistance values, attained during the MT.

where R_0 is the value of the real part of the impedance in the point where the continuous cycle is interrupted and ΔF is the difference between the martensite volume fraction at a certain time of the relaxation $F(t)$ and its initial value at the interruption of the T-scan F_0, $\Delta F(t) = F(t) - F_0$.

Under the above mentioned assumptions, within the transformation range, the MT temperature rate $\frac{\partial F}{\partial T}$ is

$$\frac{\partial F}{\partial T} \approx \frac{1}{R_{MAX} - R_{MIN}} \frac{\partial R}{\partial T} \tag{2.23}$$

To be applicable, equations (2.21), (2.22) and (2.23) require a set of quite restrictive conditions, so we could call this situation the "ideal case". In general, the condition is not valid when, during the transformation, the real part of the impedance is not a monotonous function of temperature. At the point of the extremum the real part of the impedance becomes insensitive to the change of the martensite fraction. In this case, equations (2.21), (2.22) and (2.23) are not valid.

To judge whether or not these conditions are fulfilled, one can compare the results of two different methods of evaluation of the martensite volume fraction: the temperature derivative of real part of the impedance, right hand side of equation (2.23), and the calorimetric signal given by the DSC (2.12). To simplify the relation between both methods, it is possible to make several assumptions. First, lets suppose that the transformation latent heat L is constant along the transformation range; then a differential of mass ∂m absorbs/emits a proportional differential of heat ∂q when it transforms

$$\partial q = L \partial m \tag{2.24}$$

According to the analysis in section 2.1, the transformation generates a heat flux ϕ_r

$$\phi_r = \frac{\partial q}{\partial t} = L \frac{\partial m}{\partial t} \tag{2.25}$$

To establish a relation with the martensite volume fraction F, let us assume that the density of the transforming mass units is constant. Then, as the martensite volume fraction is the normalized volume

$$\partial F = \frac{1}{V} \partial V = \frac{1}{V\rho} \partial m \tag{2.26}$$

In addition, $V \cdot \rho$ is the total mass m_T of the sample and the change of martensite volume fraction per unit of time $\frac{\partial F}{\partial t}$ will be proportional to $\frac{\partial F}{\partial T}$, because the T-scan rate $\beta = \frac{\partial T}{\partial t}$ is constant. Then, equations (2.25) and (2.26) are joined to obtain

$$\phi_r = L m_T \beta \frac{\partial F}{\partial T} \tag{2.27}$$

Now, one can obtain a relation between the calorimetric and the electrical impedance measurements by comparing the equations (2.27) and (2.23)

$$\phi_r \approx \frac{L m_T \beta}{R_{MAX} - R_{MIN}} \frac{\partial R}{\partial T} \tag{2.28}$$

However, as seen in section 2.1, the signal measured by the DSC is not directly ϕ_r, but a distorted and delayed in time heat flux ϕ. Therefore, the approximated relation between the calorimetric signal and the temperature derivative of the real part of the impedance is given by the equations (2.12) and (2.28)

$$\phi \approx -\frac{Lm_T\beta'}{R_{MAX}-R_{MIN}}\frac{\partial R}{\partial T}-\beta(C_S-C_R)-C_S\frac{\partial \Delta T}{\partial t} \tag{2.29}$$

Note that in general the temperature scan rate of both experiments can be different. Therefore, β' changes the temperature derivative of R into a time derivate: it refers to the rate of the electrical impedance experiment. By contrast, β is the T-scan rate of the DSC experiment.

Therefore, the relation between the $\frac{\partial F}{\partial T}$ obtained by two methods is rather complex, they are not proportional in general. Nevertheless, both, ϕ and $\frac{1}{R}\frac{\partial R}{\partial T}$, will show a transformation peak in the temperature spectrum and the peak temperature should be similar. In this case, the condition $\partial R \propto \partial F$ is fulfilled in an uninterrupted cycle. Otherwise, one or both methods is not a good approximation for the change of martensite volume fraction.

2.4 Measurements of the isothermal transformation rate

If the isothermal martensitic transformation exhibits a logarithmic kinetics, its rate is characterized by the Z parameter

$$\Delta F(t) = Z(T)\ln\frac{t}{t_0} \tag{2.30}$$

where t_0 is a constant. In the subsequent numerical estimations $t_0 = 1$ s is used.

This type of MT kinetics has been known for decades in steels [90, 91], and has been observed recently at metamagnetic SMA [62]. The logarithmic kinetics is typical for relaxations with a wide distribution of activation energies, like the magnetic thermal fluctuation aftereffect [92]. The logarithm diverges with time, then, a saturation of the logarithmic kinetics during long-term isothermal holdings is expected.

Using the equations (2.22) and (2.30) one gets

$$\frac{R(t)-R_0}{R_{MAX}-R_{MIN}} \approx Z(T)\ln\frac{t}{t_0} \tag{2.31}$$

Then Z was calculated from isothermal holding experiments obtaining the kinetics of DC resistance or the real part of the AC impedance. Z

calculated as in equation (2.31) is suitable to distinguish between isothermal ($Z \neq 0$) and athermal ($Z \approx 0$) transformation and to compare the isothermal behavior of different martensitic transformations (between different phases, of different compounds, with different heat treatments, under different applied magnetic fields, etc.). In addition, isothermal holding experiments were done at different temperatures to obtain T-dependence of Z, which is important to compare it with other MT properties.

The effects of phonon contribution are neglected in equation (2.31), and hence, equation (2.31) requires the same set of quite restrictive conditions that equations (2.21), (2.22) and (2.23). Therefore, the equation (2.31) is not applicable in several cases, for example when:

- the transformation range is broad or/and the impedance change within the transformation range is small (the effects of phonon scattering cannot be neglected);
- the dependence of R with T is not monotonous (so $R_{MAX} - R_{MIN}$ cannot be determined).

Yet another approximation can be made.

$$\frac{R(t) - R_0}{R_0} \approx Z'(T) \ln \frac{t}{t_0} \tag{2.32}$$

The approximation (2.32) is not equivalent anymore to the expression given by equation (2.30), unlike the equation (2.31). The approximation (2.32) introduces a temperature-dependent factor, $R_0 = R_0(T)$. This factor is introduced to obtain a normalized value of Z' (independent of the sample size). Equation (2.32) can be applied when the change of R within the martensitic transformation range is small compared with the absolute value of R, or in other words, when the temperature dependence of the impedance is weak. The condition for equation (2.32) is less restrictive than ones for equation (2.31), therefore it can be applied in more cases. Equation (2.31) was used to analyze the isothermal behavior of the MT on the Ni–Mn–In–X alloy system while equation (2.32) was used on the Ni–Ti–X alloy system.

The relation between the equations (2.31) and (2.32) is shown in equations (2.33) and (2.34).

$$Z'(T) = \alpha(T) Z(T) \tag{2.33}$$

$$\alpha(T) = \frac{R_{MAX} - R_{MIN}}{R_0(T)} \tag{2.34}$$

The value of $\alpha(T)$ can be calculated if equation (2.31) can be applied. Furthermore, in this case $\alpha(T)$ should be, as the resistance/impedance itself, a monotonic function of the temperature. The maximum and minimum values of $\alpha(T)$ are easily calculated by substituting R_0 by R_{MAX} or R_{MIN}. Then, the relative total change of the factor α with temperature is described as:

$$\frac{\Delta\alpha}{\alpha} = \frac{R_0\left(R_{MAX} - R_{MIN}\right)}{R_{MAX}R_{MIN}} \tag{2.35}$$

In Ni–Ti–X alloy system, the change of resistance/impedance during the transformation is small compared with its total value, and then, as is seen in equation (2.35), the same is true for the factor α, i.e., the temperature dependence of α is weak ($\Delta\alpha << \alpha$).

Coming back to equation (2.33), in general, Z and Z' are not of the same order and Z' does not give direct information about the martensite volume fraction, but both can describe the possible isothermal kinetics of a MT, which is our objective. However, in the case of Ni–Ti–X alloy system, the factor α is almost independent of the temperature as compared with the much stronger temperature dependence of Z and Z' in the Ni–Mn–In–X system. Therefore, Z' would be approximately proportional to Z. Thus, even when R_{MAX} and R_{MIN} cannot be known and the resistance/impedance is non-monotonic, Z' gives indirect information about the martensite volume fraction since it is somewhat proportional to Z.

2.5 Preparation of samples

An ingot of the quaternary Ni–Mn–In–Co metamagnetic alloy was produced from 99.9% purity Ni and Co and 99.99% Mn and In by arc melting followed by several consecutive remeltings in order to homogenize the alloy composition. The samples were spark cut from the ingot and subjected to 24 h annealing at 1170 K in vacuum followed by water quenching.The samples were additionally annealed for 900 s at 1070 K in the air and water quenched to obtain a low degree of long-range $L2_1$ order or annealed for 900 s at 1070 K and cooled in air at room temperature.

Samples of binary Ni–Ti alloy were prepared from a commercial 40% cold-rolled $Ni_{50.2}Ti_{49.8}$ wire with a diameter of 3 mm obtained from @Medical Technologies N. V., Herk-de-Stad, Belgium. Pieces of wire with a length of around 25 mm were annealed for 30 minutes in Ar atmosphere at different temperatures of 620, 770 and 1070 K and quenched into water. Bar-shaped samples with dimensions appropriate for the electric impedance and internal friction measurements were spark-cut from the heat treated cylinders.

An ingot of ternary alloy $Ti_{50}Ni_{47.4}Fe_{2.6}$ was produced by arc melting. The ingot was remelted several times, annealed at 1270 K during 2 hours to homogenize its composition and quenched in water. The samples of appropriate dimensions were produced using a spark cutting machine.

A $Ti_{50.5}Ni_{49.5}$ ingot was prepared by arc-melting. The ingot was homogenized at 1470 K during 3600 s and cut using a diamond saw into samples. The samples were heat treated at 920 K during 1800 s and water quenched.

Samples of a commercial ternary alloy $Ti_{52.4}Ni_{39.7}Cu_{7.9}$ were annealed at 1120 K during 30 minutes and cooled in air.

Samples used for DC resistance or AC impedance measurements were bar shaped with dimensions close to $12 \cdot 2 \cdot 1$ mm^3. Examples of typical samples prepared for these experiments are showed in Figures 2.2 and 2.3.

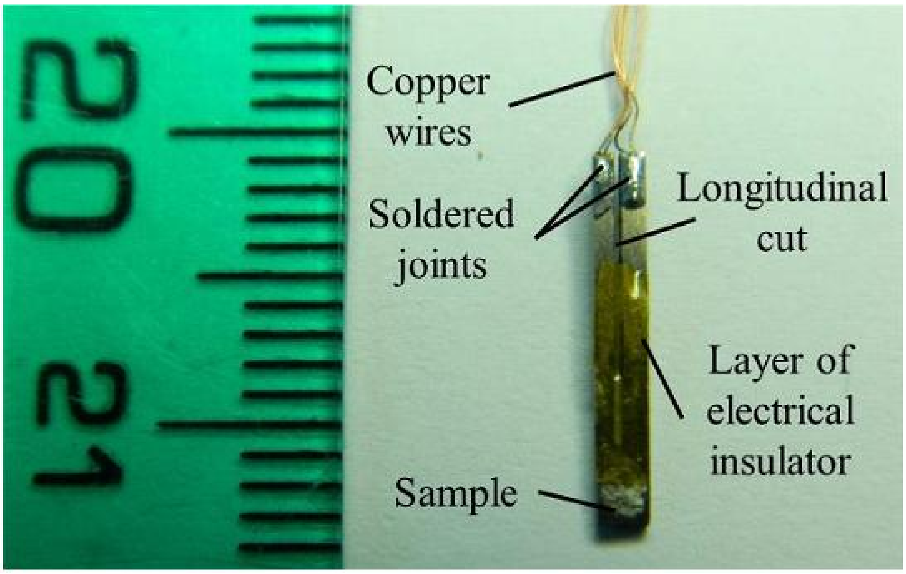

Figure 2.2: Typical U-shaped sample prepared for DC resistance measurements. The longitudinal cut permits to weld the four contacts to one side of the sample. One lateral surface of the sample is covered with a thin dielectric insulator layer above which a thermocouple is placed.

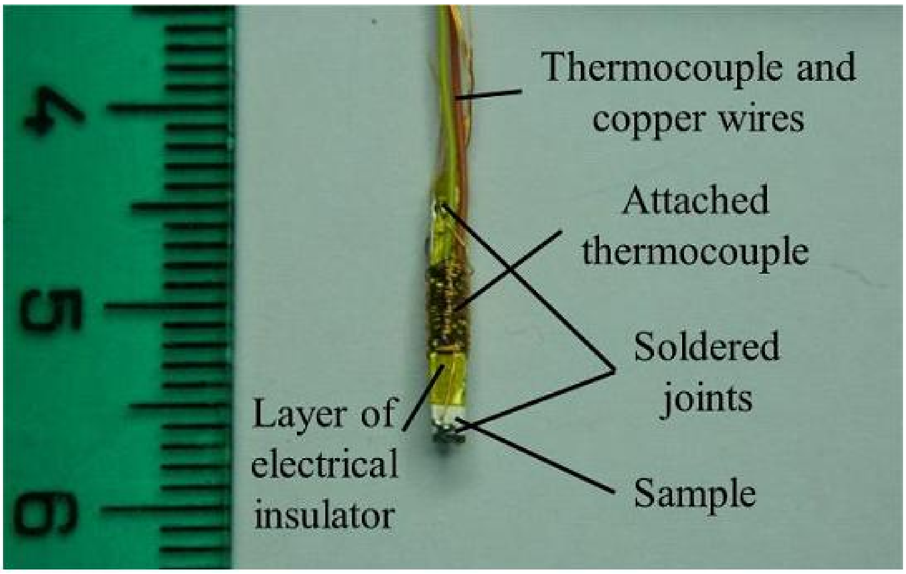

Figure 2.3: Typical sample prepared for AC impedance measurements with an attached thermocouple. The thermocouple is electrically insulated from the sample by a thin layer of an adhesive film and is placed in the center of the sample. The sample does not have a longitudinal cut and the contacts are welded to both sides of the sample.

The sample displayed on Figure 2.2 was prepared for DC resistance measurements. The sample was cut lengthways and is U-shaped. This permits to weld the copper wires to the same side of the sample which is divided in two because of the longitudinal cut. This shape eliminates the small temperature gradient between the welds, and avoids a contribution of the thermo-emf which might distort the measurement. In addition, it increases the resistance as the sample becomes longer and thinner, improving somewhat signal-to-noise ratio.

For AC impedance measurements the constant contributions to the signal are eliminated, including the contribution of the thermo-emf due to the temperature gradient between the welds, and then there is no need to make a longitudinal cut of the sample. This more simple configuration of the sample is shown on Figure 2.3. In contrast with the sample shown in Figure 2.2, the copper wires are now welded to both sides of the sample. Figure 2.3 also shows a thermocouple attached to the sample, this thermocouple measures and controls the temperature of the sample during the experiments. An electrical insulator layer is placed between the sample and the thermocouple to avoid electrical interferences.

Samples used for DSC experiments had dimensions close to $5 \cdot 2 \cdot 1$ mm^3.

2.6 Equipment and experimental procedures

2.6.1 Cooling-heating system

The cooling-heating facility employs cold/hot He gas, flashing free-standing samples with attached thermocouple. A schematic drawing in Figure 2.4 explains the principles of functioning of the cooling-heating system.

Samples with 4 welded wires were placed inside a thin quartz tube with an external diameter of 3 mm and joined (but properly electrically insulated) to a type K thermocouple, which is used to measure and control the temperature of the sample with a resolution of 0.01 K.

He gas is cooled/heated to control the sample temperature. First, He gas is cooled when it flows through a spiral heat exchange copper tube submerged into liquid N_2, represented by a loop in Figure 2.4. Afterwards, cold He gas is heated to the required temperature by a furnace mounted on a copper tube. The cold spiral heat exchanger and the furnace are mechanically connected using Teflon junctions in order to decouple thermally the cooling and heating parts of the gas circuit. Finally, He gas flows close to the sample inside the quartz tube placed immediately after the furnace in order to minimize the temperature difference between the furnace/spiral heat exchanger and the

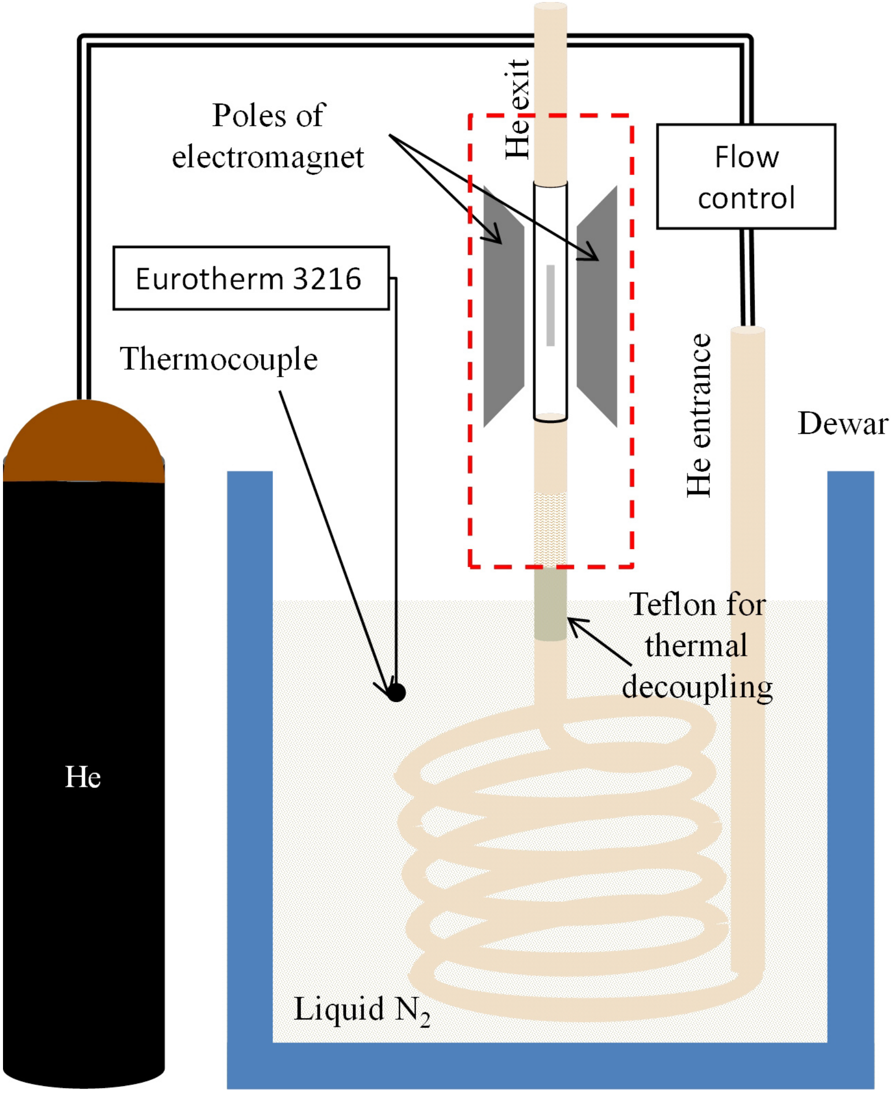

Figure 2.4: Block-diagram of the cooling-heating system. The furnace, the sample, the thermocouple and the quartz tube are shown on a dashed rectangle. This part is detailed in Figure 2.5 which also shows the electronic setup.

sample and also to reduce the time constant of the cooling/heating system.

Therefore, there are three parameters that affect the sample temperature, two of them are kept more or less static during the measurement and the third one is the control one. The first one is the flow level, which is adjusted by the pressure regulator of the helium tank and a flow controller placed before the cooling part of the gas circuit (see Figure 2.4). Generally, higher flow level means higher cooling power and the system can reach and hold lower temperatures, but the consumption of helium is higher.

The second one is the level of liquid N_2 contained in the Dewar. Liquid N_2 is introduced manually into the Dewar and a second type K thermocouple, which is in a fixed position inside the Dewar, gives vague information about the quantity of liquid N_2. Similarly to the previous mechanism, a higher level of liquid N_2 corresponds to a higher cooling power because of a larger section of the circuit is submerged into the liquid N_2.

The last one is the voltage supplied to the furnace, which is the dynamic parameter which controls the sample temperature by means of a programmable Eurotherm PID (Proportional-Integral-Derivative) controller model 3216, Figure 2.5. This third control system compensates possible minor/slow variations of the two previous parameters. Eurotherm controller reads the sample temperature from the thermocouple attached to the sample; compares the sample temperature with the target temperature and calculates the output power needed to achieve the target temperature. Then, Eurotherm controller adjusts the voltage submitted to the furnace by a SR-120 DC power supply. In addition, the controller also communicates with the PC with a Serial Bus RS232 connection so that PC can read and register the sample temperature data.

The temperature range in which the system can operate depends strongly on He flow level and liquid N_2 level. The absolute minimum and maximum are around 120 K and 400 K respectively, but both cannot be achieved under the same experimental conditions (He flow level and liquid N_2 level).

Optionally, the quartz tube can be placed between the poles of an electromagnet, Figure 2.6. The generated magnetic field for the value of gap necessary to place the quartz tube (about 5 mm) can reach 3 T. Rather small gap value compared to the poles diameter, 5 mm and 60 mm, respectively, guarantees good homogeneity of the magnetic field in the working space containing the sample. The electromagnet was used only in experiments with metamagnetic SMA. Measurements under applied polarizing field were performed in the DC mode. In this mode both ends of the sample, to which the contacts are welded, must have exactly the same temperature to avoid thermo-emf.

For example, for a typical potential difference across the sample of ~1

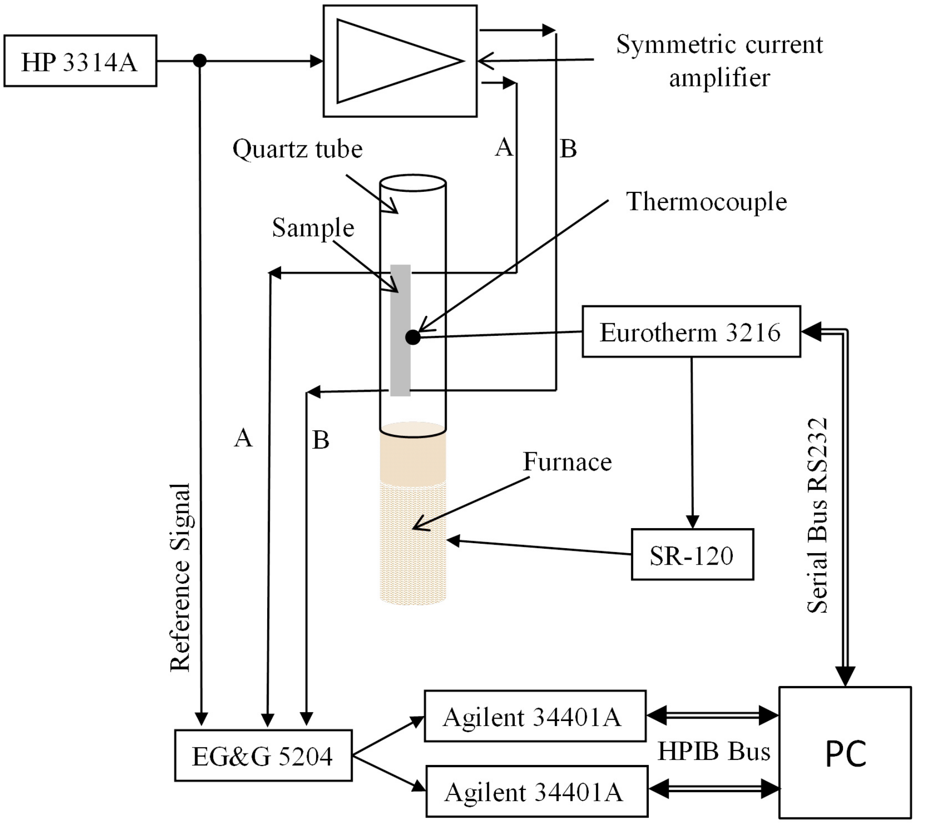

Figure 2.5: Electronic circuit for AC impedance measurements. Units which control the sample temperature and acquire data for temperature, real and imaginary part of the AC impedance are shown.

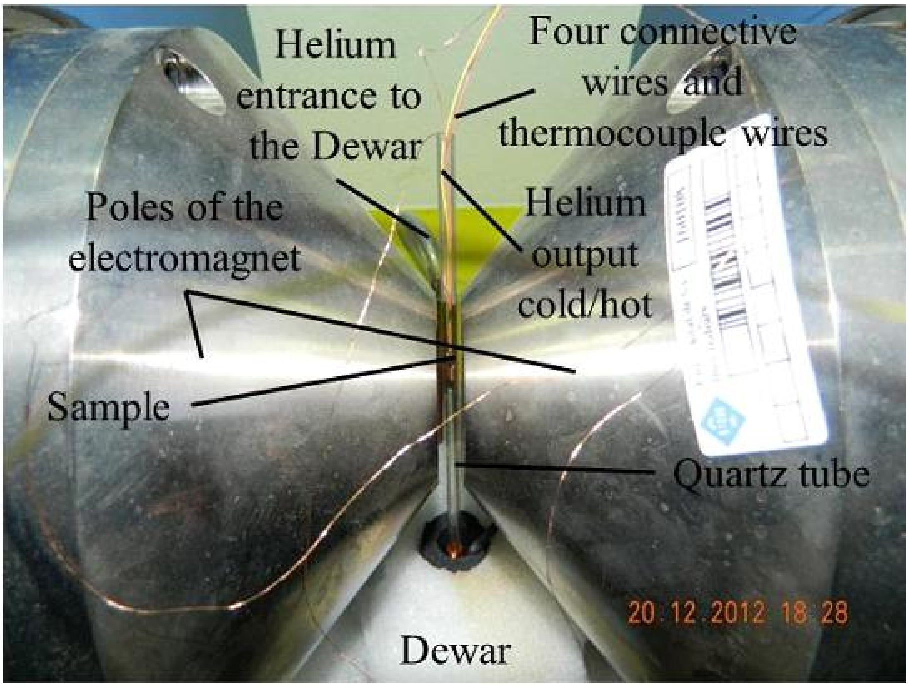

Figure 2.6: Set-up with the sample between the poles of the electromagnet. The Dewar, shown closed in the lower part of the figure, contains cooling and heating systems of the flowing helium gas. The sample is placed inside the quartz tube and is connected to the impedance measurement system by four thin wires. Another two wires that appear in the figure are chromel and alumel wires of the thermocouple.

mV, a voltage drop of only around 10 μV would correspond to a variation of martensite fraction of ~10^{-2}, which can be comparable with the isothermally accumulated martensite. The abovementioned voltage drop of 10 μV can correspond to the thermo-emf generated by temperature difference of only of the order of $10^{-1} - 10^{-2}$ K.

Since the sample is submerged into the He flux and is near the furnace, this system has very low thermal inertia and good temperature stability. These two features are crucial for isothermal holding experiments. The low thermal inertia of the system allowed us, first, to interrupt the cycle with a small overcooling/overheating, around few tenths of degree, and second, to keep constant the sample temperature with temperature fluctuations of less than 0.1 K.

An example of typical temperature versus time plot is shown in Figure 2.7.

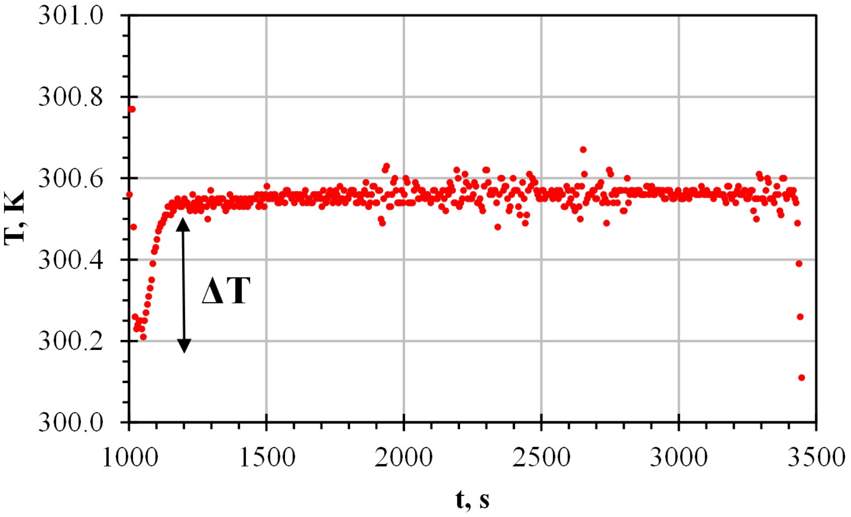

Figure 2.7: Example of the temperature evolution during an isothermal holding the sample in a cooling scan. An overcooling ΔT due to the thermal inertia of the system is shown. In addition, after the temperature is stabilized, small temperature instabilities are produced by non-controllable issues, like rapid irregularities of the helium flux.

Occasionally, a bigger thermal fluctuation could happen. If the fluctuation was big enough, it perturbed inevitably the experiment, producing a partial cycle. However, for the most part of the measurements, this did not happen; the stability was good enough to consider that registered kinetics was caused by isothermal phenomena. The typical time of isothermal holding in the present measurements was 2400 s.

2.6.2 Electronics

Figure 2.5 shows a diagram of the electronics used for AC impedance measurements. Eurotherm controller and SR-120 power supply used to control and obtain data of the sample temperature, as mentioned above. For AC measurements, the reference excitation signal, emitted by a function generator HP 3314A, is split into two current signals of opposite phases, A and B, by means of a symmetric current amplifier. These excitation current signals are applied to opposite sides of the sample to generate the voltage drop along it. The output impedance of the symmetric current amplifier is 1 kΩ, much higher than the rest of the circuit. This keeps constant the current intensity. In the present work, the current intensity was 6 mA$_{R}MS$.

The pickup signal is applied to the measuring circuit by means of remaining pair of copper wires. The signal is amplified and synchronously detected by a lock-in analyzer EG&G model 5204, Figure 2.8, providing the DC signals proportional to the real and imaginary parts of the sample impedance. These DC signals are read by two Agilent 34401A voltmeters to reach the maximum possible precision. The voltmeters are connected to the PC by means of a HPIB interface. So PC takes and saves data of time, temperature, real and imaginary parts of the impedance, and also calculates the modulus of the sample impedance.

The system is somewhat different for DC resistance measurements. HP 3314A function generator and symmetric amplifier are replaced by a HP 611A power supply and few series resistors and EG&G lock-in analyser and the two Agilent voltmeters are substituted by a HP 3457A voltmeter.

Series resistors have a large resistance, about 512 Ω, compared with the sample resistance and other possible small variations, like change of the wire resistance with temperature. Therefore the current intensity is kept constant at around 38 mA.

2.6.3 Control software

Data acquisition employed self-made software, based on Labview 7.0 package. This software allowed obtaining a high level of automation of experiments. For each iteration of pre-set time interval (typically 5s), the software acquired global experiment time, sample temperature, real and imaginary parts of the impedance for AC experiments or resistance for DC experiments. In addition,

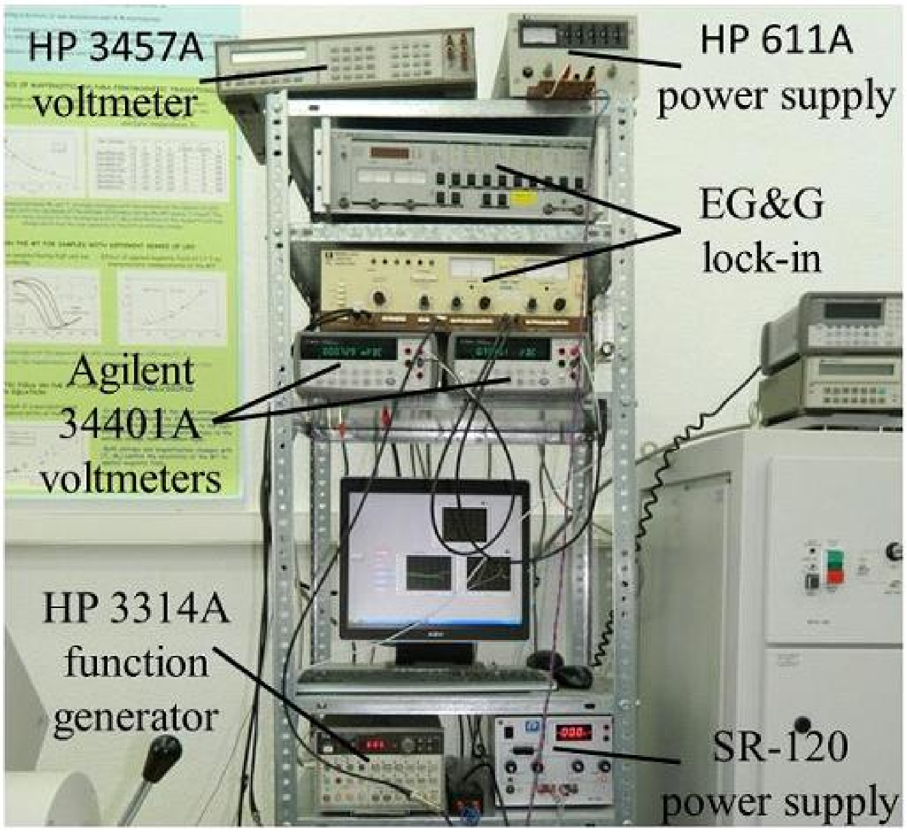

Figure 2.8: Electronics used to excite the sample and measure the sample resistance in DC mode or real and imaginary parts of the sample impedance in AC mode.

software also calculated the module of sample impedance and saved all these data in a file; one row for each iteration.

Control software read and configured the Agilent 34401A voltmeters (AC) or HP 3457A voltmeter (DC), but only used the Eurotherm 3216 module to read the data for temperature. That was because we found convenient not to program isothermal holdings by means of the Eurotherm 3216 module, but, rather to interrupt cooling/heating scans manually, depending on the actual results.

Temperature scans were programmed in the Eurotherm controller internal software. Four consecutive scans can be programmed ascribing the value for end temperature, temperature rate and holding time when the end temperature is achieved for each scan. Only four scans are insufficient to set an experiment with several isothermal holdings, but Eurotherm controller permits to interrupt and resume temperature scans. Therefore, usually only two steps, cooling and heating, were set and this cycle was manually interrupted and resumed to take isothermal data at the desired temperature.

EG&G lock-in, HP 3314A function generator and HP 611 A power supply were set manually depending on each experiment conditions. SR-120 power supply is controlled by the Eurotherm 3216 module.

2.7 Experimental protocols

2.7.1 Measurement of the DC resistance/AC impedance

Temperature dependence of DC resistance/AC impedance is registered in a temperature cycle with constant temperature scan rate of 2 K/min, see Figure 2.9 as an example. We may call it a continuous temperature cycle as opposed to the temperature cycles interrupted by isothermal holdings. As mentioned before, the system permits to perform temperature cycles between 120 K and 400 K, the range being wide enough to cover the typical transformation temperatures of the materials under study.

The resistance/impedance spectra tell us whether or not transformation is monotonic and serve to determine R_{MAX} and R_{MIN} (in the case of Ni–Mn–In type alloys) as is shown in Figure 2.1.

The continuous temperature cycle could be repeated to check its reproducibility with number of cycles. Since the isothermal holding experiments were performed in different cycles it was important that the resistance/impedance of the sample kept reasonably constant with the number of cycles. If not, it might hinder obtaining the temperature dependence of Z,

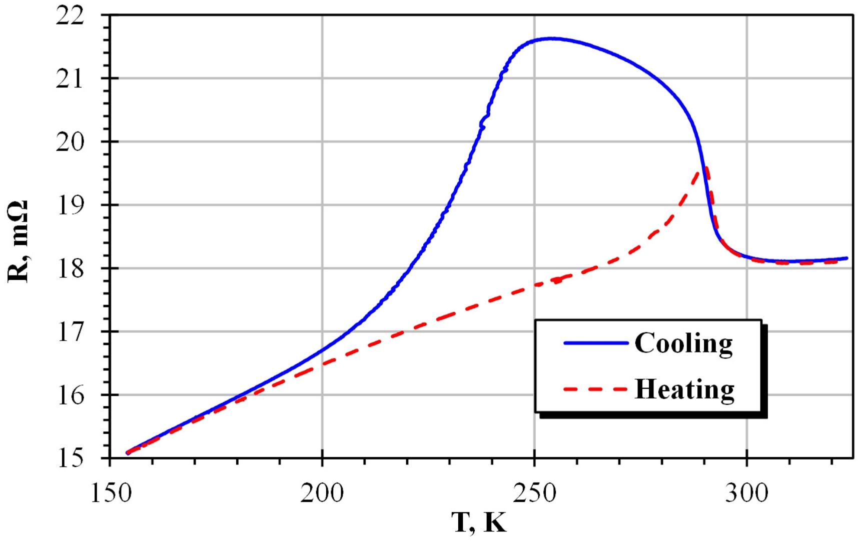

Figure 2.9: Temperature dependence of the real part of the impedance of a sample of $Ni_{50.2}Ti_{49.8}$ alloy heat treated at 770 K and quenched in water.

using data from different temperature cycles. Fortunately, this was not the case in the present work.

The summary of parameters used in experiments is shown below.

- DC resistance measurements: electric current: 38 mA, drive electric voltage: 20 V
- AC impedance measurements: frequency 686 Hz, electric current 6 mA_RMS, corresponding to approximately 3 V_RMS excitation signal in each shoulder (A and B) of the symmetric current amplifier, lock-in amplifier range: 100 or 250 μV depending on sample dimensions.

2.7.2 Measurement of the calorimetric signal

A differential scanning calorimeter Mettler Toledo DSC832 was used to characterize the MTs of the samples. Figure 2.10 shows a typical example of the DSC scan for the $Ni_{50.2}Ti_{49.8}$ alloy after annealing at 770 K and water quenching (the same heat treatment as was used for the sample whose resistance is shown in Figure 2.9). These data will not only give us information about the transformation temperatures but also yield the information about the martensitic volume fraction change rate, as prescribed by equation (2.27). So, the peak temperature will point to the maximum rate of martensitic volume fraction change.

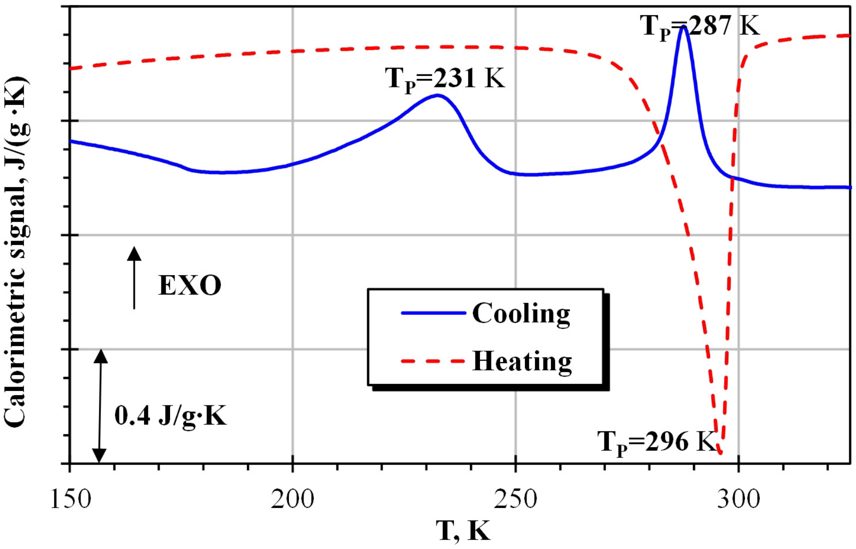

Figure 2.10: Calorimetric signal of a sample of $Ni_{50.2}Ti_{49.8}$ alloy heat treated at 770 K and quenched in water.

The following parameters were used in experiments:

- DSC measurements: temperature range: 140 K - 350 K, T-scan rate: 10 K/min.

2.7.3 Relative temperature variation rate of the DC resistance/AC impedance

The temperature derivative of resistance/impedance was calculated for continuous temperature cycles from the corresponding resistance and impedance data. Figure 2.11 shows an example calculated from data of Figure 2.9. As has been established in paragraph 2.3, the criteria of applicability of the equation (2.23) is the proportionality between the calorimetric signal and the relative temperature rate of the electrical resistance $\frac{1}{R}\frac{\partial R}{\partial T}$. Thus, to apply the algorithm provided by equation (2.23), the curves in Figures 2.11 and 2.10 should demonstrate sufficient similarity.

The relative temperature rate of resistance/impedance also helps to determine whether or not a MT is monotonic by comparing it to the temperature dependence of resistance/impedance. There should not be zeros of the relative temperature rate inside the transformation range.

As an example, the comparison of Figures 2.11 and 2.10 demonstrates a good correspondence between the calorimetric signal and $\frac{1}{R}\frac{\partial R}{\partial T}$.

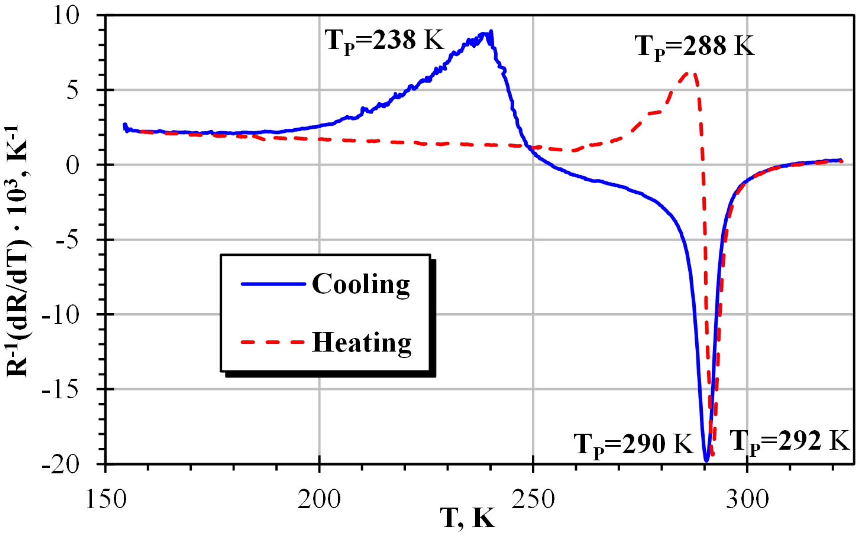

Figure 2.11: Temperature dependence of the relative temperature rate of the real part of the impedance of a sample of $Ni_{50.2}Ti_{49.8}$ alloy heat treated at 770 K and quenched in water.

2.7.4 Isothermal holding experiments

Classical isothermal holding experiments were carried out. Starting from temperatures above M_S, the sample were continuously cooled with a cooling rate of 2 K/min to a certain temperature at which cooling was interrupted and isothermal kinetics of DC resistance/AC impedance were registered during 2400 s. After this holding period, cooling was continued until new preset temperature selected for a new isothermal holding experiment was reached. These experimental steps were repeated down to the lowest temperature of interest. The same procedure was applied for experiments during heating (with also 2 K/min T-scan rate) which started from the temperature well below A_F.

There are two important possible problems with this methodology which may affect the reliability of the experiments if they are not taken into account properly. First, between the different stop temperatures there must be enough time to allow the sample to recover the continuous temperature cycle behavior. This way the isothermal experiments are not affected by the previous stop. The complete recovery is specially critical if isothermally accumulated resistance in the previous stop was large. Due to this requirement of a complete recovery of the cooling/heating trend after the isothermal exposures, the density of experiments in a single cycle is limited: it is insuffi-

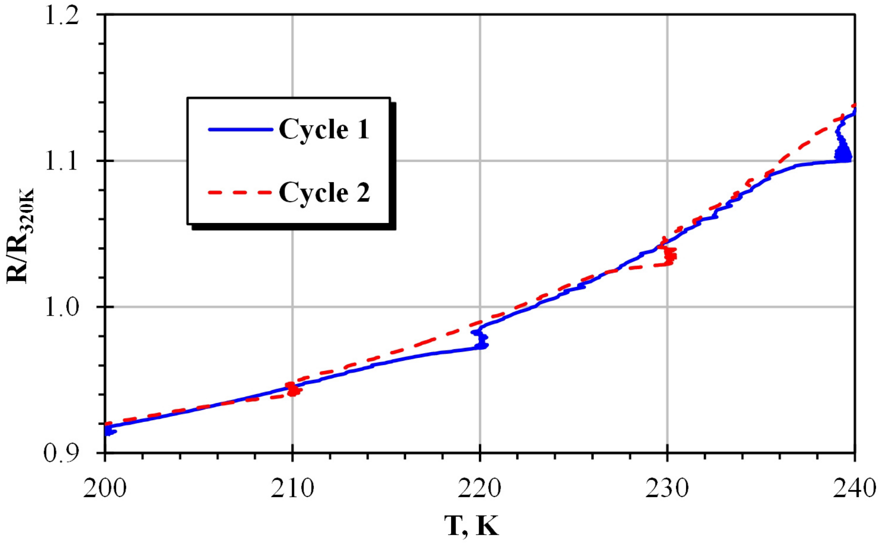

Figure 2.12: Real part of the impedance of the sample of $Ni_{50.2}Ti_{49.8}$ alloy heat treated at 770 K and quenched in water in two consecutive thermal cycles with interruptions of cooling.

cient to give a good overview of the isothermal/athermal behavior along the temperature axis. Consequently, several temperature cycles were needed to obtain a temperature dependence of the parameter Z with a good density of points. This connects with the second possible problem. In order to compare between isothermal holdings done in different runs, it is necessary a high reproducibility of the resistance cycle. This is a fundamental point that do not only will affect the quantification of the isothermal experiments, but call into question the origin of the isothermal accumulation of resistance. If a material depends strongly on the number of cycles, the isothermally accumulated resistance may not be due to the accumulation of austenite/martensite, but other effects like isothermal generation of crystalline defects or isothermal variation of the transformation temperatures. This is not the case for the present materials that exhibits the two stage B2↔R↔B19’ MT and will be treat in detail later.

As an example, Figure 2.12 shows a comparison between two series of experiments for a sample made of binary $Ni_{50.2}Ti_{49.8}$ alloy annealed at 770 K.The holding temperatures between 250 K and 180 K for the direct R→B19’ transformation were alternated. Figure 2.12 proves, first, the excellent reproducibility of the measurements and, second, a complete recovery of the continuous cycle after sufficiently high isothermal holdings. Such representation of experimental data also shows a noticeable variation of the resistance

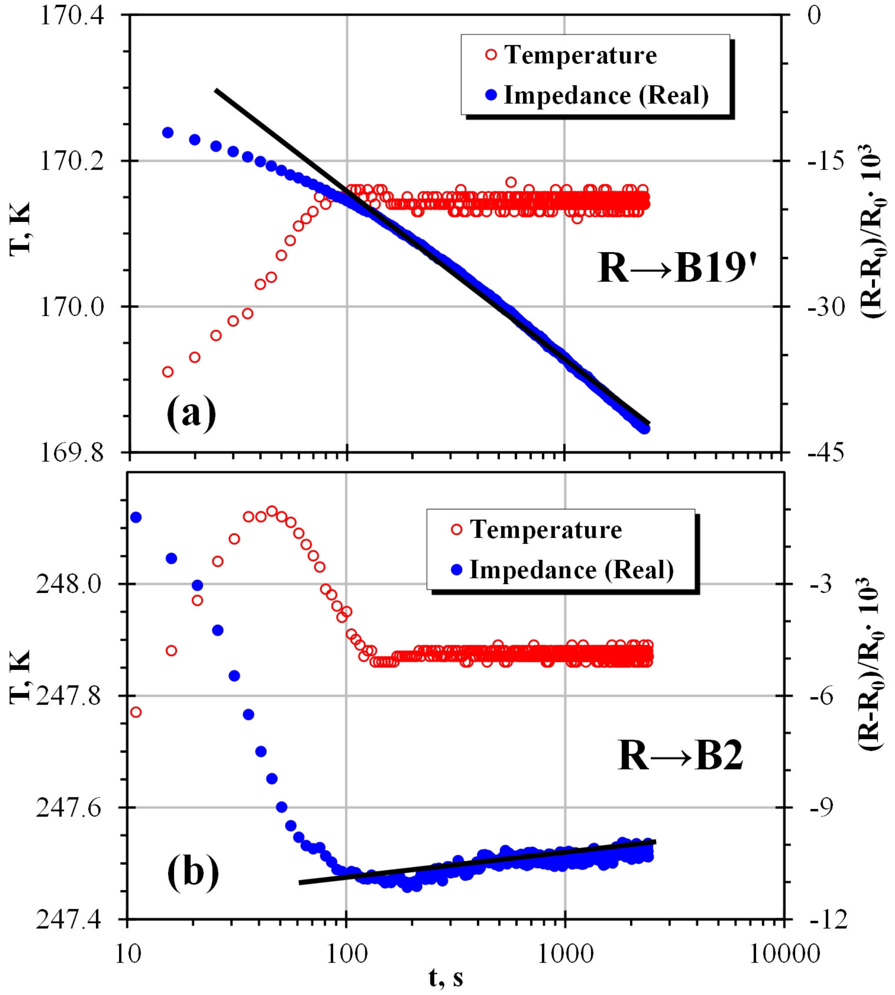

Figure 2.13: Temperature and normalized change of the real part of the impedance as function of the elapsed time since the moment of the interruption of the temperature cycle. The sample of $Ti_{50}Ni_{47.4}Fe_{2.6}$ was heat treated at 1270 K and quenched in water. Panel (a) corresponds to an isothermal holding during cooling (R→B19') which shows a prominent isothermal effect and panel (b) corresponds to an isothermal holding during heating (R→B2) without any clear isothermal effect.

during the stops; it is revealed as a drop of the resistance at constant temperature.

Isothermal kinetics can be conveniently represented as function of time elapsed after the temperature cycle interruption, Figure 2.13. Isothermal kinetics is shown to be straight on logarithmic scale of the local time. Then, it can be fitted by a logarithmic law, equation (2.31) or equation (2.32), and the Z parameter can be calculated.

Figure 2.13 also shows the temperature evolution during the isothermal stop in which two parts are well distinguished. First part is the overcooling/overheating produced just after interrupting the temperature cycle. It exceeds the set up temperature by only about 0.2-0.3 K because of the low thermal inertia of the cooling/heating system.

In the second part the temperature is very stable. The temperature takes around 100 seconds to get stabilized. The isothermal kinetics will be affected by this overcooling/overheating, for example, Figure 2.13b shows a large change of the impedance compared to its change when the temperature is stable. This is because the change during the overheating is mostly a change with temperature and not a change with time.

2.8 Mechanical Spectroscopy

2.8.1 Internal Friction

In all solids, the movement of a variety of point-like, linear or planar lattice defects is accompanied by the dissipation of elastic energy known as Internal Friction (IF). The spectrum of mechanical energy absorption is closely related to the microstructure of a solid, and then its study is an important tool to reveal meaningful characteristics of the alloy's microstructure. The mechanical spectroscopy investigates the spectra of elastic energy absorption under the conditions of applied periodic mechanical excitation [93]. This is a common technique used to investigate the SMAs since their most important functional properties (SME and SE) are directly controlled by the mobility os such structural elements as twin and interphase boundaries [94, 95].

Consider that, a periodic uniaxial stress

$$\sigma = \sigma_0 e^{j\omega t} \tag{2.36}$$

is applied to the sample, where j is $\sqrt{-1}$, σ_0 is the stress amplitude, ω is the angular frequency of oscillations and t is the time. The response of the material will be a periodic strain delayed in time because of the elastic energy loss:

$$\epsilon = \epsilon_0 e^{j(\omega t - \phi)} \tag{2.37}$$

where ϵ_0 is the maximum strain during the cycle and ϕ is the loss angle $(0 \leq \phi \leq \frac{\pi}{2})$.

The relation between the applied stress and strain is given by a complex modulus $E^*(\omega)$:

$$E^*(\omega) = \frac{\sigma}{\epsilon} = \frac{\sigma_0}{\epsilon_0} e^{i\phi} \tag{2.38}$$

Since $E^*(\omega)$ is a complex quantity, is can also be written as:

$$E^*(\omega) = E_1(\omega) + jE_2(\omega) \tag{2.39}$$

where E_1 and E_2 are known as the “storage modulus” and the “loss modulus”, respectively, due to its physical meaning. These parameters are related with the the total stored elastic energy in one cycle, W, and the energy dissipated per cycle, ΔW.

The maximum stored energy per unit volume during a cycle is:

$$W = \int_{\omega t=0}^{\frac{\pi}{2}} \sigma d\epsilon = \frac{1}{2} E_1 \epsilon_0^2 \tag{2.40}$$

Similarly, the energy loss per cycle per unit volume is the area contained by the hysteretic loop in the $\epsilon - \sigma$ plane:

$$\Delta W = \oint \sigma d\epsilon = \pi E_2 \epsilon_0^2 \tag{2.41}$$

Combining equations (2.40) and (2.41), one obtains the fraction of energy which is lost per cycle. In addition, one can express it as function of the loss angles using the equations (2.38), (2.39):

$$\frac{\Delta W}{W} = 2\pi \frac{E_2}{E_1} = 2\pi \tan\phi \tag{2.42}$$

Therefore, $\tan\phi$ gives a measure of the fractional energy loss per cycle due to anelastic behavior. Consequently, one may refer to $\tan\phi$ as the internal friction. However, there are other equivalent characteristics which may be used to represent the internal friction instead of $\tan\phi$. First, since the energy loss per cycle is, commonly, small as compared with the total stored energy, one can approximate $\tan\phi \approx \phi$. So, the loss angle ϕ can also be used as a synonym of internal friction.

On the other hand, since there is dissipation of the elastic energy of free oscillations, the amplitude of the oscillations will decay with time/number of cycles. There exist a relation between the rate of this decay and the fraction of energy dissipated per cycle, used to define the logarithmic decrement, δ:

$$\delta = \ln\frac{A_n}{A_{n+1}} = \frac{1}{2}\frac{\Delta W}{W} \tag{2.43}$$

where A_n is the amplitude after n cycles of free-decaying oscillations. δ is the IF measure referred to as logarithmic decrement of oscillations, which will be used in the present work. It is important to notice that there are several contributions to the internal friction, specifically, there are contributions which do not depend on the strain amplitude of the oscillations and the other that does depend. Then, the logarithmic decrement can be separated into the strain amplitude independent or linear IF, δ_i, and the strain amplitude dependent or non-linear IF, δ_h. These components are frequently denoted as AIIF and ADIF, respectively. Then, assuming their independence (additivity), one gets the total decrement as a sum of the AIIF and ADIF components [96]:

$$\delta(\epsilon_0) = \delta_i + \delta_h(\epsilon_0) \tag{2.44}$$

2.8.2 The piezoelectric ultrasonic composite oscillator technique

A Piezoelectric Ultrasonic Composite Oscillator Technique (PUCOT) was used in acoustic experiments to measure the internal friction and resonant frequency (and thus Young's modulus) of the samples. The setup, developed by Gremaud et al. [97] and Kustov et al. [98], is a modern realization of the classical method developed in the first half of the past century [99,100]. The PUCOT uses a piezoelectric quartz transducer to induce resonant oscillation in the sample.

There exists a broad variety of resonant systems which use magnetostrictive, capacitive, electromotive units, magnetic, eddy current transducers and the already mentioned piezoelectric ones [101, 102]. Among the piezoelectric systems, the quartz resonator composite oscillator technique has demonstrated many advantages over others due to its good temperature stability, linearity, precision, broad strain amplitude rage and relatively low background damping [100, 102].

The application of quartz resonators to measurements of elastic and anelastic properties of solids have been used extensively for decades, the first reports date back to the 20s of the past century [99]. Later on, Robinson et al. developed a detailed theory of the composite oscillator technique for longitudinal [103], torsional [104] and flexural [105] modes of oscillations. Kustov et al. [98] designed new electronics for the PUCOT system in order to achieve several substantial advantages:

- Adaptive measurement procedure, when the time-resolution depends upon current values of registered absorption of ultrasound.
- Automatic selection of an appropriate measurement range.
- Combined analog-digital control of drive voltage (strain amplitude), which substantially simplifies the electronics design.
- Resonant conditions for oscillations, checked and maintained at each measuring point quite rapidly owing to a procedure of polynomial fitting of the resonant curve.
- Wide application of highly integrated high-precision analog circuits instead of digital ones, resulting in simple and compact design.

Figure 2.14 shows schematically the assembled three-component oscillator and the block diagram of the electronics. The oscillator, in the left side of the Figure 2.14, is composed of the sample and two identical quartz transducers. The sample is glued to the transduces, forming thus a resonant system. The transducers are 18.5° X-cut α-quartz and have rectangular cross-section. Commonly, the sample also has parallelepiped shape with rectangular cross-section. However, this is not a mandatory condition. Other sample shapes, which keep constant the cross-section area, like the cylindrical shape, are acceptable. The quartz crystals are used to excite the oscillations and to pickup the strain amplitude signal. Thus, there are the drive quartz and the gauge one. The quartz crystals are plated with electrodes on two opposite sides and the electrical connections are in the center of the crystal in order to excite them with the fundamental/odd harmonics of longitudinal oscillations.

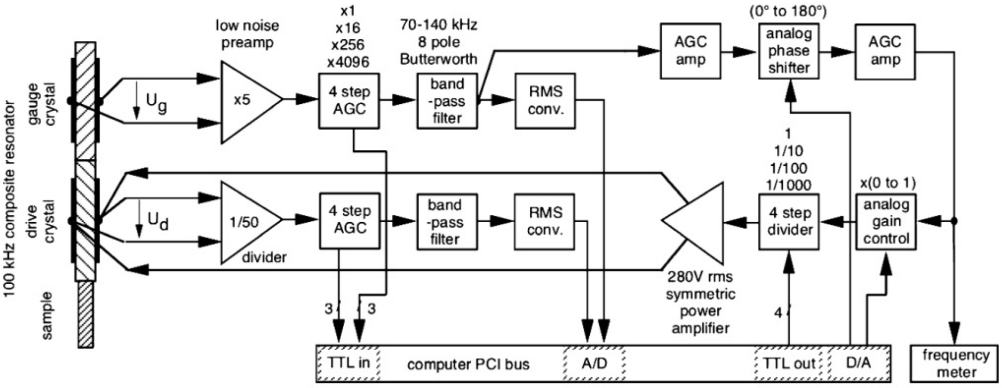

Figure 2.14: Schematic representation of the composite oscillator and the electronic circuit [98].

The quartz crystals and the specimen are cemented together at their ends, and the assembly is driven by an AC voltage U_d applied to the drive component. The voltage across the gauge component, U_g, is used to monitor the induced oscillatory strain and to maintain continuous resonant oscillations via a positive feedback loop. The angular resonant frequency, ω of the specimen depends on its length and should be similar to the resonant frequency of the quartz crystals. Therefore, for example, for the quartz transducer with a resonant frequency of 91 kHz, the length of the sample is chosen to keep the resonant frequency of the specimen within a range of 80–100 kHz during the experiments.

In operation, the system is driven by the U_d voltage and data for the resonant frequency of the full oscillator and the U_g are obtained. For longitudinal oscillations, the expressions for the total decrement of the composite oscillator, $\delta(t)$, and peak value of the strain amplitude of its ith element (normally, these elements are: sample, drive quartz and gauge quartz), $\epsilon_{11}^{max}(i)$, in terms of the parameters U_d, U_g and $\omega(t)$, have been obtained by Robinson and Edgar [103]:

$$\delta(t) = \frac{8\pi Z_m}{\omega(t)m(t)} \left(\frac{l_2 d_{311}}{S_{1111}}\right)^2 \frac{U_d}{U_g} = K_\delta \frac{U_d}{U_g} \tag{2.45}$$

$$\epsilon_{11}^{max}(i)\lambda(i) = \frac{\sqrt{2}\pi}{j\omega(i)} \frac{S_{1111}}{l_2 d_{311}} \frac{U_g}{Z_m} = K_\epsilon U_g \tag{2.46}$$

which bring out other intrinsic parameters of the system that should be known. Z_m is the electrical impedance across the gauge quartz (including connecting cables and input impedance of the measuring circuit), $\lambda(i)$ and $\omega(i)$ are the wavelength of the longitudinal wave and the angular resonant frequency in component i (being $\omega(t) \approx \omega(i)$), $m(t)$ is the total mass of the oscillator, S_{1111} and d_{311} are the elastic compliance and the piezoelectric modulus of the transducers, l_2 is the width of the plated side of the transducer and, finally, j is $\sqrt{-1}$. Equations 2.45 and 2.46 indicate that the logarithmic decrement and the strain amplitude of oscillations are simply determined from the two electric voltages across the quartz transducers. It is desirable that the electrical impedance of the measuring circuit is completely resistive or completely capacitive. One should choose between both possibilities which have their advantages and disadvantages [103, 106]. The present PUCOT system has resistive electrical impedance with negligible capacitive component.

The damping and the angular resonant frequency of the specimen can be determined from that of the total oscillator (provided that the mass, the resonant frequency and the damping of quartz transducers are known) using the following equations [103]:

$$m(t)\omega(t)^2 = \sum_i m(i)\omega(i)^2 \tag{2.47}$$

$$m(t)\delta(t) = \sum_i m(i)\delta(i) \tag{2.48}$$

where $m(i)$, $\omega(i)$ and $\delta(i)$ are the mass, the resonant frequency and the damping of the ith component of the oscillator, respectively. $\delta(i)$ of high-quality transducers is usually substantially lower than that of the specimen, therefore the logarithmic decrement $\delta(i)$ of the specimen can be derived with high precision from the measured total damping of the oscillator.

The Youngs modulus of the sample is conventionally determined from the fundamental angular frequency of longitudinal oscillations of a rod-shaped sample:

$$E = \frac{\rho\omega(s)^2 l(s)^2}{\pi^2} \tag{2.49}$$

where ρ, $\omega(s)$ and $l(s)$ are the density, the resonant angular frequency and the length of the sample.

Summarizing, measurements of the decrement, oscillatory strain amplitude and Young's modulus of the sample are reduced to measurements of two electrical voltages and the resonant frequency of the oscillator:

- The coefficients K_δ and K_ϵ, equations (2.45) and (2.46), depend on the known parameters: the geometry of the transducers, fundamental characteristics of quartz crystals and the electrical impedance Z_m of the measuring circuit. So these parameters can be included in the calculations performed by the automatized measuring system.

- The total decrement $\delta(i)$ and the strain amplitude of the ith element are easily determined from equations (2.45) and (2.46).

- The relation between the total decrement/resonant frequency of the oscillator and the ones of each element depend on their masses, as is indicated by equations (2.47) and (2.48). These calculations are rather simple since the decrement and the angular resonant frequency of the quartz crystal is nearly constant with temperature, strain amplitude and frequency.

- Finally, there is a direct relation, equation (2.49), between the resonant frequency of the specimen and its Young's modulus.

The electronics, schematically shown in Figure 2.14, are controlled via a general-purpose data acquisition PCI card. The electronic circuitry performs two basic functions: (i) maintaining resonant conditions over a wide range of oscillatory strain amplitudes and (ii) conditioning U_d and U_g signals. Therefore, the setup includes two similar channels, one for the U_g signal, seen in the upper part of Figure 2.14, and the channel for the U_d signal shown below. Both channels use symmetrical input circuits to minimize the electric pickup between drive and gauge voltage signals. This is especially important for high damping values when the U_d/U_g ratio becomes high (see Equation (2.45)) since this ratio may reach values of the order of 10^3.

The U_g channel forms a part of the positive feedback loop. Apart from the symmetric preamplifier/divider connected directly to the quartz crystals, each measuring channel includes:

- A line of three digitally-controlled amplifiers, which is controlled by a circuitry for automatic range selection (four-step automatic gain control units, AGC).

- A one-chip hybrid eight-pole octave Butterworth filter with the center frequency of 100 kHz to improve signal-to-noise ratio and thus to increase the dynamic range of measurements.

- A highly linear integrated RMS converter.

The digital part of each measuring channel contains three Transistor-Transistor Logic (TTL) lines (inputs of subrange status) and one A/D converter (for acquisition of the analogue voltage of RMS value of the U_d (U_g) signal).

Key elements of the positive feedback loop are the automatic gain control amplifier and phase-shifter units. The AGC amplifier provides a constant AC voltage at the output, independent of the gauge voltage across the transducer, which serves afterwards in control of the drive voltage level, U_d. The analog phase-shifter is used to control the overall phase shift in the positive feedback loop and, thus, to maintain the oscillator at resonance. The latter condition corresponds to a purely resistive impedance of the entire electromechanical circuit (including drive and gauge components and measuring circuit) and, hence, to a maximum voltage across the gauge quartz transducer. The phase of the feedback loop is controlled by one analog line. Before each measurement, the resonant condition (i.e. the maximum response signal) is verified and maintained.

To minimize the time for this procedure, the following algorithm is adopted. Initially and only once, before a measurement is started, the “global search” of the resonance is performed with 1000 steps over the total phase shift range from 0 to π rad. The conditions of resonance are obtained from the maximum of the strain amplitude signal and the system starts the measurement with the sample at resonance. During the experiment, the measuring conditions, like the temperature or the applied magnetic field, may vary, causing the variation of the conditions of resonance. Therefore, it is necessary to find the proper conditions of resonance before acquisition of each data point. Instead of performing a new “global search” of the resonance, only a “fine tuning” procedure is performed in the close proximity to the actual resonant conditions. In this procedure, only a few points of the resonant curve, which are close to the previous maximum value, are measured (typically, five points are sufficient). Afterwards, the position of the maximum response is found from a polynomial fitting to these few points. The “fine tuning” procedure is repeated, if necessary, until the resonant maximum is close to the middle of the tuning range and only afterwards a measurement of the decrement and the resonant frequency is carried out. This “fine tuning” procedure minimizes the tuning time as compared to the “global search” one.

An essential ingredient of the entire system is the drive voltage control circuitry, which includes a digitally-controlled four-step resistive divider and an analog gain control module based on a high-precision analog multiplier. These are key elements which control the drive voltage level and, thus, the oscillatory strain amplitude over the range exceeding 80 dB with a resolution of better than 0.5%. The last number gives an estimate of the strain amplitude resolution, when the strain amplitude should be controlled or, as a particular case, kept constant. In a single measurement of the strain amplitude dependence close to 100 kHz, the setup controls the excitation voltage in the range from ∼20 mV to 280 V_{RMS}. For a typical mass ($m \sim 0.5$ g) and damping of a specimen (Q^{-1} from 10^{-4} to 10^{-2}) these values ensure oscillations with strain amplitudes ranging typically from 10^{-7} to $2 \cdot 10^{-4}$, sufficient usually for the majority of materials science problems.

In total, there are four analogical lines (two D/A channels and two A/D) and ten digital lines (TTL). Therefore, as was previously commented, the system can be controlled via a single general-purpose data acquisition National Instruments PCI-6013 card, which is schematically shown in the bottom part of the Figure 2.14. Then, the circuitry of the actual PUCOT design is composed mainly by analog integrated circuits with analog control making it simple, compact and reliable. This have notable advantages as compared with previous designs based on digital control [97].

The lower limit for strain amplitudes of the setup is restricted by the noise level of the output power amplifier. The gauge signal, U_g, contains less noise since it is picked up from the quartz transducer and this procedure is equivalent to rather narrow band filtering of the drive voltage, U_d. In the present setup, the output noise of the amplifier (with the open positive feedback loop) is compensated in the software, assuming that this noise is not correlated with the useful signal. The upper limit of the strain amplitudes is determined either by the mechanical strength of the quartz transducers (for the case of low total damping), or by the maximum drive voltage provided by the power amplifier (for the case of high damping). According to Robinson and Edgar [103], the practical range of strain amplitudes can be extended from 10^{-12} to $5 \cdot 10^{-4}$.

The temporal resolution of the equipment is another key feature. In the present PUCOT, the temporal resolution depends on the current values of measured damping of the oscillator (specimen). In the composite oscillator technique, for not too high values of damping, the properties of the oscillator limit the temporal resolution, because each step-like change of the drive voltage leads to a transient in the time dependence of strain amplitude. If the step is small and the change of the decrement during this transient is neglected, the time constant τ_Q of the transient is simply given as $\tau_Q = T_{OSC}/(\pi Q^{-1}(t))$, where T_{OSC} is the period of oscillation. Thus, the higher is the damping, the faster can the measurements be performed. This adaptive feature of the equipment is especially important if the decrement values change orders of magnitude during measurements and if the decrement is time-dependent.

The functions of the PUCOT that are automatized (configuration and manage of the measurements, data acquisition) are computer-controlled by means of self-made programs based on Labview software, like for the resistance/impedance measurements. The set of programs, which are specialized in different kind of experiments, permits to register different dependencies (on temperature, strain amplitude or applied magnetic field) of different variables, like the decrement or resonant frequency. In this set of programs, there is one that permits to perform simultaneous measurements of temperature spectra of the decrement and Young's modulus for two values of strain amplitudes and of the strain amplitude dependence of the same parameters during single heating/cooling scan. This mode is specially useful since the stabilized strain amplitudes of the experiment can be selected to fall within strain-amplitude-independent and strain-amplitude-dependent ranges, so both linear and non-linear components of damping can be investigated at the same time. At each step of these measurements, a cycle of three measurements is performed: first, the low strain amplitude is stabilized and the data is acquired, second, the same procedure is repeated for the high strain amplitude, and third, the low strain amplitude is stabilized again and a third set of data points is registered. The values for the low strain amplitude are an average between the first and the third measurements. In this way, and since the measurements are quick enough in comparison with the temperature scan rate, one can assume that the data for low and high strain amplitudes were registered at the same temperature. Therefore, the temperature spectrum registered for the low strain amplitude value can be defined as the strain-Amplitude-Independent component of the Internal Friction (AIIF) whereas the difference between the spectra for the high and low strain amplitudes is the strain-Amplitude-Dependent part of the Internal Friction (ADIF). Similar procedure is used in measurements of the Young's modulus for low and high strain amplitudes, yielding temperature spectra of the strain-amplitude-independent Young's modulus and the amplitude-dependent modulus defect.

In addition to the temperature spectra measurements, other important mode permits the measurement of the strain amplitude dependence of decrement and modulus defect at any temperature, interrupting the temperature spectra measurement. The time to measure the strain amplitude dependence (containing about 100 experimental points) is rather short, typically about 1 min, which corresponds to the temperature variation for typical heating-cooling rates of only 1–2 K. This allows one to measure, in the majority of applications, the strain amplitude dependence at a certain temperature with a precision of about 1 K. After measurements of the strain amplitude dependence, the software returns to the registration of the temperature spectra.

During the strain amplitude dependence measurement, the drive voltage is first increased with a fixed step (10-20%) from the lowest strain amplitude to the highest one allowed for the experiment (direct run), and then it is decreased in the inverse sequence (reverse run). The direct and reverse runs can coincide, indicating thus a perfect stability of the defect system with respect to the ultrasonic excitation, or their equilibrium state. Otherwise, the direct and reverse runs may demonstrate certain strain amplitude hysteresis. The emergence of such hysteresis indicates, in its turn, that the state of the system of relevant defects/structural elements is affected by ultrasonic oscillations: it can be either excited to or relaxed from a non-equilibrium state.

Apart from the electronics which belongs to the PUCOT, displayed on Figure 2.14, the systems includes other devices which perform different additional functions. Some of these devices are employed in the control of the experimental variables like temperature, applied magnetic field or driving voltage.

The first variable is the symmetric AC signal U_d which should reach rather high values (up to 280 V_{RMS} at $\sim$ 100 kHz) to generate sufficiently high excitation strain amplitudes. The amplification of the output drive voltage is performed by means of a KRON-HITE 7602M wideband amplifier.

The temperature is another important variable. To measure and control the temperature of the composite oscillator, it is placed inside a “three-chamber” system. Each of these “chambers” is contained inside the larger one, like the Matryoshka dolls. The smallest chamber is a double-wall copper cylinder. A Ni–Cr bifilar winding is rolled around the outer surface of the inner cylinder. This bifilar winding is used to heat the chamber and utilize it as a furnace. The oscillator itself is situated inside the copper cylinder close to a temperature sensor (Pt-100 probe). The winding is fed by a HP 6002A power supply; the output current of which is controlled by the EUROTHERM 3216 controlled. The outer copper cylinder of this “sandwich” structure serves for better homogenization of temperature in the volume of the inner cylinder. The Pt-100 sensor is connected to an EUROTHERM 3216 controller. The temperature scans and isothermal stops are programmed in this EUROTHERM controller which manages the heating power of the furnace (as mentioned above) and allows for reading, with a resolution of 0.01 K, the actual temperature by means of a serial RS232 interface. The next chamber, a thin wall stainless steel, is used to keep the composite oscillator in a controlled atmosphere, normally of He gas. The atmosphere is pumped out of this volume bymeans of a OERLIKON LEYBOLD S1,5 pump and afterwards the volume of the stainless steel chamber is filled with pure He under pressure of 0.3 atm. Using pure He atmosphere guarantees the absence of condensation of gases on the surface of the oscillator and improves the heat exchange between the oscillator, the furnace and the cold surface of the stainless steel chamber. The third and last “chamber” is just an open

Dewar which, if necessary, is filled with liquid nitrogen to permit the system to cool down to temperatures close to 80 K. The upper limit for the working temperature is usually imposed by the glue between sample and drive quartz which will be damaged above 370 K.

In conclusion, the basic technical characteristics of the PUCOT are as follows:

- The frequency range 70–140 kHz (with the limitation that the resonant frequency should be relatively close, within (5-10%) to the one of the quartz transducers).
- The maximum strain amplitude typically is $2 \cdot 10^{-4}$.
- The noise level referring to quartz transducers is about $3 \cdot 10^{-9}$ for the strain amplitude channel.
- The maximum drive voltage 280 V_{RMS}.
- The noise level for the drive voltage channel is about 5 mV with the booster amplifier ON and 0.5 mV for the measuring channel alone.
- Working temperatures range cover the range from around liquid nitrogen temperature, 80 K, to about 370 K.

Chapter 3

Isothermal effects in complete diffusionless transformations

3.1 Results for the B2-R-B19' MT

The transformation between the trigonal R phase and the monoclinic B19' phase has been investigated as a part of the two-stage B2↔R↔B19' martensitic transformation. This transformation is exhibited by samples of cold-worked commercial wires of a near equiatomic binary $Ni_{50.2}Ti_{49.8}$ alloy annealed during 30 minutes at 620 K ot at 770 K and water quenched and by a sample of ternary $Ti_{50}Ni_{47.4}Fe_{2.6}$ alloy annealed during 1 hour at 1270 K followed by water quenching.

In the following, results and discussion on samples of Ni–Ti–X system, the real part of the electrical AC impedance is referred to as "resistance" to simplify the nomenclature. It was shown in section 2.2 (page 40) that the real part of the AC impedance and the DC resistance are numerically identical (see equations (2.14), (2.15), (2.17) and (2.19)) under certain condition, namely, the factor $\frac{a}{\delta}$ must be small, where a is the radius of a cylindrical ideal sample and δ is the skin depth. This condition is fulfilled in Ni–Ti–X alloys: being non-magnetic, the effective transverse magnetic permeability μ is very small, the skin depth δ is high (equation (2.16)) and the factor $\frac{a}{\delta}$ is small.

Figure 3.1 shows the temperature dependence of the resistance for several samples which exhibit the two stage B2↔R↔B19' martensitic transformation. In particular, in panel (a) the curves correspond to a sample of binary $Ni_{50.2}Ti_{49.8}$ annealed at 620 K , in panel (b), to a sample of binary $Ni_{50.2}Ti_{49.8}$ annealed at 770 K and, in panel (c), to a sample of ternary $Ti_{50}Ni_{47.4}Fe_{2.6}$ alloy quenched from 1270 K. The transformation temperatures for each transformation stage are indicated. Only one start and finish temperature is shown for the reverse transformations in panels (a) and (b). This is because the reverse B19'→R and R→B2 transformations are overlapped in the binary $Ni_{50.2}Ti_{49.8}$ alloys quenched from 620 K and 770 K. The reverse transformations are well defined for the ternary $Ti_{50}Ni_{47.4}Fe_{2.6}$ alloy since the transformations are displaced, specially the R↔B19' MT, toward lower temperatures as compared with the sample of binary Ni–Ti alloy quenched from 770 K. The variations of resistance during the MTs in the sample of binary Ni–Ti alloy annealed at 620 K are smaller than in the one annealed at 770 K. This is because the transformations in the first sample are more diffuse and, probably, not complete. It is important to recall here that the binary alloys were cold worked to 40 % before the heat treatment. Cold rolling of 40 % introduces amorphization and stabilizes the B2 phase in textured nanograins [69]. The posterior heat treatments partially recrystallize the amorphous parts of the sample and will generate different precipitates depending on the temperature of the anneal [69]. Therefore, the sample annealed at 620 K is more amorphous than the one heat treated at 770 K and a lower quantity of the material can undergo the martensitic transformation.

Figure 3.2 compares the temperature dependencies of the calorimetric signal and the relative temperature rate of the resistance of the binary Ni–Ti sample annealed at 620 K. In section 2.3 (page 42), it was shown that theses two variables ($\frac{\phi}{m\beta}$ and $\frac{\partial R}{\partial T}$) may be nearly proportional to the transformation rate in an uninterrupted temperature cycle $\frac{\partial F}{\partial T}$, equations (2.23) and (2.27). Therefore, there is a relation between the DSC signal $\frac{\phi}{m\beta}$ and the temperature rate of the resistance $\frac{\partial R}{\partial T}$ shown in equation (2.29). However, there are contributions that are ignored in equations (2.23) and (2.29) like the temperature dependence of the resistance due to phonon scattering. Then, it is important to compare these two parameters related to the transformation rate to estimate whether or not the variation of resistance is representative of the evolution of transformation.

The calorimetric signal $\frac{\phi}{m\beta}$ shows one peak on cooling at 303 K and two peaks on heating at 271 and 306 K. The single peak on cooling and the peak on heating at 306 K should correspond to the B2↔R MT which has a very small hysteresis even with a T-scan rate of 10 K/min. The other peak on heating, may be attributed to the reverse B19'→R transformation by comparison with the temperature rate of the resistance in panel (b). However, the corresponding peak on cooling of the direct transformation is missing. The relative temperature rate of the resistance shown in panel (b) indicates that the direct R→B19' MT has a peak temperature of 165 K, the transformation range is very broad (the transformation is diffuse) and M_F can

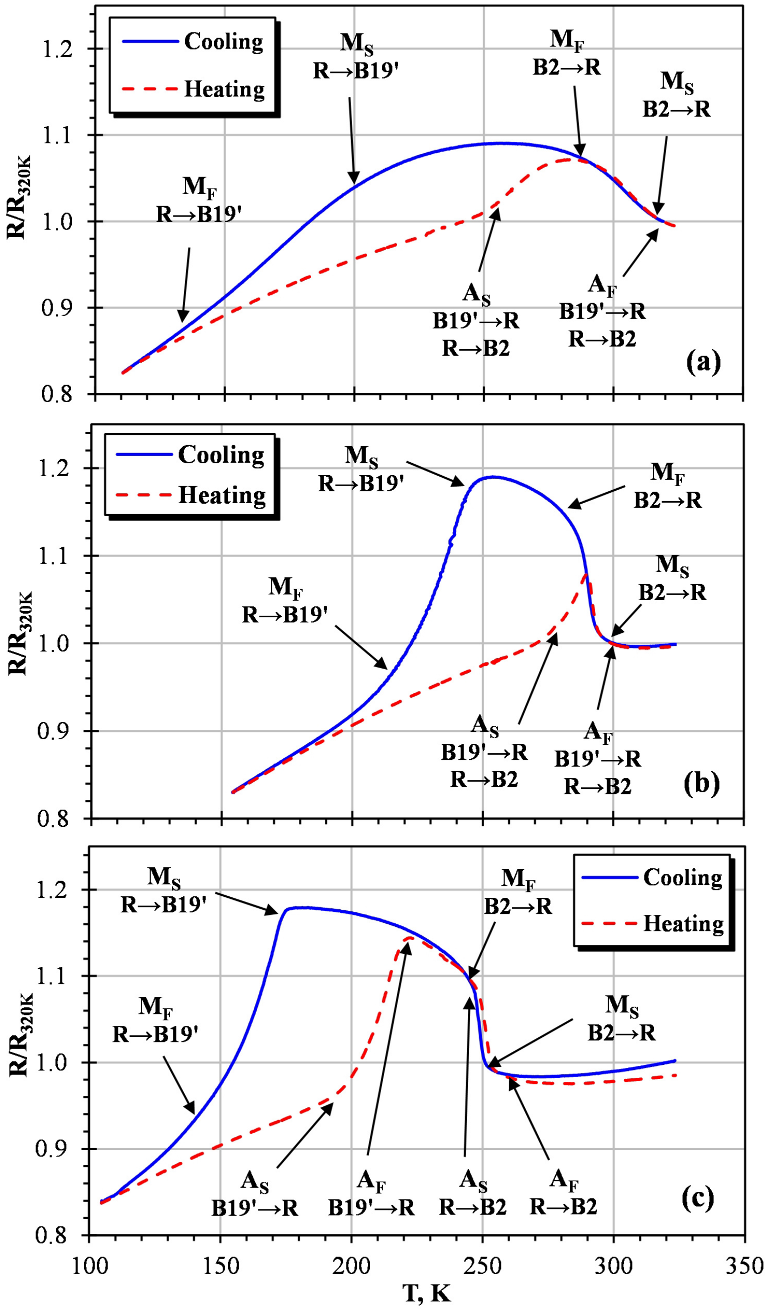

Figure 3.1: Temperature dependence of the resistance for samples of $Ni_{50.2}Ti_{49.8}$ cold worked and annealed at (a) 620 and (b) 770 K and (c) for a sample of $Ti_{50}Ni_{47.4}Fe_{2.6}$ quenched from 1270 K. Data are normalized to the value of resistance at 320 K. Measurements in an uninterrupted cycle with a cooling/heating rate of 2 K/min.

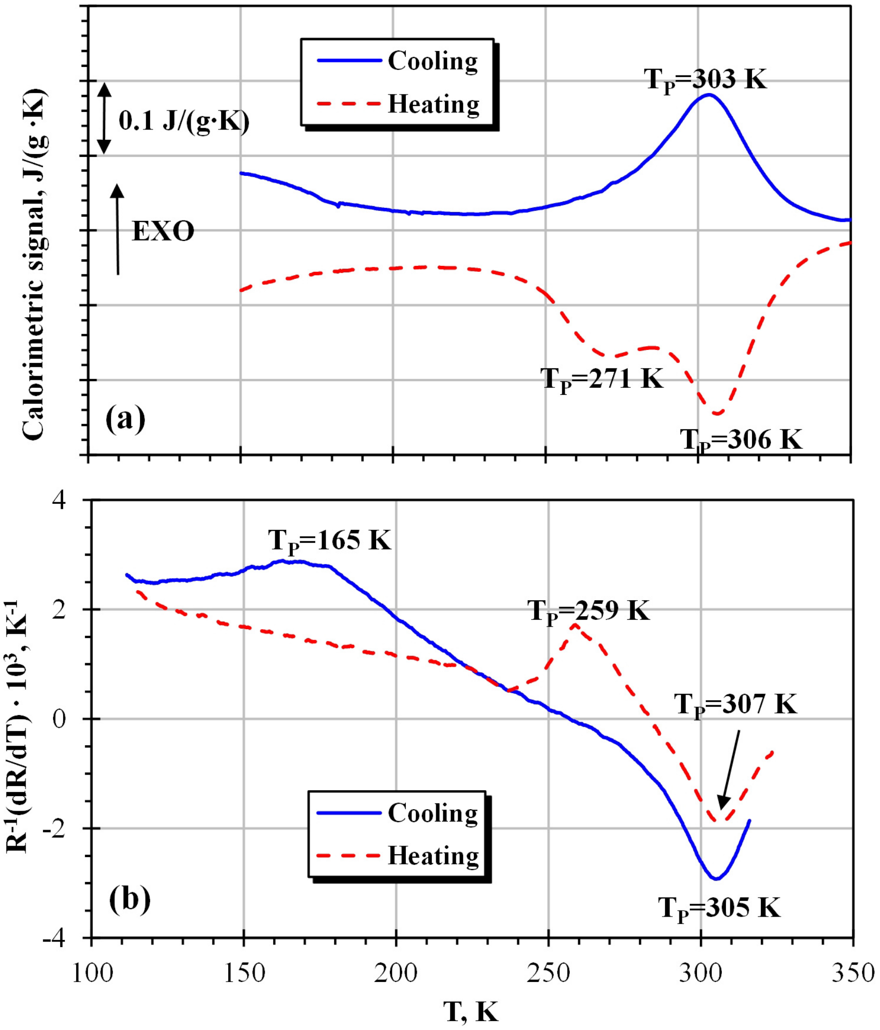

Figure 3.2: Temperature dependence of the calorimetric signal (a) and of the relative temperature rate of the resistance (b) for a sample of $Ni_{50.2}Ti_{49.8}$ alloy annealed at 620 K. The transformation peak temperatures are indicated.

be estimated as 135 K. These facts explain why this transformation is not detected in the calorimetric signal. First, the broad transformation implies a low peak in the DSC signal, that is, for broad enough transformation ranges, the transformation peak will be hardly identifiable. Second, although the DSC can reach temperatures down to 130 K, the effective lower limit of DSC scans is much higher since the DSC loses the control of the T-scan rate at certain temperature, which affects strongly the baseline. The effective lower limit depends on several technical factors of the DSC and is around 180 K. Therefore, below 180 K, the baseline varies its behavior complicating to distinguish the possible effects of a very broad peak. In conclusion, the DSC cannot give information of a very broad transformation with a transformation range contained below 180 K like the R→B19' MT in the sample of $\mathrm{Ni}_{50.2}\mathrm{Ti}_{49.8}$ alloy annealed at 620 K.

The relative temperature rate of the resistance exhibits two peaks on cooling at 165 and 305 K and two peaks on heating at 259 and 307 K. Taking into account both panels of the Figure 3.2, one notes that, similar to the R↔B19' MT, the B2↔R transformation range is also relatively broad for this heat treatment, around 50 K, between 275-325 K. On the other hand, as a consequence of the large hysteresis of the R↔B19' MT, around 85 K, the reverse transformations are slightly overlapped (this fact has been already mentioned previously, discussing Figure 3.1). This overlapping may affect the transformation peak temperatures. In fact, the peak temperatures of $\frac{\phi}{m\beta}$ and $\frac{1}{R}\frac{\partial R}{\partial T}$ are not expected to be the same: the equation (2.29) in page 45 is an approximation and even if it was exact, the term $C_S \frac{\partial \Delta T}{\partial t}$ introduces a delay with time to both parameters which shifts the peak temperatures. The magnitude of this shift depends on the T-scan rate of each experiment, β for the DSC experiment and β' for the resistance experiment. The typical values in the present work are 10 K/min for β and 2 K/min for β'. Therefore, the hysteresis of the transformation is expected to be higher in DSC measurements than in resistance ones with lower peak temperatures on cooling and higher on heating. Taking into account the above commented, the small differences in the transformation peak temperatures for the B2↔R MTs are not meaningful. Nevertheless, the difference of around 12 K in the peak temperatures of the reverse B19'→R MT is slightly above the typical temperature shift between DSC and resistance mesurements. This difference in temperature of around 12 K is attributed to the overlapping of the the B19'→R and R→B2 transformation peaks. If two peaks are overlapped, the “tail” of one peak may extend over the peak temperature of the other peak. Therefore, for each transformation, the observed peak is a superposition and its shape and peak temperature may vary with respect to the hypothetical peak generated by the contribution of a single transformation. In the case of the variables shown in Figure 3.2, the broad and diffuse peak of the reverse B19'→R transformation is affected by the close position of the sharp peak of the reverse R→B2 MT. In addition, the contribution of the R→B2 transformation generates opposite displacements of the B19'→R peak temperature in both signals, $\frac{\phi}{m\beta}$ and $\frac{1}{R}\frac{\partial R}{\partial T}$, leading to the difference in temperature of around 12 K above commented.

- In the calorimetric signal, both reverse transformations are endothermic, then the tail of the R→B2 MT is added to the B19'→R peak displacing the peak temperature of the last transformation toward higher temperatures.
- By contrast, the sign of the transformation peak in the relative temperature rate of the resistance depends on the resistance level of the phases and the direction of the temperature ramp. The signs of the $\frac{1}{R}\frac{\partial R}{\partial T}$ are opposite for the transformation peaks of the B19'→R and R→B2 MTs. Therefore, the tail of the R→B2 MT is subtracted to the B19'→R peak. Therefore, it displaces the peak temperature of the B19'→R MT toward lower temperatures.

Figure 3.3 compares the temperatures dependencies of the calorimetric signal $\frac{\phi}{m\beta}$ and the relative temperature rate of the resistance $\frac{1}{R}\frac{\partial R}{\partial T}$ of a sample of binary $Ni_{50.2}Ti_{49.8}$ alloy annealed at 770 K. The DSC signal exhibits two maxima on cooling at 232 and 288 K and a large endothermic peak on heating at 296 K. The peaks on cooling are assigned to the direct B2→R MT (288 K) and the R→B19' MT (232 K). The R→B19' MT has now much higher transformation temperatures as compared with the sample annealed at 620 K and is less diffuse, allowing this transformation to fall within the range of working temperatures of the calorimeter. The DSC measurements do not allow us to distinguish possible reverse B19'→R and R→B2 MTs, which are, likely, overlapped in a single peak centred around 296 K, without any shoulder and having a rather long low-temperature "tail". Based on the DSC data, one concludes that the reverse MT peak may corresponds either to the single stage B19'→B2 MT or to a very overlapped combination of the two stage B19'→R→B2 MT.

According to the data in panel (b), the $\frac{1}{R}\frac{\partial R}{\partial T}$ demonstrates two peaks on cooling at 239 and 290 K and two on heating at 287 and 292 K. The peaks on cooling clearly find their counterparts in the calorimetric signal on panel (a). Meanwhile, the peaks observed on heating clarify the situation with the calorimetric peak at 296 K. The signs of the relative temperature rate of the

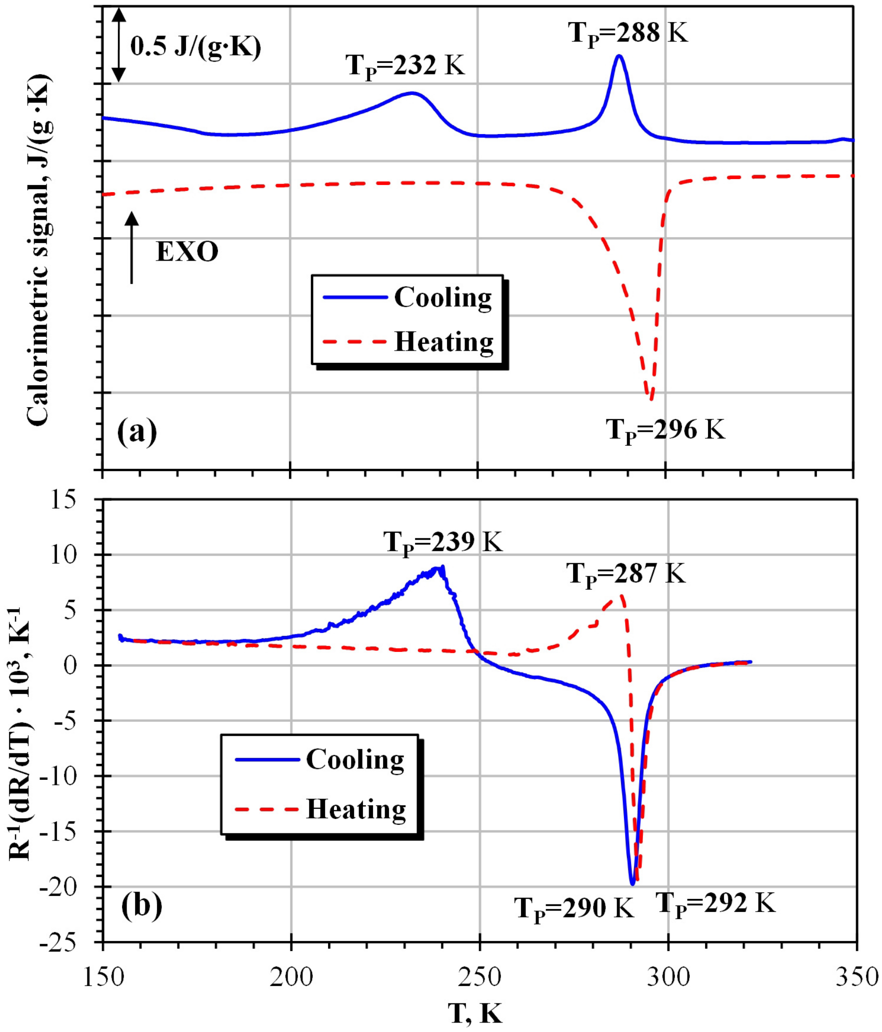

Figure 3.3: Temperature dependence of the calorimetric signal (a) and of the relative temperature rate of the resistance (b) for a sample of $Ni_{50.2}Ti_{49.8}$ alloy annealed at 770 K. The transformation peak temperatures are indicated.

resistance of the reverse B19'→R and the R→B2 MTs are opposite. This decouples the B19'→R and R→B2 MTs in the resistance data and indicates that the DSC peak on heating at 296 K, panel (a), is due to the two overlapped reverse MTs. Thus, during the reverse MT the two stage B19'→R→B2 MT and the single B19'→B2 MT may occur in parallel. It could be easier to understand the sequence of events during the reverse transformation if one compares the temperature dependence of the resistance on panel (b) and (c) of the Figure 3.1 where data for the binary alloy annealed at 770 K and the ternary Ni–Ti–Fe are shown. The curves for the binary alloy resemble the ones of the ternary alloy but somewhat "compressed" along the temperature axis. It is easy to identify in the reverse transformation in the Figure 3.1b two different parts that are joined by an abrupt maximum. These two parts behave exactly as the B19'→R and the R→B2 MTs in the data for the ternary alloy in Figure 3.1c. Therefore, as the temperature increases on heating, the B19' phase transforms to the R phase until the abrupt maximum is reached, then the B2 austenite becomes thermodynamically more stable than the R phase and the curve follows a normal path for the R→B2 MT. Since only part of the sample can transform to the R phase before reaching the abrupt maximum, after this point both reverse transformations, R→B2 and B19'→B2, may occur. The volume fraction of R phase is expected to be low during the transformation according to a relatively small increase of the resistance between A_S and the peak in Figure 3.1b as compared with the total change of resistance during a complete B19'→R MT in Figure 3.1c. Due to the overlapping and mixing of the reverse transformations, a direct relation cannot be established between the change of resistance and the martensite volume fraction on heating.

A comparison of the Figures 3.2 and 3.3 shows:

- The peak values of the $\frac{\phi}{m\beta}$ and the $\frac{1}{R}\frac{\partial R}{\partial T}$ are higher for the sample annealed at 770 K than for the one annealed at 620 K.
- The B2→R transformation temperatures are nearly the same for two different annealing temperatures. In contrast, the direct R→B19' transition is displaced towards higher temperatures by approximately 70 K after annealing at 770 K compared with annealing at 620 K.
- The R↔B19' transformation hysteresis is higher for the lower annealing temperature. Therefore, the difference between the temperatures of the reverse B19'→R transitions for samples annealed at 620 and 770 K is less than that of the direct R→B19' one.

These facts evidence that the transformations in the binary sample annealed at higher temperature are more completed, i. e., more lattice defects introduced by the cold-working were eliminated during the heat treatment.

Figure 3.4 shows the DSC scan and the temperature dependence of the relative temperature rate of the resistance for a sample of ternary $Ti_{50}Ni_{47.4}Fe_{2.6}$ alloy annealed at 1270 K and water quenched. In panel (a), the DSC signal exhibits two peaks at 250 and 165 K for the direct transformations B2→R and R→B19' and two peaks at 220 and 256 K for the reverse transformations B19'→R and R→B2, respectively. Similarly, the $\frac{1}{R}\frac{\partial R}{\partial T}$, in panel (b), shows four peaks in total, two on cooling at 169 and 213 K and two on heating at 213 and 251 K. The peak temperatures of all transformations are similar with the expected difference between the $\frac{\phi}{m\beta}$ and $\frac{1}{R}\frac{\partial R}{\partial T}$ curves: the transformations present a larger hysteresis in the DSC. There is no overlap of the reverse transformations for this alloy. The transformation ranges of the R↔B19' MTs are relatively broad, about 36 K on cooling and 32 K on heating, but their peaks are quite clear and not as diffuse as the MTs for the binary samples annealed at 620 and 770 K.

The effect of the direct R→B19' transformation is noticeably smaller in the DSC signal than for the reverse transformation. Several reasons for this difference can be mentioned:

1. The hysteresis of the R↔B19' MT is large, about 50 K, and then the temperature during the direct transformation is much lower than during the reverse one. If the entropy difference between the two phases is constant, this difference between the transformation temperatures will result in higher transformation heat for the reverse MT than for the direct one.

2. It should be noticed that the peak temperature of the direct R→B19' MT is below the temperature at which the DSC loses the control of the cooling ramp, about 180 K. Therefore, the peak of the direct transformation should be slightly distorted since the T-scan rate is not constant along the transformation range.

It is worth to note in Figure 3.1c that the resistance changes during the four transformations are high, much larger that the change due to other temperature dependencies of the resistance, like phonon scattering. In addition, the resistance do not present any maximum. Therefore, taking into account all these features, one can conclude that the resistance varies monotonously with the martensite volume fraction and that the sample of $Ti_{50}Ni_{47.4}Fe_{2.6}$ alloy quenched from 1270 K is very suitable to investigate the athermal/isothermal features of the B2↔R and R↔B19' MTs. In comparison with the binary alloys, their main drawbacks, like more diffuse transformations and

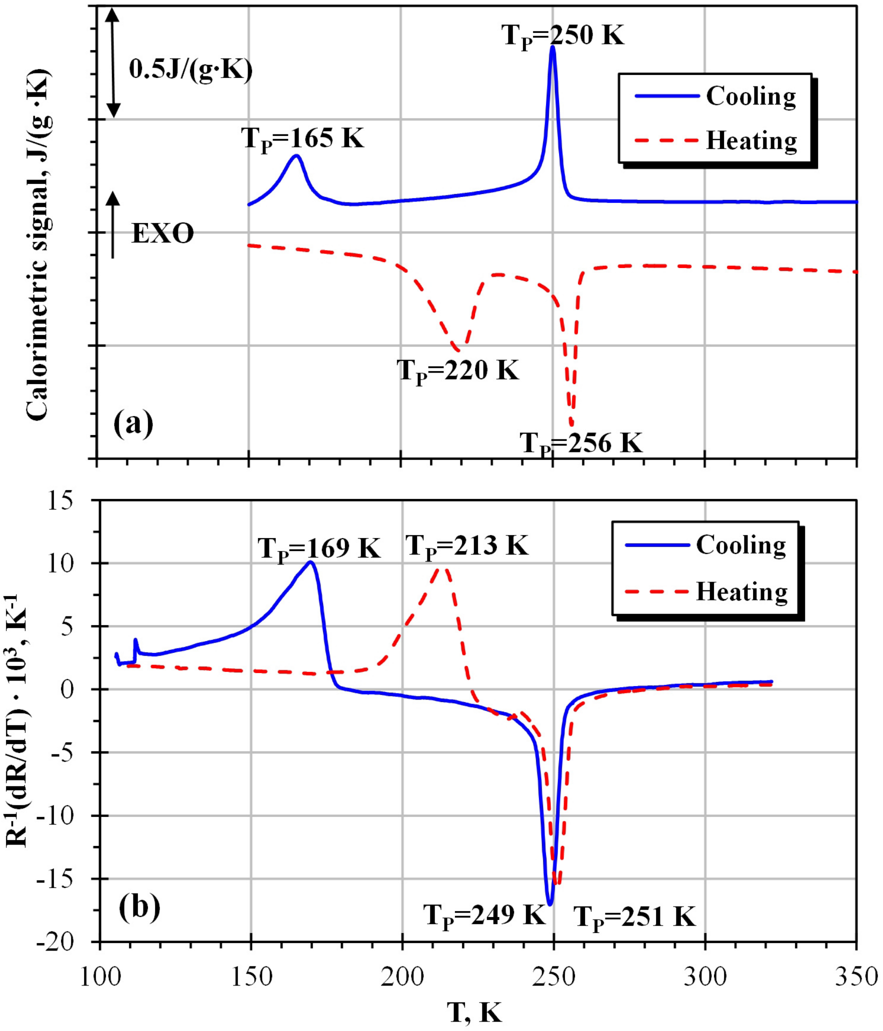

Figure 3.4: Temperature dependence of the calorimetric signal (a) and of the relative temperature rate of the resistance (b) for a sample of $Ti_{50}Ni_{47.4}Fe_{2.6}$ quenched from 1270 K. The transformation peak temperatures are indicated.

the reverse overlapped transformations, are absent in the Fe-containing alloy. For this reason, the athermal/isothermal behavior of the B2↔R↔B19' MT was investigated in the ternary alloy after the experiments with the binary alloys annealed at 620 and 770 K.

Summarizing, the data, shown in the Figure 3.1, taken as a whole, give reliable information of the evolution of the martensite volume fraction F tracked by means of resistivity experiments. Then, these alloys all were used to study the isothermal/athermal nature of all transformation paths of the two stage B2↔R↔B19' MT. In order to achieve this, the experimental protocol of isothermal stops at different temperatures were used.

Figure 3.5 presents a synthetic plot of the results of the isothermal holding experiments over the entire temperature range of the direct R→B19' MT. The figure is divided into three panels with the results corresponding to samples of the binary Ni–Ti alloy annealed at 620 K (a) and 770 K (b) and to the sample of the ternary Ti–Ni–Fe alloy heat treated at 1270 K (c). Before analysis and comparison of the results for the three samples, it is important to notice that the transformation temperatures are different for the three samples. The peak temperatures of the direct R→B19' MTs are 165 K, Figure 3.2, 239 K, Figure 3.3, and 169 K, Figure 3.4, respectively for the three types of samples mentioned. The curves depicted in panel (a) show some of the common features of the time evolution of the resistance during an isothermal martensitic transformation (IMT).

- The behavior of the isothermal kinetics of the resistance is well approximated by a logarithmic law. This was shown in section 2.4 (equation (2.31) in page 45). Therefore, the time-dependence of the resistance will follow a straight line when plotted on a logarithmic time axis, like in the Figure 3.5.

- The logarithmic law is not met during the firsts seconds of the isothermal holding, for about 100 seconds, the deviation being different for different samples and temperatures. This transitory effect may, at a first glance, be attributed to the properties of the logarithmic function. The logarithm diverges for short and long times and then the logarithmic kinetics of the resistance are inevitably approximations. However, the short-time transitory effect is, likely, an effect caused mainly by the overcooling/overheating produced during the interruption of the T-scan, as discussed in section 2.6.1, see Figure 2.7 in page 55. Despite a typical overshoot is only about or less than 0.2 K, the temperature may take about 100 seconds to stabilize at a setpoint. Therefore, since the resistance is also temperature-dependent, the overshoot is the main

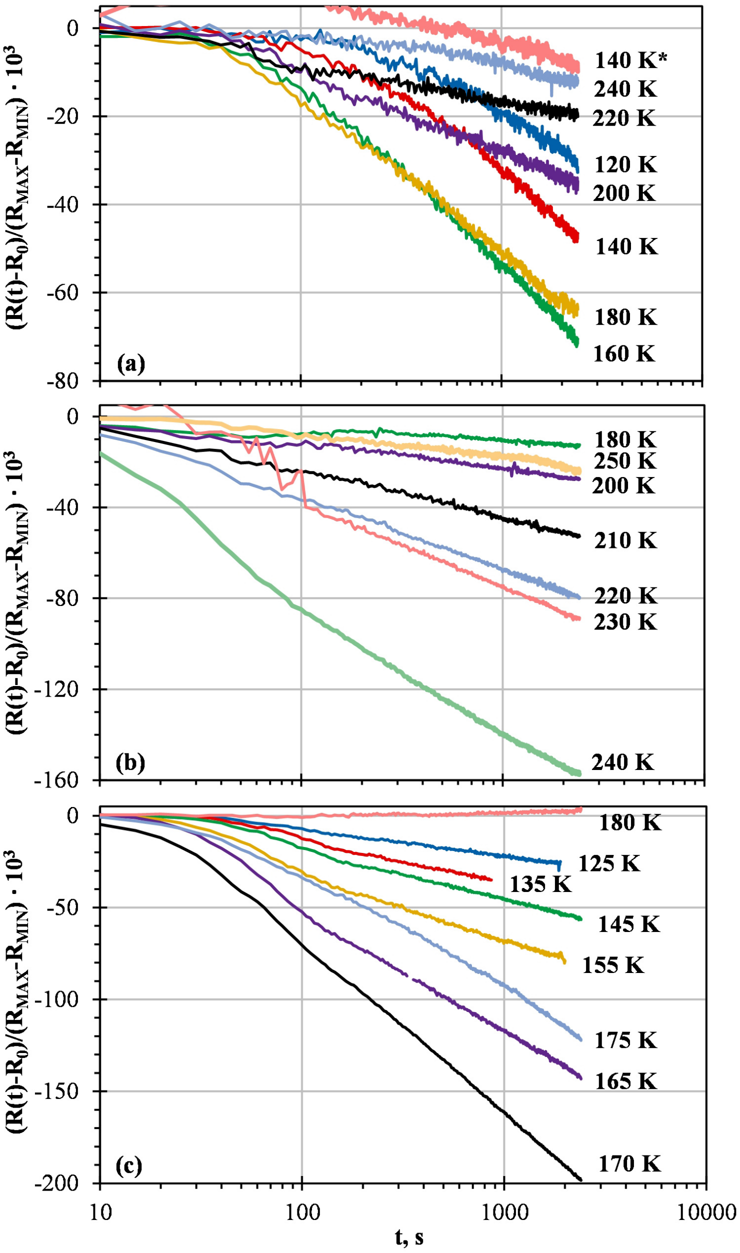

Figure 3.5: Time evolution of the resistance during interruptions of the temperature scan near and inside the direct R→B19’ transformation range for (a) a sample of binary $Ni_{50.2}Ti_{49.8}$ annealed at 620 K, (b) a sample of binary $Ni_{50.2}Ti_{49.8}$ alloy annealed at 770 K and (c) a sample of $Ti_{50}Ni_{47.4}Fe_{2.6}$ alloy annealed at 1270 K. The asterisk stands for an isothermal holding during heating. Note different ordinate scales in (a), (b) and (c).

contribution that produces the short-time transitory effect affecting the logarithmic kinetics. In addition, there is also a possibility of the existence of a certain “activation time” which delays the logarithmic behavior, see Section 5.2 in page 170.

- The variation of resistance with time $\frac{R(t)-R_0}{R_{MAX}-R_{MIN}}$ is maximum near the maximum of the DSC peak and/or the relative temperature rate of the resistance peak, in other words, near the maximum of the athermal transformation rate in an uninterrupted temperature cycle. On panel (a), which shows the results for a MT with a peak temperature at 165 K, the isothermal variation of resistance increases from the 240 K curve to the 160 K curve, where it attains a maximum speed, and then starts to decreases until the 120 K curve. This characteristic is shared by the other samples on panels (b) and (c) and for all the isothermal MTs in the Ni–Ti–X alloy system in general. However, as will be shown later, this is not necessarily the case for all isothermal MTs.

It should be mentioned that panel (a) also presents an additional curve that was registered within the direct R→B19' MT temperature range but interrupting the heating T-scan at 140 K after cooling to 115 K. This curve is marked with an asterisk. Although taken on heating, the 140K* curve is included in this figure because the isothermal kinetics of the resistance do not correspond to the reverse transformation, but to the isothermal accumulation of B19' phase. The direct R→B19' MT occurs because it is a quite diffuse transformation that is not completed upon cooling down to 115 K. So, when the sample is held at 140 K, which is inside the direct transformation range, the isothermal accumulation of the B19' martensite continues, like on cooling. This is a classical behavior [38] when the structural transition is isothermal and not completed during cooling.

Panels (b) and (c) of the Figure 3.5 depict the kinetics of the resistance during isothermal holdings inside the R→B19' transformation range for a sample of binary $Ni_{50.2}Ti_{49.8}$ alloy heat treated at 770 K and the ternary $Ti_{50}Ni_{47.4}Fe_{2.6}$ alloy annealed at 1270 K. The isothermal effect can be clearly detected and it essentially follows a logarithmic law in the transformation range of the direct R→B19' MT. The intensity of isothermal accumulation of resistance is higher for these samples than for the sample annealed at 620 K shown in panel (a). The transitory effect is also present, but the time of the transitory effect seem to be reduced. However, this is simply due to the higher isothermal variations of resistance (see different ordinate scales in (a) and (b,c)) that makes the variation of resistance due to the temperature overshoot relatively smaller. The maximum of isothermally accumulated resistance in a single holding experiment is for the 240 K curve on panel (b) and for 170 K in panel (c), near of the correspondent $\frac{1}{R}\frac{\partial R}{\partial T}$ peak temperatures: 239 and 169 K, respectively. Therefore, the samples on panels (b) and (c) show the same regularities as those observed for the binary sample annealed at 620 K.

Figure 3.6 shows the time evolution of the resistance within the temperature range of reverse MTs from the B19' phase for three different samples: two samples of binary Ni–Ti alloy quenched from 620 (a) and 770 K (b) and a sample of the Fe-containing ternary alloy alloy annealed at 1270 K (c). Many curves, which correspond to experiments outside the transformation range with little or no accumulation of resistance, are not shown for clarity. In addition, the reverse B19'→R MT has a narrower transformation range. Because of these reasons, only a few curves are displayed in the Figure 3.6 as compared to the figure 3.5. Relatively small number of isothermal experiments were performed for the binary alloy annealed at 620 K. Therefore, only one experimental point was taken close to the temperature of the maximum of the reverse B19'→R transformation rate centered around 259 K, Figure 3.2b. This point, taken at 260 K, clearly shows isothermal accumulation of the R phase, Figure 3.6a.

The number of experiments was substantially higher for the binary alloy at 770 K and the ternary Ni–Ti–Fe alloy. The sample of binary alloy quenched from 770 K has the maximum transformation rate at 287 K. This sample exhibits isothermal kinetics in curves, registered around the peak temperature, at 275, 282 and 290 K, Figure 3.6b. However, the reverse transformations are strongly overlapped for this alloy, see Figure 3.3, resulting in a mixture of the reverse B19'→R, B19'→B2 and R→B2 MTs. This overlap distorts the results, for example, complicating the choice of R_{MAX} and R_{MIN} of the B19'→R path. Therefore, the absolute values given by the Figure 3.6b are not too reliable. In addition, the kinetics during the transitory stage are rather irregular. This is, likely, because of the abrupt change of the relative temperature rate of the resistance during the reverse transformations: it is not obvious how the resistance depends on the temperature during the overshoot in a cold-worked sample with a mixture of transformations. The situation is much clear in the ternary alloy, Figure 3.6c. The data taken at 200 K and 206 K undoubtedly show isothermal logarithmic kinetics after the transitory stage. Curve registered at 214 K also shows a large time-dependence, but it is irregular and does not fit the logarithmic dependance as well as the curves at 200 and 206 K.

Therefore, the isothermal accumulation of the resistance during the direct R↔B19' is evident from the Figures 3.5 and 3.6. Nevertheless, one finds that the isothermal variation of resistance is much less intense for the reverse

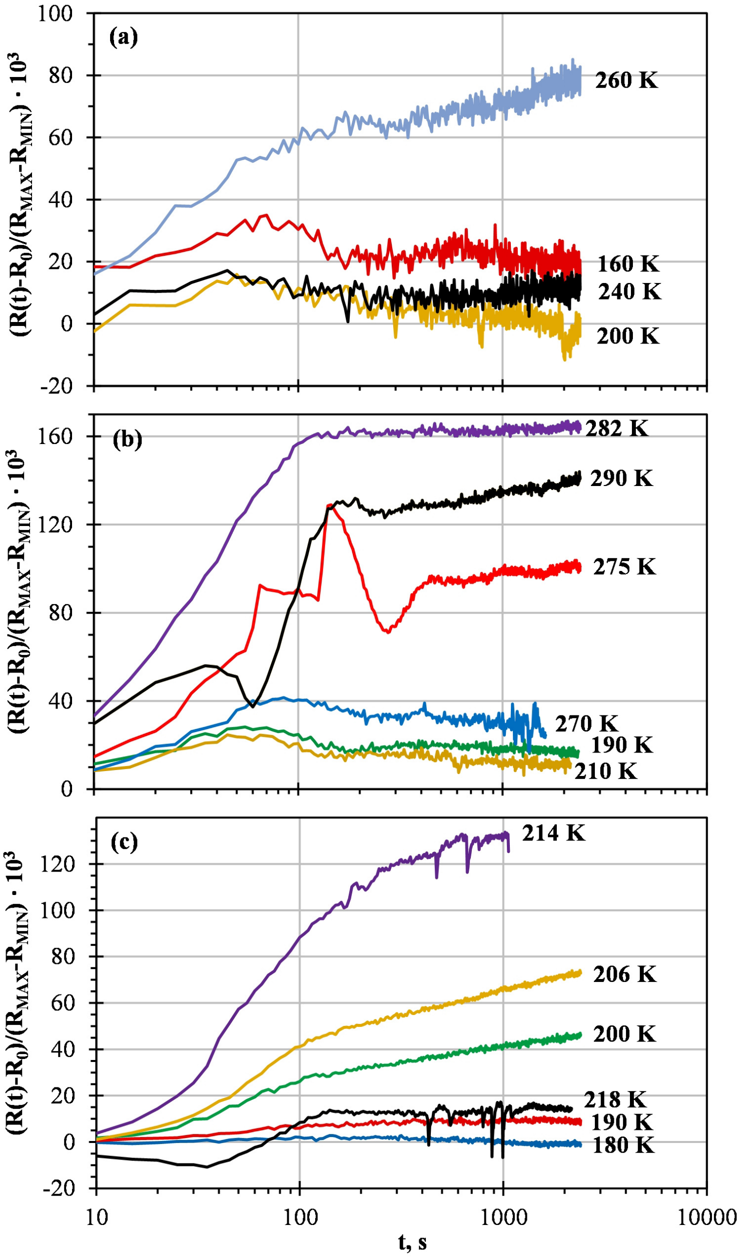

Figure 3.6: Time evolution of the resistance during interruptions of the temperature scan near and inside the reverse B19'→R transformation range for (a) a sample of binary $Ni_{50.2}Ti_{49.8}$ annealed at 620 K, (b) a sample of binary $Ni_{50.2}Ti_{49.8}$ alloy annealed at 770 K and (c) a sample of $Ti_{50}Ni_{47.4}Fe_{2.6}$ alloy annealed at 1270 K. Note different ordinate scales in (a), (b) and (c).

transformation than for the direct one.

Isothermal kinetics were also registered over the temperature range of the B2↔R MT for the same samples. Figure 3.7 depicts the results for the direct B2→R MT for these samples: (a) $Ni_{50.2}Ti_{49.8}$ annealed at 620 K, (b) $Ni_{50.2}Ti_{49.8}$ annealed at 770 K and (c) $Ti_{50}Ni_{47.4}Fe_{2.6}$ quenched from 1270 K. A few isothermal holding experiments were performed for the binary Ni–Ti alloys within the transformation range of the B2↔R MT. Only two curves at 280 and 300 K are shown in Figure 3.7a for the direct transformation for the sample annealed at 620 K. For this sample the peak temperature of the transformation is 305 K. The curves registered at 260, 280 and 300 K are shown in Figure 3.7b for the sample annealed at 770 K having a transformation peak temperature of 290 K. Much more extensive experiments were done near the peak temperature of the transformation (249 K) for the sample of ternary alloy, Figure 3.7c.

For the sample of ternary alloy Figure 3.7c, the resistance registered at 300 K demonstrates an important decrease with time but do not show a clear logarithmic kinetics. In panel (b), the resistance is essentially constant during the isothermal holding experiments; especially taking into account strongly expanded ordinate scale in Figure 3.7b. However, the temperatures of isothermal dwellings of 260, 280 and 300 K are relatively far from the sharp transformation peak at 290K, Figure 3.3b . Therefore, the data for binary alloys, Figures 3.7a and 3.7b, do not seem to be too conclusive. The experiment for the Fe-containing alloy performed at 250 K (close to the MT peak temperature), presents an important change of the resistance during the initial transitory stage, Figure 3.7c. However, after the transitory stage, the accumulation of resistance with time becomes small. One can realize that the higher variations of the resistance during the transitory period seem to coincide with the transformation range. However, this is not related with the isothermal accumulation of martensite/austenite. As has been commented previously, the variation of resistance during the transitory effect is mainly due to the temperature overshoot on interrupting the T-scan. During the overshoot, the resistance varies due to several reasons:

- During the T-scan, the actual temperature of the sample, T_{ACT}, is delayed with respect to the set temperature, T_{SET}. This difference may depend on several factors, but in the present work it has a typical value of 0.5 K. Then, when the cycle is interrupted, the value of the resistance at “local” time $t = 0$ s (time at the interruption event) R_0 is taken at $T = T_{ACT}$. Later, the overshoot takes place and the temperature goes back and stabilizes. However, it does not go back to T_{ACT}, but to the T_{SET} of the controller at the moment of interruption. Therefore, since

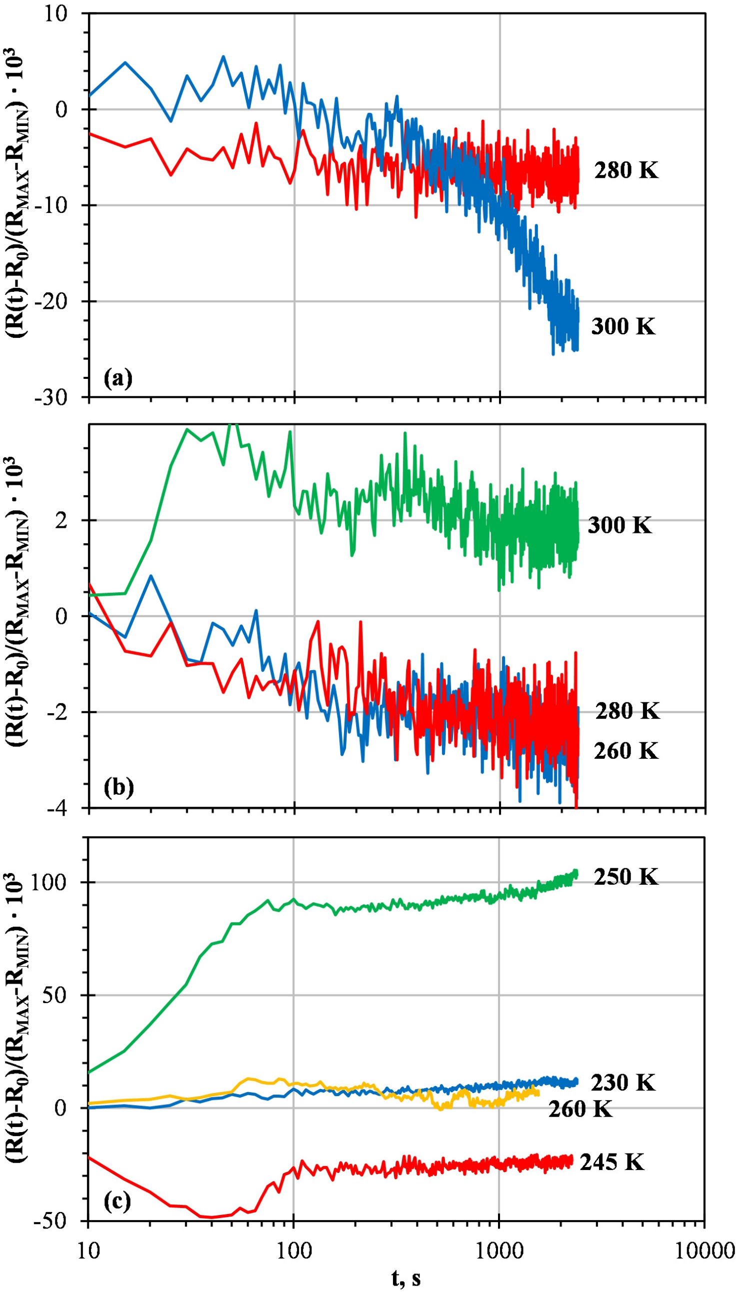

Figure 3.7: Time evolution of the resistance during interruptions of the temperature scan near and inside the direct B2→R transformation range for (a) a sample of binary $Ni_{50.2}Ti_{49.8}$ annealed at 620 K, (b) a sample of binary $Ni_{50.2}Ti_{49.8}$ alloy annealed at 770 K and (c) a sample of $Ti_{50}Ni_{47.4}Fe_{2.6}$ alloy annealed at 1270 K. Note different ordinate scales in (a), (b) and (c).

the resistance depends on the temperature, independently of whether or not the resistance varies with time, there will be inevitable a difference between the final resistance $R(t \approx 2400$ s) and the initial resistance R_0. This difference should be approximately $R(T_{SET}) - R(T_{ACT})$ or, typically, $R(T_{SET}) - R(T_{SET} \pm 0.5$ K). The higher the temperature derivative of the resistance, the higher is this difference. Then, this difference may be maximum at the peak temperature of the transformations when the variation of resistance with temperature is the strongest. However, other reasons for the temperature-dependence of the resistance, like phonon scattering, can also contribute.

- The typical overshoot will not exceed 0.4 K, as seen in the Figure 2.7 in page 55. However, inside the transformation domain, this will be enough to produce a small hysteretic loop, which results in a permanent variation of resistance. This possible effect should be more important near the maximum of the temperature rate of the resistance, since this is the point where the transformation rate is more sensitive to the variation of the temperature.

- In addition to the non-recoverable variation of resistance during the overshoot, introduced in the two previous points, since the resistance depends on the temperature, there is part of the variation of resistance during the overshoot which is recovered when the temperature goes back to reach the T_{SET}. This does not contribute to the R versus t curves once the temperature is stabilized, about 100 s. However, it may be the main contribution to the kinetics during the overshoot for some curves, like the curve at 300 K in the Figure 3.7b.

In conclusion, these three points explain why there are some curves with a strong variation of resistance during the overshoot, but quite small after it, and why they are likely to be those curves correspondent to isothermal holding experiments performed near the maximum of the transformation peak. The curve at 250 K in Figure 3.7c is a good example. Therefore, if the effects of the overshoot are not considered, the curves shown in the Figure 3.7 have a very small or no change of resistance with time; especially if they are compared to the results of the isothermal experiments for the R↔B19' MT shown in Figures 3.5 and 3.6.

Some isothermal effect can be distinguished in Figure 3.7a, where the scale is strongly expanded. However, this effect has a opposite sign to the expected in the case of isothermal MT. Moreover, the kinetics of the resistance variation is essentially linear, as is shown in Figure 3.8. Since the temperature control during this isothermal experiment was good (instabilities of a few hundredths of a degree), the feasible reason for this minor effect is the heating of the electronics. This reasoning is additionally confirmed by the fact that this isothermal experiment was the first one in a series of consecutive isothermal holding experiments. This example illustrates the necessity of serious precautions in these delicate experiments.

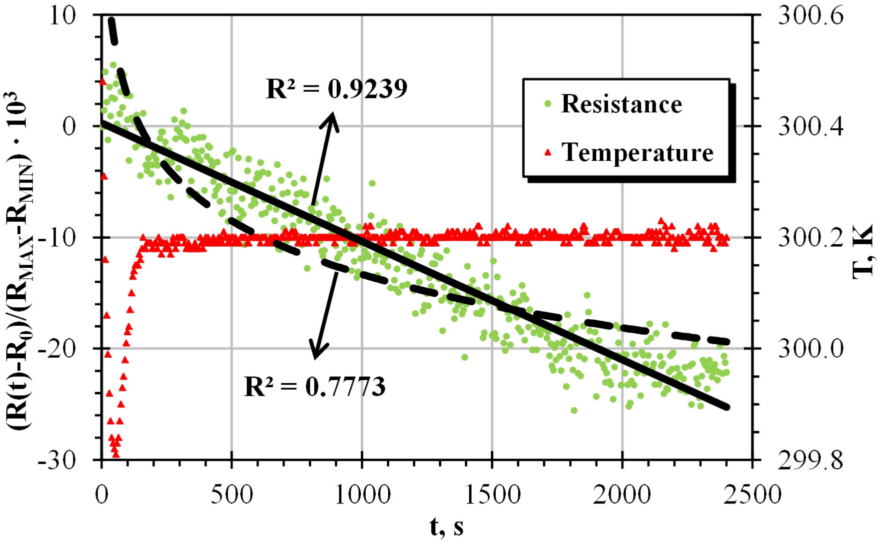

Figure 3.8: Time evolution of the resistance and the temperature during interruption of cooling at 300 K for a sample of $Ni_{50.2}Ti_{49.8}$ alloy annealed at 620 K. The resistance curve is fitted by two curves, linear (line) and logarithmic (dashed), and the R^2 coefficient is shown for each fitting curve.

Figure 3.9 shows representative plots of the time dependencies registered on heating within the range of the reverse R→B2 MT. The results of the experiments performed in the sample annealed at 620 K are shown in the panel (a). Both curves manifest a slight increase of the resistance with time. However, the resistance decreases when going from the R phase to the B2 phase. Then, this very small isothermal accumulation of resistance is, likely, irrelevant to the isothermal MT. In panel (b), the results for the sample of binary Ni–Ti alloy annealed at 770 K are shown. Since the reverse MTs are very overlapped for this alloy, the curve at 290 K is in between both transformations and was shown also in the Figure 3.6b. Therefore, the 290 K curve presents logarithmic kinetics after the transitory effect, which can be attributable to either the B19'→R MT or the B19'→B2 MT. Furthermore, the peak temperature is 292 K; the curve at 295 K is also very close to this transformation temperature but does not show any variation of resistance with time. The results for the direct B2→R MT in ternary Ti–Ni–Fe alloy, in Figure 3.9c, show a large variation of the resistance during the transitory stage near to the maximum of the relative temperature rate of the resistance at 251 K. However, the subsequent variation of the resistance is much less significant.

In conclusion, the isothermal holding experiments do not demonstrate a clear isothermal behavior of the resistance in the B2↔R MTs within the experimental resolution. By contrast, the experiments performed within the transformation range of the R↔B19' show logarithmic kinetics of the resistance variation, pointing to the isothermal accumulation of B19' phase (direct MT) and R phase (reverse MT).

The data exposed in Figures 3.5, 3.6, 3.7 and 3.9 give a rather clear idea about the athermal/isothermal behavior of the different transformation paths of the two stage B2↔R↔B19' MT. However, it is necessary to quantify these effects in order to analyze and compare different alloys/heat treatments and transformations. To this end, the time evolution curves are fitted by a logarithmic dependence following equation (2.31) in section 2.4

$$\frac{R - R_0}{R_{MAX} - R_{MIN}} \approx Z(T) \ln \frac{t}{t_0} \tag{3.1}$$

from where the “viscosity” Z is calculated. In this calculations, the constant t_0 is set to 1 s. Since Z quantifies the rate of the transformation during an isothermal holding experiment, one can refer to it as the isothermal transformation rate or the relaxation rate or viscosity. These calculated values of Z are shown as function of temperature in Figures 3.10, 3.11 and 3.12. In these figures, the Z-points are separated in series depending on which sample the experiment was done and if the T-scan was interrupted on cooling or on heating. Consequently, data are arranged in a different way than in previous figures, from 3.5 to 3.9, where there is one figure for each MT type. Therefore, with this configuration we will compare, separately for each alloy/heat treatment and for cooling and heating scans, the temperature dependence of the isothermal transformation rate $Z(T)$ with the relative temperature rate of the resistance in an uninterrupted cycle. Since the latter is an approximation to the athermal transformation rate, see equation (2.23) in page 43, this comparison establishes a relation between the behavior of the transformation under isothermal conditions and under “anisothermal” conditions.

Since in the synthetics plots, Figures 3.10, 3.11 and 3.12, different Z points may correspond to different types of MTs (B2↔R, R↔B19' and B2↔B19'), the points corresponding to different types of MTs require their own normalization conditions, $R_{MAX} - R_{MIN}$ in equation (3.1). The normal-

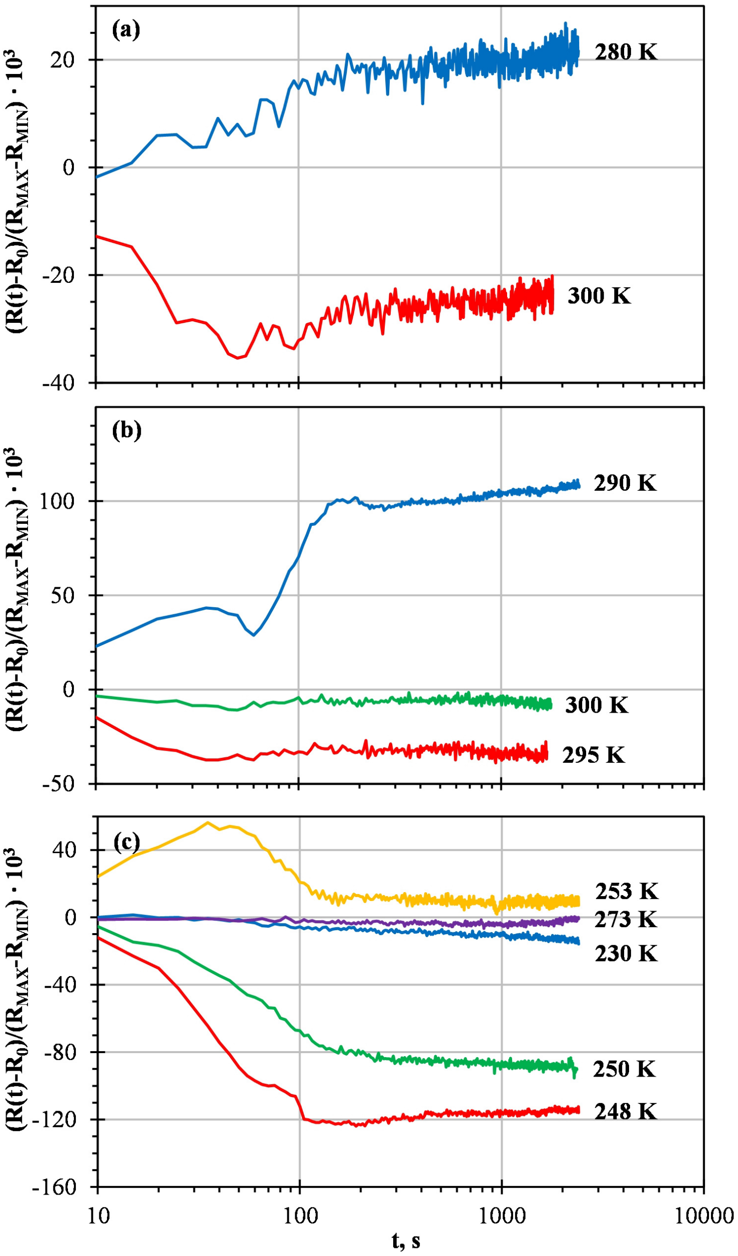

Figure 3.9: Time evolution of the resistance during interruptions of the temperature scan near and inside the reverse R→B2 transformation range for (a) a sample of binary $Ni_{50.2}Ti_{49.8}$ annealed at 620 K, (b) a sample of binary $Ni_{50.2}Ti_{49.8}$ alloy annealed at 770 K and (c) a sample of $Ti_{50}Ni_{47.4}Fe_{2.6}$ alloy annealed at 1270 K. Note different ordinate scales in (a), (b) and (c).

ization condition imply that the total variation of resistance during the MT, $R_{MAX} - R_{MIN}$, corresponds to 100% transformed fraction. For example, if a plot shows the direct B2→R and R→B19' MTs:

- the points of Z within the transformation range of B2→R and at higher temperatures are calculated using the $R_{MAX} - R_{MIN}$ corresponding to the B2→R MT;
- the points of Z within the R→B19' transformation range and at lower temperatures are calculate using the resistance data of the R→B19' MT and
- finally, for the points at intermediate temperatures between both transformations the value $R_{MAX} - R_{MIN}$ was selected depending on the proximity to each transformation.

There is one exception to these rules. The curve registered during the isothermal holding at 290 K on heating for the binary sample annealed at 770 K is repeated in Figures 3.6b and 3.9b due to the strong overlap of both reverse transformations. In this case the corresponding point of the relaxation rate was calculated using the R_{MIN} and R_{MAX} of the direct R→B19' MT.

Figure 3.10 shows a synthetic plot of the Z-parameter (relaxation rate) obtained between 120 K and 300 K in several scans on cooling (a) and heating (b) for a sample of $Ni_{50.2}Ti_{49.8}$ alloy annealed at 620 K. The relaxation rate is confronted with the relative temperature rate of the resistance in an uninterrupted temperature scan. In panel (a), the "-Z Cooling" curve shows the values of the relaxation rate calculated from the data of the isothermal holding experiments on cooling. Between 120 and 240 K, the points of the "-Z Cooling" curve form a broad peak, similar to the peak in the $\frac{1}{R}\frac{\partial R}{\partial T}$. The existence of such peak points to the isothermal nature of the direct R→B19' MT. Note that the $\frac{1}{R}\frac{\partial R}{\partial T}$ curve has several contributions, and represents not only the change of resistance due to the transformation, but other possible temperature dependencies of the resistance as well, like the phonon scattering. Therefore, independently of whether of not the parameter Z is proportional to the temperature rate of the martensite volume fraction in an uninterrupted cycle $Z \propto \frac{\partial F}{\partial T}$, it will not fit perfectly with the $\frac{1}{R}\frac{\partial R}{\partial T}$ curve. In its turn, no pints of "-Z cooling" curve are shown in the transformation domain of the direct B2→R MT.

An extra point of the relaxation rate is shown apart from the "-Z Cooling" curve: the point for the curve made at 140 K interrupting the T-scan on heating (Triangle). The "140 K Heating" point is shown on cooling since the isothermal accumulation of resistance during the corresponding isothermal

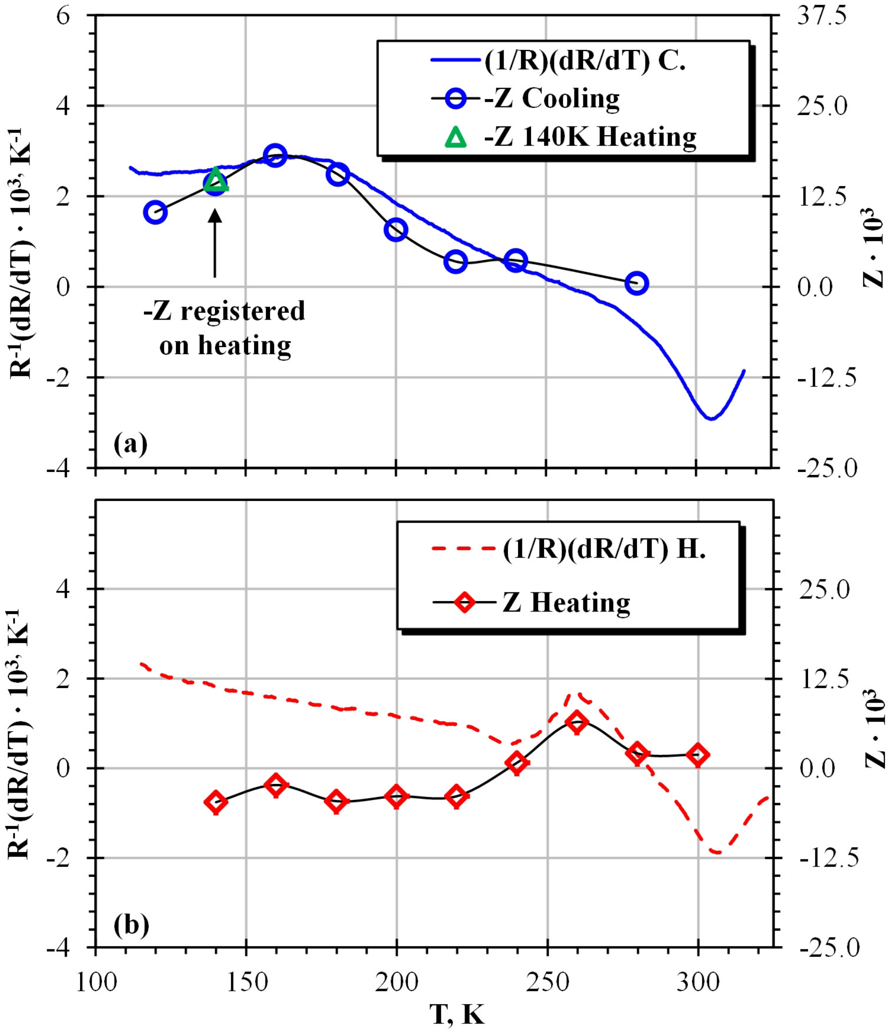

Figure 3.10: Comparison of the temperature dependence of the relative temperature rate of the resistance, $\frac{1}{R}\frac{\partial R}{\partial T}$ and of the relaxation rate Z for a sample of $Ni_{50.2}Ti_{49.8}$ quenched from 620 K; (a): $\frac{1}{R}\frac{\partial R}{\partial T}$ on cooling (continuous line), -Z calculated from isothermal holdings upon interruptions of cooling (open circles) and -Z calculated from an isothermal holding experiment after stop the heating at 140 K (open triangle); (b):$\frac{1}{R}\frac{\partial R}{\partial T}$ on heating (dashed line), Z calculated from isothermal holdings upon interruptions of heating (open diamonds).

experiment is due to the isothermally accumulated B19' phase. Surprisingly, the value of Z in "140 K Heating" is very similar to the point obtained at the same temperature but interrupting the cycle on cooling. This happens despite the fact that before the experiment on heating the sample was cooled down to 115 K. This fact suggests that the transformation is not only incomplete on cooling below 140 K, but also is arrested.

Note also from Figure 3.10a that the data for the relaxation rate is shown as $-Z$. This is done to compare the values of Z with the $\frac{1}{R}\frac{\partial R}{\partial T}$ due to the different behavior of both parameters:

- The relaxation rate normally changes its sign between cooling and heating. For example, for the R↔B19' MTs, the level of resistance is higher in the R phase than in the B19' phase, see Figure 3.1. Then, the sign of the isothermal accumulation of resistance is negative when going from R to B19' phase, Figure 3.5, and positive when doing the reverse path, Figure 3.6.

- By contrast, the temperature derivative of the resistance does not have into account the direction of the transformation. Therefore, following the above example, the $\frac{1}{R}\frac{\partial R}{\partial T}$ shows a positive peak for both transformation paths, see, for example, Figure 3.4.

Despite it does not have the same origin, a similar effect is observed when comparing the DSC signal and the relative temperature rate of the resistance in Figures 3.2, 3.3 and 3.4.

Similar synthetic plot $Z(T)$ and $\frac{1}{R}\frac{\partial R}{\partial T}$ for heating is shown in panel (b) of the Figure 3.10. According to the data presented in the panel (b), only the kinetics registered at 260 K might point to the reverse transformation: all experimental $Z(T)$ points that are inside the reverse transformations range are quite close to zero level, except for the point at 260 K. This temperature is clearly within the range of the reverse MT as DSC data show, see Figure 3.2. Moreover, taking into account much lower sensitivity of the resistance to the reverse MT, one has to conclude that possible athermal/isothermal nature of the reverse B19'→R MT can not be clearly corroborated based on the results for the sample made of binary $Ni_{50.2}Ti_{49.8}$ quenched from 620 K.

Finally, a reasonable correlation between $Z(T)$ and $\frac{1}{R}\frac{\partial R}{\partial T}(T)$ over the range of the direct R→B19' MT, Figure 3.10a, might be an indirect evidence of the proportionality between the resistance and the martensitic volume fraction, $\partial R \propto \partial F$. It should be reminded that this proportionality could not be checked directly from the comparison of the $\frac{1}{R}\frac{\partial R}{\partial T}(T)$ and the calorimetric signal $\frac{\phi}{m\beta}(T)$ since this MT is not detected by DSC due to a very broad transformation range and quite low transformation temperature, which is below the lower limit of the calorimeter.

Figure 3.11 shows a comparison between the temperature-dependence of the relative temperature rate of the resistance $\frac{1}{R}\frac{\partial R}{\partial T}(T)$ and the isothermal transformation rate Z for interruptions of cooling (a) and of heating (b) for a sample of binary Ni–Ti quenched from 770 K. In panel (a), there are two points of the Z parameter inside the transformation range of the direct B2→R martensitic transformation. These points are zero within the scatter of experimental data. Therefore, the direct B2→R MT does not show isothermal accumulation of resistance and should be classified as athermal. However, as commented above, the low number of isothermal experiments within the B2→R temperature range makes highly desirable confirmation of this conclusion by data for other samples. On the other hand, high Z values for the direct R→B19' MT, correlated with the $\frac{1}{R}\frac{\partial R}{\partial T}(T)$ clearly point to its isothermal nature. The situation is less clear for the reverse transformations in panel (b) since these MTs are overlapped. Relaxation rate for the isothermal holdings at 275, 282 and 290 K seems to be high enough to indicate isothermal accumulation. Despite overlapping of the reverse transformations, these points are at the initial stage of the reverse transformation, which is associated with the reverse B19'→R transformation. In addition, they are in clear contrast with the small or zero value of Z for the points at 295 and 300 K. This suggests that, despite the overlap of the transformation peaks, the reverse B19'→R MT may be considered as isothermal and the reverse B19'→R as experimentally athermal. The results for the binary Ni–Ti annealed at 770 K point in the same direction as the results obtained for the sample annealed at 620 K. The results on the ternary Fe-containing alloy are desirable to finally confirm these conclusions , especially, concerning the reverse transformations.

The temperature dependence of the relaxation rate Z derived from the data shown in Figures 3.5c 3.6c 3.7c and 3.9c is compared with the relative temperature rate of the resistance $\frac{1}{R}\frac{\partial R}{\partial T}$ in the Figure 3.12 for cooling (a) and heating (b) for the ternary Ti–Ni–Fe alloy. In panel (a), three points of the "-Z Cooling" curve corresponding to isothermal holdings performed close to the peak temperature of the direct B2→R MT are shown. These points demonstrate that, despite the substantial change of R during the first 100 seconds (during the transitory stage) is high, Figure 3.7c, the time dependence under isothermal conditions is very weak: the resistance does not depend on time within the experimental resolution. In the same way, panel (b) shows three points of Z close to the maximum of the reverse R→B2 MT which indicate very small or no time dependence on this reverse path. On the other hand, the points of the relaxation rate spread over the transfor-

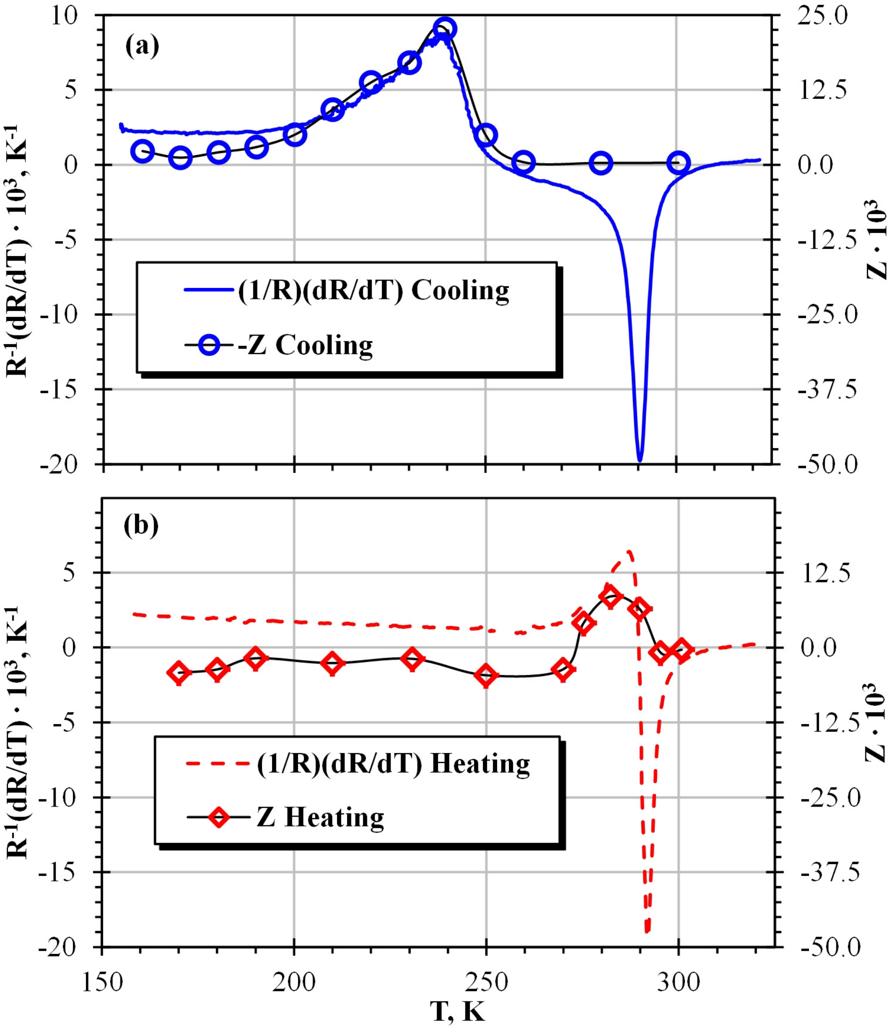

Figure 3.11: Comparison of the temperature dependence of the relative temperature rate of the resistance, $\frac{1}{R}\frac{\partial R}{\partial T}$ and of the relaxation rate Z for a sample of $Ni_{50.2}Ti_{49.8}$ quenched from 770 K. In panel (a): $\frac{1}{R}\frac{\partial R}{\partial T}$ on cooling (continuous line), -Z calculated from isothermal holdings upon interruptions of cooling (open circles). In panel (b):$\frac{1}{R}\frac{\partial R}{\partial T}$ on heating (dashed line), Z calculated from isothermal holdings upon interruptions of heating (open rhombus).

mation range of the direct R→B19' MT in panel (a) show a temperature dependence trend clearly different from zero. This trend has a good correspondence with the $\frac{1}{R}\frac{\partial R}{\partial T}$ during the direct transformation. The behavior of the relaxation rate Z is also typical of an isothermal MT during the reverse B19'→R transformation. It is also similar to the $\frac{1}{R}\frac{\partial R}{\partial T}$ peak during the reverse transformation. However, the isothermal accumulation of resistance is lower during the reverse B19'→R MT than during the direct one.

Since the good correlation between the relative temperature rate of the resistance and the DSC signal has been proved, see Figure 3.4, then there is an implicit relation between the isothermal variation of resistance and the isothermal transformed martensite/austenite, in other words, one can conclude that the isothermal accumulation of resistance is proportional to isothermally accumulated product phase, see equation (2.22) in page 42. Therefore, the data obtained for the ternary alloy confirms our preliminary conclusions based on the experimental data for the binary alloy: the direct B2→R MT has to be classified as athermal, whereas the direct R→B19' MT as isothermal. Due to the clear separation of the reverse B19'→R and R→B2 MTs the data for the ternary alloy clarify the issue of the athermal/isothermal nature of these MTs. Namely, the reverse B19'→R MT has to be undoubtedly classified as isothermal, whereas the R→B2 one as athermal.

3.2 Results for the B2-B19' MT

As discussed previously, the one stage B2↔B19' martensitic transformation is typical for a sample of binary $Ni_{50.2}Ti_{49.8}$ alloy annealed at 1070 K during 30 minutes and water quenched. This is the only alloy and heat treatment from the studied Ni-rich samples which result in a single stage transformation. Other samples with identical composition which were heat treated at lower temperatures demonstrate a two stage transformation B2↔R↔B19'. The decisive factor that differentiates one stage and two stage transformations is the annealing temperature, which was above or below the recrystallization temperature, respectively.

In the present work, the one stage B2↔B19' MT has also been investigated in a sample of $Ti_{50.5}Ni_{49.5}$ alloy heat treated at 920 K and water quenched. The Ti-rich sample has a composition with different deviation from stoichiometry than in the previous Ni-rich samples and exhibits a MT which, although is the same transformation type, presents many differences to the one exhibited by the Ni-rich sample annealed at 1070 K.

Figure 3.13a shows the temperature dependance of the resistance, R, in an uninterrupted temperature cycle for a sample of $Ni_{50.2}Ti_{49.8}$ alloy annealed

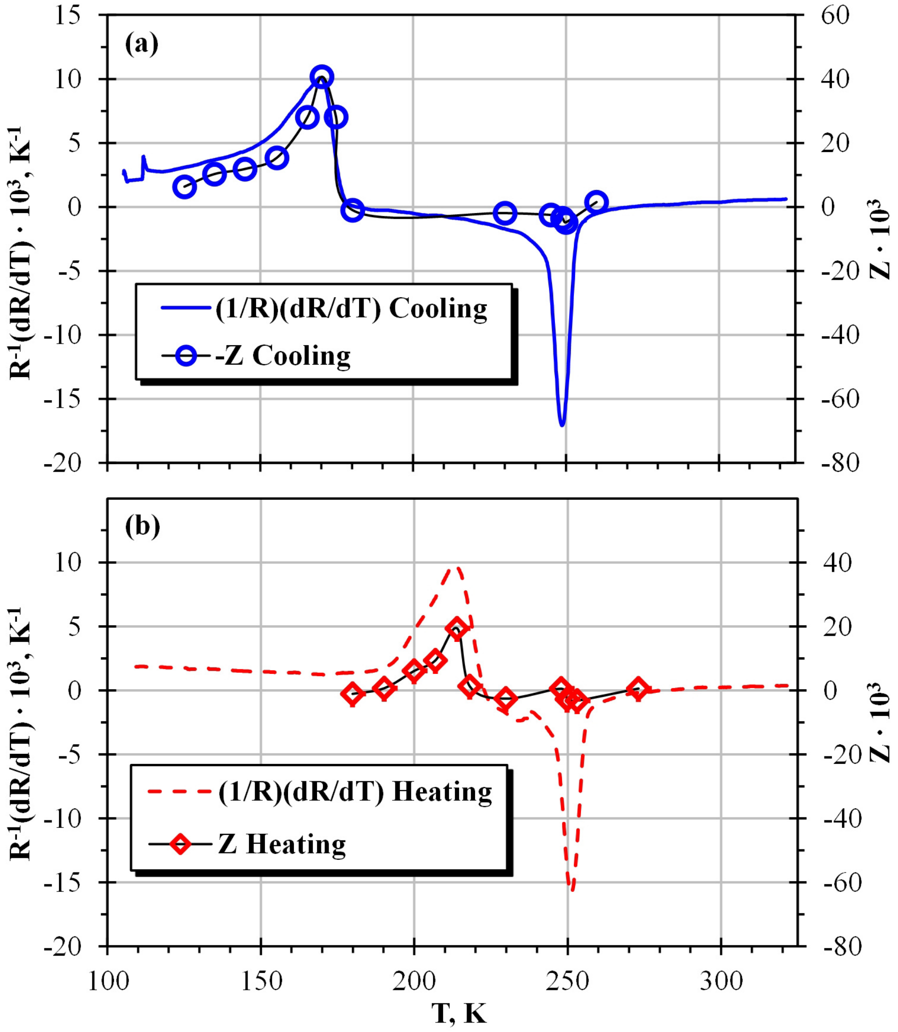

Figure 3.12: Comparison of the temperature dependence of the relative temperature rate of the resistance, $\frac{1}{R}\frac{\partial R}{\partial T}$ and of the relaxation rate Z for a sample of $Ti_{50}Ni_{47.4}Fe_{2.6}$ annealed at 1270 K. In panel (a): $\frac{1}{R}\frac{\partial R}{\partial T}$ on cooling (continuous line), -Z calculated from isothermal holdings upon interruptions of cooling (open circles). In panel (b):$\frac{1}{R}\frac{\partial R}{\partial T}$ on heating (dashed line), Z calculated from isothermal holdings upon interruptions of heating (open rhombus).

at 1070 K. The T-scan rate is 2 K/min and the value of the resistance is normalized to its value at 320 K on cooling (well above M_S). This sample exhibits the one stage B2↔B19' transformation. It is not obvious the transformation temperatures (which were calculated from the DSC data) from the resistance data. This is due to the abnormal increase of the resistance on decreasing the temperature in austenite. This resistance behavior is caused by a strong premartensitic effect which is missing in the other composition and heat treatments and spreads over a range of over 60 K above M_S. Then, the premartensitic effect is the responsible that there are two maxima of the resistance, one on cooling and another on heating. The maximum on cooling coincides with M_S temperature while the one on heating lies between A_S and A_F. This observation is in agreement with previously published results [68, 107–109]. The combination of the effects of the martensitic transformation and the premartensitic effects also makes that the total resistance change during the MT on heating is significantly smaller than on cooling.

Several temperature dependencies of the resistance of a sample of the Ti-rich $Ti_{50.5}Ni_{49.5}$ alloy annealed at 920 K are shown in Figure 3.13b. Three different cycles are plotted. Cycle 1 is an continuous cycle whereas cycles 2 and 3 were stopped several times at different temperatures inside the MT range to perform isothermal holding experiments: cycle 2 was interrupted along the reverse B19'→B2 MT and cycle 3 over the direct B2→B19' MT range. The resistance data is normalized to the resistance at 320 K (in martensite) on cooling during the first cycle. The temperature dependence of the resistance during a continuous temperature ramp is quickly recovered after resuming the cooling/heating ramp. Therefore, despite cycles 2 and 3 were interrupted, their resistance data should give a very similar cycle when plotted versus temperature than a continuous temperature cycle. The last sentence implicitly includes the important assumption that the accumulation of resistance during the isothermal holdings is only due to the progression of the MT and there is not "permanent accumulation of resistance", like isothermal generation of crystalline defects.

These three different cycles were included because of the strong dependence of the resistance with the number of cycles (which is missing in previous samples, see Figure 2.12 in page 62). Then, there is a substantial increase of the resistance with the number of cycles: only between the cycle 1 and 3 the resistance increases nearly 2% in austenite and 5% in martensite. Furthermore, Figure 3.13c shows that, for the three cycles represented in panel (b), all characteristic transformation temperatures, excluding A_S, decrease with thermal cycling. By contrast, the A_S slightly increases. Therefore, the reverse B19'→B2 MT range, $A_F - A_S$, slightly decreases, whereas the transformation hysteresis increases with the number of cycles. A similar effect

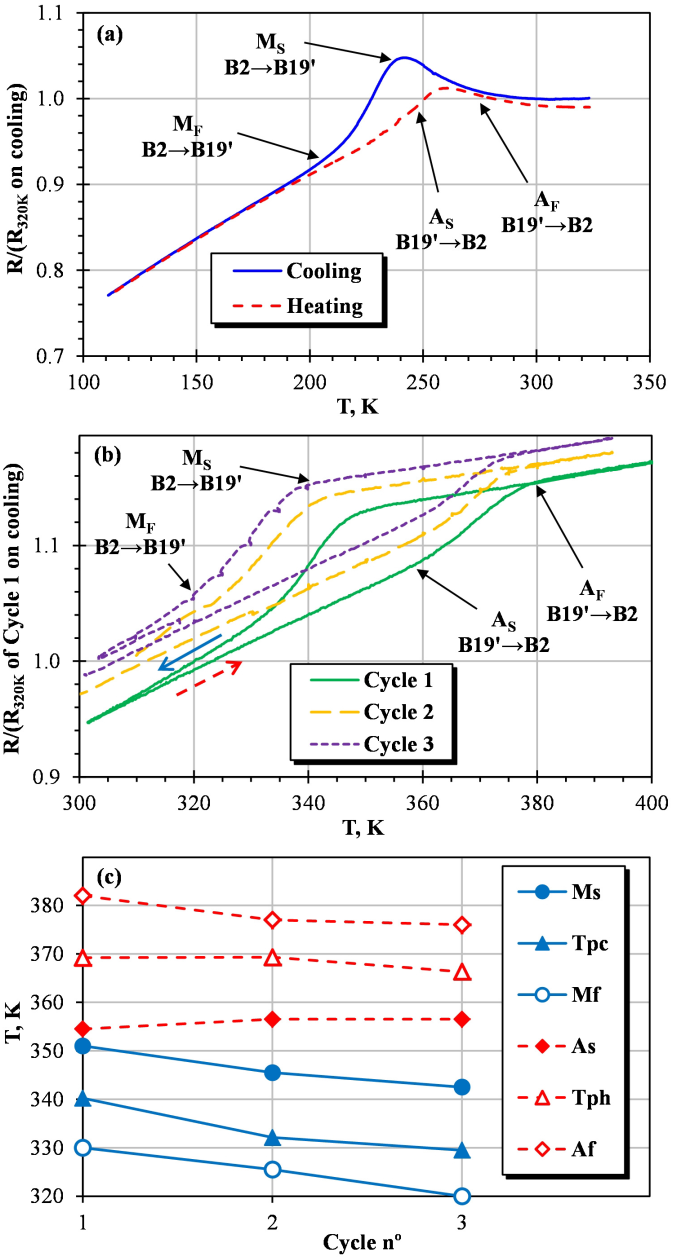

Figure 3.13: Temperature dependence of the normalized resistance of (a) a sample of $Ni_{50.2}Ti_{49.8}$ alloy annealed at 1070 K in a single temperature cycle and (b) a sample of $Ti_{50.5}Ni_{49.5}$ annealed at 920 K in three consecutive thermocycles: cycle 1 non-interrupted, cycles 2 and 3 are interrupted several times on heating and cooling, respectively. Panel (c) shows the evolution of temperatures M_S, M_F, T_{PC}, A_S, A_F and T_{PH} along the cycles represented in panel (b).

of thermal cycling was observed in previous studies of the B2↔B19' MT in Ni-rich Ni-Ti alloys [107, 110] and Ti-rich ones [111].

It is important for the present study to figure out whether the effect of thermal cycling on the resistance and the transformation temperatures of the MT stems from the exposure of material to high temperatures or from the martensitic transformation. To clarify this point, two different samples of $Ti_{50.5}Ni_{49.5}$ were subjected to the same heat treatment, heated at 920 K during 1800 s and water quenched, and prepared for calorimetric experiments. Figure 3.14a shows the experimental protocol, T versus t, followed by these two samples while their heat flux was registered. The first sample (continuous line) was cycled 3 times between 270 and 400 K. As is shown by the Figure 3.14a, this range includes both direct and reverse B2↔B19' MTs. The second sample (dashed line) was also subjected to 3 thermocycles within the same temperature limits. However, for this sample each cycle was interrupted on heating at 383 K (slightly above the reverse MT) for 3600 s. The panels (b) and (c) of the Figure 3.14 presents the temperature dependance of the calorimetric signal on cooling registered during the continuous and the interrupted scans, respectively. The DSC peak of the direct transformation is displaced towards lower temperatures with thermal cycling for both experimental protocols. The evolution of the peak temperature of the direct transformation, T_{PC}, is shown for both samples in an inset in Figure 3.14c. The T_{PC} of the first sample changes from 337.2 to 334.3 K and of the second one from 335.2 to 332.2 K. The effect of thermal cycling over T_{PC} is essentially the same for both experimental protocols, showing no appreciable effect of the aging at 383 K. Since the isothermal holdings were above A_F, the absence of a meaningful contribution of the isothermal holding indicates that the dependencies with n have their origin during the MT. Hence, the change of the MT temperatures is not produced by any isothermal process not related to the MT, like atomic diffusion.

As in the previous section 3.1 (page 77), in order to check wether the resistance variations during the martensite transformation reflects the change of the martensite volume fraction F, one should compare the temperature dependance of calorimetric signal $\frac{\phi}{m\beta}$ and of the relative temperature rate of the resistance $\frac{1}{R}\frac{\partial R}{\partial T}$.

Figure 3.15a shows the temperature dependance of the calorimetric signal for a sample of binary $Ni_{50.2}Ti_{49.8}$ alloy annealed at 1070 K. One broad transformation peak is observed, both for cooling and heating at 225 K and 259 K, respectively. There is a small shoulder at the onset of the direct transformation, but the transformation is considered as a one stage MT. From this figure, the following transformation temperatures are obtained: $M_S = 242$

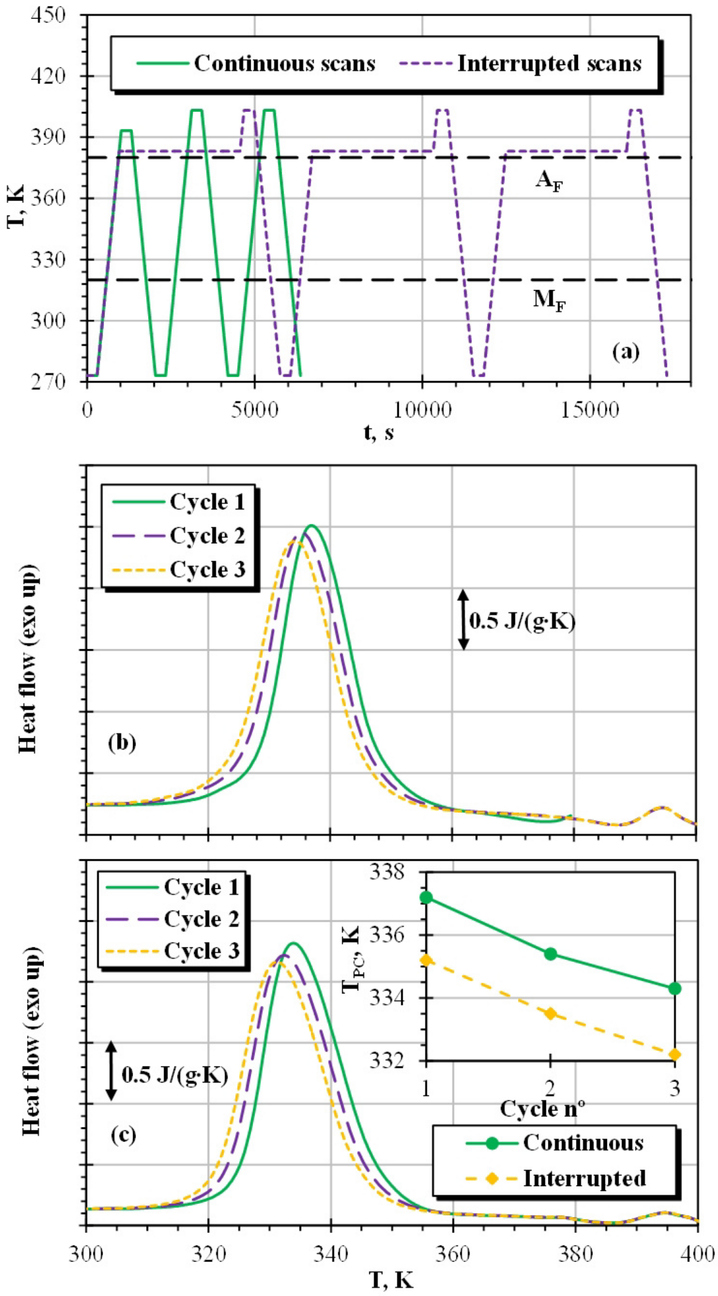

Figure 3.14: Experimental protocols (a) followed by the DSC experiments performed with two different $Ti_{50.5}Ni_{49.5}$ samples. The horizontal dashed lines marks A_F and M_F temperatures. DSC signal on cooling registered using the protocols shown in (a) is shown in (b) and (c), for continuous and interrupted scans, respectively. The inset in (c) shows the change of T_{PC} through the experiments in (b) and (c).

K, $M_F = 205$ K, $A_S = 240$ K and $A_F = 275$ K. For the binary Ni-rich Ni–Ti sample annealed at 1070 K is was easier to determine the transformation temperatures from the calorimetric signal than from the electric resistance. This is because of the above mentioned unusual temperature dependence of the resistance in the austenitic phase above the M_S/A_F temperature: it increases notably on cooling. This is normally considered as a premartensitic effect.

Figure 3.15b shows the temperature dependence of the relative temperature rate of the resistance. The $\frac{1}{R}\frac{\partial R}{\partial T}$ shows one maximum on cooling and one on heating, as the calorimetric signal. The peaks temperatures are 227 K on cooling and 251 K on heating. In addition, due to the premartensitic effect, there is a deep minimum in the right side of the peaks, specially on cooling. A comparison between both curves on cooling in panels (a) and (b) points to a good correspondence of peak temperatures, 225 and 227 K, in spite of the deep minimum in the $\frac{1}{R}\frac{\partial R}{\partial T}$ curve. On the other hand, the peak temperatures on heating differ significantly, 259 and 251 K, especially, taking into consideration that the temperature of the maximum of the $\frac{\phi}{m\beta}$, 259 K, is close to a zero of the $\frac{1}{R}\frac{\partial R}{\partial T}$ at 260 K. This discrepancy is due to the high negative temperature dependence of the resistance during the premartensitic effect which displaces the peak temperature of the $\frac{1}{R}\frac{\partial R}{\partial T}$ towards lower temperatures. The transformation peak on heating is more affected because it is lower than on cooling, it is at higher temperature (obviously) and the contribution of the premartensitic effect to the resistance is independent from the direction of the temperature scan.

Note that the premartensitic effect affects quite differently to the resistance and to the exchanged heat flux. During the premartensitic effect there is the generation of martensitic nuclei. The formation of nuclei do not generates/consumes a detectable quantity of heat, and then, the DSC will only register the heat exchanged produced by the growth of the nuclei during the martensitic transformation. By contrast, the formation of nuclei affects strongly the electrical conductivity of the sample which is sensitive to the characteristics of the crystalline lattice, like the density of crystalline defects.

The temperature dependence of the calorimetic signal $\frac{\phi}{m\beta}$ of the Ti-rich sample annealed at 920 K is presented in Figure 3.16a. The peak temperature for the direct B2→B19' transformation is 332 K and the one for the reverse transformation is 367 K. In its turn, the panel (b) of the same figure shows the temperature dependance of the relative temperature rate of the resistance. The $\frac{1}{R}\frac{\partial R}{\partial T}$ of the Ti-rich sample is obtained by subtracting the baseline due to the temperature dependence of the resistance in austenite

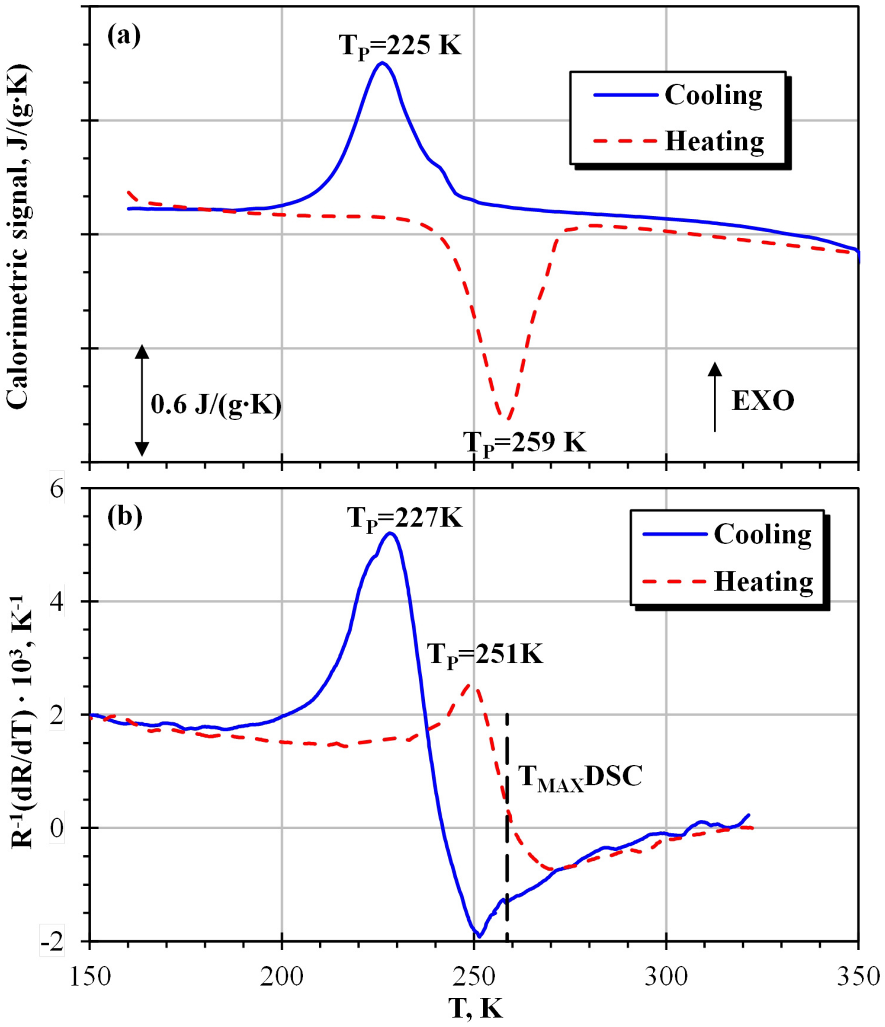

Figure 3.15: Temperature dependence of the calorimetric signal (a) and of the relative temperature rate of the resistance (b) for a sample of $Ni_{50.2}Ti_{49.8}$ alloy annealed at 1070 K. The transformation peak temperatures are indicated. The peak temperature of the calorimetric signal on heating is indicated.

and martensite outside the MT range. Similarly to the $\frac{\phi}{m\beta}$ in panel (a), the temperature derivative of the resistance presents two well defined peaks, one on cooling at 330 K and a second one on heating at 368 K. There is a very good correspondence between these peak temperatures a the ones of the DSC signal. This confirms the applicability of resistivity measurements in studying the isothermal/athermal nature of Ti-rich alloy.

For the case of the Ni-rich binary alloy annealed at 1070 K, two "different" samples (S1 and S2) were used in isothermal holding experiments. The only difference between samples S1 and S2 was their length: sample S1 was longer than the regular 12 mm for the rest of the used samples (about 22 mm). Thermal cycles and isothermal holding experiment were done with the sample S1, after that, the sample was cut to become the usual 12 mm length, renamed as S2 and more experiments registering the resistance were done. This was done for the following reason:

During the temperature ramp, there inevitably exists some temperature gradient in the sample. The temperature along the sample depends on the distance to the furnace because the nearer parts respond quicker to changes of the furnace's power. This gradient is reduced when the temperature is stabilized during an isothermal holding. Then, since the resistance is, in general, temperature dependent, the homogenization of the temperature along the sample produces an isothermal variation of resistance.

The relative changes of the resistance during the isothermal holding experiments may be quite smalls, for example, for the ternary iron-doped alloy, the maximum change of resistance during a single isothermal holding experiment is about 3% (with respect to the total resistance, $\frac{R(t)-R_0}{R_0}$), see curve registered at 170 K in Figure 3.5c. Thus in the majority of experiments the resistance variation will be smaller than a 1%. Therefore, using two samples of different length we can estimate whether or not this effect is comparable (in magnitude) with the isothermal transformation effect on the resistance.

On the other hand, for the same resistivity and sample's cross-section, longer samples have higher total electrical resistance and then higher isothermal variations of resistance. Therefore, the measurements of the small variations of resistance with time were more precise for larger samples. Then, short samples will avoid the contribution of the temperature gradient's change, but will not allow us to study small accumulation of the martensite volume fraction. In any case, if not meaningful effect of the length is observed when comparing the results of S1 and S2 samples, the contribution of the temperature gradient will be secondary and negligible.

Following the experimental protocol shown in section 2.7 in page 58, isothermal holding experiments were performed in the samples of binary Ni–Ti annealed at 1070 K and of binary $Ti_{50.5}Ni_{49.5}$ annealed at 920 K. The

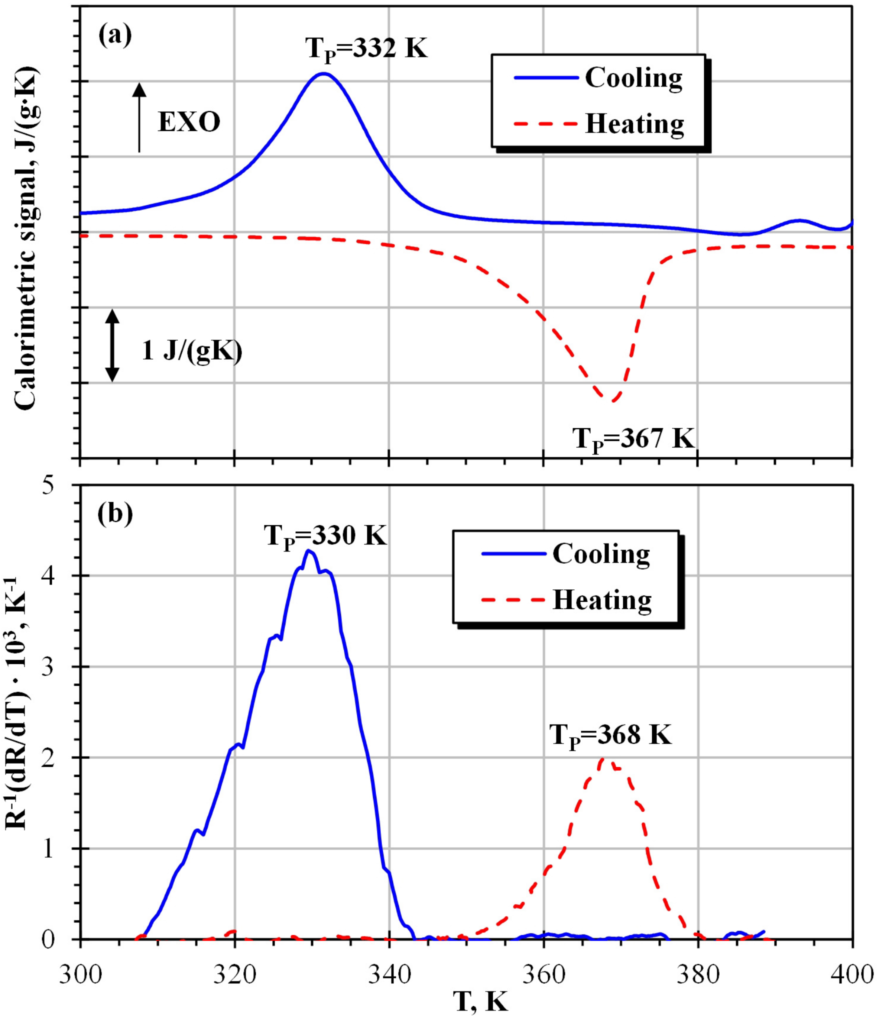

Figure 3.16: Temperature dependence of the calorimetric signal (a) and of the relative temperature rate of the resistance (b) for a sample of $Ti_{50.5}Ni_{49.5}$ alloy annealed at 920 K. The DSC scans were performed after 3 thermal cycles in the resistance experiments. The $\frac{1}{R}\frac{\partial R}{\partial T}$ data correspond to the cycles 2 and 3 in Figure 3.13b where the majority of isothermal dwellings were performed

x-axis represents the time elapsed from the moment when the temperature cycle is interrupted. R_0 is the value of the resistance at the inerruption of the cooling scan ($t = 0$ s). R_{MAX} and R_{MIN} are the values of the resistance at M_S and M_F, respectively. Naturally, R_{MAX} and R_{MIN} is different between the Ni-rich and Ti-rich samples.

Figure 3.17 shows a synthetic plot of the results of the isothermal holding experiments over the entire temperature range of the direct B2→B19' MT. The figure presents the time evolution of the resistance during these experiments. Specifically, panels (a) and (b) presents the results corresponding to the samples S1 and S2 of $Ni_{50.2}Ti_{49.8}$ alloy annealed 1070 K, respectively, and panel (c) the same for a sample of Ti-rich alloy. The results for the sample S1 in panel (a) show a clear change of the real part of the impedance with time. The isothermal variation of resistance clearly follows a logarithmic law (the curve is straight on a semilogarithmic scale) like in the previous cases in the R↔B19', Figures 3.5 and 3.6. The results for the sample S2 in panel (b) are similar to the results of the sample S1, as we would have expected: first, sample S2 is the sample S1 after have been cut, and second, the B2→B19' MT for this alloy/heat treatment is weakly dependent on the number of thermal cycles. The measurements in the sample S2 complete the points over the temperature spectra (spectra over the range of the direct and reverse B2↔B19' transformations). In addition, isothermal stop at 227 K was done in both, S1 and S2, obtaining a similar result. This proves than the contribution of the temperature gradient to the isothermal variation of resistance is negligible as compared to the contribution of the isothermal transformation. Therefore, the isothermal accumulation of resistance is maximum near the maximum of the relative temperature rate of the resistance at 227 K. In general, the effects of the thermal activated transformation is observed for the curves between 210 and 240 K, coinciding with the direct B2→B19' range.

In the other hand, the results for the Ti-rich sample shown in panel (c) of Figure 3.17 also shows clearly the isothermal variation of resistance. Specifically, the the accumulation of resistance is noticeable in the experiments performed at 320, 325, 330, 335 and 340 K, coinciding with the domain of the direct B2→B19' MT, Figure 3.16, like for the Ni-rich samples. Note the different resistance scale between the Ni-rich samples S1 and S2 (panels (a) and (b)) and the sample of $Ti_{50.5}Ni_{49.5}$ (panel (c)). A smaller amount of normalized resistance is accumulated in the last case.

As have been shown in the panels (b) and (c) of the Figure 3.13, both, the resistance and the transformation temperatures depends on the number of cycles n. Furthermore, the DSC exposed in Figure 3.14 demonstrates that these dependencies with n should take place during the martensitic transformation. Therefore, it is important to discern if the origin of these dependen-

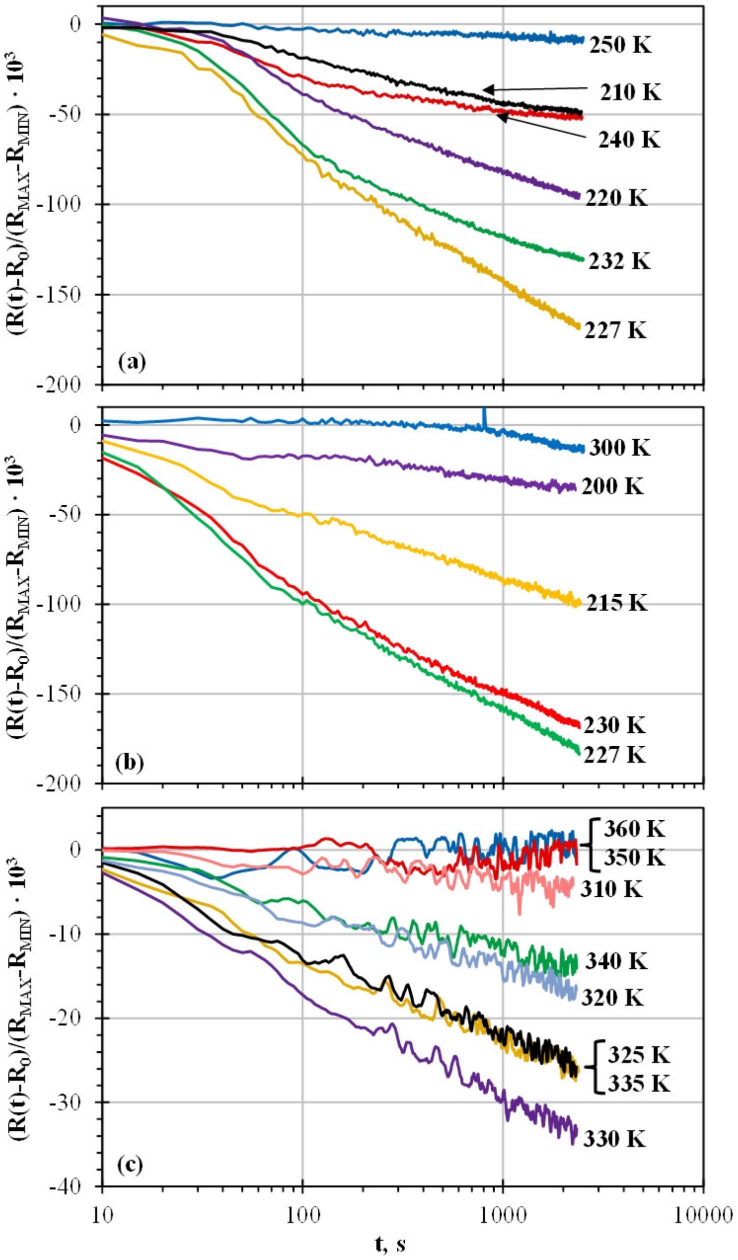

Figure 3.17: Time evolution of the resistance during interruptions of the temperature scan near and inside the direct B2→B19' transformation range for (a) the sample S1 of binary $Ni_{50.2}Ti_{49.8}$ annealed at 1070 K, (b) the sample S2 of binary $Ni_{50.2}Ti_{49.8}$ alloy annealed at 1070 K and (c) a sample of $Ti_{50.5}Ni_{49.5}$ alloy annealed at 920 K. Note different ordinate scales in (c) as compared with (a) and (b).

cies is an athermal process or can take place during the isothermal holding experiment. In the last case, that process can affect the resistance distorting the measurements or even being responsible of the isothermal accumulation of resistance in an otherwise athermal MT.

- First, the resistance increases as a consequence of thermal cycling, but it decreases during isothermal holding, Figure 3.17c. Therefore, the isothermal resistance variations and variations of resistance provoked by thermal cycling have different origins. The increase of resistance upon thermal cycling might be induced by the athermal generation of lattice defects during the MT.

- Second, if the MT temperatures decrease were produced during the isothermal stops, the austenite would get stabilized against martensite and the time-dependent reverse transformation would proceed. Since the resistance of the austenite is higher than that of the martensite, the increase of resistance would occur under isothermal conditions. This effect is also opposite to the observed kinetics of resistance in isothermal experiments. Thus, the experimentally observed isothermal variation of R is provoked neither by resistance variation nor by MT temperature shift during thermocycling.

Therefore, the isothermal change of resistance for curves from 320 to 340 K in Figure 3.17 should be attributed to the isothermal accumulation of B19' martensite. The same is true for the Ni-rich samples whose MT depend weakly on thermal cycling. Therefore, there is isothermal accumulation of martensite is the direct B2→B19' MT.

Figure 3.18 presents in a synthetic plot the time evolution of the resistance registered in different isothermal holding experiments within the transformation domain of the reverse B19'→B2 MT. Likely the Figure 3.17, panel (a) and (b) shows the results for the samples S1 and S2 of binary $Ni_{50.2}Ti_{49.8}$ alloy annealed 1070 K and panel (c) presents the results for the sample of $Ti_{50.5}Ni_{49.5}$ alloy annealed at 920 K. It is important to note that the ordinate scales in Figure3.18 is expanded per two as compared with the same scales in Figure 3.17. Even with the expanded scale, small or no isothermal variation of resistance are observed as compared with the equivalent results for the direct transformation. Results in panel (a) do not show isothermal accumulation of resistance. Only the curve registered at 240 K is clearly separated from zero. However, after the transitory period (the first 100 seconds where the temperature is not perfectly constant but there is the small overcooling/overheating), the variation of resistance is minor. The change of resistance with temperature during the transitory period have already been commented and is related with the magnitude of the relative temperature rate of the resistance. This effect is more evident for the curves registered at 247 K in panel (b), very close to the maximum of $\frac{1}{R}\frac{\partial R}{\partial T}$ at 251 K. Then, for the samples S1 and S2 the only curve which shows isothermal variations of resistance is the one registered at 252 K in Figure 3.18b. However, this isothermal change of resistance is small as compared with the ones within the direct B2→B19' transformation and, in addition, it has the opposite sign to the expected isothermal accumulation of B2 austenite.

Normally, if there is isothermal accumulation of resistance at a certain temperature, the logarithmic kinetics start when the temperature is stable after the overcooling/overheating. However, for some curves the logarithmic behavior starts at longer expositions than the time of the transitory effect, for example the curve at 300 K in Figure 3.17a or the curve at 259 K in Figure 3.18b. This phenomenon might be attributed to a need for an incubation time for the isothermal transformation.

On the other hand, for the case of the Ti-rich sample in panel (c) of the Figure 3.18, the resistance during interruptions of heating seems to decrease slightly with time. These isothermal variations of resistance are very small as compared with the effects observed for the direct transformation in Figure 3.17c. Furthermore, this small isothermal decrease of the resistance is observed even outside of the MT range, and, therefore, not related to the MT. The origin of this minor time-dependent decrease of the resistivity remains unclear. Note that precautions were taken to ensure that this effect is not equipment-related.

Figure 3.19 shows a comparison between the temperature-dependence of the relative temperature rate of the resistance $\frac{1}{R}\frac{\partial R}{\partial T}(T)$ and the isothermal transformation rate Z for interruptions of cooling (a) and of heating (b) for the samples S1 and S2 of binary $\mathrm{Ni}_{50.2}\mathrm{Ti}_{49.8}$. The curves "-Z Cooling" in panel (a) and "Z Heating" in panel (b) are composed by Z values calculated from curves of experiments performed with the samples S1 and S2. They are plotted together because both samples have the same composition and heat treatment, furthermore, sample S2 is a part of the sample S1. Therefore, the $Z(T)$ curves are composed by values of the sample S1 (open circles) and values of the sample S2 (open diamonds).

Panel (a) demonstrates that Z and $\frac{1}{R}\frac{\partial R}{\partial T}$ within the range of the direct B2→B19' transformation are nearly proportional. Moreover, Z values of the both samples (S1 and S2) are in good agreement. It corroborates that the temperature gradient contribution to the isothermal accumulation of resistance is small as compared with the contribution caused by the isothermal transformation. Concluding, results show that direct martensitic transfor-

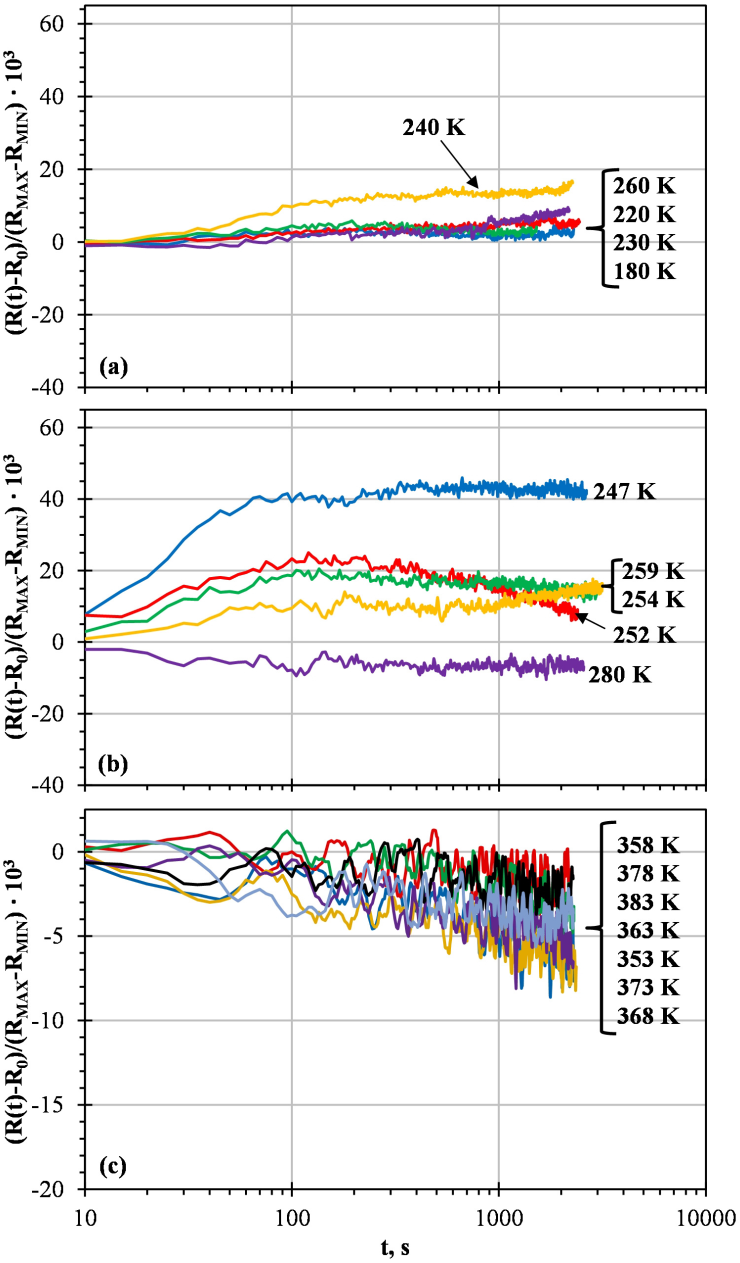

Figure 3.18: Time evolution of the resistance during interruptions of the temperature scan near and inside the reverse B19'→B2 transformation range for (a) the sample S1 of binary $Ni_{50.2}Ti_{49.8}$ annealed at 1070 K, (b) the sample S2 of binary $Ni_{50.2}Ti_{49.8}$ alloy annealed at 1070 K and (c) a sample of $Ti_{50.5}Ni_{49.5}$ alloy annealed at 920 K. Note different ordinate scales in (c) as compared with (a) and (b).

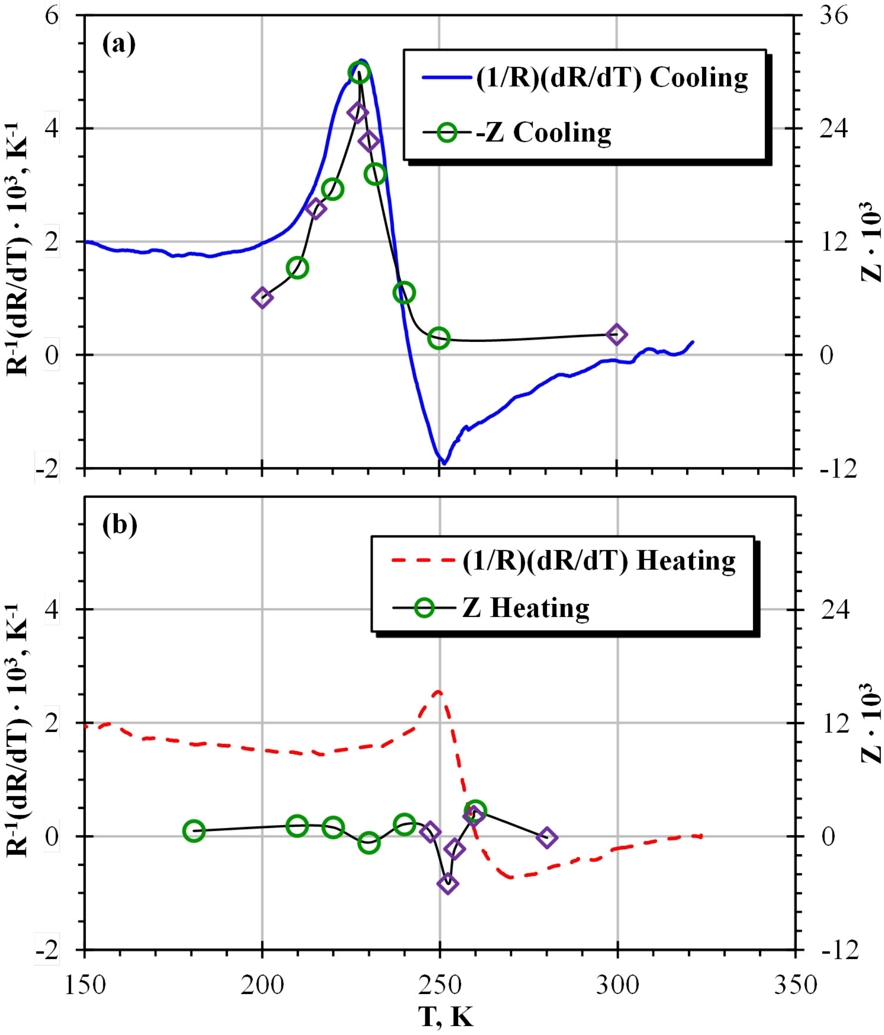

Figure 3.19: Comparison of the temperature dependence of the relative temperature rate of the resistance, $\frac{1}{R}\frac{\partial R}{\partial T}$ and of the relaxation rate Z for a sample of $Ni_{50.2}Ti_{49.8}$ quenched from 1070 K. In panel (a): $\frac{1}{R}\frac{\partial R}{\partial T}$ on cooling (continuous line), -Z calculated from isothermal holdings upon interruptions of cooling from sample S1 (open circles) and from sample S2 (open rhombus). In panel (b):$\frac{1}{R}\frac{\partial R}{\partial T}$ on heating (dashed line), Z calculated from isothermal holdings upon interruptions of heating from sample S1 (open circles) and from sample S2 (open rhombus).

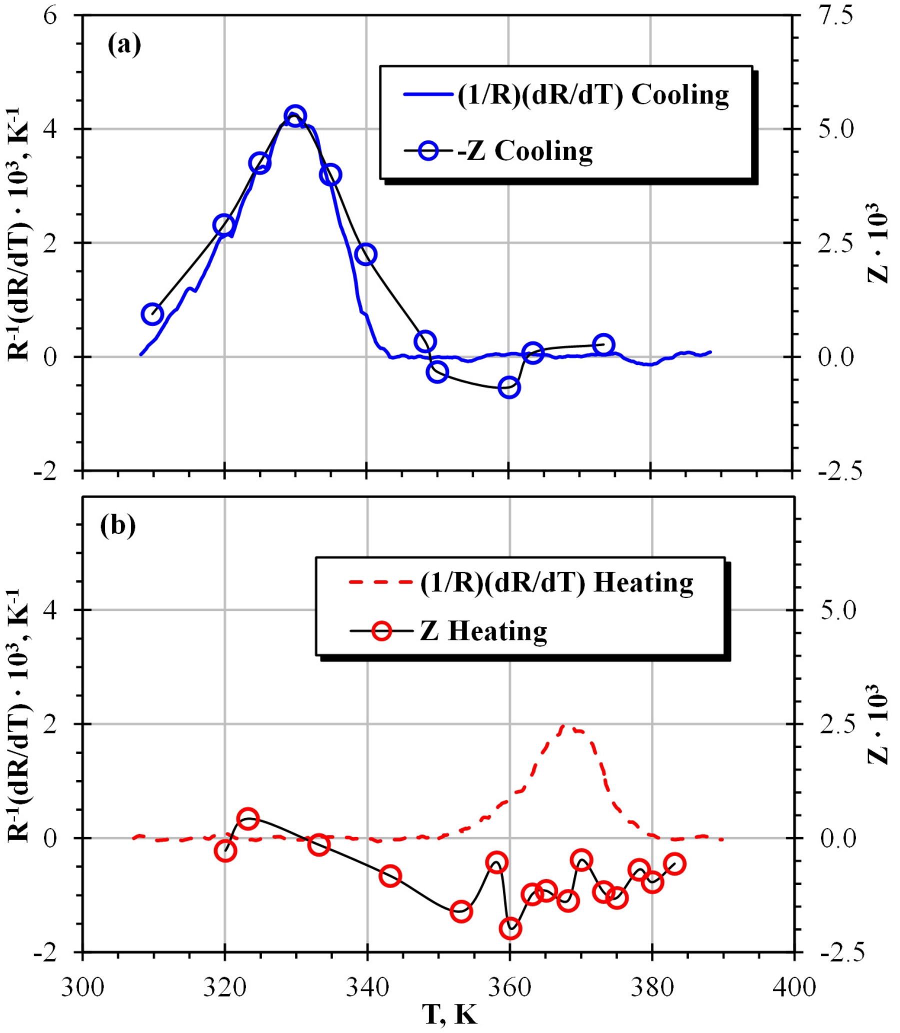

Figure 3.20: Comparison of the temperature dependence of the relative temperature rate of the resistance, $\frac{1}{R}\frac{\partial R}{\partial T}$ and of the relaxation rate Z for a sample of $Ti_{50.2}Ni_{49.8}$ annealed at 920 K. In panel (a): $\frac{1}{R}\frac{\partial R}{\partial T}$ on cooling (continuous line), -Z calculated from isothermal holdings upon interruptions of cooling (open circles). In panel (b):$\frac{1}{R}\frac{\partial R}{\partial T}$ on heating (dashed line), Z calculated from isothermal holdings upon interruptions of heating (open circles).

mation B2→B19’ has isothermal character.

Panel (b) of the figure 3.19 shows that the data on the relaxation rate Z are scattered around 0. The only point that stand out is the diamond (sample S2) at 252 K which correspond to the isothermal holding experiment exposed in Figure 3.18b. However, the magnitude of this isothermal decrease of resistance is small and the resistance is expected to increase with the accumulation of austenite. Then, there is no isothermal accumulation of austenite or his effect produced over the resistance is too small in our experimental observation time window. The reverse B19’→B2 transformation shows an athermal behavior.

The temperature dependence of the relaxation rate Z derived from the data shown in Figures 3.17c and 3.18c is compared with the relative temperature rate of the resistance $\frac{1}{R}\frac{\partial R}{\partial T}$ in the Figure 3.20 for cooling (a) and of heating (b) for a samples of Ti-rich Ti–Ni annealed at 920 K. The data demonstrate excellent correspondence between these parameters for the direct MT. On the other hand, the isothermal effects during the reverse MT are very small and have a sign opposite to the one expected for the IMT, see Figure 3.18c. Thus, panels (a) and (b) of the Figure 3.20 show that isothermal effects during the reverse MT, if any, are at least four times less intense than during the direct one, and are comparable with the scatter of experimental data. Then, the reverse B19’→B2 MT may be considered as an athermal MT, at least, from an experimental point of view.

3.3 Results for the B2-B19-B19’ MT

The athermal/isothermal behavior of the two stage B2↔B19↔B19’ MT has been investigated. These were the transformations paths which present more difficulties: some characteristics of these transformations complicate the analysis of the isothermal accumulation by means of the resistance variations, which do not allow us to have the same level of certainty of the conclusions as for the B2↔R↔B19’ and B2↔B19’ transformation paths.

The B2↔B19↔B19’ MT has been studied in different samples of ternary Ni–Ti–Cu alloys with different Cu content, but the data for only one of these alloys are shown in the present work: $Ti_{52.4}Ni_{39.7}Cu_{7.9}$ heat treated during 30 minutes at 1120 K, followed by air cooling. This composition exhibits the two stage B2↔B19↔B19’ transformations as shown by Nam et al. [112,113].

Figure 3.21 presents in panel (a) the temperature dependence of the resistance in a continuous temperature cycle for a sample of $Ti_{52.4}Ni_{39.7}Cu_{7.9}$ alloy annealed at 1120 K. The cooling and heating curves follow different paths for around 100 K. However, the maximum hysteresis along this temperature domain is about 15 K. This datum indicates that the direct and reverse transformation ranges are very broad. Moreover, two clear shoulders appear at 326 K on cooling and at 339 K on heating. These shoulders are due to the fact that the hysteresis is generated not by a single transformation, but by the overlapped two stage B2↔B19↔B19’ MTs. To clarify the behavior of the resistance, its relative temperature rate, $\frac{1}{R}\frac{\partial R}{\partial T}$, is shown in panel (b) and is compared with the calorimetric signal presented in panel (c). $\frac{1}{R}\frac{\partial R}{\partial T}$ curve shows a sharp peak on cooling at 333 K and a similar one on heating at 344 K. These peaks are overlapped with lower intensity and very broad maxima that extend down to about 200-250 K. According to previous studies [112, 114], the sharp peaks correspond to the B2↔B19 MTs while the broad ones to the direct and reverse B19↔B19’ MTs. In its turn, the DSC signal in panel (c) shows only one peak for either cooling and heating scans. However, these peaks are somewhat asymmetric: they demonstrate a tail that extends to temperatures at least 50 K lower than the peak temperatures [112]. The sharp peaks are associated again with the direct and reverse B2↔B19 transformations. The DSC signal peaks are at 332 K on cooling and 347 K on heating. These peak temperatures are in excellent agreement with the resistance data, Figure 3.21b. The difference between the peak temperatures on cooling and heating of around 11-15 K indicates a substantially larger hysteresis than that of B2↔R transformation. Although the long tail may be related to the direct and reverse B19↔B19’ transformations, they are not clearly revealed in the calorimetric signal. However, the existence of the B19↔B19’ MTs is evident from the resistance data in panels (a) and (b). The resistance data show that the transformation range of direct B19→B19’ and reverse B19’→B19 MTs are about 74 K and 77 K, respectively. Therefore, these transformations are too diffuse to be clearly revealed by the DSC scan. The existence of the two stage transformation is also corroborated in alloys of similar composition by other techniques in the literature, for example, by measurements of the internal friction where the temperature-dependence of the frequency reveals both transformations [115, 116].

One may note that there are zeros of the relative temperature rate of the resistance, Figure 3.21b. Inside the B19↔B19’ transformation range: there is one zero on cooling at 263 K and the other one on heating at 270 K. There is a relation of proportionally between the relaxation rate Z of an IMT and the relative temperature rate of the resistance $\frac{1}{R}\frac{\partial R}{\partial T}$ that arises from some of the previous results, see, for example, Figure 3.12 in Section 3.1. This relation seem to suggest that the zeros of $\frac{1}{R}\frac{\partial R}{\partial T}$ implies a zero of Z. Then, if the cycle is interrupted at the temperature of one of these zeros, there will not be any isothermal variation of resistance independently of whether or not the martensite volume fraction varies with time. However, this reasoning is

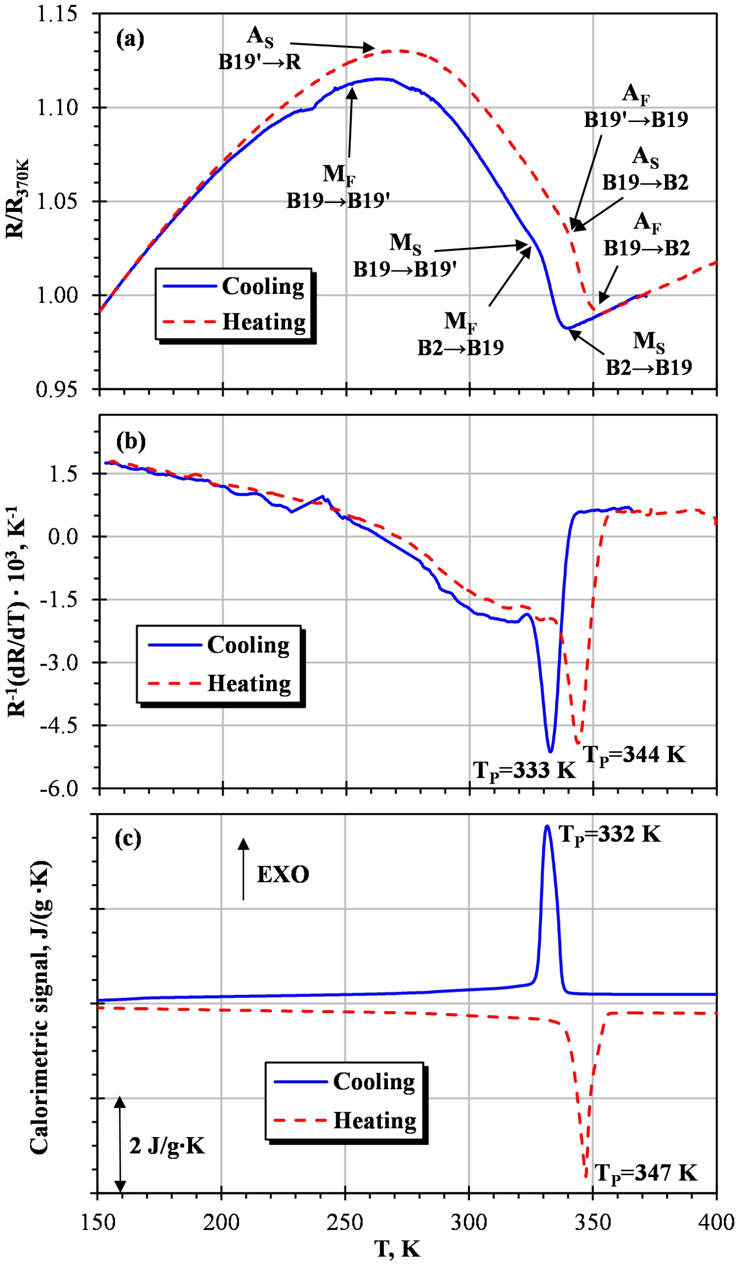

Figure 3.21: Temperature dependence of (a) the resistance, (b) the relative temperature rate of the resistance and (c) the calorimetric signal for a sample of $Ti_{52.4}Ni_{39.7}Cu_{7.9}$ alloy annealed at 1120 K. Resistance data in (a) are normalized to the value of resistance at 370 K. The transformation temperatures are pointed in (a) and the peak temperatures are indicated in (b) and (c).

incorrect.

First, as commented previously, $\frac{1}{R}\frac{\partial R}{\partial T}$ curve is a sum of several contributions and the resistance variation is caused not only by the MT.

- The resistance increases upon cooling from B19 phase to B19' martensite. Hence, this MT produce a negative $\frac{1}{R}\frac{\partial R}{\partial T}$ peak.

- On the other hand, the resistance increases with temperature due to scattering of conduction electrons by thermal phonons. Therefore, its contribution to the temperature derivative of the resistance is positive.

Therefore, a zero of the temperature dependence of the resistance appears when the different contributions compensate each other.

Second, Z may only be proportional to the contribution to $\frac{1}{R}\frac{\partial R}{\partial T}$ caused by the MT. Therefore, the good correspondence between Z and the total $\frac{1}{R}\frac{\partial R}{\partial T}$ in the case of the R→B19' MT for the alloy of $Ti_{50}Ni_{47.4}Fe_{2.6}$ quenched from 1270 K is only a good approximation. This good correspondence is because the contribution of scattering of conduction electrons by thermal phonons to $\frac{1}{R}\frac{\partial R}{\partial T}$ is quite small as compared with the contribution due to the MT. This is not true in general, especially, within the transformation range of the B19↔B19' MTs where both contributions should be of similar order.

Third, even if the different temperature dependencies of the resistance compensate each other, the time dependence of the resistance would be different of zero since the contribution to the resistance caused by the scattering of conduction electrons by thermal phonons does not depend on time.

Fourth, since the resistance is stable with the number of cycles and the transformation temperatures are not quite high, other effects that can isothermally vary the resistance, like the atomic diffusion and the isothermal generation of crystalline defects, are discarded in the ternary Cu-doped alloy. Therefore, the unique time dependence of the resistance may be originated by the isothermal variation of martensite.

In conclusion, the isothermal variation of resistance will be zero if there is no variation of the martensite volume fraction (the MT is athermal) or if the resistance is insensitive to the variation of martensite (the resistivity of both phases are equal, being this one a quite hypothetical case). Therefore, the behavior of Z should be independent of whether or not there is a zero in the temperature derivative of the resistance. Hence, these zeros of the $\frac{1}{R}\frac{\partial R}{\partial T}$ may not affect the study of the isothermal accumulation of austenite/martensite by means of the isothermal variation of resistance. The comparison between the data shown in the panels (b) and (c) of Figure 3.21 indicate that the isothermal evolution of the resistance is a good method to analyze the behavior of the transformation for the B2↔B19 MTs, but could not be suitable for the very diffuse B19↔B19' MTs.

Next, many isothermal holding experiments were performed in the ternary $Ti_{52.4}Ni_{39.7}Cu_{7.9}$ alloy annealed at 1120 K. The number of experiments is larger than in the previous samples with different composition/heat treatment temperature due to the difficulty to determine whether or not there is isothermal accumulation of martensite/austenite: the isothermal holding experiments were usually repeated for the most problematic temperatures.

This difficulty mainly stems from the characteristics of the B19↔B19' transformation:

- The B19↔B19' transformation range is very broad, about 75 K, see Figure 3.21. Consider that: first, the isothermal transformation rate Z, and then also the amount of isothermally transformed martensite in a single holding experiment, is often proportional to the transformation rate in a continuous cycle; second, a broader transformation means a lower relative temperature rate of the resistance as compared with narrow transformations that produces similar total resistance variations. Therefore, if the B19↔B19' MTs are isothermal, they will produce a small isothermal change of the martensite volume fraction during a normal isothermal holding experiment.

- The total variation of resistance within the range of the B19↔B19' MTs is quite small. The total change is about 9% of R_{370K}, but this change includes the temperature dependence of the resistance due to phonon scattering. Since the B2↔B19 and B19↔B19' MTs are overlapped on both, cooling and heating, it is hard to estimate the contribution of the phonon scattering. This contribution has the sign opposite to the resistance variation due to the transformation. Then, subtracting the baseline from Figure 3.21b and integrating one gets a approximate variation during the B19→B19' MT of about 11%. This value is relatively small as compared with other transformations which show isothermal accumulation of resistance. The total variation of resistance within the range of the B2→B19' MT varies between 10–13%, Figure 3.13, and within the range R→B19' MT between 16–23%, Figure 3.1.

Therefore, the B19↔B19' MTs have a relatively small variation of resistance and a broad range. As a result, the relative temperature rate of the resistance of the B19↔B19' transformation is around $2 \cdot 10^{-3}$ K^{-1}, whereas the previous studied alloys present values for the $\frac{1}{R}\frac{\partial R}{\partial T}$ of the order of 10^{-2} K^{-1}.

The conclusion is that, even whether this transformation is isothermal, the isothermally accumulated martensite during the experiments will be low. In addition, and since the sensitivity of the resistance to the change of F is poor as compared with other alloys, the possible isothermal small variation of F will produce a tiny change of R. These resistance variations are in the low limit of the real experimental accuracy of our measuring system. In other words, electronic noise and small change in the conditions may generate changes of resistance of similar order than the ones produced by the IMT, and hence, it is difficult to discern between the athermal/isothermal behavior. That is why these measurements required special care and often resulted in doubtful points.

On the other hand, the data of the isothermal holding experiments in the Cu-doped Ti–Ni–Cu alloy were treated differently from the same data for the B2↔R↔B19' and B2↔B19' cases. Formerly, the viscosity or isothermal transformation rate Z was calculated using equation (2.31) (page 45) which needs the normalization conditions R_{MAX} and R_{MIN}. However, it is hard to estimate precisely these variables in the present case:

- The B2↔B19 and B19↔B19' MTs are noticeably overlapped on both, cooling and heating. This fact only permits to give the transformation temperatures (M_S, M_F, A_S and A_F) for the partial transformation. In addition, both transformations coexists as shown by Fukuda et al. [117]: B19' phase grows inside orthorhombic B19 plates at the same time that these are growing concluding the B2→B19 transformation. This fact ensures a non monotonic relation between the accumulation of the martensite volume fraction and the variation of resistance. Therefore, only an apprxomation to the variation of resistance during the partial transformation can be estimated and, furthermote, it should be a quite roughly calculation since it is not possible to choose a realistic baseline. The baseline is always an approximation, but since the transformations are overlapped it is not possible to intuit its behavior during the transformations.

- The B19↔B19' MTs are very broad and the variation of resistance within the transformation range is relatively low. Then, the contribution of the phonon scattering to the change of resistance is neither negligible nor can be estimated precisely.

- The change of resistance during the B2↔B19 MTs is tiny. These transformations have the advantage, as compared with the B19↔B19' MTs, that the transformation range is narrow. However, the small variation of resistance makes that the above mentioned error in calculating R_{MAX} and R_{MIN} is huge in comparison.

Therefore, instead of calculate Z, Z' is calculated using equation (2.32) in page 46 which is always applicable. This is calculated using R_0, the resistance at the interruption of the thermal cycle ($t = 0$). Then, Z' is independent of the sample's shape. Unfortunately, thus way has two disadvantages. First, calculated Z' for different transformation paths in samples with different composition/annealing temperature cannot be compared. And second, the temperature dependence of R_0 introduces a temperature dependence to Z' external to the isothermal accumulation of product phase. In the present case, the temperature dependence of R_0 is small and do not affect significantly the results.

Time evolution of the resistance, expressed as $\frac{R-R_0}{R_0}$, after interruption of the thermocycle at different temperatures is shown in Figure 3.22 for interruptions during cooling and in Figures 3.23 and 3.24 for interruptions on heating.

In Figures 3.22 and 3.23, the data from the isothermal holding experiments have been separated in three panels. This separation is not made depending on the temperature of the interruption. Instead, in any panel may appear data corresponding to stops inside and outside the B2↔B19 and B19↔B19' transformations. These time-dependence curves are classified as "good", "regular" or "bad" based on the degree of certainty that they visually transmit. The curves classified as "good" are the ones which seems quite straight in logarithmic axis and its data is fairly scattered. The ones classified as "regular" have no or little time-dependence in comparison with the quick variations due to noise or have a large change of resistance during the transitory period, as compared with the ulterior time dependence. They may also correspond to experiments performed at temperatures that require long incubation times. Finally, the curves named as "bad" present important irregularities: the data is very high scattered, there are jumps and/or abnormal changes of the time dependent slope. As commented above, a large number of isothermal holding experiments were performed, then only some representative curves are shown in Figures 3.22, 3.23 and 3.24 for clarity.

Panels (a), (b) and (c) of Figure 3.22 show the "good", "regular" and "bad" curves, respectively, for interruptions on cooling. Panels (a) and (b) demonstrate that, in general, there is an increase of resistance with dwelling time and during the transitory period. The variation of resistance during the transitory stage is important for curves registered between 300 and 340 K, specially within the range of the direct B2→B19 MT since the T-dependence of R is the highest. There is decrease of resistance during the transitory stage

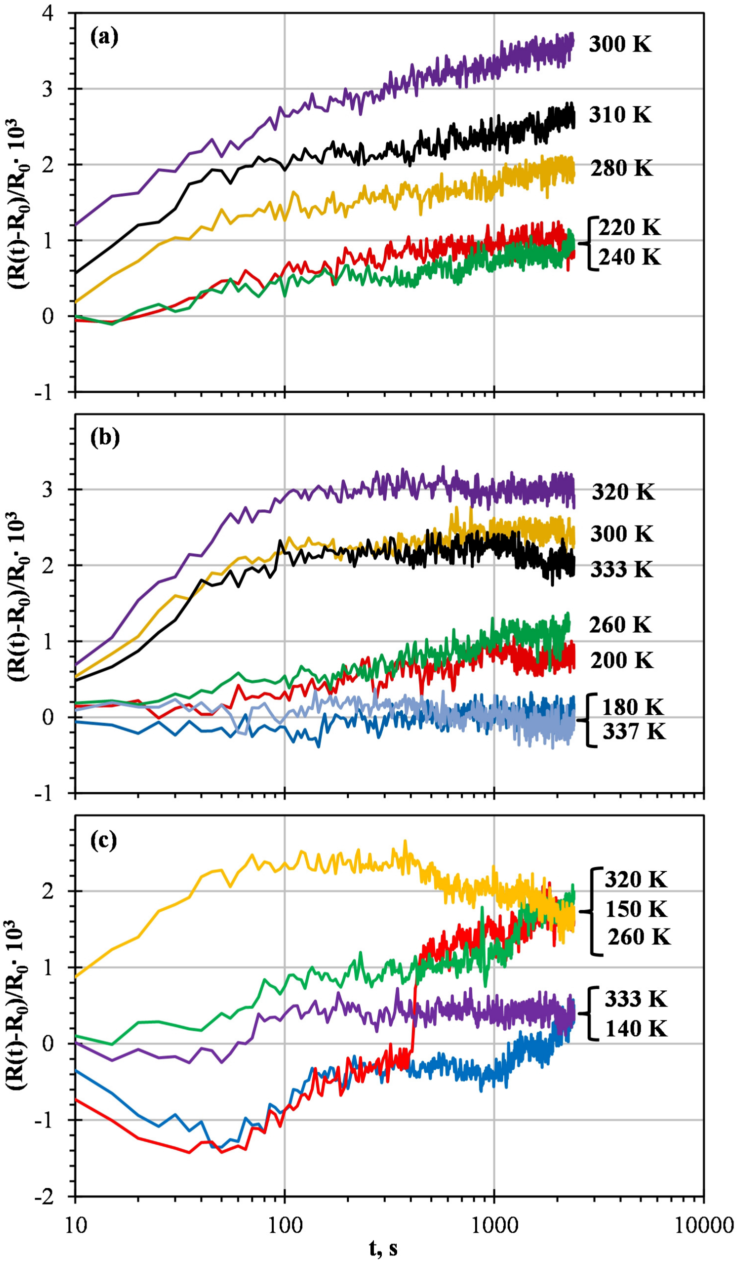

Figure 3.22: Time evolution of the resistance during interruptions of the temperature scan near and inside the direct B2→B19 and B19→B19’ MTs range for a sample of $Ti_{52.4}Ni_{39.7}Cu_{7.9}$ alloy annealed at 1120 K. Curves are classified as (a) “good”, (b) “regular” and (c) “bad” depending on how much they resemble a logarithmic dependence without jumps and scattered data.

only for the curves registered at 140 K and 150 K in panel (c) which are far below the maximum of R, ~270 K, and M_F. The curves registered at 300 and 310 K in panel (a) present clear isothermal accumulation of resistance. These curves are within the range of the B19→B19’ MT. However, some isothermal accumulation seems to take place for stops at lower temperature, even at temperature below M_F (about 252 K). This fact points to the possibility that the very diffuse B19→B19’ transformation is not completed during a normal temperature cycle.

Panel (a) of the Figure 3.23 present the data for the interruptions of the T-scan on heating classified as “good”. Only three curves were classified as “good” which show a clear isothermal decrease of the resistance without much signal-to-noise ratio. These curves, registered at 300, 320 and 335 K, are within the transformation range of the reverse transformations. If these data is compared with the one shown in panel (a) of Figure 3.22, one can observe that the isothermal effects registered on both, cooling and heating, are quite similar in magnitude, but have opposite sign. The last is the expected situation for a isothermal MT, while the former is different from previous transformation paths where the accumulation of resistance during isothermal holding experiments on heating were noticeable smaller than during experiments on cooling; compare, for example, data shown in Figures 3.5 and 3.6. The resistance data obtained from the interruptions of the heating scan which are classified as “regular” are shown in the panel (b) of the Figure 3.23. These curves were taken in a wide range of temperatures and do not show important accumulation of resistance. The decrease of resistance shown by the curve registered at 260 K may correspond to isothermal accumulation of B19 phase after some incubation time. However, this temperature is close to the start temperature of the reverse B19’→B19 MT, about 262 K, and, comparing with previous cases, little isothermal accumulation is expected. Therefore, it is risky to suggest that the curve at 260 K show isothermal accumulation of B19 phase.

The data shown in the panel (c) of the Figure 3.23 and in the Figure 3.24 correspond to the isothermal holding experiments performed on heating which present more irregularities. These curves were classified as “bad” for both plots. The data are separated in different plots because the variation of resistance of the curved presented in Figure 3.24 is very large in comparison with any other. Note that the vertical axis in Figures 3.22 and 3.23 have the same magnitude, but displaced by 2. In its turn, the scale of the resistance axis in the Figure 3.24 is more than three times larger than its homonyms in the Figures 3.22 and 3.23. The curves in panel (c), Figure 3.23, correspond to stops between 200 and 280 K. This is below and above A_S (B19’→B19, 262 K), but far from the overlap between the revers transformations, ~330 K.

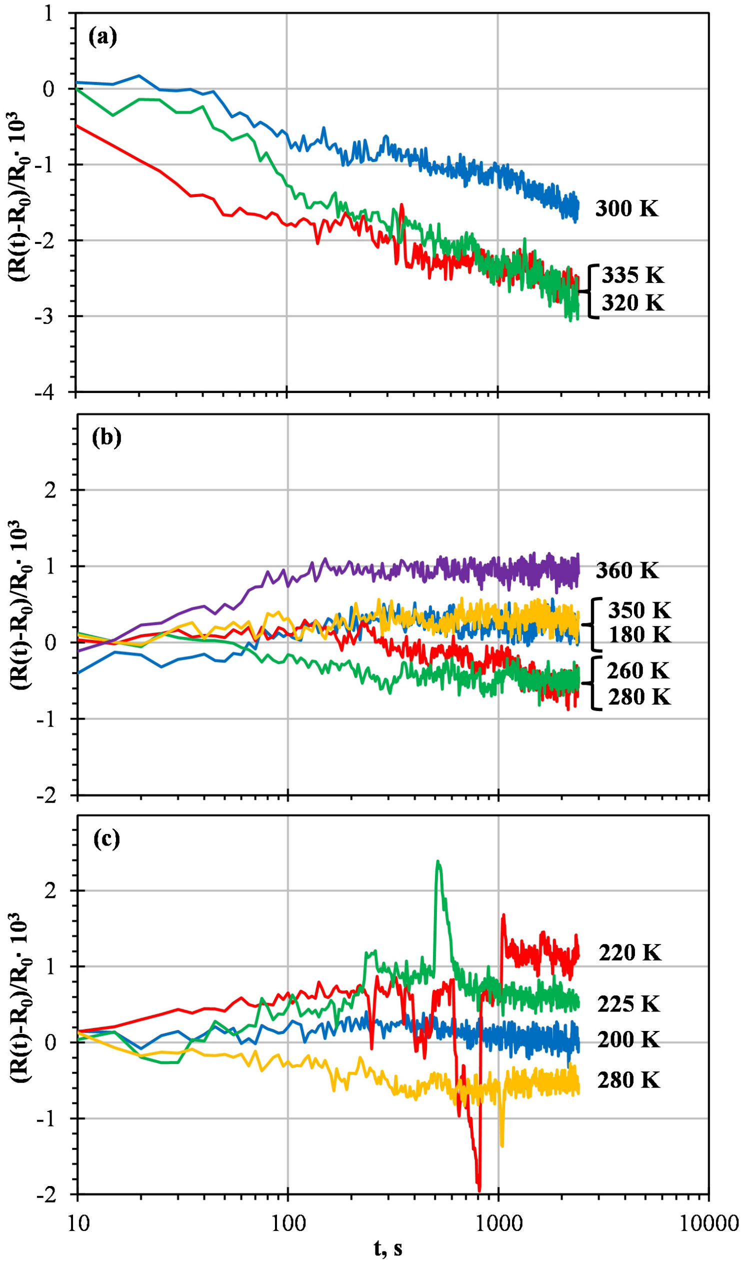

Figure 3.23: Time evolution of the resistance during interruptions of the temperature scan near and inside the reverse B19’→B19 and B19→B2 MTs range for a sample of $Ti_{52.4}Ni_{39.7}Cu_{7.9}$ alloy annealed at 1120 K. Curves are classified as (a) “good”, (b) “regular” and (c) “bad” depending on how much they resemble a logarithmic dependence without jumps and scattered data.

Therefore, for this range of temperatures, some curves present big instability, like the ones at 220 and 225 K, but the final change of resistance during the isothermal period is relatively small.

In Figure 3.24, data are from experiments performed between 320 and 344 K. The curves present a big change of resistance over time, big jumps and, even, extreme noise-to-signal ratio (see the upper curve at 344 K). The resistance variation with time is not consistent along these curves, for example, they show a big total change of the resistance, but curves at 340 K and both at 344 K present nearby no change between 100 and 400 seconds. Also the curve at 320 K has relatively low time-dependence in this range, as compared with its posterior evolution after some big jumps. All these curves were performed at temperatures within the range of the reverse MTs, specially, three of them are inside the domain of the reverse B19→B2 MT. Despite the important total variations of resistance over time in these curves, it is hardly attributable to the possible isothermal transformation, specially for the curves within the range of the reverse B19→B2 MT.

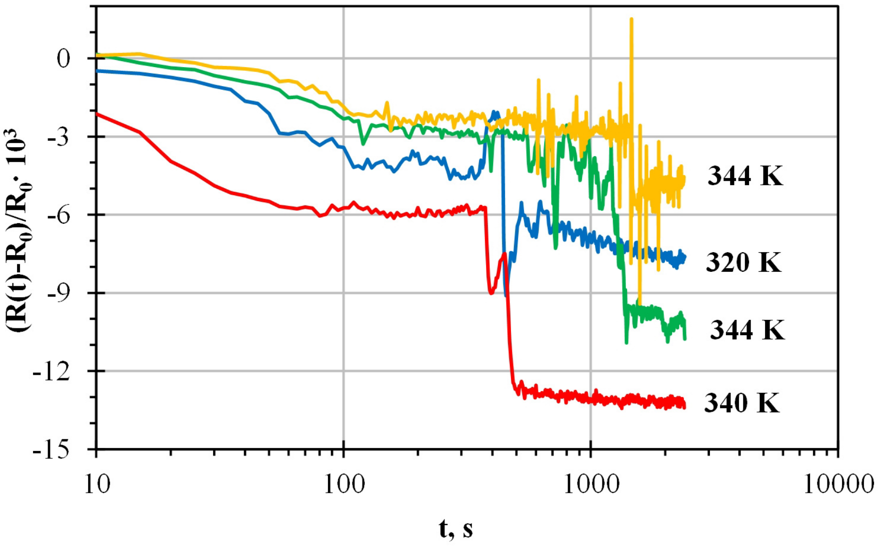

Figure 3.24: Time evolution of the resistance during interruptions of the temperature scan near and inside the reverse B19'→B19 and B19→B2 MTs range for a sample of $Ti_{52.4}Ni_{39.7}Cu_{7.9}$ alloy annealed at 1120 K. Shown curves are classified as "bad" and demonstrate bigger isothermal variation of resistance that the curves presented in panel (c) of the Figure 3.23.

The classification of the data from the isothermal holding experiments as "good", "regular" or "bad" is rather subjective (the limits are unclear/undefined), but it will be helpful in an attempt to extract more reliable information from the experimental data in this specially complicate case.

Figure 3.25 shows a synthetic plot of the relaxation rate Z' calculated from data obtained between 150 K and 360 K in several scans on (a) cooling and (b) heating for a sample of $Ti_{52.4}Ni_{39.7}Cu_{7.9}$ alloy annealed at 1120 K. The relaxation rate is confronted with the relative temperature rate of the resistance in an uninterrupted temperature scan. The points of Z' are represented with different symbols depending on the classification used in the Figures 3.22, 3.23 and 3.24: open circles ("good" curves), plus signs ("regular" curves) and open diamonds ("bad" curves).

The values of Z' do not show a good correlation with the relative temperature rate of the resistance $\frac{1}{R}\frac{\partial R}{\partial T}$ neither on cooling nor on heating. This correlation was the criteria for choose the scale of the Z-axis in previous transformation paths, e.g. Figure 3.19. In the present case, these axis were chosen arbitrary to keep the Figure 3.25 clear. As a consequence, the points may seem to be undoubtedly different from zero. However, in fact the obtained isothermal resistance variations are very small. This do not indicated that these transformations are athermal because, as has been already commented, it is expected by the transformation characteristics that the isothermal accumulation of martentise will be low and produce tiny variation of resistance.

The distribution of the "good", "regular" and "bad" points of Z' indicates:

- On cooling, the points for the isothermal results classified as "good" are spread between 170 and 320 K, being the Z'-points at 300 K and at 310 K the ones with higher values. The accumulation of the "good" values within the range of the direct B19→B19' MT points to the isothermal nature of this transformation path. However, the isothermal effects are observed well below M_S in some experiments classified as "good" or "regular". Therefore, the direct B19→B19' MT may not be completed during a normal temperature scan.

- Within the range of the direct B2→B19 transformation there is an accumulation of "regular" and "bad" points. The data is quite scattered and many of the points have negative value (note that $-Z'$ is displayed in panel (a)). Then, there were a decrease of the resistance during many experiments within this range. This is in contradiction with the increase of the resistance during the direct B2→B19 MT: it is expected that if there were isothermal accumulation of B19 phase, the resistance would increase with time. Therefore, no clear isothermal effects are observed during the direct B2→B19 MT.

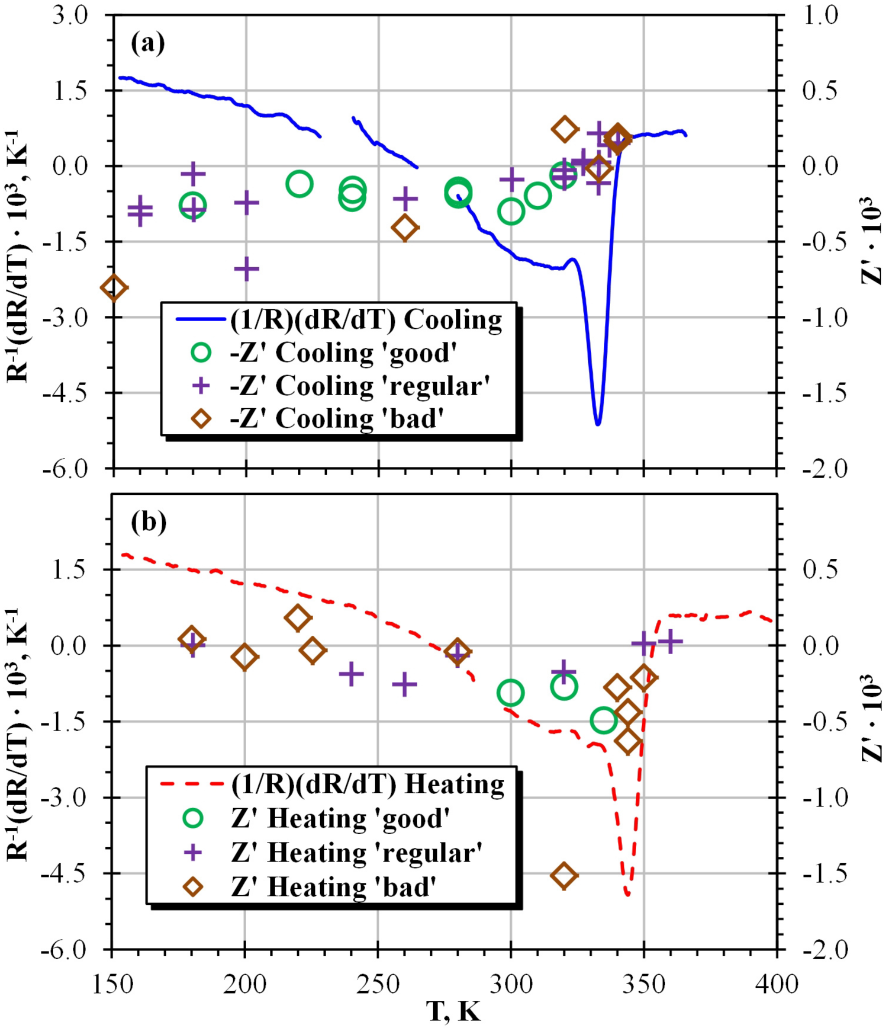

Figure 3.25: Comparison of the temperature dependence of the relative temperature rate of the resistance, $\frac{1}{R}\frac{\partial R}{\partial T}$ and of the relaxation rate Z for a sample of $Ti_{52.4}Ni_{39.7}Cu_{7.9}$ alloy annealed at 1120 K. In panel (a): $\frac{1}{R}\frac{\partial R}{\partial T}$ on cooling (continuous line), -Z calculated from isothermal holdings upon interruptions of cooling which are classified as "good" (open circles), "regular" (plus signs) or "bad" (open diamonds). In panel (b):$\frac{1}{R}\frac{\partial R}{\partial T}$ on heating (dashed line), Z calculated from isothermal holdings upon interruptions of heating which are classified as "good" (open circles), "regular" (plus signs) or "bad" (open diamonds).

- On heating, panel (b) of the Figure 3.25, only the data from three experiments were classified as “good”: 300 K, 320 K and 335 K. They were performed within the domain of the reverse B19’→B19 MT. This facts reinforces the idea that the B19↔B19’ MTs are isothermal. However, as shown by Figure 3.24, the system seem to be very unstable within this range, and the data have limited credibility despite the experiments within the range of the B19↔B19’ MTs have the cleanest and best fitted time dependencies.

- In both panels, (a) and (b), the points classified as “regular” or “bad” are more likely to be at low temperatures, below M_F, and within the B2↔B19 transformation range, specially on heating. While on cooling the experiments within the direct B2→B19 MT are scattered, but the average value of Z' is close to zero, on heating the data for the reverse B19→B2MT are more problematic but are clearly different from zero in average. Z' is calculated for these experiments with the data previous to the jumps, see Figure 3.24. They gives values of Z' comparable to the ones within the B2↔B19 transformation range supposed to be isothermal. However, the quality of the logarithmic fitting is evidently different. As commented above, the variation of resistance with time within the range of the reverse B19→B2 transformation is inconsistent and includes periods with almost no time-dependencies.

In conclusion, despite the relative uncertainty, the B19↔B19’ MTs are likely to be classified as isothermal, the direct B2→B19 MT is athermal, and the reverse B19→B2 MT lacks on appropriate data corroborating its isothermal nature, and then it may be classified as athermal like the direct transformation.

3.4 Classification of the athermal/isothermal transformations in the Ni–Ti–X system

According to the results obtained for different samples and heat treatments, the following classification for the different MTs of the Ni-Ti-X alloy system can be suggested, Figure 3.26.

The nature of the two stage B2↔R↔B19’ MT was discussed in Section 3.1. According to the results obtained for the ternary $Ti_{50}Ni_{47.4}Fe_{2.6}$ alloy (see e.g. Figure 3.12 in page 104), the “viscosity” parameter, Z, takes non-zero values only within the transformation ranges of the direct R→B19’

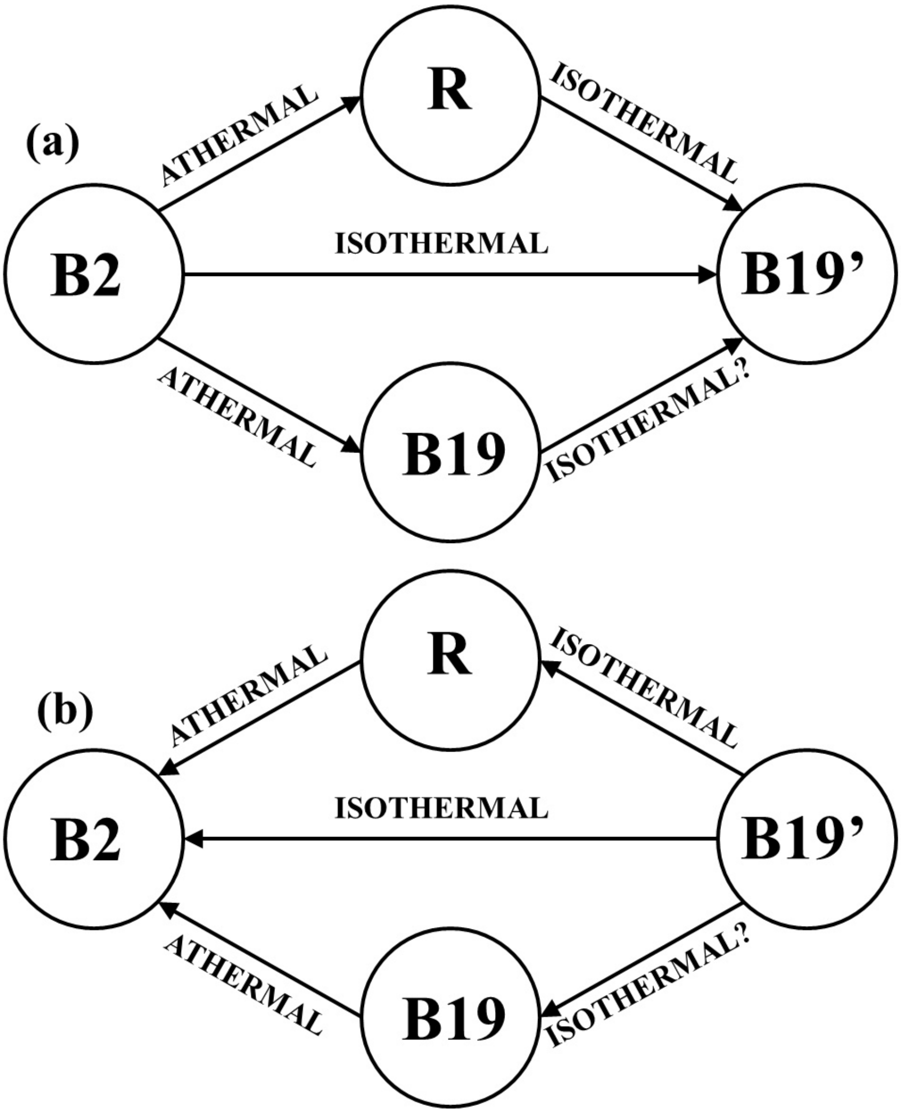

Figure 3.26: Schematic diagram showing classification of the (a) direct and (b) reverse transformation paths between the B2 and the B19' phase as athermal/isothermal. Isothermal: clear accumulation of the product phase during the isothermal holding experiments; Athermal: the transformation is time-independent within the experimental resolution; Isothermal?: there is no clear isothermal accumulation of the product phase but there is indirect evidence pointing to the isothermal nature of the transformation path.

and the reverse B19'→R MTs. In other words, the B2↔R MTs are time-independent within the experimental resolution and the R↔B19' transformations are IMTs.

The binary alloys which exhibit the two stage B2↔R↔B19' MT, Section 3.1, in general, confirm the behavior shown by the ternary alloy. The main results for binary alloys are exemplified by Figures 3.10 and 3.11. In the sample annealed at 620 K, the characterization of the direct B2→R and R→B19' MTs is rather straightforward: there are only few points within the range of the transformations to confirm/deny their athermal/isothermal behavior, Figure 3.10a. The situation is better for the binary alloy annealed at 770 K. The results firmly support the isothermal behavior of the direct R→B19' MT, Figure 3.11a. However, are not sufficient experimental data for the sample annealed at 770 K to be conclusive about the direct B2→R MT. On the other hand, the existing data do not contradict the results of the ternary alloy. The situation is even less clear in the case of the reverse MTs in the binary samples, as discussed in Section 3.1, due to overlapping of the B19'→R and R→B2 MTs, Figures 3.10b and 3.11b. Still, there are data supporting the isothermal behavior of the reverse B19'→R MT.

By contrast to the binary alloys, the reverse B19'→R and R→B2 are not overlapped in the sample of ternary $Ti_{50}Ni_{47.4}Fe_{2.6}$ alloy. In addition, the resistance change due to the transformation is considerable, this means higher sensitivity of the resistance to the variations of F. Therefore, the problems with the binary alloys are not present in the ternary alloy making the results shown by the Figure 3.12 very reliable.

The one stage B2↔B19' transformations were studied in the sample of binary $Ni_{50.2}Ti_{49.8}$ alloy heat treated at 1070 K and binary $Ti_{50.5}Ni_{49.5}$ alloy heat treated at 920 K. For the former alloy, the direct B2→B19' MT shows isothermally accumulation of B19' martensite, see panels (a) and (b) of the Figure 3.17. However, the isothermal holding experiments performed on the reverse B19'→B2 transformation, panels (a) and (b) of the Figure 3.18, do not show any time-dependence of the resistivity distinguishable from data scattered near $\frac{R(t)-R_0}{R_{MAX}-R_{MIN}} = 0$. Then, isothermal experiments performed on the binary $Ni_{50.2}Ti_{49.8}$ alloy points to an isothermal direct B2→B19' MT and an athermal reverse B19'→B2 MT.

The isothermal holding experiments registered with the sample of Ti-rich alloy give similar results, see Figure 3.17c for the direct MT and Figure 3.18c for the reverse transformation. The direct B2→B19' MT is clearly isothermal and also show a good correspondence with the relative temperature rate of the resistance, Figure 3.20a, like in other IMTs. On the other hand, the values of Z obtained during the reverse transformation, Figure 3.20b, are scattered and their sign is opposite to the expected one for the isothermal accumulation of B2 phase. Therefore, in the experiments with the sample of Ti-rich alloy the reverse B19'→B2 MT also has an athermal behavior.

Therefore, experiments neither in the $Ni_{50.2}Ti_{49.8}$ nor in the $Ti_{50.5}Ni_{49.5}$ are clear enough to reveal an isothermal behavior of the B19'→B2 MT inside our laboratory time window. However, the isothermal change of resistivity during this transformation has been observed by Fukuda et al. [118] in a $Ni_{51.2}Ti_{48.8}$ alloy quenched from 1270 K. The solution for this discrepancy about the athermal/isothermal nature of the reverse B19'→B2 MT is discussed in Section 5.5 were the effect of temperature in the intensity of isothermal effects is investigated in detail. This discussion is placed in Section 5.5 in order to use the concepts related to the model of bistable units introduced in Chapter 5. The conclusion, which emerges from the Section 5.5, is that this discrepancy is mostly due to the decrease of the isothermal accumulation of martensite in a single interruption with the increase of temperature. Taking this temperature-dependence into consideration, one may expect the isothermal accumulation of B2 phase in the sample $Ni_{50.2}Ti_{49.8}$ alloy, $T_P(DSC) = 259K$, to be more intense that the isothermal effects in the sample of Ti-rich alloy, $T_P(DSC) = 367K$ (as it actually happens with the direct transformation). The absence of observable isothermal effects during the reverse transformation with the sample of $Ni_{50.2}Ti_{49.8}$ alloy, apart from the decrease of the intensity of isothermal effects with temperature, is caused by two characteristics:

1. In general, it has been systematically observed that the relaxation rate Z is smaller for a reverse IMT than for a direct IMT; usually it is about two times smaller, see Figures 3.11 and 3.12. Part of this difference may be because the reverse transformation takes place at higher temperatures.

2. For this composition and heat treatment, the peak of the relative temperature rate of the resistance is nearby three times higher on cooling than on heating, see Figure 3.15b.

Since Z is proportional to $\frac{1}{R}\frac{\partial R}{\partial T}$, equation (5.26), the sum of the above two characteristics imply that the possible values for Z in the reverse transformation will be much lower than its values in the correspondent direct MT, even if there is isothermally accumulation of the parent B2 phase.

Therefore, the reverse B19'→B2 transformation may be classified as isothermal. However, this transformation type is experimentally athermal for samples that transforms at temperatures superior or comparable to the room temperature.

The two stage B2↔B19↔B19’ martensitic transformation presents, as commented in the Section 3.3, important difficulties, which are explained in detail since page 124.

The direct and reverse B19↔B19’ MTs appears in Figure 3.26 with a question mark (isothermal?) due to the experimental difficulties which makes the conclusions less reliable. On one hand, the accumulation of martensite/austenite within the transformation range of both, the direct and reverse B19↔B19’ MTs, is small as compared with other isothermal transformations. For example, the variation of resistance during the isothermal dwelling on cooling at 300 K is about $2 \cdot 10^{-3} R_0$, Figure 3.22a. If the same calculation is made for the kinetics registered for the sample of ternary Ni–Ti–Fe alloy during an interruption on cooling at 170 K, Figure 3.5c, it gives that the variation is about $27 \cdot 10^{-3} R_0$. On the other hand, the data of the time-dependences within this transformation range are less scattered and fit better a logarithmic law. Therefore, despite the absence of more clear isothermal accumulation of resistance, like in other IMTs, there actually exist isothermal effects and the characteristics of the material (temperature dependence of the resistance and transformation temperatures) predicts that the quantity of transformed material ΔF and its effect over the resistance during an isothermal holding experiment should be small. Then, these transformation paths may be considered as isothermal.

The values of Z' calculated from the data of the resistance inside the range of the direct B2→B19 MT are quite scattered around $Z' = 0$, Figure 3.25a in page 132. Some of the Z'-points has the sign opposite to the expected one for the accumulation of B19 phase (and B19’ too). Thus the direct B2→B19 transformation path has been classified as athermal, Figure 3.26.

The reverse B19→B2 MT is more complicated. There actually is isothermal accumulation of resistance during interruptions of heating within the the range of the reverse transformation. However, all the attempts to measure the isothermal kinetics of this transformation path results in problematic data with big jumps and/or high noise-to-signal ratio (Figure 3.24 shows some examples); there is no a steadily variation of resistance like in the isothermal transformations. Furthermore, B2↔B19 and B19↔B19’ MTs are more overlapped on heating than on cooling. This fact implies that it is risky to classify the points of Z' to be inside the B19’→B19 range or inside the B19→B2 one; since the sample is in a mixed state when the reverse B19→B2 MT starts. The system seems to be specially unstable within this transformation range and it is hard to associate the observed variation of resistance to the isothermal accumulation of B2 phase. Consequently, the reverse B19→B2 MT is classified as athermal, like the direct one.

3.5 Isothermal nature versus hysteresis and range of the MT

An important fact that arises from the experimental results is the existence of the relationship between the athermal/isothermal character of the MT and its hysteresis and its temperature range; see Table 3.1.

In the Figure 3.26, the transformation paths that are classified as clearly athermal are the direct and reverse B2↔R and B2↔B19 MTs. The hysteresis of the former transformation is about 2.5 K in the binary Ni–Ti alloy annealed at 620 K, about 6.5 K for the binary alloy annealed at 770 K (note that the reverse transformations are overlapped affecting this value) and about 4 K for the sample of ternary $Ti_{50}Ni_{47.4}Fe_{2.6}$ alloy (Figures 3.2a, 3.3a and 3.4a, respectively). In its turn, the hysteresis of the B2↔B19 MT is about 13 K for the sample of $Ti_{52.4}Ni_{39.7}Cu_{7.9}$ alloy annealed at 1120 K, Figure 3.21b (page 122).

By contrast, the isothermal transformations demonstrate a substantially broader hysteresis. For the R↔B19' MT the hysteresis is about 94 K (sample of $Ni_{50.2}Ti_{49.8}$ annealed at 620 K), 56 K (sample of $Ni_{50.2}Ti_{49.8}$ annealed at 770 K) and 49 K (sample of ternary $Ti_{50}Ni_{47.4}Fe_{2.6}$ alloy annealed at 1270 K). The hysteresis of the B2↔B19' MT is about 34 K in the sample of binary Ni–Ti annealed at 1070 K and about 36 K in the sample of Ti-rich Ti–Ni alloy, see Figures 3.15a and 3.16a, respectively.

Following the fundamentals of the MTs [6], the hysteresis of a transformation is related with the frictional work produced during the transformation. Therefore, it is supposed that for larger hysteresis the motion of interphase interfaces is more difficult since the energy barrier U opposing the movement of the interfaces is higher.

The activation energy ΔE is supposed to be the difference between two effects

$$\Delta E = U - \gamma\sigma \tag{3.2}$$

where U is the total height of the energy barrier, γ the activation volume and σ the stress caused by the transformation driving force.

In the transformation with a narrow hysteresis, the total height of the barrier U is low and then the activation energy ΔE will be also low, see equation (3.2). Then, as expected from the equation (5.35), τ_r is also small. Therefore, following the interpretation of Kurdjumov [38] and Kakeshita [42], supposing that all MTs are intrinsically isothermal, the system likely satisfies the condition $\tau_r << \tau_w$. Ergo the B2↔R and B2↔B19 MTs are, in fact,

Composition Heat treatment	MT type	T_S K	T_F K	T_P K	T_P $\partial_T R$ K	Range K	Hysteresis K	Character
$Ni_{50.2}Ti_{49.8}$	B2→R	315	282	303	305	33	2.5	Athermal
	R→B2	285	317	306	307	32		
620 K	R→B19’	200	135	^{a}	165	65	94	Isothermal
	B19’→R	252	274	271	259	22		
$Ni_{50.2}Ti_{49.8}$	B2→R	294	281	288	287	13	6.5	Athermal
	R→B2	290^{b}	295	296	292	5^{b}		
770 K	R→B19’	247	218	232	239	29	56	Isothermal
	B19’→R	280	290^{b}	296	292	10^{b}		
$Ti_{50}Ni_{47.4}Fe_{2.6}$	B2→R	252	243	250	249	9	4	Athermal
	R→B2	245	257	256	251	12		
1120 K	R→B19’	176	140	165	169	36	49	Isothermal
	B19’→R	190	222	220	213	32		
$Ni_{50.2}Ti_{49.8}$ 1070 K	B2→B19’	240	210	225	227	30	34	Isothermal
	B19’→B2	244	272	259	251^{c}	28		
$Ti_{50.5}Ni_{49.5}$ 920 K	B2→B19’	344	318	332	330	26	36	Isothermal
	B19’→B2	353	374	367	368	21		
$Ti_{52.4}Ni_{39.7}Cu_{7.9}$	B2→B19	338	326	333	332	12	13	Athermal
	B19→B2	339	355	344	347	16		
1120 K, AC	B19→B19’	326	252	^{a}	315^{d}	74	15^{d}	Isothermal?
	B19’→B19	262	339	^{a}	330^{d}	77		

Table 3.1: Start temperature, finish temperature and peak temperature from DSC signal, peak temperature from $\frac{1}{R}\frac{\partial R}{\partial T}$, transformation range, hysteresis and athermal/isothermal character of the different transformation paths studied for the Ni–Ti–X alloy system. ^{a}No peak on DSC signal. ^{b}Data correspond to partial transformations since they are very overlapped. ^{c}Affected by pre-martensitic variation of resistance.^{d}Non-precise data because the transformations are diffuse.

not athermal transformations, but pseudo-athermal ones. In this case the activation energy is low, the interfaces can overcome the barriers with a very short waiting time for the fluctuation and these transformations will follow a path close to the equilibrium.

By contrast, in a transformation with broader hysteresis the energy barriers are higher, and, within a broad distribution of the number of relaxing units versus energy, there will be the cases with the activation energy ΔE comparable to $k_B T$, $\Delta E \sim k_B T$. Hence, the characteristic relaxation time τ_r will be comparable with the laboratory time window τ_w. Therefore, in this case the isothermal accumulation of the product phase is experimentally observable and this should be the case for the B2↔B19' and R↔B19' transformations.

The B19↔B19' MTs are, again, more complicated. From the Table 3.1 one can see that the width of the hysteresis of the B19↔B19' transformation is similar to the one of the B2↔B19 MT, but the B19↔B19' transformation has, by far, the widest temperature range of all the transformation paths in the Ni–Ti alloy system.

The range of a MT depends on the stored elastic energy, the frictional work and the driving force of the transformation. A very wide transformation range implies a small driving force per kelvin and then the effect of the driving force in equation (3.2) will be very small, increasing the effective activation energy.

This fact offers a possible explanation for the different behavior between B2↔B19 and B19↔B19' MTs. Despite the total energy barrier height U is low in both cases, the very low driving force for the B19↔B19' transformation keeps ΔE at higher values than in the B2↔B19 MT and makes their behavior quite different. In summary, whereas the B2↔B19 transformation is pseudo-athermal, the lower driving force of the B19↔B19' MT enables certain accumulation of martensite/austenite to be detected in our laboratory time scale.

Table 3.1 shows the relationship between the athermal/isothermal character of the transformation and its hysteresis and range; the hysteresis being the decisive factor which distinguishes between isothermal transformations and athermal ones. The transformation range appears to be a secondary factor, according to the way in which it affects the behavior of the MT.

In addition, Table 3.1 also shows that all MT in the Ni–Ti–X alloy system which show isothermal behavior are related to the monoclinic B19' phase, whereas MTs that do not involve the B19' martensite are athermal. This remarkable observation enables us to conclude that the isothermal/athermal nature of the MT in Ni–Ti system is related to the crystallography of martensite phase and to recall specific reason of the high friction stress for the MT to/from B19' phase. As was advanced in Section 1.3.4 (page 26) and will be further discussed in Section 4.2, the isothermal behavior can be related to the thermally activated motion of the martensitic interphases mainly due to their interaction with lattice defects. Therefore, we suggest that the distinction between the transformations to/from the B19' phase and the transformations connecting the B2, R and B19 phases is in the fact that the self accommodation between the B19' phase and the other phases is far more complicated than between the B2, R and B19 phases [119]. Then, more defects are generated during the transformations to/from B19' phase and the interphase boundaries find a higher resistance to their motion, promoting the isothermal behavior.

Chapter 4

Athermal/isothermal behavior of the nucleation and growth processes

4.1 The role of the nucleation process

A generally accepted doctrine is that the isothermal nature of the MT originates from the thermally activated character of the nucleation stage. This position has been explicitly stated by Kakeshita et al. in derivation of their universal theory of IMT [42], despite observations of the reverse isothermal transformation [46] which in fact does not imply nucleation stage. The same idea that only the nucleation stage can be responsible for the time dependence of the MT has been used by Massalski in his recent review [36].

Otsuka et al. [45] in their study of the B2-B19' martensitic transformation in binary NiTi also assumed that only the nucleation stage of the MT is time-dependent, whereas the growth stage should be athermal. Consequently, they performed isothermal holding of the samples at a temperature slightly above M_S to determine whether or not the isothermal development of martensitic nuclei occurred in Ni–Ti. They expected that if there were martensitic nuclei generated isothermally, the resistance would have changed quickly after restart of the cooling scan because the hypothetical isothermally generated nuclei would start to grow upon resuming of cooling. The temperature domain studied by Otsuka et al. [45] is characterized by an increase of the electrical resistance on cooling: in the Figure 3.15b one can see than the reduced temperature derivative of the resistance $\frac{1}{R}\frac{\partial R}{\partial T}$ is negative along 80 K above M_S. This increment along a wide temperature range should be attributed to a "preparatory" stage of the MT, which includes the incubation/creation of nuclei or tweed structure, also known as pre-martensitic effects.

Otsuka et al. [45] found that there was no effect on the MT of the isothermal dwelling of the sample above M_S (i.e. within the pre-martensite effect temperature range). Based on this observation and assuming that only the nucleation stage can be isothermal, they concluded that the B2→B19' MT is athermal. Furthermore, the pre-martensitic stage is also athermal, according to Otsuka et al. data, in the sense that no isothermal effect is observed in the laboratory time window. However, they did not verify the absence of the effect of isothermal exposure on the MT for points inside the transformation range, between M_S and M_F. Following our experiments that were done for a wide range of temperatures, both inside and outside the transformation range, the isothermal accumulation of B19' phase is restricted to the range between M_S and M_F temperatures, see, for example, Figures 3.19 (page 118), 3.20 (page 119) for B2→B19' transformation path or the Figure 3.12 (page 104) for the R→B19' MT. This range of temperatures was not investigated by Otsuka et al. [45].

Concerning the pre-martensitic temperature range, our data corroborate the lack of any isothermal effect just above M_S. Take as an example of this fact the time evolution of the resistance for an isothermal experiment performed at 250 K in the Figure 3.17a (page 114) or the one at 350 K for the Ti-rich sample in panel (c) of the same figure. In all cases, there is a large difference between the values of Z for the experiments performed outside and inside B2→B19' MT range.

Thus, the classical assumption that only the nucleation stage is responsible for the isothermal nature of the MTs has lead Otsuka et al. to the erroneous general conclusion that the MT in NiTi system is athermal. This brief analysis indicates that the issue of the thermally activated/athermal nature of nucleation is a crucial one and an additional experimental verification of its athermal/isothermal nature is highly desirable. Therefore, we have employed mechanical spectroscopy measurements to confirm the hypothesis of the athermal nature of the nucleation. The measurements of the linear and non-linear Internal Friction (IF) components is a different approach to the characteristics of the MT as compared with the resistivity measurement, and then, such experiments can additionally reinforce or throw into doubt our conclusions based on the resistance studies.

The material selected for the IF experiments was the same near equiatomic $Ni_{50.2}Ti_{49.8}$ alloy, but annealed at 870 K after cold working. This is the alloy and the heat treatment, for which the microstructure was studied in detail by Srivastava et al. [69]. The present alloy after this annealing treatment recovers a complete MT, which becomes well localized and demonstrates transformation hysteresis of around 30 K, much narrower than the one after partial annealings at 623 and 773 K, see Table 3.1 in page 139. At the same time, the grain size obtained remains relatively small of order of a few microns [69] and the microstructure contains a high density of defects, like dislocations and Ni_3Ti_2 precipitates [69]. The high density of defects is expected to create a rich spectrum of local stresses and this way to promote nucleation [120].

Measurements of the linear and non-linear IF components were performed at ultrasonic frequencies, by means of the PUCOT technique described in Section 2.8.2, page 66. Using ultrasonic frequencies is advantageous for the purpose of nucleation detection, since ultrasonic experiments yield only the structural IF component and render negligible possible transitory IF term [121, 122].

This kind of experiments requires precise localization of the MT temperatures in the IF temperature spectra. To meet this prerequisite, the IF studies were combined with the DSC scans and resistance measurements, the latter were performed for the same sample as the IF investigations. To minimize errors/discrepancies in the MT temperatures, as seen by different techniques, all types of experiments were conducted under the same cooling-heating rate of 2 K/min. The results of the calorimetry scans together with resistance and IF temperature spectra are shown in Figure 4.1. As expected, the heat flow shows a significant activity above the M_S temperature on cooling and above the A_F on heating, Figure 4.1a. Moreover, this NiTi alloy after the heat treatment employed demonstrates an extremely intense premartensitic relaxation peak in the linear IF component, which is depicted in Figure 4.1b.

A comparison of the DSC data with the resistance and IF temperature spectra in Figure 4.1b reveals the following notable features:

- As usually, the M_S temperature, determined by means of the DSC, corresponds to the temperature of the resistance maximum during cooling.

- According to Figure 4.1b, the IF demonstrates perfect reversibility between the cooling and heating scans over a very broad temperature range, except for the MT range, wherein its behavior is quite remarkable. On cooling, the IF starts to increase strongly well above (at least 50 K) the M_S temperature and shows an extremely high peak at this temperature, which is unusual for non-transient IF in Ni–Ti [123–125]. The IF drops rapidly below the M_S temperature, as soon as the MT starts. The direct MT peak in the DSC data at around 220 K is revealed in the IF spectrum only as a small shoulder on the low temperature side of the IF maximum. The IF in the MT range remains much lower

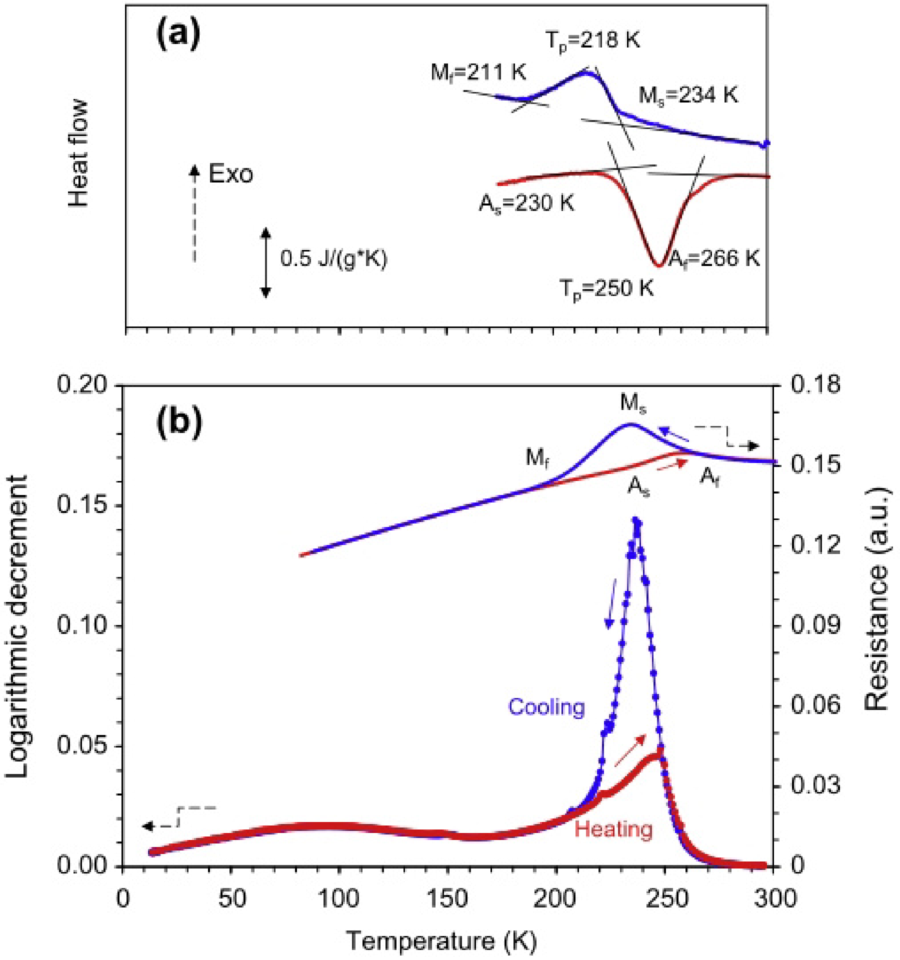

Figure 4.1: (a) Calorimetry scan for a sample of $Ni_{50.2}Ti_{49.8}$ alloy annealed for 1.8 ks at 870 K after cold working. (b) Temperature spectra of the internal friction measured at a frequency of around 90 kHz and strain amplitude of 10^{-6}, represented by the logarithmic decrement, and the resistance on cooling and heating.

during heating than during cooling, whereas, above the MT range, the IF patterns on cooling and heating coincide perfectly.

- The IF over the temperature range of 10-15 K above the engineering A_F temperature remains much higher even than damping in the martensitic state. It only drops to very lower levels typical for the austenite at temperatures substantially higher than A_F.

Since the IF peak on cooling occurs at M_S, at which temperature macroscopic martensitic variants only start to appear and grow, it is not related to the macroscopic MT or to the coexistence of macroscopic martensite variants and austenite. Another important proof of this fact is the observation that the IF spectra on cooling and heating coincide perfectly over a broad temperature range above A_F. Since a substantial thermal activity is detected well above the M_S, as shown in Figure 4.1a, the intense IF growth beyond M_S should be related to this premartensitic activity. As for the microstructural elements responsible for this premartensitic anelasticity, the most plausible candidates are martensite-like nanodomains or nuclei, revealed in Ni-rich Ni–Ti alloys well above the M_S temperature by transmission electron microscopy [126–128].

Additional experiments employing the non-linear strain amplitude-dependent IF, ADIF, which is exclusively related to linear, planar or 3-dimensional structural elements, can confirm that the origin of this unusual behavior of anelasticity is the nucleation process. Figure 4.2 shows the behavior of the linear IF, AIIF, and non-linear, ADIF, components in a partial temperature cycle down to 273 K, that is, above the M_S, but within the range of the intense strong rise of damping, see Figure 4.1b. The experimental results indicate, firstly, that the ADIF emerges from the very low values at around 300 K, over the temperature range of the very intense increase of the linear IF. Secondly, the increase of the non-linear IF with approaching the M_S temperature is essentially reversible: the thermal hysteresis between cooling and heating scans is of the order of only 2 K. This small hysteresis may be attributed to the error of the sample temperature determination between cooling and heating scans under cooling/heating rate of 2 K/min used in the experiments.

The emergence of non-linear anelastic effects simultaneously with the linear IF indicates that the increase of both IF components is related to linear, planar or volume structural elements, the only feasible candidates being pre-martensitic phenomena/martensite nuclei. Moreover, according to these data, generation of nuclei is controlled only by temperature, the absence of the temperature hysteresis implies that this increase is not related to the

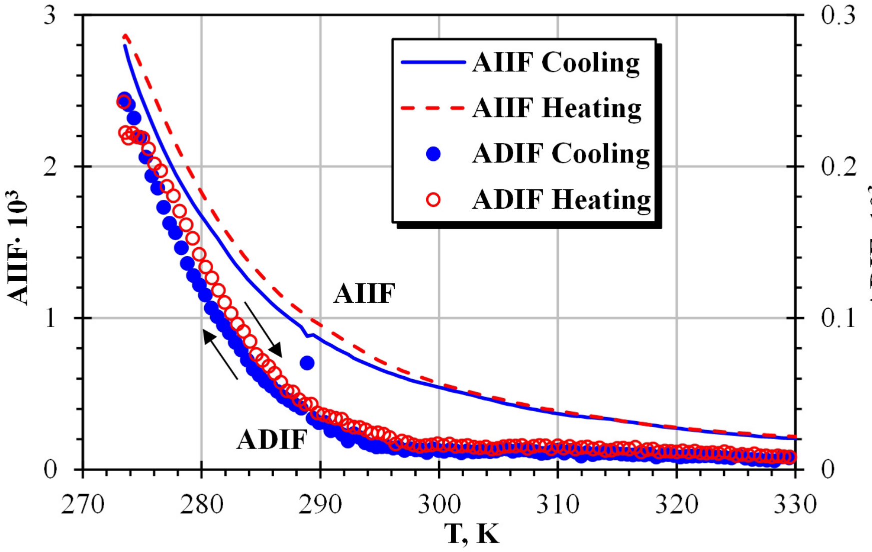

Figure 4.2: Temperature dependence of the AIIF on cooling (solid line) and on heating (dashed line) and of the ADIF on cooling (full circles) and on heating (open circles) during a partial temperature cycle performed above M_S but within the temperature range of strong pre-martensitic effect for a sample of $Ni_{50.2}Ti_{49.8}$ alloy annealed for 1.8 ks at 870 K after cold working. The resonant frequency is about 90 kHz, the low strain amplitude is $2 \cdot 10^{-6}$ and the high strain amplitude is $5 \cdot 10^{-5}$.

creation of macroscopic martensitic structure/variants. The same feature (the absence of the hysteresis) also indicates that the generation of nuclei is an equilibrium process on the laboratory time scale.

To further confirm the equilibrium nature of nucleation process, isothermal holding experiments on cooling between 293 and 253 K with registration of the linear IF were performed. The corresponding time dependence of the temperature and the IF, shown in the panel (a) of the Figure 4.3, confirm that no detectable time-dependent increase of the IF is observed during isothermal holdings. Note that the temporal increase of the IF just after interruptions of cooling process is due to the unavoidable temperature overshooting (overcooling). Panel (b) of the Figure 4.3 shows the same data as in the panel (a) but depicted versus temperature. It evidences that, despite the interruptions of the cooling scan, the data points follow the curve of a continuous cooling, like the one of the Figure 4.2.

To additionally confirm that the non-linear anelastic effects above M_S are not related to the macroscopic variant structure, it is instructive to analyze the ADIF strain amplitude dependences above M_S and below M_F. In order to do this, it is necessary first to analyze the strain amplitude dependence of the total damping, which includes both linear and non-linear components. Figure 4.4 shows the strain amplitude dependence of damping measured at several fixed temperatures during interruptions of cooling between 294 and 254 K (above M_S) in panel (a) and between 207 and 13 K (below M_F) in panel (b). Data shown in Figure 4.4 were registered using the experimental procedure introduced in the Section 2.8.2 (in page 73). In a strain amplitude cycle, performed between the low and high strain amplitudes, the drive voltage is increased first with a fixed step of 10% during the direct run of this cycle, and after this, it is decreased in the inverse sequence (reverse run). A comparison between the direct and reverse runs can provide meaningful information about the stability of the system of crystalline defects and the twin boundaries. If the direct and reverse runs of the strain amplitude dependence coincide, the system of defects is in equilibrium or demonstrates a perfect stability with respect to the ultrasonic excitation. This is the case of most dependencies shown in Figure 4.4.

In panel (a), curves between 294 and 264 K present very small or no hysteresis. Therefore, these data demonstrate that for this range of temperatures, which are inside the pre-martensitic range, the structure is in equilibrium. These curves also show that the damping dramatically increases as the temperature decreases from well above M_S. This fact is consistent with the analysis of the temperature spectra, Figures 4.1 and 4.2.

In panel (b), some of the strain amplitude dependence curves demonstrate hysteresis, the damping during the reverse run is slightly higher than during

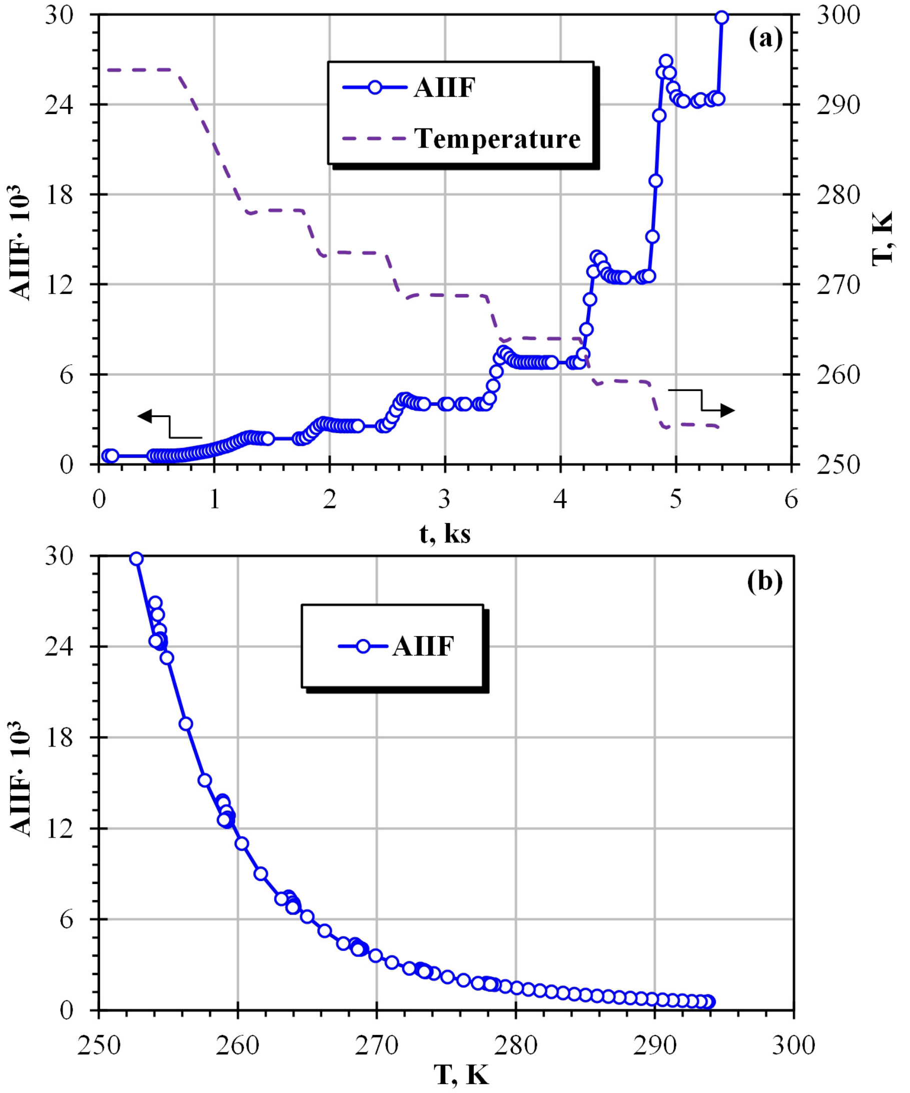

Figure 4.3: (a) Time dependence and (b) temperature dependence of the linear component of the internal friction, AIIF (open circles), during interrupted cooling for a sample of $Ni_{50.2}Ti_{49.8}$ alloy annealed for 1.8 ks at 870 K after cold working. In panel (a), the AIIF kinetics is compared with the time dependence of the temperature (dashed line). The AIIF was registered using a strain amplitude of 10^{-6}.

the direct run. This hysteresis is a typical characteristic of the martensites where the point defects have moderate mobility [129–131]. Thus hysteresis is higher for the curves registered at 119 K, 157 K and 177 K. One can notice from Figure 4.1 that these strain amplitude dependences correspond to temperatures which are on the high temperature side of a small secondary peak at around 90 K. The origin of this low-temperature peak will not be discussed in the present work. We mention only that it is related to the presence of hydrogen in the lattice.

The strain amplitude dependences of the IF registered at 254 K and 259 K, in panel (a) deserve a closer look because of their unusual behavior. These curves have a notable hysteresis which is different from the one presented by the curves below M_F: the hysteresis is higher and the level of damping is lower during the reverse run than during the direct one. Therefore, on reducing the strain amplitude, the decrement decreases and, in addition, forms a minimum with the IF level lower than the level of damping under low strain amplitude. If, as usually, one assumes that the AIIF and ADIF are additive [96], this unusual form of the strain amplitude dependence implies that the ADIF takes negative values, which is physically meaningless. Actually, this behavior is a spurious effect and occurs due to the self-heating of the sample during the experiment. The reasoning is as follows:

- The specimen dissipates energy in the form of heat, due to the energy loss in a cycle of oscillations.
- The energy dissipated in a cycle of oscillations, ΔW is proportional to the logarithmic decrement, δ, and to the strain amplitude squared, ϵ_0^2, as can be derived from the definition of the logarithmic decrement itself, equation (2.43), and of the stored elastic energy, W, equation (2.40) (page 66):

$$\Delta W = 2\delta W = \delta E_1 \epsilon_0^2 \tag{4.1}$$

- Since the higher the damping, the higher the energy dissipated, this effect becomes important for the higher levels of damping between 200 and 260 K, see Figure 4.1.
- Since the energy dissipated grows with the strain amplitude squared and the strain amplitude is increased by a factor of 1000 during the measurement of the strain amplitude dependence, the heat dissipated is 10^6 times larger for the highest strain amplitude than for the lowest

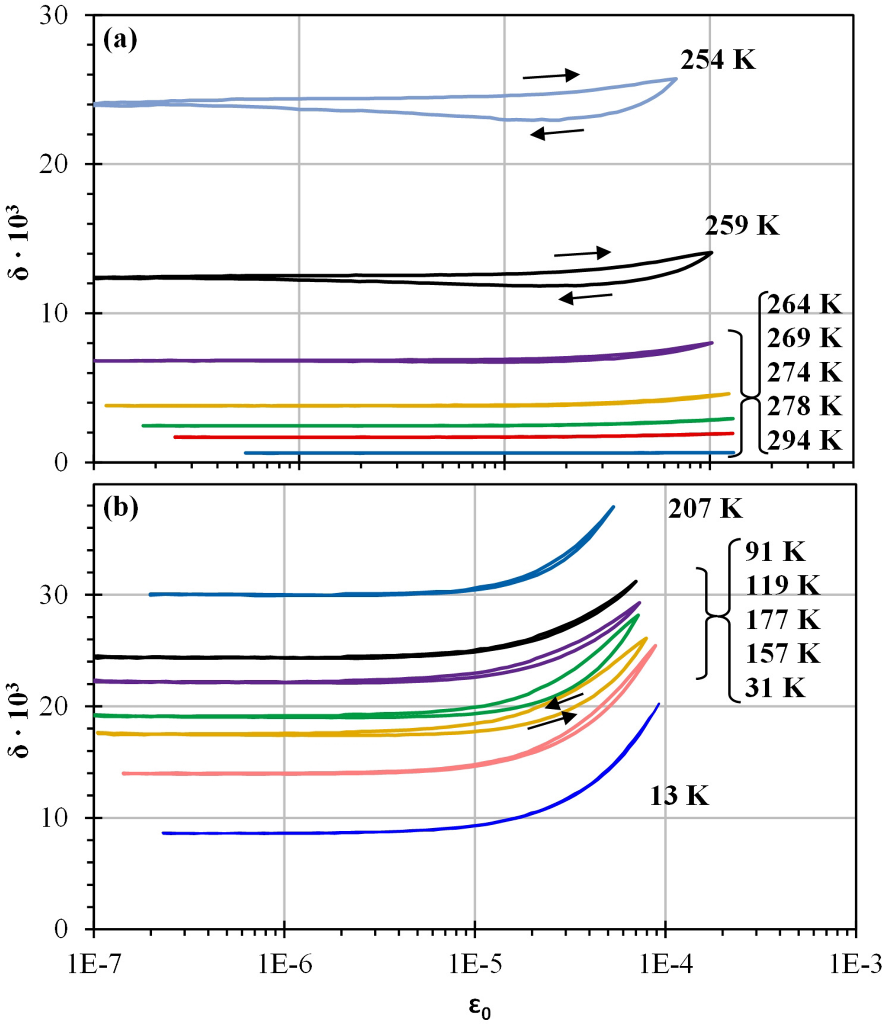

Figure 4.4: Strain amplitude dependence of the internal friction for a sample of $Ni_{50.2}Ti_{49.8}$ alloy, annealed at 870 K after cold working, registered at different temperatures during cooling between 294 and 13 K. (a) Strain amplitude dependences above the M_S temperature; (b) strain amplitude dependences below the M_F temperature. Arrows indicate the direction of the strain amplitude variations.

one. The intensity of self-heating increases strongly with the strain amplitude.

- In addition, the internal friction is very sensitive to the variation of temperature in this range of temperatures since it corresponds to the high-temperature side of the sharp IF peak, see Figure 4.1. Hence, a small increase of the temperature causes a notable reduction of the IF.
- The hysteresis appears because the temperature of the sample remains higher on reducing the strain amplitude than during the strain amplitude increase.
- Thus, a strong coupling between the strain amplitude and dissipated heat (parabolic dependence), high damping values around the IF peak (high dissipated energy), and, most importantly, a very strong coupling between the temperature and the IF level (sharp IF peak), results in a strong distortion of the strain amplitude dependence and even the strange minimum versus ϵ_0 for decreasing strain amplitude.

Using the equation (4.1), one can obtain a rough numerical estimate of the sample self-heating by the energy dissipated. For the present specimen, being $\delta \approx 2.5 \cdot 10^{-2}$ for a strain amplitude $\epsilon_0 \approx 5 \cdot 10^{-5}$ and assuming that the Young's modulus in austenite is approximately $E_1 \approx 45$ GPa [132], the energy dissipated per cycle is $\Delta W \approx 2.8$ J/(m^{3}cycle). In order to obtain the total energy dissipated during a experiment, one can consider that the frequency is $f \approx 90$ kHz= 90000 cyles/s, that the density of the Ni–Ti is $\rho \approx 6.45$ g/cm^3 $= 6.45 \cdot 10^6$ g/m^3, that the mass of the specimen is $m = 0.326$ g and that the experiment lasts around 50 s (but may be at high strain amplitudes only for about 25 s). Then, the total energy dissipated in the sample in an experiment is $\Delta W \approx 3.2 \cdot 10^{-1}$ J. Finally, the energy is dissipated as heat and absorbed by the sample increasing its temperatures following:

$$\Delta W \rightarrow Q = m c_p \Delta T \tag{4.2}$$

Then, given the mass of the sample ($m = 0.326$ g) and the specific heat capacity ($c_p = 0.32$ J/(g K)), the increase of temperate of the sample caused by the energy dissipation is $\Delta T \approx 3$ K. Is it a good approximation? Let us assume that the curves registered at 254 K and 259 K, in Figure 4.4a, will not have any hysteresis if the temperature were constant. Then, the difference in decrement during the hysteresis is caused the temperature variation and has a maximum value of $\Delta\delta \approx -1.8 \cdot 10^{-3}$ for the curve registered at 254 K and a value of $\Delta\delta \approx -0.9 \cdot 10^{-3}$ for the one registered at 259 K. From the data shown in Figure 4.3b, the values of the temperature-derivative of the decrement are $\frac{\partial\delta}{\partial T} = -3.3 \cdot 10^{-3}$ K^{-1} at 254 K and $\frac{\partial\delta}{\partial T} = -1.8 \cdot 10^{-3}$ K^{-1} at 259 K. Therefore, the increase of temperature between cooling and heating at the maximum of the hysteresis is $\Delta T \approx 0.55$ K at 254 K and $\Delta T \approx 0.5$ K at 259 K. The last calculation is not equivalent to the first estimation where the total adiabatic heating of the sample during the experiment is calculated. However, the comparison of the results of these two calculations demonstrates that the hypothetical total temperature variation due to the energy loss and the maximum difference in temperature between two points of the strain amplitude dependences, one on cooling and the other on heating with the same ϵ_0, are of the same order of magnitude. This fact corroborates the above assumptions about the origin of the hysteresis in the strain amplitude dependences above M_S.

There is another way to check the interpretation of the anomalous IF strain amplitude dependence behavior close to the damping peak: the hysteresis should depend on the strain amplitude step since it varies the time of measurements and the total dissipated heat during the amplitude dependence cycle. The normal amplitude step was 10%, i.e., each new point is done with the excitation voltage 1.1 times the one of the previous point. In this way, the points are nearly uniformly spaced when plotted with logarithmic strain amplitude axis. All the curves represented in Figure 4.4 were registered with a strain amplitude step of 10%. Then, in order to check the above assumptions, the strain amplitude scan was performed with an excitation step of 1.2, two times larger than the normal one. Figure 4.5 shows a comparison of the strain amplitude dependence of the IF in two experiments with different strain amplitude step, 10% and 20%. There are two facts that strongly support the above interpretation of this hysteresis:

1. The variation of the IF between the lowest and the highest value of the strain amplitude is higher for the amplitude step of 20%. During this experiment, since it is faster, the sample suffers a smaller self-heating and, as the heating of the specimen decreases the damping, the total variation of IF is higher for the shorter running time.

2. The hysteresis is lower in the curve registered with a strain amplitude step of 20%. Again, the sample has less time to be heated up during this experiment and then, the temperature difference between points for increasing and decreasing strain amplitude is less.

Therefore, a higher strain amplitude step reduces the effect of the heating of the sample. However, the increase of the strain amplitude step does not

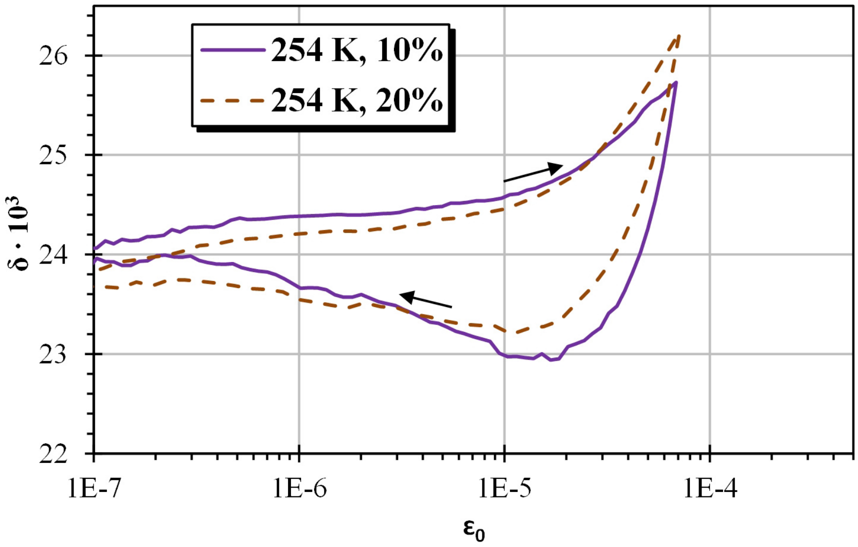

Figure 4.5: Strain amplitude dependence of the internal friction for a sample of $Ni_{50.2}Ti_{49.8}$ alloy annealed at 870 K after cold working registered at 254 K with two different strain amplitude steps, 10% (solid line) and 20% (dashed line). The arrows indicate the direction of the strain amplitude variations.

seem to be a solution to completely avoid this problem, since, to render the self-heating negligible, one needs to reduce dramatically the number of experimental points loosing this way the possibility to analyze the functional form of the IF strain amplitude dependence. One should conclude, thus, that: a) the strain amplitude dependence of the IF is reversible, indicating that the pre-martensitic structure is in an equilibrium state, and that b) the observed unusual hysteresis close to the very high IF peak is caused by self-heating of the sample.

Once one has the strain amplitude dependence of the total damping, introduced in Figure 4.4, the ADIF strain amplitude dependences can be analyzed to confirm/refute that the non-linear anelastic effects above M_S are not related to the macroscopic variant structure. Figure 4.6 shows the non-linear part of the total damping, the ADIF or δ_h, derived for different temperatures above M_S and below M_F. Note that the data for the experiments performed at 254 K and 259 K are not shown since it is not possible to decouple the effect of the self-heating of the sample from the strain amplitude dependence of the non-linear IF. The most important feature revealed by these experimental data is the different functional form of the ADIF versus strain amplitude in the range of pre-martensitic/nucleation stage and in the martensitic phase. In general, in both states, above M_S and below M_F, the strain amplitude dependence is well fitted by a power law:

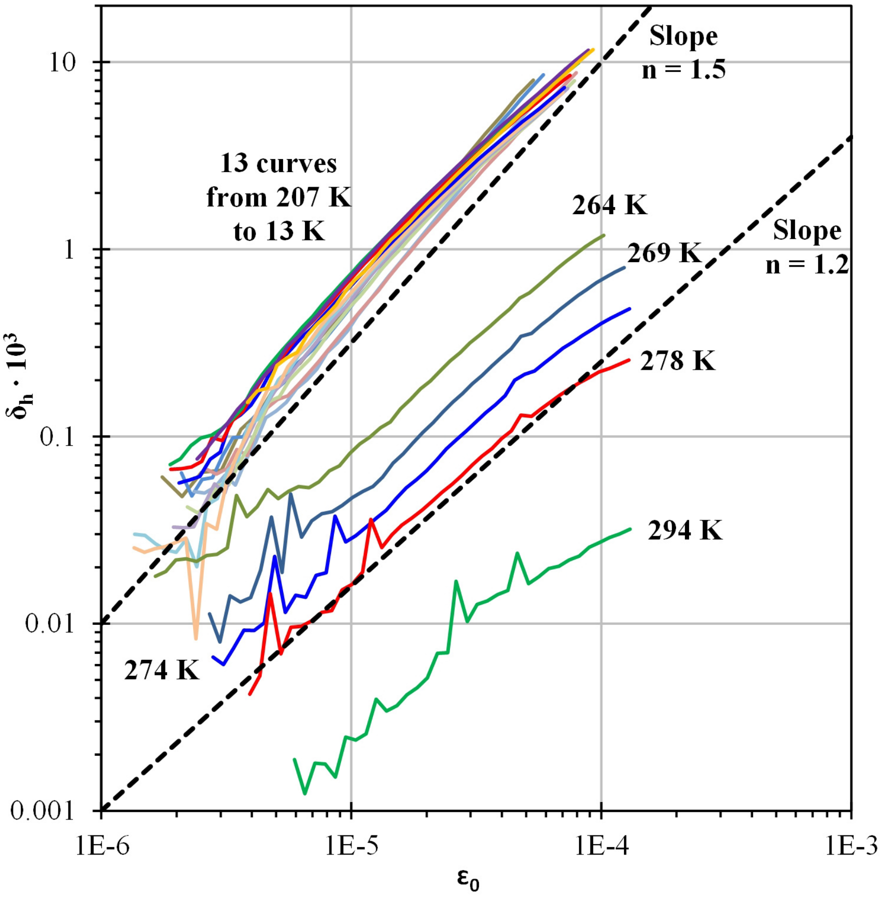

Figure 4.6: Strain amplitude dependent part of the internal friction (ADIF) derived for different temperatures between 300 and 13 K for a sample of $Ni_{50.2}Ti_{49.8}$ alloy annealed at 870 K after cold working. For comparison, dashed lines are guides that show power laws with strain exponents $n = 1.2$ and $n = 1.5$ ($\delta_h \propto \epsilon_0^n$).

$$\delta_h \cong A(T)\epsilon_0^n \tag{4.3}$$

being $A(T)$ a function only of temperature, and n the strain amplitude exponent.

All curves in the Figure 4.6 fit reasonably well equation (4.3). The experimental data evidence that the exponent n is nearly constant above M_S and in the martensitic state, but the absolute values of n are substantially different: $n \approx 1.2$ at high temperatures and $n \approx 1.5$ in the martensitic state. This difference confirms the difference in the nature of structural elements responsible for the non-linear dissipation of energy.

As have been already commented, the dependence of the amplitude-dependent logarithmic decrement with temperature, $A(T)$, is stronger within the austenite/pre-martensitic state, than in martensite. In fact, the weak temperature dependence below M_F forces all curves nearly to collapse when depicted on a double logarithmic scale. For curves above M_S, $A(T)$ is a strong function of temperature due to the increase of the number/size of the martensitic nuclei, whereas, below M_F, it is nearly constant for finally formed twin structure of the material in the martensitic state.

In summary, various experiments employing anelastic properties of the $Ni_{50.2}Ti_{49.8}$ alloy confirm, independently of the resistance data, that the formation of the martensitic nuclei is a time-independent process on a laboratory time scale.

This evidence, however, is not enough to claim that the nucleation/incubation process is intrinsically athermal. Our data cannot discard the possibility that the nucleation/incubation would be thermally activated with levels of activation energies quite different from the available thermal energies, so the probability of a thermally activated event is too low or too high to be observable inside our laboratory time window, which is, approximately, from 5 s to around 3000 s, i.e., covers only around 3 orders of magnitude.

4.2 Thermally activated motion of interfaces

The martensitic transformation, as any first order transition, includes nucleation and growth stages. Usually, the isothermal behavior of an MT is attributed exclusively to the nucleation process [4, 36, 86]. By contrast, the growth is considered as a rapid and athermal process. However, there is strong evidence that the growth process can also be isothermal: Kakeshita et al. observed in situ the isothermal growth of martensite plates for a sample of Fe–24.9Ni–3.9Mn wt% [43].

In the case of the Ni–Ti–X alloy system, it has been shown in the present work that both direct and reverse R↔B19' MT exhibit isothermal accumulation of resistance within the transformation range, see Figures 3.5 (page 88) and 3.6 (page 91). In addition, the experiments performed in samples that exhibit the one stage B2↔B19' MT indicate that the transformation is time-dependent between M_S and M_F, Figure 3.17 (page 114). However, the transformation does not show a clear evolution with time above M_S, see reference [45] or data registered at 350 K and 360 K in Figure 3.17c.

These results indicate that both direct and reverse MTs can be isothermal and that the nucleation and growth stages may be influenced differently by thermal activation. As has been introduced in Section 4.1, Otsuka et al. [45] observed the absence of isothermally accumulated B19' above M_S. They concluded from this result that the diffusionless B2↔B19' MT is athermal and that isothermal MTs reported in literature may be related with certain kind of migration of atoms. However, the time-dependence of the B2↔B19' MT within M_S and M_F has been found in the present work. In order to reconcile the results, we suggest that the isothermal behavior of the growth stage generates the main contribution to the experimentally observed time-dependence of the transformations to/from the B19' phase in the Ni–Ti–X alloy system.

The isothermal growth in a diffusionless MT is an option which has been scarcely explored in literature as compared with the thermally activated nucleation. Atomic diffusion is a thermally activated process that can be responsible of the isothermal nature of the growth stage, as had been found in a sample of Au–Cd alloy by Kozuma et al. [133]. However, the Ni–Ti alloy system is known for not having detectable atomic diffusion around transformation temperature [134]. Therefore, other mechanisms that can explain the isothermal nature of the growth in displacive and diffusionless MTs are needed.

Grujicic et al. [135] studied the thermally activated motion of an interphase interface through a perfect crystal and the interaction of the interface with crystal defects. Following Grujicic et al., the kinetics of the interface can be modeled using the formalisms developed to describe dislocation mobility.

Olson and Cohen had previously proposed a general dislocation description of the interface [136]. They modeled the interface as a set of discrete dislocations of two different types. The first kind, the coherency or transformation dislocations, deform the lattice while maintaining the continuity of the crystal planes and directions across the interface. The second type, the misfit or anticoherency dislocations, disrupt the lattice correspondence and produce the simple shears in the product phase which constitute the lattice invariant strain.

According to Grujicic et al. [135], those dislocations during their motion interact with the Peierls barrier and the crystalline defects. The Peierls barrier is an intrinsic periodic resisting force of the lattice which opposes the dislocation motion. The origin of this force is the periodic potential of the lattice, which is a consequence of its translational symmetry. Therefore, the Peierls barriers is present even in a perfect crystal. However, despite the Peierls barrier strongly affects the mobility of dislocations below the Bordoni relaxation temperature [137], it is unlikely that this barrier controls the velocity of the interface under accessible experimental conditions.

Therefore, following Grujicic et al. [135], it is more likely that the motion of a macroscopic interface is determined by its interactions with the crystalline defects. The interfaces can interact with different types of crystalline defects: point, linear or planar ones. However, the defects that are more likely to control the speed of the thermally activated motion of the interfaces are those that are involved in the point-surface type interactions with a tridimensional distribution of discrete obstacles.

However, the equivalence between the motion of dislocations and of martensitic interface has its limitations. Following Barsch [67] , the strain fields, the dynamic behavior of interphase interfaces and of dislocations are quite different. For example, for dislocations the strain field decreases as an inverse power of distance, whereas for the twin boundaries the strain field decreases exponentially with distance. As an alternative to the models based on the motion of dislocations, Barsch et al. [138] show that planar, stress free and coherent martensitic interfaces in three dimensions can be described consistently in terms of topological solitons (a self-reinforcing solitary wave which maintains its shape while it travels at constant speed through a nonlinear medium). Therefore, Barsch developed the “phonon viscosity” model [67]. This model describes the motion of the interphase interfaces as solitons and the frictional forces opposing their motion as the intrinsic attenuation experienced by the solitons caused by its interaction with the thermal phonons. Note that the mathematical equivalence that this model introduces between the motions of interfaces and solitons does not suggest that thermal phonons are involved in the IMTs.

In order to attribute the isothermal behavior of the diffusionless transformations to/from the B19’ phase in the Ni–Ti alloy system to the growth stage, it is important that the interaction between the interphase interfaces and the lattice defects has experimental support.

Following Zhang et al. [139], the dislocations can either help to accommodate elastic stresses associated with the formation of martensite or act as obstacles. They studied the microstructure of a Ni-rich alloy which exhibits a B2↔B19’ MT. As a result, the decrease of M_S and the increase of the density of defects with the number of cycles were found. The generation of dislocation during the temperature-induced transformation demonstrates the difficult accommodation between the monoclinic B19’ and the cubic B2 phases as was previously found by other authors, like Wasilewski [140] or Miyazaki et al. [107], who associated the crystalline defects with the variation of the transformation temperatures.

Zhang et al. [139] and Pelton et al. [141] observed the formation of dislocations around the growing martensitic plates. Following Zhang et al., the dislocations formed during the direct transformation have a unique substructure with leaf-like features. The leaf dislocations are generated during the direct transformation to accommodate the growth of the martensitic plate. However, after the thermal cycle is completed and during the subsequent direct transformation, the leaf dislocations appear to impede the nucleation of the same type of martensitic needle which generated the dislocation in the previous thermocycles. Therefore, the leaf dislocations oppose the nucleation and growth of the martensite and delay these processes. In its turn, the results shown by Pelton et al. [141] corroborate the generation of dislocations during the thermally induced B2→B19' MT and the interaction between the motion of the interphase boundaries and these dislocations. Following Pelton et al., during the first transformations, the growth of the martensite generates shear loops. Next, with the subsequent thermocycles, the moving interfaces act as crystallographic "snowplows" that force the initial shear loops to slip (and cross slip) in a certain crystallographic direction. This mechanism generates sessile bands of dislocations which can lock the interfaces. Another consequence of the generation of dislocations is the increase of both the frictional and elastic energy with increasing cycles. The increase of frictional work establishes a link with the already discussed high transformation hysteresis of the transformations to/from B19' phase (IMTs) as compared with the athermal transformation paths, see Section 3.5 on page 138.

On the other hand, the fact that most part of the dislocations are formed on cooling may explain the systematic differences observed in the intensity of isothermal effects between the direct and the reverse transformations. Along the present work, the isothermal accumulation of resistance on interrupting the heating scan is usually lower than for dwellings during the direct transformation; furthermore, in some cases the direct transformation demonstrates clear isothermal behavior but the reverse transformation was essentially time-independent, like the B2↔B19' transformation in the Ti-rich $Ti_{50.5}Ni_{49.5}$ alloy. Therefore, the mechanism which induces the isothermal behavior of these transformations should depend on the direction of the transformation, as does the generation of crystalline defects.

In conclusion, the interaction of the martensitic interfaces with crystalline defects is a thermally activated mechanism that can act in both direct and reverse MT and can explain the isothermal nature of the MT in the absence of a thermally activated nucleation process and diffusion. Therefore, this interaction can be the origin, by itself, of the isothermal behavior of diffusionless growth process in Ni–Ti alloys.

Chapter 5

Kinetics of the isothermal martensitic transformation

5.1 Logarithmic time dependence

The hallmark of many IMTs, also revealed by the experiments performed in the present work is the logarithmic kinetics of accumulation of martensite. As has been discussed in the section 2.4 (page 45), the logarithmic kinetics of the isothermal MTs was already observed and studied in the 50s [90, 91] in iron-based alloys. Furthermore, it has also appeared in recent studies in modern Ni-based ferromagnetic and metamagnetic SMAs [62]. Results on the isothermal behavior of the $L2_1 \rightarrow 2M$ martensitic transformation in the metamagnetic $Ni_{45.0}Mn_{36.7}In_{13.3}Co_{5.0}$ alloy will be shown in Chapter 6 (page 191). However, this material possesses additional problems for understanding of the isothermal nature of the MT due to the existence of the magnetic subsystem. The metamagnetic SMAs have a magnetostructural martensitic transformation during which, in addition to the conventional structural modification during the MT, the magnetic properties also change between the ferromagnetic austenite and the non-magnetic martensite. The magnetic subsystem adds an extra degree of freedom that is not present in the conventional SMAs.

At this stage, a universal phenomenological description of the IMT, based only on the activation energy concept, will be introduced. Therefore, this description disregards both specific mechanisms responsible of the IMT (nucleation and growth), and additionally degree of freedom, introduced by the magnetic subsystem in MMSMAs. The experimental results obtained for MMSMA will be discussed later on in a reference frame of this elaborated discussion.

As shown in Section 2.4 (page 45), the martensite volume fraction F ($0 < F < 1$) can vary under isothermal conditions. The variation of martensite volume fraction, $\Delta F(t,T) = F(t,T) - F_0(T)$, during a single isothermal holding experiment follows the logarithmic kinetics. This kinetics are usually characterized by the viscosity/relaxation rate $Z(T)$:

$$\Delta F(t,T) = Z(T) \ln \frac{t}{t_0} \tag{5.1}$$

It has been repeatedly confirmed that the isothermal evolution of resistance fits the logarithmic kinetics, equation (5.1), during an IMT, see, for example, Figure 3.5 in page 88. As discussed in the Section 2.4 on page 45, logarithmic kinetics of the IMT has a strong phenomenological support in different fields of physics. In the following, the basic theoretical concept, although also essentially phenomenological, describing logarithmic kinetics of relaxation, will be introduced. The advantage of the phenomenological approach is that it can be applied to describe the IMT independently of whether its kinetics is controlled by the nucleation and/or growth. The description below remains essentially the same. First we analyze the main principles underlying the model and the analytical solutions will be obtained in terms of the basic IMT characteristics.

Undoubtedly, one should search the origin of the isothermal behavior of the transformation in the thermally activated nature of the nucleation and/or growth processes. The existence of time dependence indicates that during the MT the system is out of equilibrium, but can approach it by means of the thermally activated relaxation. Eventually, the system will arrive to the vicinity of the state of minimum free energy for a given temperature, applied stress and, in the case of a magnetic alloy, external magnetic field. However, since the free energy profile has a complicated structure, the system is trapped in local energy minima for long times, until thermal fluctuations offer a chance to overcome one of the energy barriers that separate the system from neighboring states with lower free energy. In this way, the system can isothermally transform to the most energetically favorable phase while it progressively jumps to the states of lower energy. This relaxation mechanism is also present when the material transforms under anisothermal conditions because the high activation energy, U, of the energy barriers depends, in general, on the temperature, applied stress and external magnetic field. For example, when cooling during a direct MT, the height of the energy barriers decreases and, consequently, also decreases the time required for the thermally activated jumps over the selected energy barrier. Of course, this straight forward consideration is applicable under assumption that small temperature variations do not perturb significantly the free energy profile in the vicinity of the energy barrier under consideration.

The presence of thermal activated processes indicates that the transformation will depend on the T-scan rate and/or the field rate. This dependence emerges because these rates modify the time spent by the system in front of a certain energy barrier and consequently modify the probability that the barrier may be overcome by thermal fluctuations rather than through the increase of the transformation driving force.

In any case, equation (5.1) is only an approximation: the logarithm diverges both for $t \to 0$ and $t \to \infty$ whereas ΔF should be 0 when $t \to 0$ and it should tend to a certain saturation value less than 1 for $t \to \infty$. The description at short times can often be improved by adding a small value to the argument of the logarithm, for example, 1:

$$\Delta F = Z(T) \ln \left(1 + \frac{t}{t_0} \right) \tag{5.2}$$

The addition of this constant to the argument of the logarithm makes it zero when $t = 0$ s, as is expected from the isothermal variation of martensite volume fraction ΔF. Furthermore, it only slightly affects the value of Z since this constant quickly becomes negligible for long times. However, the equation (5.2) will only describe correctly the evolution of the system when it is still far from equilibrium: the logarithm in equation (5.2) in fact diverges for $t \to \infty$ and then this equation cannot describe the system when it approaches the saturation. On the other hand, it has to be taken into account that the initial stages of the relaxation may be the only ones accessible to experiment: the time needed to reach equilibrium in systems with a complicated energy landscape and barriers widely distributed in amplitude may easily exceed the age of the universe. Therefore, it is physically plausible that the limitation of the equation (5.2) for long times will not come into play in IMTs. In this case, equation (5.2) is a very accurate approximation.

The isothermal martensitic transformation presents two main features that are shared with other well-known thermally activated processes, in particular, the Thermal Fluctuation Magnetic Aftereffect (TFMA). These features are:

1. Both effects involve the diffusionless motion of two dimensional interfaces: the habit plane interfaces between austenite and martensite for the isothermal MTs and the magnetic domain walls in the case of the magnetic aftereffect.

2. Both show isothermal kinetics. These kinetics are characteristic of a system that relaxes due to the thermally activated jumps over energy barriers with a broad distribution of activation energies.

The thermal fluctuation magnetic aftereffect is discussed in detail by a number of authors [92,142,143] who use the Néel model [144,145] to describe the behavior of the system of magnetic domain walls. Taking into account the profound similarities between TFMA and IMT, the latter can be described in a similar way to the description of the former [92, 142, 143]. The same approach have been already used to describe the behavior of the IMT in investigation with alloys of the Ni–Ti [66,146] alloy system and with samples of metamagnetic $Ni_{45.0}Mn_{36.7}In_{13.3}Co_{5.0}$ alloy [62,147]. In reference [147], Pérez Landazábal et al. applied the model to the particular case of a magnetically induced transformation (instead of the present temperature-induced transformations). They have shown that there are many equivalences between the behavior of the transformation on interrupting the temperature scan and the applied magnetic field scan. The most remarkable similarities are the accumulation of magnetization/electrical resistance which presents logarithmic kinetics during isothermal isofield experiments and the relation (close to the proportionality) between the relaxation rate or viscosity of the system Z and the magnetic field derivative/temperature derivative of the martensite volume fraction ($\frac{\partial F}{\partial H}$ or $\frac{\partial F}{\partial T}$). Therefore, equation (5.1), as already commented, corresponds to a particular case with no applied magnetic field nor applied stress. Thus in general:

$$\Delta F(t, T, H, \sigma_0) = Z(T, H, \sigma_0) \ln \frac{t}{t_0} \tag{5.3}$$

and the following experimental relations were revealed (note that, in the present work, this relationship is met by all isothermal transformations with disregard of sample's composition/heat treatment, excepting the arrested magnetostructural transformation of the high ordered sample of Ni–Mn–In–Co, see Section 6.2 in page 201):

$$\left(\frac{\partial F}{\partial T}\right)_H \propto \left(\frac{\partial F}{\partial H}\right)_T \propto Z(T, H) \tag{5.4}$$

which can be extended to the case of a stress-induced MT. However, our attempts to investigate the IMT by means of tensile experiments were not successful. Those experiments failed to describe quantitatively the evolution of the transformation because there occur other time-dependent relaxations of the internal stresses in a loaded sample which affect the strain ϵ. Consequently, the time dependence of ϵ had a high noise-to-signal ratio and it was not possible to decouple the possible isothermal accumulation of strain due to the variation of F from other effects.

In the following, the model of bistable units is applied to the temperature-induced MT. Here, despite no reference is made to H or σ_0, any variable that depends on T, as Z, will also depend, in general, on any thermodynamic variable that affects the phase stability, as an applied stress σ_0 or an external magnetic field H (for the magnetic materials). The possibility of shuch solutions should be taken into account but this fact will not be mentioned for non-magnetic materials for clarity.

The model considers a collection of units with two non-degenerate energy minima, (+) and (–) (bistable units). These units can pass from one state to the other by overcoming a certain energy barrier. Since the level of energy of both minima is different in general, the activation energy should be asymmetric between both states. With this model, one makes the drastic assumption that the overall metastable behavior of the system, related to a complicated free energy surface with a large number of local minima, can be decomposed into the superposition of many bistable units. This strong phenomenological hypothesis is hard to justify rigorously. But, following [92], it has far-reaching consequences that lead to important progress in the comprehension of the thermal fluctuation aftereffect and the magnetic hysteresis phenomena. In the same way, it leads to a model that reproduces the characteristics of the isothermal MTs.

For this system composed by a large number of bistable units, we shall ignore the possible existence of quasi-degenerate energy levels, for which the difference in the Gibbs free energy is smaller than k_BT, $|\Delta G| \leq k_BT$. This means that the relaxation of each unit is described uniquely by the probability of jumping from the higher to the lower energy minimum. The probability of jumps in the opposite direction is ignored. Under this approximation, the relaxation time τ_r for a single unit overcoming an energy barrier with an effective activation energy U becomes

$$\tau_r(U) = \tau_0 \exp\left(\frac{U}{k_BT}\right) \tag{5.5}$$

where τ_0 is the characteristic time constant that summarizes other details of the free energy profile and its temperature dependence and k_B is the Boltzmann constant. τ_0 is not strictly a constant, but its dependence with temperature should be negligible as compared with the strong exponential dependence on $\frac{U}{k_BT}$ present in the equation (5.5). τ_0 can also be named as the “inverse attempt frequency” which evidences the probabilistic nature of the process.

One can simplify the growth of the martensitic plates as a set of elements which can be in austenite (+) or martensite (–). Starting from a high enough temperature, all the elements are in austenite, then the material is cooled inside the transformation range and isothermally held. At this temperature, the set of hypothetical elements can be classified in three groups [92]:

1. The units which have already made the transition to the martensitic state prior to the interruption of the cooling ramp.
2. The units which remain in austenite but they will not participate in the isothermal relaxation since they are in stable minima (or, at least, stable within the experimental time window).
3. The units which have not transformed on cooling and are metastable at the holding temperature. So the thermal fluctuations will, eventually, make them overcome the energy barrier to the martensitic state.

Thus, only the third group takes part in the relaxation. The number of elements in the third group when the T-scan is interrupted depends strongly on temperature. Then, let $N(T)$ be the number per unit volume of metastable units at the beginning of the isothermal relaxation. Equation (5.5) indicates that the charasteristic time required by each unit to relax depends on the effective activation energy U. Therefore, let $n(T, U)$ be the number of units per unit volume in front of an energy barrier with an activation energy between U and $U + dU$

$$N(T) = \int_0^\infty n(U, T) dU \tag{5.6}$$

Each unit produces a certain variation of the total martensite volume fraction when it relaxes. Then, let $\Delta f(T, U)$ be the variation of the martensite volume fraction when a unit with an activation energy between U and $U + dU$ relaxes. It is useful to introduce the average variation of martensite volume fraction per transformed unit

$$\langle \Delta f \rangle (T) = \frac{1}{N(T)} \int_0^\infty \Delta f(T, U) n(T, U) dU \tag{5.7}$$

With this variable, one can estimate the maximum ΔF that can be achieved during a single isothermal holding experiment, i.e., the martensite volume fraction at the saturation. The saturation corresponds to the state when all N units have jumped to the martensitic state. Therefore, since each unit produces an average change of the martensite volume fraction $\langle \Delta f \rangle$, the saturation limit of ΔF is

$$\lim_{t \to \infty} \Delta F = N(T) \langle \Delta f \rangle (T) \tag{5.8}$$

The saturation marks the final stage of the isothermal activity. Note that the initial stage is known and corresponds by definition to the moment of the interruption of the cycle when $N(T)$ metastable units are still present in austenite. Then

$$\Delta F(t = 0) \equiv 0 \tag{5.9}$$

Summarizing the previous definitions, both the time $\tau_r(T, U)$ required for a specific unit to relax and the effect produced by this unit over the martensite volume fraction $\Delta f(T, U)$ depend on temperature T and on the height U of its corresponding energy barrier. Therefore, the time evolution of the martensite volume fraction $\Delta F(t, T)$ can be obtained by integrating over the energy the distribution of units $n(T, U)$, taking into account their effect over F and the characteristic relaxation time:

$$\Delta F(t, T) = \int_0^\infty \Delta f(T, U) \left[1 - exp\left(-\frac{t}{\tau_r(T, U)} \right) \right] n(T, U) dU \tag{5.10}$$

Equation (5.10) involves the product $\Delta f(T, U) n(T, U)$, so it can be expressed in terms of the effective energy barrier distribution

$$p(T, U) = \frac{\Delta f(T, U) n(T, U)}{N(T) \langle \Delta f \rangle (T)} \tag{5.11}$$

which describes the effect of $n(T, U)$ relaxing units with an activation energy between U and $U + dU$ over the martensite volume fraction normalized by the total possible ΔF during the relaxation. Then, the condition imposed by normalization is

$$\int_0^\infty p(U) dU = 1 \tag{5.12}$$

Substituting equation (5.11) in (5.10), one gets

$$\Delta F(t,T) = N(T)\left\langle \Delta f \right\rangle (T) \int_0^{\infty} \left[1 - exp\left(-\frac{t}{\tau_r(T,U)} \right) \right] p(T,U) dU \quad (5.13)$$

Note that the integral in equation (5.13) fulfills the "boundary conditions" shown in equations (5.8) and (5.9), being 0 when $t = 0$ and 1 when $t \to \infty$. According to equation (5.5), the argument of the exponent in equation (5.13) is itself an exponential function of the energy. Then, $\left(1 - exp\left(-\frac{t}{\tau_r(T,U)}\right)\right)$ has an abrupt change between two levels, 0 and 1. Figure 5.1a shows the schematic energy dependence of $\left(1 - exp\left(-\frac{t}{\tau_r(T,U)}\right)\right)$ for two different times t_1 and t_2 being $t_2 > t_1$. If one assumes that the energy dependence of $p(T,U)$ is much weaker than the one of the exponential term, since the transition is very abrupt, the integral in the equation (5.13) indicates that energy barrier with higher activation energies U needs longer times t to be overtaken. Consequently, the units transform following the "transformation front" shown in the Figure 5.1a, reaching higher energies as the time of the isothermal holding increases. Due to the strong energy dependence of the exponent, at a certain time, only the units with an activation energy close to U^* for which $\tau_r(T,U^*) \approx t$ are transforming. More precisely, we define U^* as the solution to the equation $\tau_r(T,U^*) \equiv t + \tau_0$, which yields

$$U^*(t,T) = k_B T \ln\left(1 + \frac{t}{\tau_0(T)}\right) \quad (5.14)$$

Since U^* is a value marking the sharp transition of the double exponential one has that

$$\begin{cases} 1 - exp\left(-\frac{t}{\tau_r(T,U)}\right) \approx 0 & U > U^* \\ 1 - exp\left(-\frac{t}{\tau_r(T,U)}\right) \approx 1 & U < U^* \end{cases} \quad (5.15)$$

This behavior is very close to the behavior of the Heaviside step function $\theta(U^*(t,T) - U)$. This step-like function is shown in panel (b) of the Figure 5.1 for two different values of time t_1 (blue) and t_2 (red), being $t_2 > t_1$. The similarity between $\left(1 - exp\left(-\frac{t}{\tau_r(T,U)}\right)\right)$ and $\theta(U^*(t,T) - U)$ is obvious if the panels (a) and (b) of the Figure 5.1 are compared. Therefore, substituting the function $\left(1 - exp\left(-\frac{t}{\tau_r(T,U)}\right)\right)$ by the step function into the equation (5.13) gives

$$\Delta F(t,T) \approx N(T)\left\langle \Delta f \right\rangle (T) \int_0^{U^*(t,T)} p(T,U) dU \quad (5.16)$$

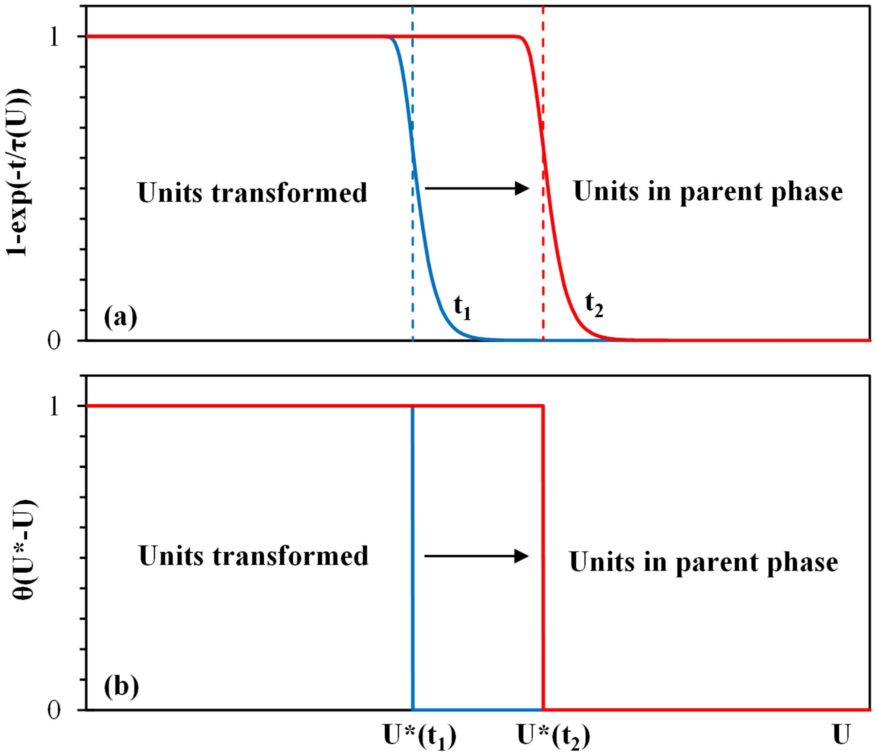

Figure 5.1: Diagram comparing the energy dependence of (a) $\left(1 - exp\left(-\frac{t}{\tau_r(T,U)}\right)\right)$ and (b) the approximate step function $\theta(U^*(t,T) - U)$ for two different values of time t_1 (blue) and t_2 (red), being $t_2 > t_1$. The arrow indicates the displacement of the moving front towards higher energy barriers values with increasing time of the isothermal holding experiment. The vertical dashed blue and red lines in (a) indicate the energies corresponding to the step-like transitions of approximating functions in (b).

Equation (5.16) can be solved analytically if one makes certain assumptions about the effective energy barrier distribution $p(T, U)$. The logarithmic kinetics of equation (5.2) arises from the assumption that the effective energy barrier distribution is essentially flat over a broad range of energies. Within this energy range, one can approximate the effective energy barrier distribution $p(T, U)$ by its average value p_{avg} between 0 and $U^*(T, U)$

$$p_{avg} = \frac{1}{U^*} \int_0^{U^*} p(T, U) dU \tag{5.17}$$

Then, taking into account equations (5.14) and (5.17), the equation (5.16) becomes

$$\Delta F(t, T) \approx N(T) \langle \Delta f \rangle (T) p_{avg} k_B T \ln \left(1 + \frac{t}{\tau_0} \right) \tag{5.18}$$

and yields the logarithmic kinetics.

5.2 Incubation time

Equation (5.18) yields a rather general result that predicts the experimental behavior represented by equation (5.2). However, it does not reflect the existence of an incubation time for the isothermal MT. The incubation time consists in a time-independent behavior of the resistance over a certain time span previous to the logarithmic behavior. This behavior has appeared in several isothermal holding experiments described in the Chapter 3, see, for example, curve at 120 K in the Figure 3.5a in page 88.

Since the logarithmic function diverges for $t \to \infty$, the real effective energy barrier distribution $p(T, U)$ should decrease to zero for activation energies higher than a certain upper limit U_{MAX}, i.e., the barriers with infinite activation energy do not exist or cannot be overcome in a thermally activated way. In addition, knowing the behavior of the relaxing front represented in the Figure 5.1, the incubation time can naturally be introduced in the model of equation (5.13) if one assumes that the distribution $p(T, U)$ is depleted of the low energy barriers up to certain energy limit U_{MIN}.

Figure 5.2a shows two curves that schematically represent the assumed behavior of the effective energy barrier distribution. These curves correspond to distributions that generate kinetics with (dashed red line) and without (solid blue line) incubation time. Different characteristic regions are observed in the $p(T, U)$, starting from the lower energies:

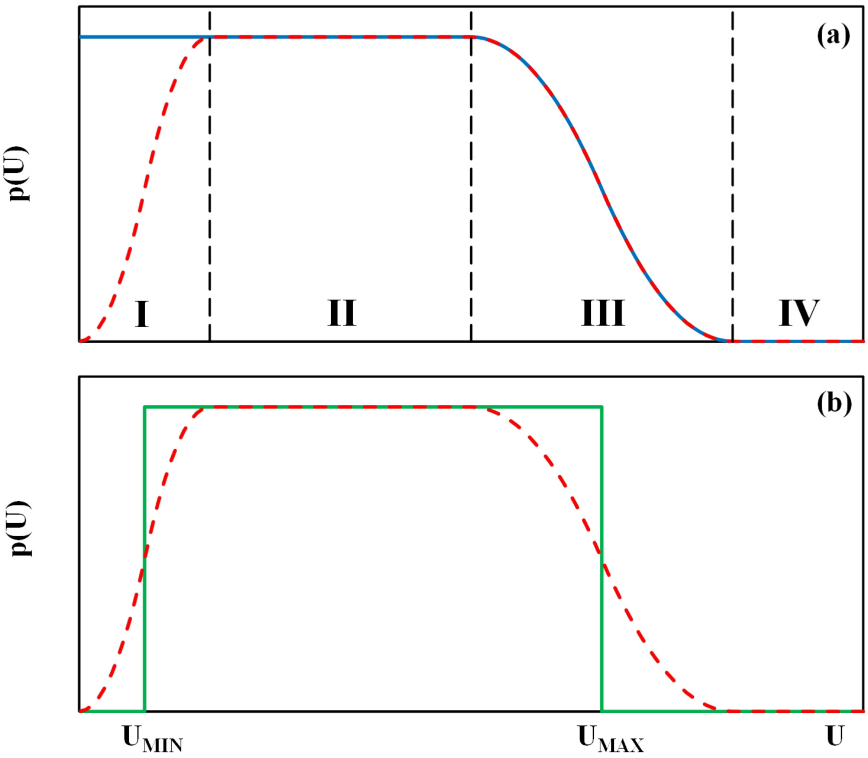

Figure 5.2: Diagrams showing different effective energy barrier distributions as function of the height of the energy barriers. (a) Two fairly realistic approximations to the behavior of $p(U)$ which generate two different types of kinetics, with (dashed red line) and without (solid blue line) incubation time. (b) The same approximation to $p(U)$ that generates logarithmic kinetics with an incubation time (dashed red line) compared with a step function which generates similar kinetics (solid green line). Panel (a) is separated in four different regions (I–IV) , which are mentioned in the text, by vertical dashed lines.

- The domain I is different for both curves. The distribution represented by the dashed line increases from zero to a certain constant value. This implies the low number of barriers with low activation energy which results in the absence of relaxation events for low isothermal holding times, the existence of the incubation time before the logarithmic kinetics sets in. On the other hand, the distribution represented by the solid line is flat and will give a relaxation with logarithmic kinetics starting from $t = 0$.

- The domain II is an energy range with approximately flat distribution of the number of energy barriers. While the relaxing front is "passing through this section", the relaxation fits the logarithmic kinetics of equation (5.2). These are the intermediate stages of the relaxation far from the initial stage (and the incubation period) and from the saturations stage.

- The domain III corresponds to a decrease of the number of the energy barriers with high activation energy. This stage of the kinetics represents approaching to the saturation and the loose of the logarithmic kinetics.

- The domain IV shows the nonexistence of barriers with very high activation energy. At this point, the kinetics are saturated and the relaxation does not proceed anymore.

Given the simple form of the effective energy barrier distribution $p(T, U)$, it is possible to approximate $p(T, U)$ by a step function in order to integrate analytically the equation (5.16). This way, the transitions of $p(T, U)$ are replaced by two abrupt step functions at the characteristic energies U_{MIN} and U_{MAX} as is shown in Figure 5.2b. Thus, the effective energy barrier distribution has the approximate form

$$p(T, U) = p_{rel}(T)\theta(U(t, T) - U_{MIN}(T))\theta(U_{MAX}(T) - U(t, T)) \quad (5.19)$$

where $p_{rel}(T)$ is the constant value of the effective energy barrier distribution during the relaxation. U_{MIN} and U_{MAX} are related with the experimental incubation time t_{inc} and saturation time t_{sat}, respectively. Then, one can define them in a similar way as U^* in equations (5.5) and (5.14)

$$U_{MIN}(T) = k_B T \ln\left(1 + \frac{t_{inc}(T)}{\tau_0(T)}\right) \quad (5.20)$$

$$U_{MAX}(T) = k_B T \ln\left(1 + \frac{t_{sat}(T)}{\tau_0(T)}\right) \tag{5.21}$$

Under this approximation, the constant value of the effective energy barrier distribution during the relaxation $p_{rel}(T)$ can be calculated since this function must fulfill the normalization condition (5.12). Then,

$$p_{rel}(T) = \frac{1}{U_{MAX}(T) - U_{MIN}(T)} \tag{5.22}$$

Now it is easy to integrate equation (5.16) using (5.19) and (5.22)

$$\Delta F(t,T) \approx N(T) \left\langle \Delta f \right\rangle (T) \frac{U^*(t,T) - U_{MIN}(T)}{U_{MAX}(T) - U_{MIN}(T)} \tag{5.23}$$

The energy terms of equation (5.23) can be replaced by means of the equations (5.14), (5.20) and (5.21) to obtain a final theoretical expression for the isothermal variation of martensite volume fraction:

$$\begin{cases} \Delta F(t,T) = 0 & 0 < t < t_{INC} \\ \Delta F(t,T) \approx N(T) \left\langle \Delta f \right\rangle (T) \frac{\ln\left(\frac{t+\tau_0}{t_{inc}+\tau_0}\right)}{\ln\left(\frac{t_{sat}+\tau_0}{t_{inc}+\tau_0}\right)} & t_{INC} < t < t_{SAT} \\ \Delta F(T) \approx N(T) \left\langle \Delta f \right\rangle (T) & t_{SAT} < t \end{cases} \tag{5.24}$$

Equation (5.24) is more complicated as compared to the simple experimentally observed equation (5.1). In principle, all the parameters different from the time t in (5.24) are temperature-dependent constants that can be incorporated in (5.1).

Let us check the solutions that the model of bistable units generates and compare these theoretical solutions with the experimental results. Figure 5.3 shows the time evolution of the variation of martensite volume fraction for different temperatures as calculated following equation (5.24). Several assumptions have been made for these numerical estimations. First, $Z(T)$ usually shows a maximum as function of temperature. Therefore, a simple Gaussian peak has been chosen to represent $N(T) \left\langle \Delta f \right\rangle (T)$. This choice will be justified further on in Section 5.4. The height of the peak is 0.3, i.e, up to the 30% of the material can transform during an isothermal holding experiment at the peak temperature T_P. The width of the peak is arbitrary and has no major importance. It is difficult to estimate precise values for the saturation time t_{sat}. As an example, Kustov et al. [62] found that for a sample of $Ni_{45.0}Mn_{36.7}In_{13.3}Co_{5.0}$ the kinetics start to deviate from the logarithmic behavior after 10 ks. However, the complete saturation was not reached after 20 hours. Within the same order, a saturation time of 48 hours (172800 s) has been taken for the numerical estimations. Althouth this value will not be precise approximation to the saturation times of the studied transformations in the present work, t_{sat} does not affect strongly the shape of the curves, but it changes only the absolute value of the curves. In its turn, in some experimental data, there is an evident incubation time t_{inc}, see, for example, Figure 3.5a in page 88. This period seems to increase with decreasing temperature. Then, it is arbitrarily chosen to increase in a geometrical progression from $1.6T_P$ ($t_{inc} = 1$ s) to $0.6T_P$ ($t_{inc} = 100$ s). Finally, the constant τ_0 is assumed to be negligible as compared with t, t_{inc} and t_{sat}.

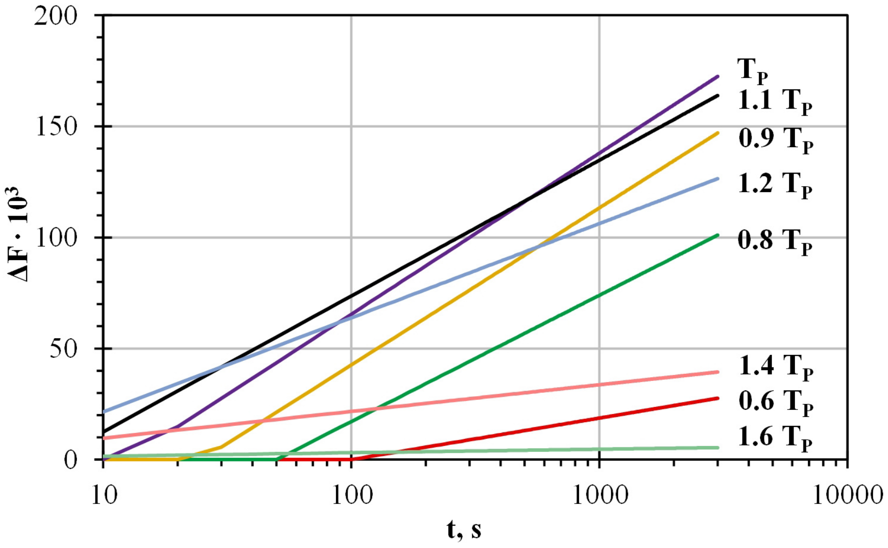

Figure 5.3: Time evolution of the martensite volume fraction during interruptions of the temperature scan as calculated following the Néel-type model of bistable units. Different curves represent numerical estimations of different isothermal holding experiments after interruptions at and around the peak temperature T_P.

Several similarities can be found comparing experimental data in Figure 3.5a (page 88) and results of calculations shown in Figure 5.3.

The slope of the curves (straight lines with logarithmic x-axis) is mainly proportional to $N(T)\left\langle \Delta f \right\rangle(T)$, but also depends on t_{inc}: for the same values of $N(T)\left\langle \Delta f \right\rangle(T)$ (for example, $0.8T_P$ and $1.2T_P$) the slope is higher with increasing value of incubation time. The difference in slope seems oversized since t_{inc} is small as compared with the total time available to the relaxation $t_{sat} - t_{inc}$. However, it is only a visual effect caused by the logarithmic axis. It is difficult to translate this effect to the real case in Figure 3.5a (page 88) since the real $Z(T)$ maximum is not perfectly symmetrical. However, a similar behavior can be observed if the experimental curves at 140 K and 180 K or the curves at 120 K and 200 K are compared.

Closely related to the point mentioned above, the total accumulated ΔF during the isothermal holding experiment increases until the temperature of the $Z(T)$ maximum, and starts to decrease for temperatures below $Z(T)$ maximum. For the same value of $N(T)\left<\Delta f\right>(T)$, it is smaller for the curves with longer incubation time, although they should coincide at the saturation time. All these features are observed experimentally, as Figure 3.5 shows (page 88). In panel (a) accumulated ΔF is higher for the curve at 180 K than the one at 140 K and the same is true for curves at 200 K and 120 K. This effect is not observed in panels (b) and (c) of Figure 3.5. However, one may note that $\frac{1}{R}\frac{\partial R}{\partial T}$ peak is not symmetrical for the isothermal R↔B19' MT in Figures 3.3b (page 83) and 3.4b (page 86).

In conclusion, the kinetics predicted by the model of bistable units is a good approximation to the experimentally obtained dependencies, both with and without incubation period.

5.3 Massalski approach to the incubation time

A phenomenological qualitative scheme, explaining the existence of the incubation time was suggested recently by Massalski [36]. According to Massalski, the athermal/isothermal behavior of the MT, analogously to the thermally activated precipitation reactions, is confined to a certain region of the time-temperature domain (plane). MT exhibits isothermal features only inside a C-shaped zone of the time-temperature domain (plane). Therefore, one can construct a pseudo-TTT diagram (time-temperature-transformation), Figure 5.4, to identify when the transformation is affected by thermal activation in a t-T plane. In this diagram, the area in which the transformation is thermally activated and the area in which it is not are separated by a C-shaped curve. Thus, the area surrounded by the C-shaped curve (the C-shaped area) is the one which corresponds to the IMT. As a consequence, the kind of a MT (isothermal, athermal, anisothermal) can change depending on the time-temperature trajectory of the experiment.

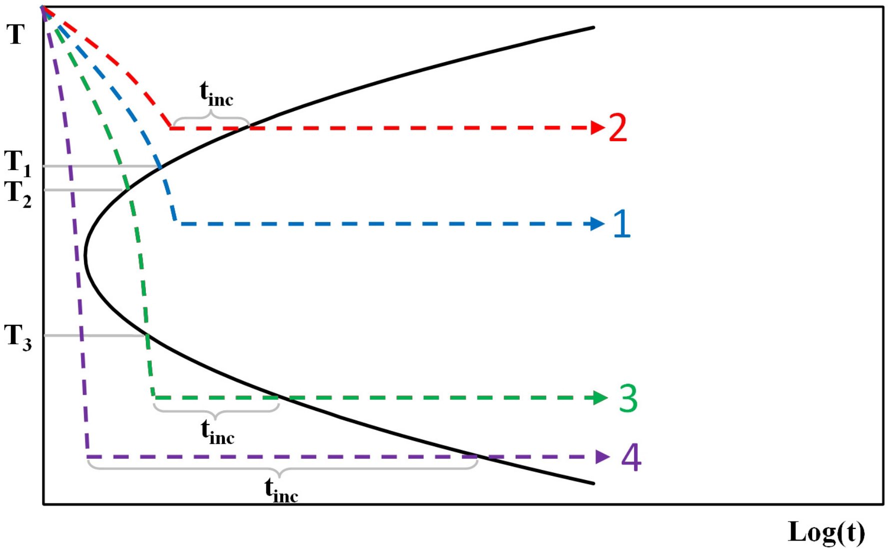

Figure 5.4: Sketch of a pseudo TTT diagram suggested by Massalski [36] in which the transformation changes its behavior depending on the *t*-*T* trajectory of the experiment. Curve 1 follows an athermal→anisothermal→isothermal trajectory, curves 2 and 4 show an athermal→isothermal trajectory while curve 3 presents an athermal→anisothermal→athermal→isothermal trajectory. The temperatures T_1, T_2 and T_3 indicate the points where the *t*-*T* trajectories cross the transition curve between athermal and anisothermal/isothermal transformation type. t_{inc} is the incubation time between the interruption of cooling and the start of the isothermal accumulation of martensite.

In Figure 5.4, the t-T trajectory will be a curve or a horizontal straight line depending on if the material is being cooled/heated or isothermally held. The trajectory represented by curve 1 in Figure 5.4 corresponds to a typical isothermal holding experiment: the material is cooled from above M_S to a certain temperature within the transformation range and is isothermally held. This becomes a t-T trajectory which starts from $t = 0$ outside the C-shaped area where the MT is athermal. The trajectory enters the C-shaped area at T_1 where the MT becomes anisothermal. Then, after interruption of cooling, the MT continues isothermally and exhibits isothermal kinetics. Curves 2, 3 and 4 in Figure 5.4 also represent a typical isothermal holding experiment which demonstrate an incubation period prior to the isothermal MT.

In the experiment represented by curve 2, the material is cooled from above M_S and the cooling is interrupted before it enters the C-shaped area and is isothermally held. It needs a certain incubation time t_{inc} to become a thermally activated transformation. The transformation type changes directly from athermal to isothermal. This case can also describe a transformation where the nucleation is thermally activated. In the last case, the cooling can be interrupted slightly above M_S and the transformation will take place after the incubation time.

The trajectory followed by curve 3 correspond to an experiment in which the cooling is interrupted at lower temperature that curve 1. Here, the t-T trajectory is again outside of the C-shaped area (the MT is not thermally activated), but will reenter this area after waiting a certain incubation time t_{inc}. Then, during cooling, the MT type changes first from athermal (above T_2) to anishothermal (between T_2 and T_3) and becomes again athermal (below T_3). Finally, the MT becomes isothermal after interruption of cooling and incubation time t_{inc}, see Figure 5.4.

Curve 4 represents the same kind of athermal to isothermal transition as curve 2, but well below the nose of the C-shaped curve. The material in this experiment should be cooled very rapidly, in order that the trajectory does not enter into the C-shaped before the interruption of cooling. For both types of experiments represented by curve 3 and 4, if the cooling rate is the same, the incubation time increases by decreasing the isothermal holding temperature.

Summarizing the transitions shown in Figure 5.4, the curve 1 shows an athermal→anisothermal→isothermal trajectory, the curve 2 and 4 represents a direct transition athermal(including the incubation time)→isothermal and the curve 3 draws a athermal→anisothermal→athermal(including the incubation time)→isothermal sequence.

The scheme proposed by Massalski [36] does not imply a particular physical origin of these changes in the experimental behavior of the transformation. Therefore, this diagram will be compatible with the results of the present work and the interpretation of the incubation time as a depletion of energy barriers with low activation energy.

The transformations in the Ni–Ti alloy system exemplify isothermal MTs which cannot be suppressed by rapid quenching. These MTs can be induced both isothermally and by temperature/stress variations. Therefore, following Massalski and Laughlin et al. [37], these MTs should be classified as anisothermal MTs during the continuous temperature scan. Furthermore, for the most part of the isothermal experiments there were no incubation time. Then, the curve 1 of the Figure 5.4 represents the majority of the results for the Ni–Ti alloy system. The few isothermal experiments that demonstrate some incubation time will correspond to the cases represented by curves 2 and 3.

5.4 Isothermal relaxation rate Z

The model of thermally activated relaxation of bistable units provides a link between the isothermal relaxation rate Z determined from experimental data and the model parameters. Comparing equations (5.2) and (5.24) (taking into account that in equation (5.2) there is no incubation time):

$$Z(T) = N(T) \langle \Delta f \rangle \ln^{-1} \left(\frac{t_{sat} + \tau_0}{t_{inc} + \tau_0} \right) \tag{5.25}$$

where N is the total number of units that can isothermally transform during a single experiment at a certain temperature, $\langle \Delta f \rangle$ is the average change of the martensite volume fraction produced by the transformation of a single unit, t_{inc} is the incubation time, t_{sat} is the saturation time and τ_0 is a characteristic time constant. All these parameters will depend, in general, on temperature. Therefore, the temperature dependence of the relaxation rate is quite complicated. It has been shown in our experiments, chapter 3, that there is a strong correlation between the isothermal transformation rate Z and the relative temperature rate of the resistance $\frac{1}{R}\frac{\partial R}{\partial T}$ within the transformation range of an IMT.

$$Z(T) \propto \frac{\partial R}{\partial T}(T) \tag{5.26}$$

This correlation, equation (5.26), is a common feature of different studied systems: apart of the Ni–Ti system of conventional alloys studied in the present work, it has been found in MetaMSMA Ni–Mn–In–Co [62].

One can relate the equations (5.25) and (5.26) in order to estimate which one of the parameters in (5.25) controls the temperature dependence of $Z(T)$. As has been introduced in Section 2.3 (page 42), if some conditions are met, as in the present case, there exist a relation between the martensite volume fraction and the temperature derivative of the resistance

$$\frac{\partial F}{\partial T} \approx \frac{1}{R_{MAX} - R_{MIN}} \frac{\partial R}{\partial T} \tag{5.27}$$

Therefore, Z is proportional to the transformation rate $\frac{\partial F}{\partial T}$. In addition, it is shown in Section 5.1 that the maximum of ΔF which can be produced during the relaxation (corresponds to the saturation) is $N \langle \Delta f \rangle$, terms which are present in equation (5.25). This fact demonstrates that both relationships, obtained from the model and experimentally, should be interrelated. However, to find a closer relation one needs to briefly recall the model of bistable units.

At the starting point (onset) of an isothermal holding experiment, the system of bistable units is stopped at certain temperature within the transformation range. At this point, the bistable units can be subdivided into three different groups. The group of interest for the relaxation process is composed by the N bistable units which can relax at that temperature. Since, at least during the major part of the transformation range, there might be a second group of units which will remain in austenite (without being transformed) up to saturation, the transformation in general cannot be completed isothermally. Therefore, N is different from the total number of units that are in austenite at the beginning of the relaxation. N is not necessarily a decreasing number with the progression of the transformation. Instead, it may depend strongly on temperature. However, what is its temperature dependence?

One can use the same concepts of the model to analyze the anisothermal transformation during a continuous cooling. On cooling, the transformation rate $\frac{\partial F}{\partial T}$ describes a peak. A higher value of $\frac{\partial F}{\partial T}$ at a certain temperature means that there is higher volume of the material which transforms at this temperature, and, in terms of the model, there are more bistable units which transform. It is reasonable to assume that the number of units which are transforming anisothermally at a certain temperature should be proportional to the number of units in front of a barrier with relatively low activation energy. In other words, the number of units which can relax isothermally, N, at certain temperature is closely related to the units that are transforming during a continuous cooling at the same temperature. Therefore, it is assumed that

$$N(T) \propto \frac{\partial F}{\partial T}(T) \tag{5.28}$$

and then, the number of available units to relax depends strongly on temperature, forming a peak along the MT range.

Taking into account the equations (5.25) to (5.28), two different approximations to the temperature dependence of the isothermal relaxation rate are obtained.

$$\begin{cases} Z(T) = N(T)\left\langle \Delta f \right\rangle(T) \ln^{-1}\left(\frac{t_{sat}+\tau_0}{t_{inc}+\tau_0}\right) \\ Z(T) \propto \frac{\partial F}{\partial T}(T) \propto N(T) \end{cases} \tag{5.29}$$

Equations (5.29) show that, for those transformations which fulfill equation (5.26), the temperature dependence of the relaxation rate is mainly due to the variation of the units available to the relaxation $N(T)$. Then, within the MT range, the other temperature dependencies are relatively weak: $\left\langle \Delta f \right\rangle$ and $\ln^{-1}\left(\frac{t_{sat}+\tau_0}{t_{inc}+\tau_0}\right)$ are approximately constants.

According to the Néel-type model [144, 145], the intensity of the isothermal effects is expected to increase linearly with temperature. This dependence is not directly observed in equations (5.29), but it is explicitly seen in equation (5.18) where p_{avg} is not substituted for its solution. In fact, in other thermally activated systems, like the thermal fluctuations magnetic aftereffect, this linear dependence with temperature is fulfilled [148, 149] and p_{avg} is found to be mostly temperature-independent. It may be similar for the case of the thermally activated martensite. However, according to experimental data, the intensity of the isothermal effects are strongly dominated by the transformation rate, and then, the linear dependence is negligible as compared to the temperature dependence of $N(T)$. If the transformation range $M_S - M_F$ is narrow, variations proportional to the temperature can be negligible as compared to variations of $N(T)$. For example, if $M_S - M_F = 30$ K and $M_S = 300$ K, then the relative change of $Z(T)$ due to its linear dependence with temperature is $\frac{M_S - M_F}{M_S} = 0.1$ (10%). By contrast, the temperature dependence of N forms a peaks that goes to zero at M_S and M_F. Therefore, the relative change of $Z(T)$ caused by the temperature dependence of N within the same range is $\frac{(N(T_P)-N(M_S))+(N(T_P)-N(M_F))}{N(T_P)} = 2$ (200%).

If one assumes that in the IMT the effective distribution of activation energy barriers may have a weak temperature dependence, like in the thermal fluctuation magnetic aftereffect, then, following equation (5.22), U_{MAX} and U_{MIN} are temperature-independent. Therefore, following equations (5.20) and (5.21), t_{inc} and t_{sat} increase exponentially with the reduction of the temperature. Although the increase of t_{inc} at lower temperatures is observed in the results, it is not demonstrated in the present work that its growth is exponential. However, being a speculation, the key point is that if U_{MAX} and U_{MIN} are approximately temperature-independent, substituting equation (5.14) in (5.23) would yield

$$\Delta F(t,T) \approx N(T) \left\langle \Delta f \right\rangle \frac{1}{U_{MAX} - U_{MIN}} \left(k_B T \ln \left(1 + \frac{t}{\tau_0} \right) - U_{MIN} \right) \quad (5.30)$$

and thus

$$Z(T) = N(T) \left\langle \Delta f \right\rangle \frac{k_B T}{U_{MAX} - U_{MIN}} \quad (5.31)$$

where the linear temperature dependence of equation (5.18) reappears (as predicted by the Néel model). One may conclude that the linear temperature dependence missing in equation (5.25) is implicitly included in the temperature dependence of $\ln^{-1}\left(\frac{t_{sat}+\tau_0}{t_{inc}+\tau_0}\right)$. Summarizing, $Z(T)$ may depend linearly on temperature, but this dependence is expected to be hidden by the stronger temperature variation of $N(T)$.

However, the interpretation of the temperature dependence of the intensity of isothermal effects deduced from the model of bistable units do not match with a common interpretation of the C-shaped curve in the pseudo TTT-diagram. Following Massalski et al. [36], the cause of this C-shaped boundary is the competition between two contributions to the intensity of isothermal effects:

1. The transformation driving force increases with the decrease of the temperature, reducing the effective activation energy.

2. The available thermal energy decreases at lower temperatures, increasing the time τ_r necessary to jump the energy barriers.

On the other hand, it has been shown above that, following the model of bistable units, the temperature-dependence of the intensity of the isothermal accumulation of martensite/austenite is due mostly to the temperature-dependence of $N(T)$ as long as the temperature-dependence caused by the variation of available thermal energy is negligible in most cases. In addition, $Z(T)$ also forms a peak/C-shaped curve in the isothermal reverse transformations. It is hard to deduce this behavior from the interpretation of Massalski, since for the reverse transformation the driving force increase with temperature, and then, both contributions will be additive.

Above, the model of independent bistable units have been used to describe the kinetics of the isothermal transformation because of its utility to explain the logarithmic kinetics, the relation between relaxation rate Z and the temperature rate of the resistance during a continuous temperature cycle $\frac{\partial R}{\partial T}$ and the incubation time. In addition, in Section 4.2, the thermally activated movement of the interphase boundaries are considered as responsible of the isothermal behavior of the present diffusionless transformations. This approach introduces two important parallelisms between an isothermal martensitic transformation and the magnetic thermal fluctuation aftereffect (MTFA), which is usually described by the model of bistable units:

1. In both cases, there exist the isothermal progression of the system, the elastic system for the IMT and the magnetic system for the MTFA, by means of the thermally activated motion of the interphase interfaces, in the IMT, or magnetic domain walls, in the MTFA.

2. Both IMT and MTFA are diffusionless processes.

5.5 Isothermal behavior of the B19’→B2 MT and the role of temperature

In the present work, the reverse B19’→B2 transformation have been investigated in two different alloys, $Ni_{50.2}Ti_{49.8}$ alloy annealed at 1070 K and $Ti_{50.5}Ni_{49.5}$ alloy annealed at 920 K. The time evolution of the resistance within the range of this transformation is synthesized in Figure 3.18 in page 117 and the temperature dependence of Z is shown in Figures 3.19b (page 118) and 3.20b (page 119). No isothermal change was detected that can be clearly associated to the isothermal accumulation of B2 austenite. The relaxation rate Z showed small values comparable with the scatter of experimental points. Therefore, most of the small variations of resistance produced during isothermal dwellings could not be related unambiguously with possible isothermal accumulation of austenite.

However, Fukuda et al. found certain (although also quite small) isothermal effects in $Ni_{51.2}Ti_{48.8}$ alloy and classified the reverse B19’→B2 MT as IMT [118]. In order to explain this discrepancy, we suggest analyzing the effect of temperature on the isothermal effects during the direct MT for a variety of Ni–Ti alloy compositions and heat treatments available. The intensity of isothermal effects can be characterized by the amount of product phase that isothermally transforms during a given time. In the present work, the typical holding experiment lasts about 2.4 ks. Therefore, it is natural to take the isothermally accumulated product phase during 2.4 ks, ΔF_{ISO}, as a measure of the intensity of isothermal effects.

Following equation (5.30), and assuming that $\langle \Delta f \rangle$, U_{MAX} and U_{MIN} depend very weakly on temperature (k_B is the Boltzmann constant), one sees that the temperature dependence of the isothermal effects is reduced to

$$\Delta F_{ISO}(T) \propto N(T)T \tag{5.32}$$

which is the same temperature dependence as that of $Z(T)$, equation (5.31). Therefore, in the framework of the model of bistable units, the temperature dependence of this function is dominated by the availability of metastable units. This fact disagrees with the use of a C-shaped TTT-diagram by Fukuda et al. [118] to describe the temperature dependence of the isothermal effects. Fukuda et al. constructed a classical TTT-diagram for the IMT in a sample of $Ni_{51.2}Ti_{48.8}$ alloy. They stoped the temperature ramp at different temperatures and determined the time required for a 1% decrease in the electrical resistivity. Observation of such diagram is actually equivalent to the temperature dependence of the Z parameter with a maximum, exemplified by Figure 3.11a (page 102) or 3.20a (page 119). We believe, however, that the analogy between this type of temperature dependence of isothermal effects and classical TTT-diagrams is confusing. According to equations (5.31) and (5.32), the Z (or ΔF_{ISO}) versus T spectra, as well as the C-shaped TTT-diagram, is mainly controlled by the temperature dependence of the number of relaxing units $N(T)$ which is proportional to the athermal transformation rate and is a parameter essentially not controlled by thermal activation. In other words, the temperature dependence along the transformation range is more conditioned by the progression of the transformation than by the effectiveness of the isothermal processes, whereas the effect of thermal activation on the intensity of isothermal accumulation of martensite is reduced to a relatively weak linear temperature dependence, equation (5.32).

We suggest, instead of comparison between the intensity of isothermal effects along the single MT for one sample, to compare the transformations to the B19' phase in different samples of the Ni–Ti–X alloy system. We have one direct transformation to the B19' phase for each composition and heat treatment. Then, the maximum value of the $\Delta F_{ISO}(T)$ function is selected to represent the intensity of isothermal effects for each composition and heat treatment. Since the isothermally accumulated martensite in 2.4 ks is essentially proportional to $N(T)$, the temperature at which its maximum value,

ΔF_{MAX}, is attained is the peak temperature T_P of the athermal transformation rate (this temperature also corresponds to the "nose" of the C-shaped TTT-like diagram). Therefore, from equation (5.32)

$$\Delta F_{MAX} = \Delta F_{ISO}(T_P) \propto N(T_P)T_P \tag{5.33}$$

Table 5.1 shows T_P and the correspondent values of ΔF_{MAX} for alloys with different compositions/annealing temperatures for the transformation to the B19' phase (B2→B19' or R→B19'). The temperature dependence of ΔF_{MAX} is shown in Figure 5.5. Each point in this dependence represents an alloy composition/annealing temperature from Table 5.1. Note that this temperature dependence refers to the peak temperature of each transformation and it is different from the variation of temperature along a single transformation/sample frequently used in the present work. A clear variation of ΔF_{MAX} with temperature is revealed: ΔF_{MAX} decreases nearly 5 times for the Ti-rich $Ti_{50.5}Ni_{49.5}$ alloy annealed at 920 K as compared with Ni-rich $Ni_{51.2}Ti_{48.8}$ one [118]. Therefore, considering that

- the intensity of isothermal effects decreases with temperature as shown in Figure 5.5,
- the transformation temperature in the alloy studied by Fukuda et al, $Ni_{51.2}Ti_{48.8}$, are lower than the one of the $Ni_{50.2}Ti_{49.8}$ annealed at 1070 K and of the $Ti_{50.5}Ni_{49.5}$ annealed at 920 K: 130 K, 227 K and 329 K, respectively,
- the relaxation rate Z is usually much smaller for a reverse IMT than for its corresponding direct IMT (cf. panels (a) and (b) of the Figure 3.12 in page 104),

it is not surprising that

- minor isothermal effects can be detected for the $Ni_{51.2}Ti_{48.8}$ alloy [118], whereas
- no isothermal effects are discernible during the isothermal holding experiments in the samples of $Ni_{50.2}Ti_{49.8}$ annealed at 1070 K and of the $Ti_{50.5}Ni_{49.5}$ annealed at 920 K, see Figures 3.19 (page 118) and 3.20 (page 119).

According to equation (5.33), ΔF_{MAX} is proportional to the maximum number of relaxing units during the transformation $N(T_P) = N_{MAX}$ which

Alloy/annealig temperature	MT Type	T_P K	ΔF_{MAX}	ΔT K	ΔF_C K
$Ni_{51.2}Ti_{48.8}$/1270 K [118]	B2→B19'	130	0.22	38	8.4
$Ni_{47.4}Ti_{50}Fe_{2.6}$/620 K	R→B19'	170	0.20	36	7.1
$Ni_{50.2}Ti_{49.8}$/1070 K	B2→B19'	227	0.17	30	5.1
$Ni_{50.2}Ti_{49.8}$/770 K	R→B19'	239	0.16	25	3.9
$Ti_{50.5}Ni_{49.5}$/920 K	B2→B19'	329	0.05	27	1.35

Table 5.1: Transformation peak temperature, T_P, estimated maximum value of the isothermally accumulated B19' phase during 2.4 ks, ΔF_{MAX}, MT range, $\Delta T = M_S - M_F$, and the corrected intensity of isothermal effects ΔF_C for IMTs to B19' phase in different Ni-Ti based alloys/heat treatments.

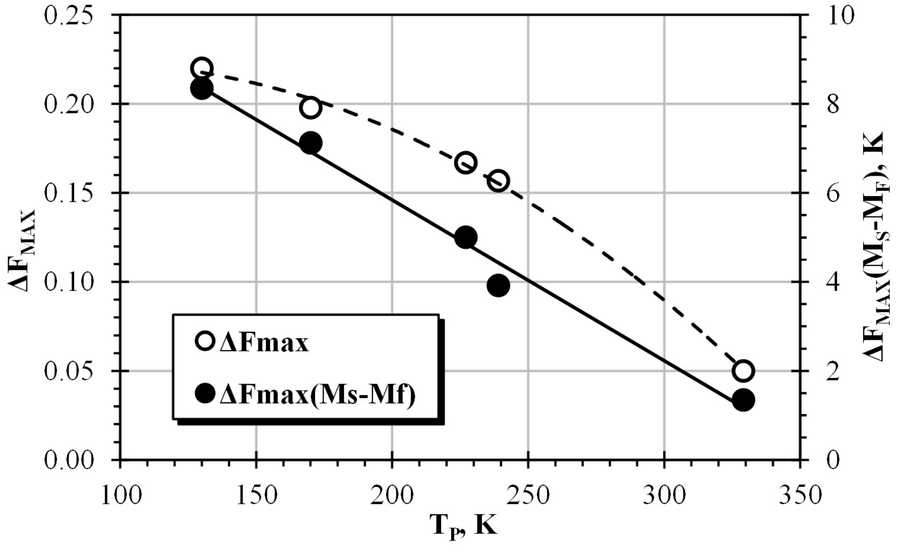

Figure 5.5: Temperature dependence of the maximum value of the martensite fraction isothermally accumulated during 2.4 ks, ΔF_{MAX}, for different transformations to B19' martensite in different Ni–Ti alloys listed in Table 5.1 (open symbols, left scale). The same parameter, corrected by the transformation "intensity" $\frac{1}{M_S - M_F}$ (full circles, right scale).

is attained at the maximum of the IMT rate. N_{MAX} depends on the range and shape of the peak of the MT and should vary for each alloy composition and heat treatment shown in Table 5.1. Then, N_{MAX} introduces a contribution to ΔF_{MAX} not related with the effect of thermal activation on the intensity of IMT. Supposing that $N(T)$ spectrum has a similar shape for all samples, N_{MAX} becomes inversely proportional to the transformation range, $\Delta T = M_S - M_F$. For example, this inverse proportionality relation is exactly fulfilled if the transformation peaks are approximated by Gaussian functions. Then, the wider is the peak the lower is its height. Therefore, one can define a corrected parameter, ΔF_C, which should eliminate the contribution of the shape of the temperature dependence of the athermal transformation rate to ΔF_{MAX}. It is defined as

$$\Delta F_C = \Delta F_{MAX} \Delta T \propto \frac{\Delta F_{MAX}}{N_{MAX}} \tag{5.34}$$

and can be interpreted as the intensity of isothermal effects corrected by the "intensity" of the athermal transformation. The values for ΔF_C, shown in the last column of Table 5.1, fit the linear temperature dependence, Figure 5.5, which might represent the high-temperature side of the expected temperature "window" of the isothermal effects inherent in the MT to B19' phase. We believe that temperature dependence of ΔF_C represent the "global" effect of temperature on the IMT to the B19' phase.

In summary, the analysis of isothermal transformations to the B19' phase in different Ni–Ti–X alloys reveals a gradual decrease of the intensity of the isothermal effects with temperature over a broad range of around 200 K. The observed sharp maximum in the temperature dependence of the intensity of the IMT for each alloy should not be related to the classical C-shaped TTT diagram: this sharp maximum is provoked by the variation of the number of relaxing units, rather than reflects variations of the efficiency of thermal activation with temperature.

Therefore, the reverse B19'→B2 MT may be classified as isothermal MT. However, the intensity of isothermal experiments decrease for the studied range of temperatures, and then no isothermal evolution of the transformation will be observed for temperatures close to or above to the room temperature.

5.6 Amount of isothermally transformed martensite

Following the results obtained in the Ni–Ti alloy system, the amount of martensite generated isothermally is, as usually [4], within a small percentage. This fact implies that the sample is normally in a mixed state when the saturation of the logarithmic kinetics is achieved, i.e., the transformation is not fully completed isothermally. In addition, the maximum of the accumulation of martensite in a single interruption is close to the peak temperature of the transformation T_P. Then, as the transformation is more completed there is less material which will transform isothermally whether the temperature ramp is interrupted. Consequently, the transformation is very alike to be completed isothermally and will reach before a relaxed state, which is also a mixed state of austenite and martensite. In the framework of the model of bistable units, this behavior implies that there exist units which are stable in the non-transformed state at the beginning of the isothermal dwelling even close to the engineering transformation finish temperature, M_F of A_F.

From table 5.1, a typical value of the maximum variation of the martensite volume fraction during a single isothermal dwelling is about $\Delta F_{MAX} \approx 0.15-$ -0.20. Therefore, one may conclude that despite the anisothermal MT is a process out of equilibrium, it is not far from a stable (time-independent) state during the continuous cycle for the alloys of the Ni–Ti–X alloy system.

5.7 Relaxation time constant versus laboratory time

In general, since the MT is a first order transformation, it needs to overcome energy barriers to proceed (during the nucleation events as well as during the movement of the interphase boundaries). The experimental behavior of the MT will be isothermal if the laboratory time window τ_w of the experiment is comparable with the characteristic relaxation time window τ_r.

The relaxation time for a single unit was shown in Section 5.1. Following equation (5.35), τ_r is a function of the effective activation energy U:

$$\tau_r(U) = \tau_0 \exp\left(\frac{U}{k_B T}\right) \tag{5.35}$$

where τ_0 is a constant, k_B is the Boltzmann constant and T is the temperature.

If the laboratory time window and the characteristic relaxation time differ substantially, one can expect two distinct cases.

- The relaxation time is much higher than the laboratory time $\tau_r >> \tau_w$ (high activation energies U). In this case, in the framework of the model of bistable units, only few units are in front of barriers that can be overcome within the typical duration of an isothermal holding experiment. Therefore, the transformation can be considered as athermal.

- By contrast, when the relaxation time is much lower than the laboratory time, $\tau_r << \tau_w$, the effective activation energies U are very low. This does not only imply a faster relaxation after the interruption of the temperature scan, but the lower activation energies also increases the number of units that transform anisothermally during the cooling/heating scan rather than by the continuous increase of the transformation driving force. In other words, just after the interruption of the T-scan, the system has a configuration close to the relaxed state at the holding temperature. In this state, similarly to the previous case, very few units are metastable once the scan is interrupted: the material will not show any time-dependence under isothermal conditions. However, thermal activation plays an active role in the $\tau_r << \tau_w$ case.

From the experimental point of view, both cases are athermal since no time-dependent behavior of the MT is detected within the experimental observation time window, but they are opposite cases concerning the role played by the thermal activation during the transformation. To distinguish both cases, Massalski classified the second case as “pseudo-athermal” [36].

There is a possible method to experimentally distinguish between the athermal and pseudo-athermal cases. This method is related to the material behavior slightly above M_S temperature, but below the temperature of thermodynamic equilibrium T_0.

On one hand, between M_S and T_0, the athermal MT will not show any isothermal accumulation of martensite (or displacement of the M_S temperature). This is the situation for the nucleation of B2→B19’ transformation in Ni–Ti [45] and the $\beta \leftrightarrow$18R transition in Cu–Zn–Al [49].

On the other hand, a pseudo-athermal behavior opens the possibility for the isothermal accumulation of martensite to occur above M_S (or the time-dependent displacement of the M_S temperature well above the value for M_S measured on a continuous cooling ramp). The reason why the time-dependence is now observable within the laboratory time window is that the driving force is strongly reduced above M_S and, hence, the activation energy barrier U is higher compared to the driving force, increasing the relaxation time τ_r. Therefore, an example of a pseudo-athermal transformation is the $\beta \leftrightarrow$2H transformation in Cu–Al–Ni [46, 49] and the MT in Fe–Ni [44].

However, the growth process needs the martensite nuclei to proceed. Therefore, if the nucleation is athermal, there will not be isothermal accumulation of martensite above M_S regardless of the behavior of the growth process. Otsuka et al. [45] demonstrates that there was no isothermal effects above M_S in a sample of $Ni_{50}Ti_{50}$ alloy furnace-cooled from 1273 K. Therefore, the nucleation process of the B2→B19' is athermal. By contrast, a clear isothermal behavior is revealed between M_S and M_F which indicates the thermally activated nature of the transformation. Then, the method explained above to distinguish between athermal and pseudo-athermal transformations will not reveal the pseudo-athermal behavior of a growth process if the nucleation is athermal.

Chapter 6

Magnetostructural transformations

6.1 An isothermal magnetostructural transformation

Ni–Mn–In–Co alloys used in the present work are based on the Ni_2MnIn Heusler alloy. The present $Ni_{45}Mn_{36.7}In_{13.3}Co_5$ alloy is modified by replacing In atoms by Mn atoms. This variation promotes the magnetic behavior of the parent phase because of the different couplings between Mn atoms in the "Mn sublattice", which are ferromagnetic, and between the Mn atoms situated in "Mn sublattice" and "In sublattice", which are antiferromagnetic, as pointed in Section 1.5.2 (page 32). In addition, some Ni is replaced by Co atoms which increase the saturation magnetization of the alloy and increase the Curie temperature, T_C, of the austenite [56,150], and, through the Clausius-Clapeyron-like relation, the effect of an applied magnetic field on the transformation. In the samples of $Ni_{45}Mn_{36.7}In_{13.3}Co_5$ alloy, the austenite is ferromagnetic and the martensite is weakly magnetic. Consequently, the magnetic ordering of the material changes during the structural martensitic transformation, converting the transformation in a magnetostructural transformation.

As for the crystallographic structure of the present sample, Ito et al. [151] found that there exists a B2-$L2_1$ ordering transformation for the parent phase of the alloy of the same composition: $Ni_{45}Mn_{36.7}In_{13.3}Co_5$. The characteristic temperature of the $L2_1$ordering transition, i.e., the temperature at which the B2 ordered austenite transforms into the $L2_1$ ordered one, was approximately 900 K. Therefore, the sample quenched from 1070 K may present the B2 phase. However, Ito et al. [150] have shown for other sample of similar characteristics, same composition and water quenched from 1170 K, that it can also posses a $L2_1$-like austenite after the heat treatment, that is, $L2_1$ ordering is not completely suppressed by quenching from 1170 K. Nevertheless, the strong difference between the transformation behavior of quenched and slowly cooled samples is observed [60, 152, 153], pointing to the strong variation of the degree of long-range orger (LRO) with heat treatment.

The martensite of the $Ni_{45}Mn_{36.7}In_{13.3}Co_5$ alloys quenched from annealing temperatures above 900 K can have several types of monoclinic structures. From Ito et al. experiments [150, 151], a sample quenched from 920 K showed a nonmodulated monoclinic 2M martensite (also known as $L1_0$) and a sample quenched from 1170 K presented a mixture of ten-layered (10M) and fourteen-layered (14M) monoclinic martensites, which are nanotwinned structures. Therefore, one can assume that the highly disordered sample of $Ni_{45}Mn_{36.7}In_{13.3}Co_5$ alloy quenched from 1070 K should exhibit a transformation similar to the B2↔2M MT.

Figure 6.1 shows a comparison between the temperature dependence of the resistance, panel (a), the temperature rate of the resistance, panel (b), and the DSC signal, panel (c), for a sample of $Ni_{45}Mn_{36.7}In_{13.3}Co_5$ alloy quenched from 1070 K, registered during a continuous temperature cycle. We will refer to this sample as WQ sample.

The resistance, in panel (a), strongly varies between austenite and martensite: the level of the resistance in martensite is much higher than in austenite, approximately by a factor of 2.5. This fact implies that the sensitivity of the electrical resistance R to the variation of the martensite volume fraction F during the transformation is high, which is very convenient for the study of the isothermal transformation. The resistance increases with temperature above M_S/A_F, which is a common situation. However, the resistance is almost independent of the temperature below M_F/A_S. This behavior is unusual since it extends to low temperatures; the resistance spectra showing this behavior have been obtained for temperatures down to 13 K.

The characteristic transformation temperatures are determined from the relative temperature rate of the resistance in panel (b). They are: $M_S = 329$ K and $M_F = 298$ K for the direct transformation, and $A_S = 318$ K and $A_F = 346$ K for the reverse one. Then, the transformation range is about 31 K for the direct transformation and 28 K for the reverse one. The hysteresis of the transformation is 19 K. These points indicate that the transformation is well localized and its isothermal/athermal behavior can be characterized properly from the resistance data registered during isothermal holding experiments. In addition, the transformation peaks of the DSC signal $\frac{\phi}{m\beta}$, shown in panel (c) of the Figure 6.1, closely resemble the ones of the relative temperature rate of the resistance $\frac{1}{R_{MAX}-R_{MIN}}\frac{\partial R}{\partial T}$, in panel (b), and the peak temperatures are

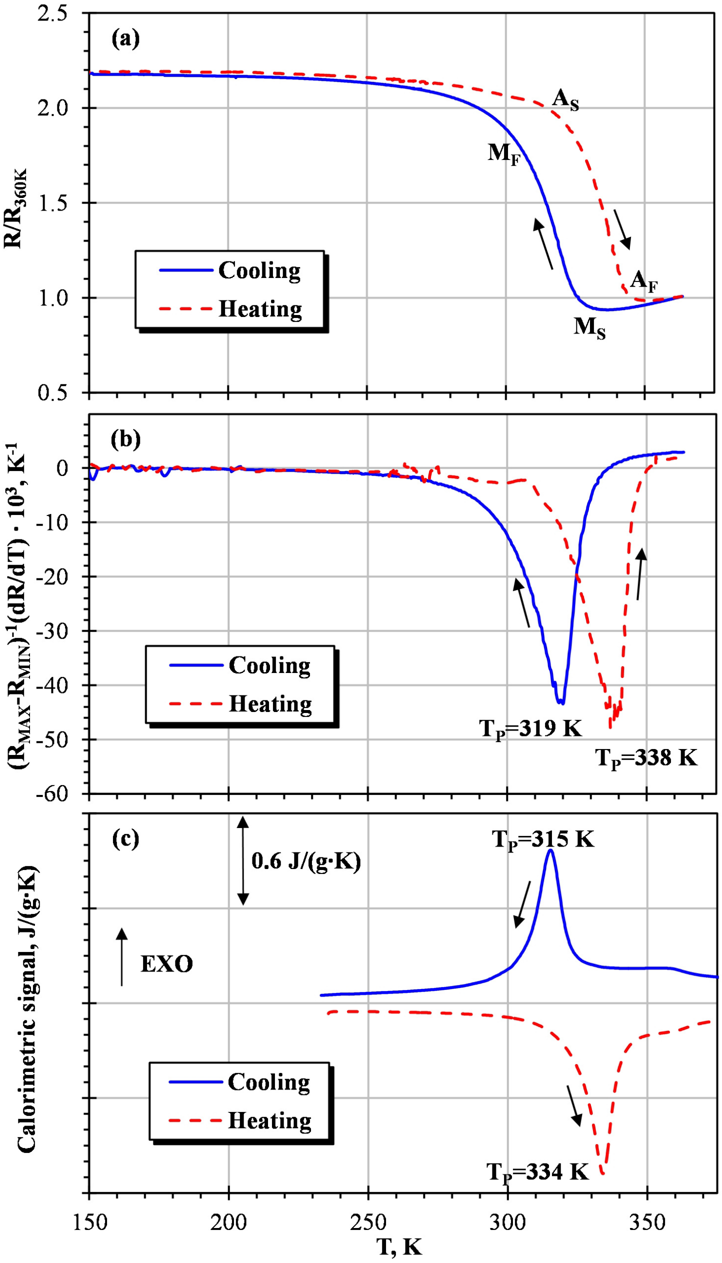

Figure 6.1: Temperature dependence of (a) the resistance, (b) the relative temperature rate of the resistance variation and (c) the calorimetric signal, for a sample of $Ni_{45}Mn_{36.7}In_{13.3}Co_5$ alloy quenched from 1070 K, registered during a continuous temperature cycle. Resistance data in (a) are normalized to the value of resistance at 360 K. The transformation temperatures are indicated in (a) and the peak temperatures are shown in (b) and (c). Arrows indicate the temperature scan direction, cooling or heating.

similar. As commented in Section 2.7 (page 58), the temperature dependence of ϕ and of the $\frac{\partial R}{\partial T}$ are two different approximations to the temperature dependence of the temperature rate of the martensite volume fraction $\frac{\partial F}{\partial T}$. Therefore, the good correspondence between the temperature dependences of $\frac{\phi}{m\beta}$ and $\frac{1}{R_{MAX}-R_{MIN}}\frac{\partial R}{\partial T}$ indicates a proportionality between the resistance and the martensite volume fraction $\partial R \propto \partial F$.

Given the different magnetic behavior of he austenite and martensite in the sample of Ni–Mn–In–Co alloy, the thermodynamical equilibrium of the phases, and then the transformation temperatures, should be affected by the application of an external magnetic field. Resistivity experiments without applied magnetic field (0 T) and with a magnetic field of 2.9 T were performed with the WQ sample. Figure 6.2 shows the effect of the application of a magnetic field on the resistance of the metamagnetic sample with low degree of order for continuous cooling scans.

Panel (a) of the Figure 6.2 compares the temperature dependence of the resistance on cooling without applied magnetic field (cooling under zero field) and with an applied magnetic field of 2.9 T (2.9 T field cooling). The transformations temperatures decrease with the application of the magnetic field: M_S varies from 329 to 325 K, M_F from 298 to 285 K and T_P from 319 to 312 K. This is the expected behavior since the magnetic field stabilizes the ferromagnetic austenite. Then, the application of a sufficiently high magnetic field can induce the reverse MT, as shown by Kainuma et al. [56]. Both resistance curves almost coincide below 260 K. This fact suggests that the transformation is completed in both cases or, at least, achieve similar value of F, i.e., the transformation is not arrested by the magnetic field.

Panel (b) displays the relative temperature rate of the resistance curves shown in panel (a). $\frac{1}{R_{MAX}-R_{MIN}}\frac{\partial R}{\partial T}$ corroborates the decrease of the transformation temperatures with the applied magnetic field and the identical temperature dependence of both curves in martensite. In addition, the value of the relative temperature rate of the resistance is reduced at the peak temperature, from about -43 K^{-1} for the cooling under zero field to about -34 K^{-1} for the field cooling. Since for both experiments, the resistance varies between the same two points of the (R, T) coordinates, the areas below the $\frac{1}{R_{MAX}-R_{MIN}}\frac{\partial R}{\partial T}$ curves should be nearly equal. Therefore, the lower peak value of $\frac{1}{R_{MAX}-R_{MIN}}\frac{\partial R}{\partial T}$ for the field cooling curve is caused by the broader temperature transformation range: the transformation range is 31 K for the cooling under zero field and about 40 K for the field cooling data. A comparison of the values of $\frac{1}{R_{MAX}-R_{MIN}}\frac{\partial R}{\partial T}$ and of $M_S - M_F$, shows an approximately inverse proportionality between them. This relation confirms that the area below the relative temperature rate of the resistance curves are similar and

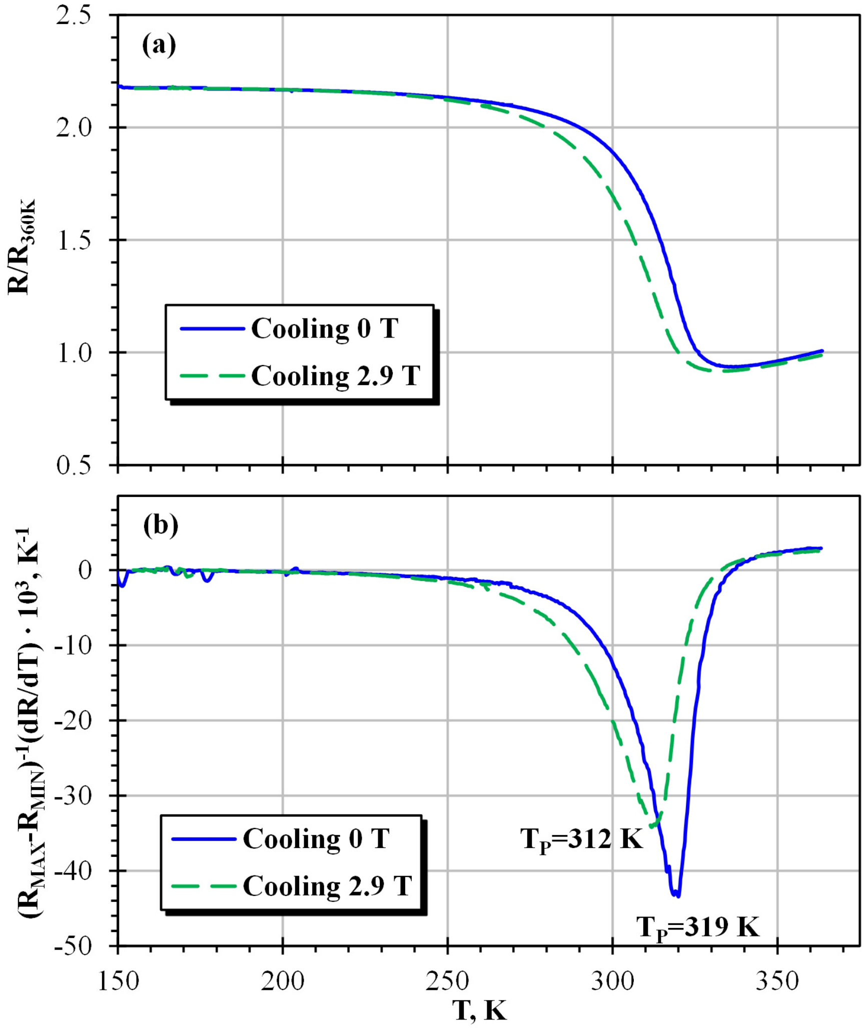

Figure 6.2: Temperature dependence of (a) the resistance and (b) the relative temperature rate of the resistance, for a sample of $Ni_{45}Mn_{36.7}In_{13.3}Co_5$ alloy quenched from 1070 K, registered during two cooling scans, without (0 T, continuous line) and with (2.9 T, long dashed line) applied magnetic field. Resistance data in (a) are normalized to the value of resistance at 360 K.

also confirms that the transformation is not arrested.

As a next step, conventional isothermal holding experiments were performed, in which the temperature ramp was interrupted and the sample is isothermally held at a certain temperature for a typical time of 2400 seconds. The kinetics of the resistance during this isothermal isofield experiments were registered. This procedure was repeated with stops at different temperatures along the transformation range to obtain the temperature dependence of the possible isothermal effects. Figure 6.3 presents in a synthetic plot the time evolution of the resistance registered in different isothermal holding experiments within the transformation domain of the direct MT for the WQ sample. These experiments were performed without applied magnetic field. Thus these data are related to the zero field resistance curve or “0 T” shown in Figure 6.2. For clarity, curves are separated between panels (a) and (b) of the Figure 6.3 depending on the total resistance accumulated during the isothermal dwelling. The time evolution curves with larger isothermal effect, which are near the transformation peak, are displayed in panel (a). In its turn, a representative selection of curves with small or no isothermal accumulation of resistance, which are at the high or low temperature sides of the transformation peak, are shown in panel (b). Note the different scale of the ordinate axes in Figures 6.3a and 6.3b.

The isothermal accumulation of resistance, which is proportional to the variation of the martensite volume fraction, is evident from the Figure 6.3. In fact, it is comparable or larger than the effects demonstrated by other isothermal MTs, see, for example, Figure 3.5 in page 88. Similar to the previous results for the Ni–Ti data from the present work, the kinetics of the isothermal magnetostructural transformation can be fitted by a logarithmic function of time, equation (2.31) in page 45. In panel (a) of the Figure 6.3, the time evolution curve which presents the largest accumulation of resistance and larger time-dependence was registered at 318 K, very close to the transformation peak 319 K, Figure 6.1b. For the other curves, the isothermal accumulation of martensite decreases as the experimental holding temperatures get away from the peak temperature.

Similarly to Figure 6.3, Figure 6.4 collects in a synthetic plot the time evolution of the resistance registered in different isothermal holding experiments on cooling under external magnetic field of 2.9 T for the WQ sample. It is important to notice that the whole experimental procedure took place under a magnetic field of 2.9 T, which was applied at the beginning of the cooling process slightly above 360 K. Then, the magnetic field is present and is not removed during the cooling, the interruption of the temperature scan, the isothermal holding time and the restart of cooling. As commented above, the application of the magnetic field decreases the transformation

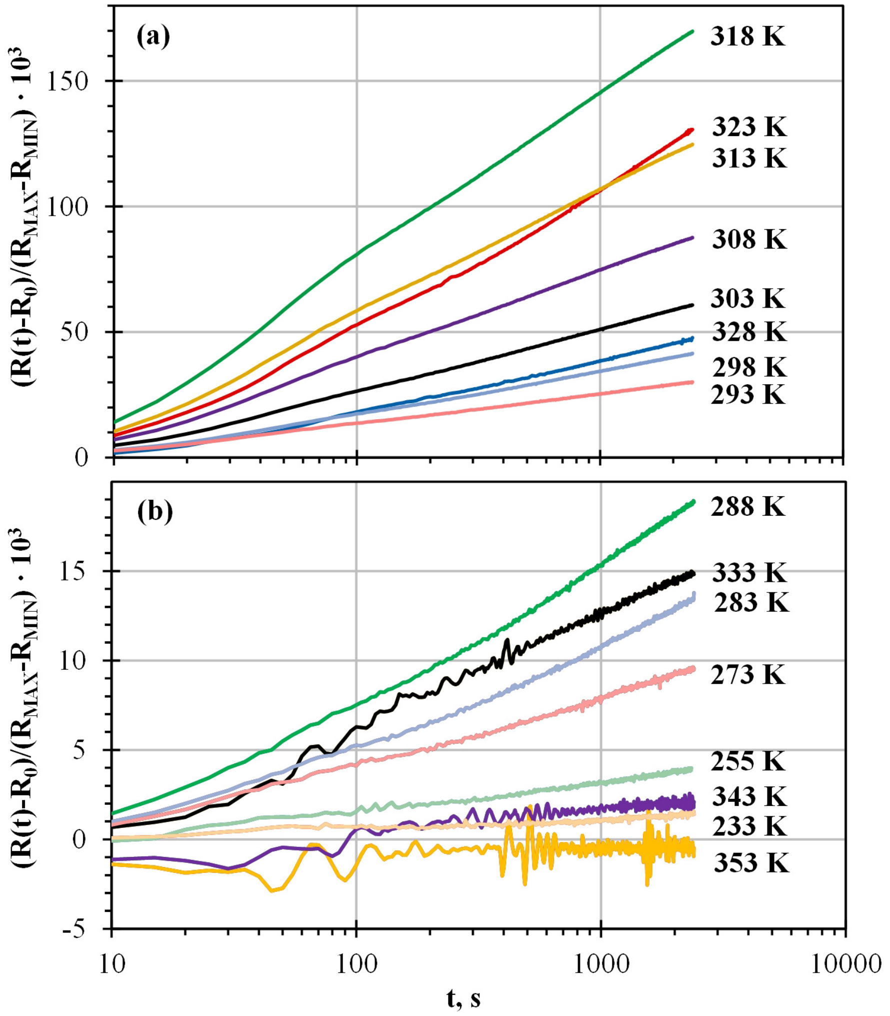

Figure 6.3: Time evolution of the resistance during interruptions of the cooling under zero field scan near and inside the transformation range of the direct transformation for a sample of $Ni_{45}Mn_{36.7}In_{13.3}Co_5$ alloy quenched from 1070 K. The time dependences with higher accumulation of resistance are shown in panel (a), while a representative selection from the rest of the measured time dependences is displayed in panel (b). Note different ordinate scales in (a) and (b).

temperatures and increases the transformation temperature range. Figure 6.4 reveals that the effect of the magnetic field is reflected in the isothermal accumulation of resistance:

- The maximum accumulation of resistance and largest time-dependence takes place during the experimental holding performed at 313 K, instead of 318 K, as it was in the zero field experiments. This difference corresponds to the shift of the transformation peak temperature during the continuous field cooling experiment to 312 K, Figure 6.2b.

- The total accumulation of resistance during 2400 s is reduced as compared with the zero field isothermal experiments. Note the different ordinate axis of the Figure 6.3a and of the Figure 6.4a. This effect is in agreement with the decrease of the height of the $\frac{1}{R_{MAX}-R_{MIN}}\frac{\partial R}{\partial T}$ peak with applied magnetic field. Since the decrease of $\frac{1}{R_{MAX}-R_{MIN}}\frac{\partial R}{\partial T}$ and the increase of the MT range are correlated, the decrease of the intensity of the isothermal effects under polarizing field is also correlated with the broadening of the MT range.

Figure 6.5 compares the temperature dependence of the relaxation rate Z derived from the data shown in Figures 6.3 and 6.4 with the relative temperature rate of the resistance $\frac{1}{R_{MAX}-R_{MIN}}\frac{\partial R}{\partial T}$, already shown in Figure 6.2b, for the WQ sample. More specifically, panel (a) shows the calculated data from experiments performed without applied magnetic field and panel (b) depicts the same dependence under an applied magnetic field of 2.9 T.

Figure 6.5a shows that, for this alloy composition and heat treatment, there exists almost perfect proportionality between the relaxation rate, Z, and the relative temperature rate of the resistance. This fact suggests that in the present case the resistance variation is a very good measure of the change of martensite volume fraction, ΔF. The behavior of the direct transformation is clearly isothermal. As shown by Figure 6.3a, approximately 15% of the material can transform isothermally when it is held near the transformation peak temperature. In other words, the transformation may not be completed isothermally, but instead it will reach a saturation state were the material is in a mixed state of austenite and martensite. In this direction, it has been shown by Kustov et al. [62] for a sample of the same composition ($Ni_{45}Mn_{36.7}In_{13.3}Co_5$) that the saturation is approached after $\sim 10^4$ seconds and the saturation occurs before the transformation is completed. The saturation time was not exhaustively investigated in the present work. However, assuming, first, that the transformation reaches the saturation in a isothermal dwelling at T_P before the MT is completed, and, second, that

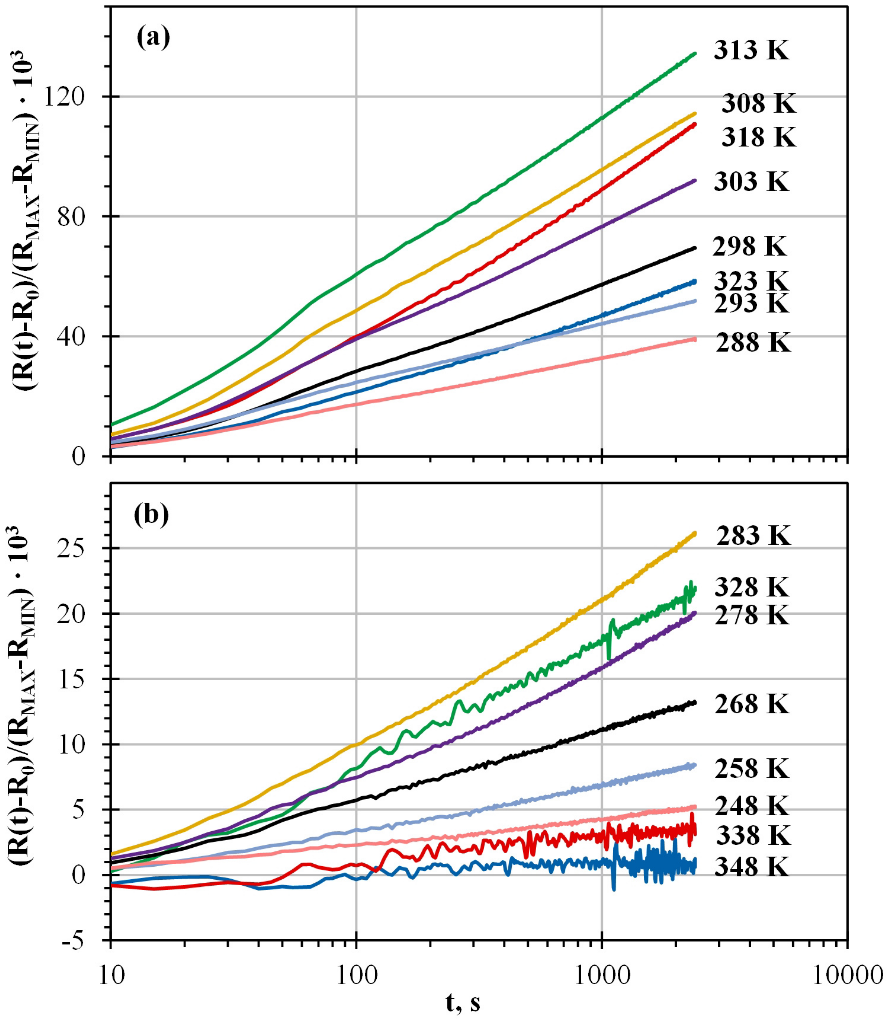

Figure 6.4: Time evolution of the resistance during interruptions of the field cooling scan (3 T) near and inside the transformation range of the direct transformation for a sample of $Ni_{45}Mn_{36.7}In_{13.3}Co_5$ alloy quenched from 1070 K. The time-dependence curves with higher accumulation of resistance are show in panel (a), while a representative selection from the rest of the measured time dependences is displayed in panel (b). Note different ordinate scales in (a) and (b).

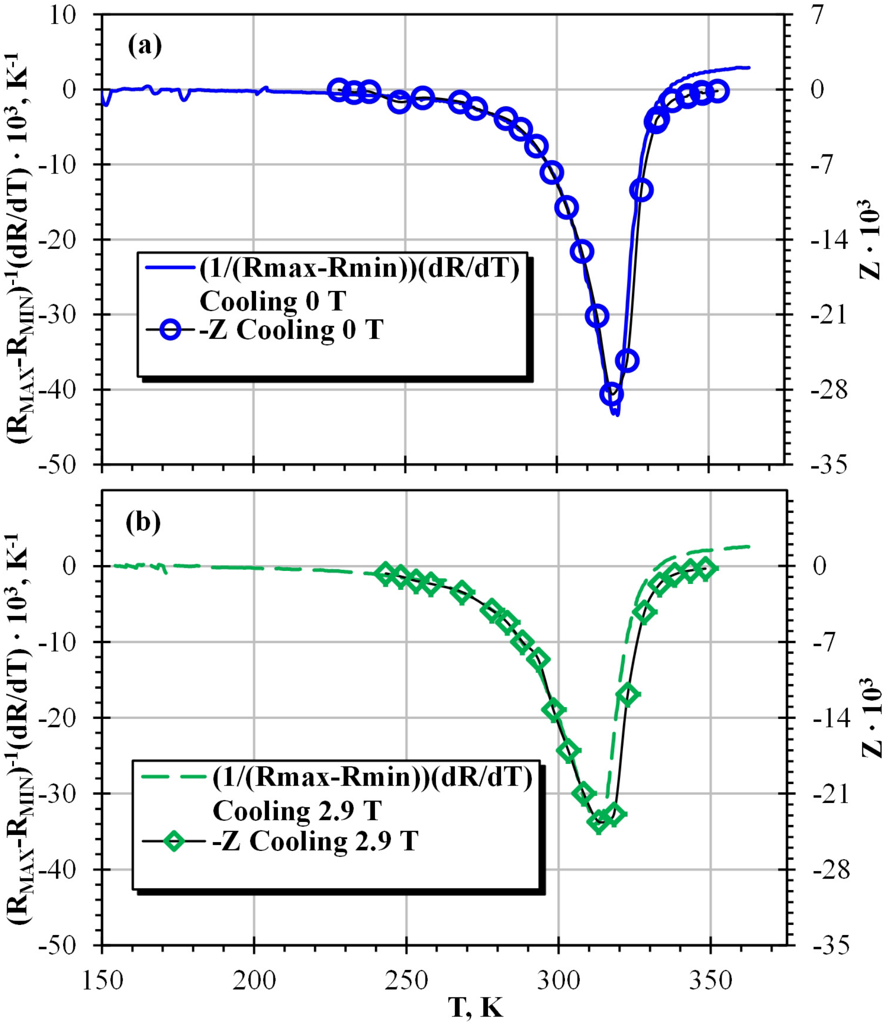

Figure 6.5: Comparison of the temperature dependence of the relative temperature rate of the resistance, $\frac{1}{R_{MAX}-R_{MIN}}\frac{\partial R}{\partial T}$ and of the relaxation rate Z for a sample of $Ni_{45}Mn_{36.7}In_{13.3}Co_5$ alloy quenched from 1070 K; (a): $\frac{1}{R_{MAX}-R_{MIN}}\frac{\partial R}{\partial T}$ for cooling under zero field (continuous line), -Z calculated from isothermal holdings upon interruptions of cooling under zero field (open circles); (b): $\frac{1}{R_{MAX}-R_{MIN}}\frac{\partial R}{\partial T}$ for field cooling (2.9 T, long-dashed line), -Z calculated from isothermal holdings upon interruptions of field cooling (2.9 T, open diamonds).

the accumulation of martensite decreases with temperature proportionally to $\frac{\partial R}{\partial T}$, then the transformation may not be completed isothermally for dwellings along the most part of the transformation range, even relatively close to M_F. This speculation reinforces the idea of the IMT as an process out of equilibrium but which is never far from the saturation state and would behave athermally if the relaxation process was much more rapid.

The material can be classified as a thermally activated martensite (behaves anisothermally during cooling and isothermally under dwelling conditions), which transformation is never very far from an equilibrium/saturation state. Therefore, the isothermal magnetostructural transformation behaves quite similar to the isothermal MTs studied in the non-magnetic Ni–Ti–X alloy system.

The results for the field cooling experiments, depicted in the panel (b) of the Figure 6.5, demonstrate, again, the good correlation between Z and $\frac{\partial R}{\partial T}$. In addition, since the ordinate axis in the panel (b), for both the relaxation rate and the temperature derivative of the resistance, have the same scale as the ordinate axis in the panel (a), then proportionality factor between Z and $\frac{\partial R}{\partial T}$ is independent of the applied magnetic field.

Referring to the model of bistable units introduced in Section 5.1 (page 161), one should conclude that the number of units which can transform during an isothermal holding experiment $N(T)$ is determined by the free energy balance of the phases, which depends on the external variables, T, H and σ_0, and by the T-scan rate β of the experiment, since $N(T)$ depends on the quantity of anisothermally transforming material. Therefore, the application of the magnetic field affects the isothermal transformation. However, the thermally activated process is the same and yields the same logarithmic kinetics and intensity of isothermal effects. In other words, as $Z(T)$ and $\frac{\partial R}{\partial T}$ are related to $N(T)$, the application of H changes $N(T)$, and thus changes $Z(T)$ and $\frac{\partial R}{\partial T}$ in a similar way, not affecting the proportionality between $Z(T)$ and $\frac{\partial R}{\partial T}$, $Z(T) \sim \frac{\partial R}{\partial T}$.

6.2 Arrested isothermal magnetostructural transformation

The athermal/isothermal behavior of the $L2_1 \rightarrow 2M$ transformation of a sample of $Ni_{45}Mn_{36.7}In_{13.3}Co_5$ alloy heat treated at 1170 K and cooled in air at room temperature was investigated. A sample, slowly cooled from temperature above the B2-$L2_1$ ordering one, possess a high degree of LRO, as has been mentioned in Section 6.1.

Following Ito et al. [151], the highly ordered material transforms to the six-layered monoclinic martensite (6M). Therefore, the air cooled sample exhibits the $L2_1 \leftrightarrow 6M$ martensitic transformation.

However, the most important is that the characteristics of the MT exhibited by the quaternary Ni–Mn–In–Co alloy depend strongly on the degree of $L2_1$ long-range atomic order. This dependence stems primarily from the decrease of the chemical driving force of the transformation, related to the entropy difference between austenite and martensite.

The effect of the long-range atomic ordering over the entropy change, Δs, has been investigated previously [60, 154]. A variety of samples of $Ni_{45}Mn_{36.7}In_{13.3}Co_5$ alloy with different heat treatments was used. The temperature-induced MTs exhibited by these samples were characterized by means of DSC measurements, the Curie temperature of the austenite, T_C, and the transformation peak temperature, T_P. The variation of entropy were calculated for both direct and reverse transformations. The dependence of the entropy change on $T_C - T_P$ is shown in Figure 6.6.

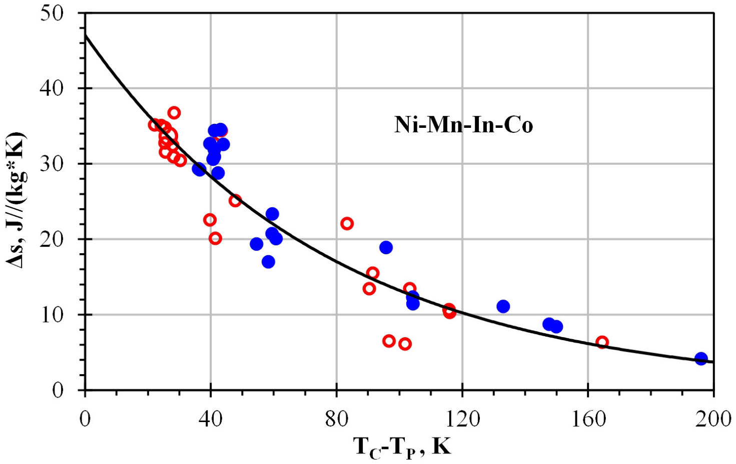

Figure 6.6: Dependence of the transformation entropy change Δs on the difference between the Curie temperature and the transformation peak temperature $T_C - T_P$ for samples of $Ni_{45}Mn_{36.7}In_{13.3}Co_5$ alloy subjected to different heat treatments. Full circles: direct MTs; open circles: reverse MTs. The continuous line fits the data by a power law, $\Delta s = a(T_C - T_P)^b$.

The degree of $L2_1$ atomic order affects the transformations temperatures; the Curie temperature increases and the transformation temperatures strongly decrease as the degree of order is increased. Therefore, the points on the left of the Figure 6.6 corresponds to the samples with low degree of LRO order, like the WQ sample, which have low $T_C - T_P$ and the points on the right of the same figure - to the highly ordered samples. The data are fitted by a power law, $\Delta s = a(T_C - T_P)^b$, which, despite the scatter of data, shows that there is an inverse relationship between Δs and $T_C - T_P$. The extrapolation of the observed decrease in Δs with increasing $T_C - T_P$ shows that for even lower MT temperatures the entropy change could likely become zero or even change its sign. That means that the MT could be completely thermodynamically arrested for higher $T_C - T_P$ values.

On the other hand, the entropy change was calculated as $\Delta s = l/T_P$, where l is the latent heat per kilogram of the material undergoing the transformation. Therefore, the obtained value of the entropy change is actually an average over the transformation range. In fact, the "true" entropy change between austenite and martensite will depend on temperature [154]: it is higher in the beginning of the transformation than close to M_F. This difference is important for the transformations with low driving force because they require higher overcooling in order to complete the MT and then the transformation range is broader. Therefore, since the entropy change is low and the transformation is broad, the variation of entropy along the transformation range may be comparable with the average Δs. This fact makes possible the "effective" Δs to reach zero or negative values during the direct transformation. In this case, the transformation becomes partially arrested: some austenite will not transform to martensite even if the temperature is further decreased.

The above phenomena are explained in terms of the lattice, $\Delta s^{P\to M}_{lattice}$, and magnetic, $\Delta s^{P\to M}_{magn}$, contributions to the transformation entropy change [57, 60]. The magnetic contribution to the entropy change is large for the MMSMAs because of the different magnetic behavior of the ferromagnetic austenite and the weakly magnetic martensite. During the direct transformation, the sample goes from a ferromagnetic state (high order) to a strongly disordered magnetic state. Then, the entropy of the magnetic subsystem notably increases during the transformation. By contrast, the contribution of the lattice (or of the elastic subsystem) is, as usually, negative. $\Delta s^{P\to M}_{lattice}$ should have a higher absolute value than $\Delta s^{P\to M}_{magn}$ for the MT to proceed. If one assumes that the two contributions are additive [154]:

$$\Delta s^{P\to M} = \Delta s^{P\to M}_{lattice} + \Delta s^{P\to M}_{magn} \tag{6.1}$$

one should conclude that, in the magnetostructural transformations, the positive magnetic contribution reduces the total entropy change, $\Delta s^{P\to M}$, and thus the driving force of the transformation.

The samples with high degree of LRO have a larger difference between the Curie temperature and the transformations temperatures than the disordered ones. Consequently, the order of the magnetic subsystem is higher during the transformation (since the MT range is far from T_C) and then the positive magnetic contribution is also higher, reducing the total entropy change, see equation (6.1). This behavior explains the inverse relationship between Δs and $T_C - T_P$.

These considerations explain remarkable differences between the transformation properties of samples with high degree of LRO, obtained by air cooling to room temperature, which we will refer to as SC samples, and the WQ sample.

Figure 6.7 shows the temperature dependence of the resistance, in panel (a), the relative temperature rate of the resistance, in panel (b), and the exchanged heat, in panel (c), for the SC sample during a continuous temperature cycle.

Some of the characteristics mentioned above, of the samples with high degree of LRO order, are clearly shown in the Figure 6.7:

1. The higher degree of LRO shifts the transformation temperatures to lower temperatures. They are, approximately, $M_S = 280$ K and $M_F = 160$ K for the direct transformation and $A_S = 200$ K and $A_F = 310$ K for the reverse one.

2. The low driving force implies that the transformation needs higher overcooling to proceed. Therefore, the MT range for the SC sample is very broad: it is 120 K for the direct path and 110 K for the reverse one.

3. Since the transformation is rather diffuse, the height of the $\frac{1}{R_{MAX}-R_{MIN}}\frac{\partial R}{\partial T}$ peak, in Figure 6.7b, is approximately $\frac{1}{3}$ of its value for the WQ sample, Figure 6.1b. In addition, the DSC signal, in Figure 6.7c, does not show any clear transformation peak.

4. From the relative temperature rate of the resistance in Figure 6.7b, the peak temperatures of the direct transformation is 245 K and the one of the reverse path is 274 K.

5. Then, the MT hysteresis is around 30 K, which is much lower than the transformation range but is comparable with the hysteresis for IMTs in Ni–Ti alloys.

As a consequence of the absence of transformation peak on the DSC signal, the temperature dependence of $\frac{\phi}{m\beta}$ cannot be used to confirm/reject the correspondence between the variation of resistance and the change of

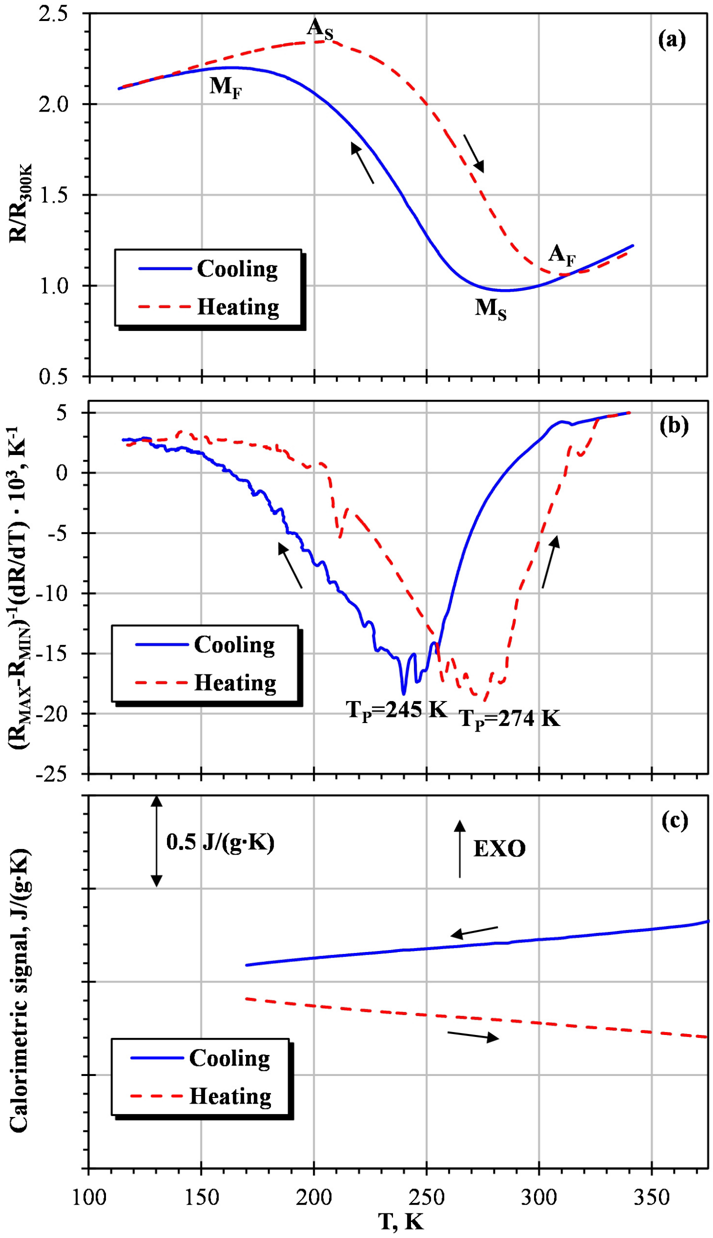

Figure 6.7: Temperature dependence of (a) the resistance, (b) the relative temperature rate of the resistance and (c) the calorimetric signal, for a sample of $Ni_{45}Mn_{36.7}In_{13.3}Co_5$ alloy annealed at 1070 K and air cooled, registered during a continuous temperature cycle. Resistance data in (a) are normalized to the value of resistance at 300 K. The transformation temperatures are indicated in (a) and the peak temperatures are shown in (b). Arrows show the temperature scan direction, cooling or heating.

the martensite volume fraction, i.e., the $dR \propto dF$ condition. However, the total variation of resistance during the martensitic transformation is high and negative factors which could affect the proportionality between dR and dF, like the strong T-dependence of the resistance due to the scattering of phonons, are not present. Indeed, for the SC sample, the temperature dependence of the resistance outside the transformation range is rather weak. Therefore, the resistance is expected to have a monotonous relation with the martensite volume fraction.

As in the case of WQ sample, the resistance of the SC sample was measured both under the action of a constant applied magnetic field and without field: resistivity data for cooling under zero field, 1.7 T field cooling and 2.9 T field cooling were obtained. The effect of the applied magnetic field on the resistance during a continuous cooling is shown in Figure 6.8.

Panel (a) shows the temperature dependence of the resistance registered for the three different values of the applied magnetic field. Similar to the behavior of the WQ sample, the M_Sa and T_S temperatures decrease with the application of the magnetic field: M_S varies from 280 K for cooling under zero field to 265 K and 260 K for the 1.7 T and 2.9 T field coolings, respectively; and T_P, from the data for the relative temperature transformation rate, in Figure 6.8b, changes from 245 K, for the cooling under zero field, to 233 K (1.7 T) and to 223 K (2.9 T).

However, the SC sample presents two substantial differences as compared to the WQ sample. For the present composition/heat treatment they are as follows.

1. M_F seems to be almost independent of the applied magnetic field: it is about 160 K for all three dependences. Furthermore, below a certain temperature, about 210 K, the three $\frac{\partial R}{\partial T}$ curves are very similar; they seem to follow a kind of a “master curve” which is independent of the applied magnetic field.

2. The total variation of resistance during the transformation, $\Delta R_{TOT} = R_{MAX} - R_{MIN}$, is reduced with the applied magnetic field. In this way, it decreases to about $0.82\Delta R_{TOT}$ for the 1.7 T field cooling and to about $0.44\Delta R_{TOT}$ for the 2.9 T field cooling experiment.

These two points indicate that the transformation for the ordered sample becomes incomplete under magnetic field: it is “arrested”. Thus, the transformation is frozen below approximately 160 K and is not completed even though the temperature is further reduced. Below the apparent M_F, the material is in a mixed state of austenite and martensite. The origin of this behavior is fourfold:

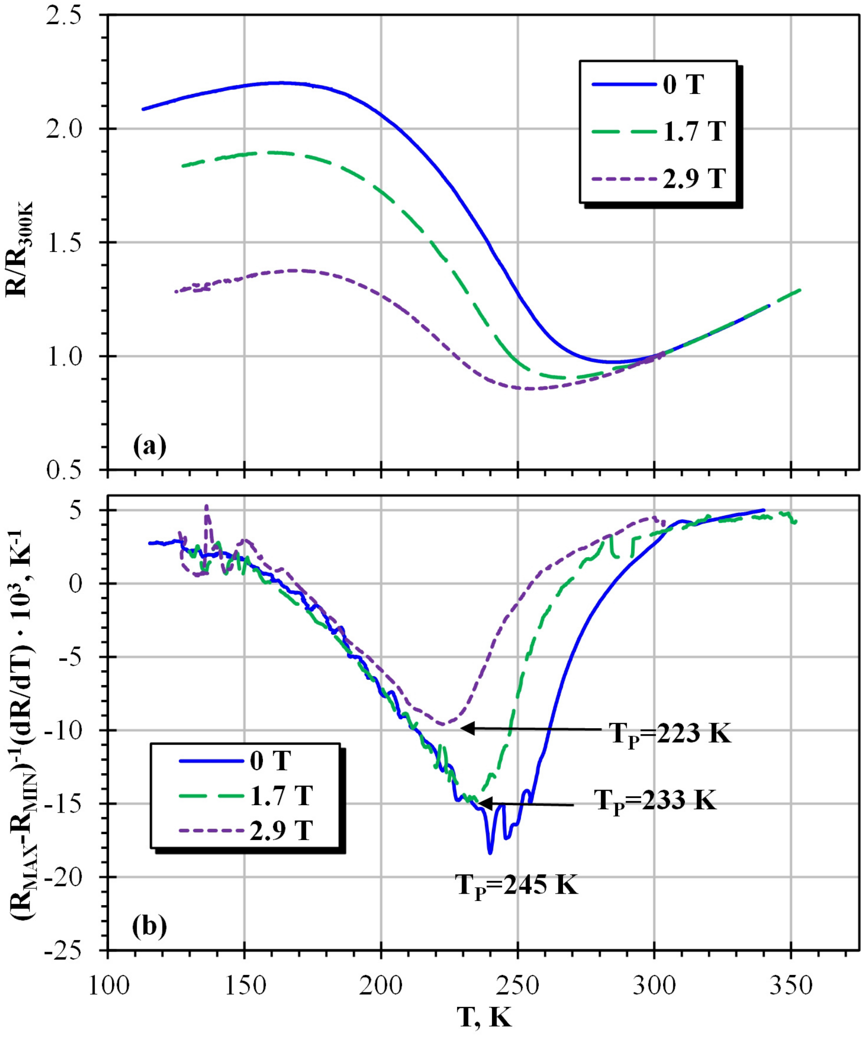

Figure 6.8: Temperature dependence of (a) the resistance and (b) the relative temperature rate of the resistance for a sample of $Ni_{45}Mn_{36.7}In_{13.3}Co_5$ alloy annealed at 1070 K and air cooled. Measurements registered during different cooling scans: cooling under zero field (continuous line), 1.7 field cooling (long-dashed line) and 2.9 T field cooling (short-dashed line). Resistance data in (a) are normalized to the value of resistance at 300 K.

1. The application of the polarizing field increases the magnetization and the magnetic order of the ferromagnetic austenite, so the $\Delta s_{magn}^{P \to M}$ term in equation (6.1) increases.

2. The driving force of this MT, even without applied magnetic field, is small. Therefore, the variations of the magnetic contribution with the applied magnetic field to the total entropy change can reduce it to zero value.

3. As has been commented above, the true entropy change decreases with temperature, permitting the partial arrest of the transformation.

4. The temperature dependence of the resistance for cooling under zero field collapses into the other two, obtained under field, below 210 K, Figure 6.8b. However, the variation of resistance over this temperature range remains high, Figure 6.8b; comparable to the total resistance change in the non-arrested WQ sample, Figure 6.1a. These two points indicate that the transformation may be partially arrested even without applied magnetic field, but this arrest should be only minor, since the total variation of the resistance under zero field is close to the one for the WQ sample.

Therefore, the direct $L2_1 \to 6M$ MT exhibited by the SC sample represents a situation when the amount of arrested austenite can be controlled by the applied magnetic field.

On the other hand, since the variation of resistance during the transformation depends on the applied magnetic field, one can obtain different R_{MAX} and R_{MIN} for each curve. Following equation (2.21) on page 42, R_{MAX} and R_{MIN} are used to calculate the relation between the resistance and the martensite volume fraction, neglecting other contributions to the temperature dependence of the resistance. If the resistance increases during the direct transformation, $F = 1$ when $R = R_{MAX}$ and $F = 0$ when $R = R_{MIN}$. Then, $\frac{1}{R_{MAX} - R_{MIN}}$ is the factor of proportionality between ΔF and ΔR. As a consequence of the arrest, ΔR is reduced because of the reduced change of martensite volume fraction δF. However, the proportionality factor between ΔR and ΔR is likely not affected by the arrest. This consideration has to be taken into account when one calculates the isothermal transformation rate Z from the resistance data, equations (2.30) and (2.31) in page 45. Given a certain sample and experimental conditions, the R_{MAX} and R_{MIN} which correspond to the full transformation should be used for all calculations disregarding the effect of the applied magnetic field on R_{MAX} and R_{MIN}, as has been the done in the present case. However, as commented before, the transformation might be slightly arrested even during cooling under zero field. Thus, the values of R_{MAX} and R_{MIN} used for the following calculation might not correspond to the full transformation. However, since this arrest, if any, should be only minor, this effect will be neglected.

As the next step, the kinetics of the resistance were registered during isothermal isofield dwellings after interruptions at different temperatures in three cases, cooling under zero field, 1.7 T field cooling and 2.9 T field cooling. Figure 6.9 presents in a synthetic plot the results of the isothermal holding experiments for the SC sample. For clarity, a selection of the dependences which yield higher values of the relaxation rate Z are shown for the interruptions of cooling under zero field, in panel (a), 1.7 T field cooling, in panel (b), and 2.9 T field cooling, in panel (c). The time evolution curves shown in Figure 6.9 follow the typical logarithmic kinetics in all three cases.

In panel (a), the variation of resistance is higher in the isothermal experiments performed at 232 K and 252 K, and it decreases on reducing the dwelling temperature. The major reason for this reduction appears to be the shift (on a logarithmic time scale) of the curves along the time axis, i.e., the emergence of the increase of the incubation time of the MT. This scheme is repeated for the results of field cooling curves in panels (b) and (c). The major effect of the applied field, in its turn, appears to be the decrease of the temperature of the highest intensity of the isothermal effects.

Figure 6.10 shows a comparison between the temperature dependence of the relative temperature rate of the resistance $\frac{1}{R_{MAX}-RMIN}\frac{\partial R}{\partial T}$ and the isothermal transformation rate Z for interruptions of cooling for a SC sample of $Ni_{45}Mn_{36.7}In_{13.3}Co_5$ alloy. The curves "-Z 0 T" in panel (a), "-Z 1.7 T" in panel (b) and "-Z 2.9 T" in panel (c) are composed by Z values calculated from curves of experiments performed by interrupting the cooling under zero field, 1.7 T field cooling and 2.9 T field cooling, respectively.

The main features revealed by Figure 6.10 are as follows:

- The temperature dependence of relative temperature rate of the resistance and of the isothermal transformation rate Z are not proportional. This makes the SC samples of quaternary Ni–Mn–In–Co alloy with a high degree of LRO quite a special case, because, until this point, all the isothermal MTs studied in the present work demonstrated a close correlation between Z and $\frac{\partial R}{\partial T}$. This includes the IMT investigated in the conventional Ni–Ti–X alloys system and isothermal magnetostructural transformation of the WQ sample, which has low degree of long-range order.

- The Z peak is broader than the $\frac{\partial R}{\partial T}$ peak and seems to form some kind of "plateau", specially for the data from the zero field experiments;

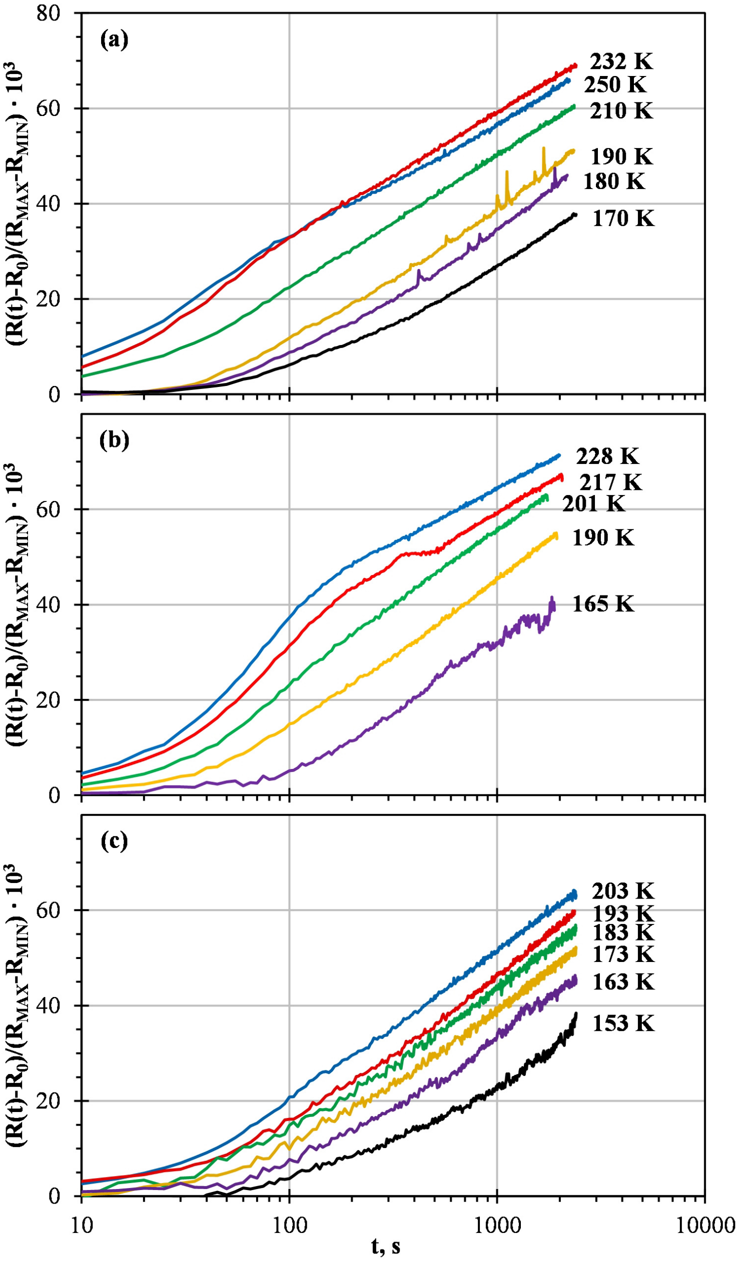

Figure 6.9: Time evolution of the resistance during interruptions of cooling for the direct $L2_1 \rightarrow 6M$ transformation range for a sample of $Ni_{45}Mn_{36.7}In_{13.3}Co_5$ alloy annealed at 1070 K and air cooled. A selection of representative isothermal holding experiments which presents notable isothermal accumulation of resistance are shown for interruptions of (a) the cooling under zero field, (b) the 1.7 T field cooling and (c) the 2.9 T field cooling.

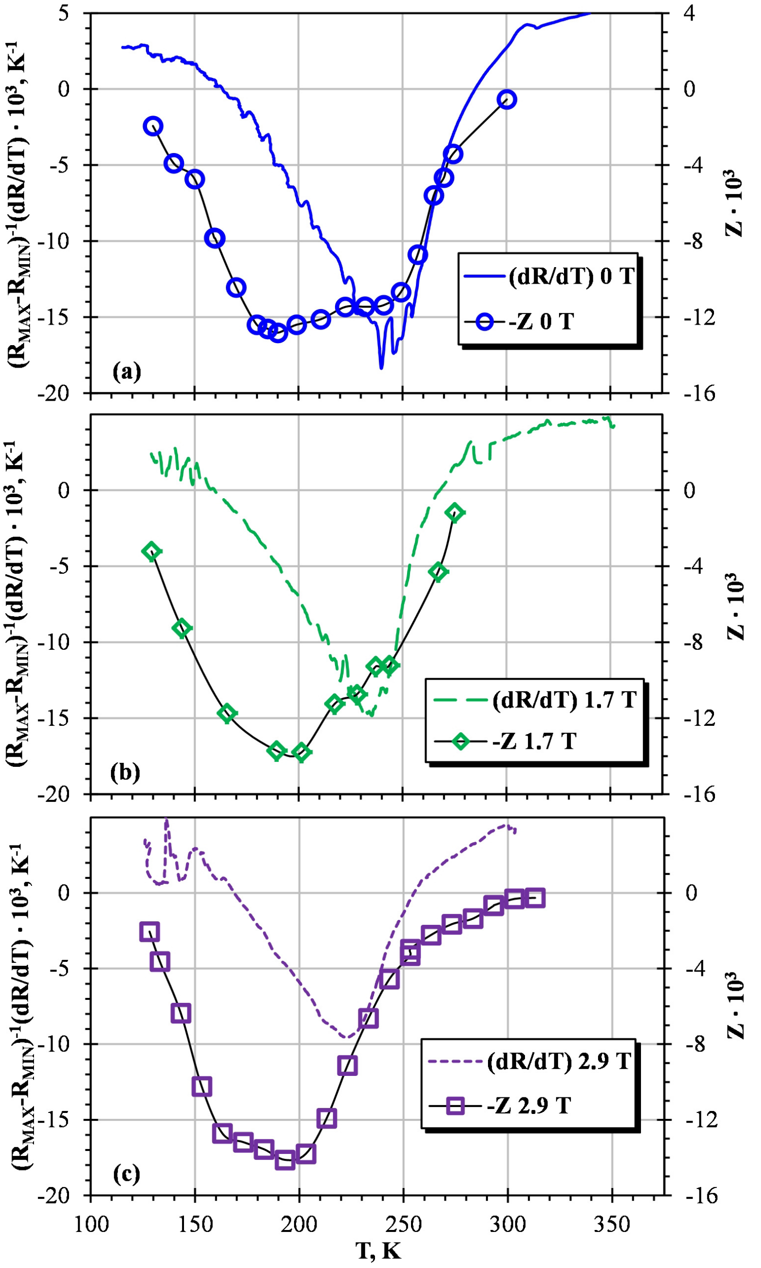

Figure 6.10: Comparison of the temperature dependence of the relative temperature rate of the resistance and of the relaxation rate for a sample of $Ni_{45}Mn_{36.7}In_{13.3}Co_5$ alloy annealed at 1070 K and air cooled. $\frac{1}{R_{MAX}-R_{MIN}}\frac{\partial R}{\partial T}$ for (a) a cooling under zero field (continuous line), (b) a 1.7 T field cooling (long-dashe line) and (c) a 2.9 T field cooling (short-dashed line). $-Z$ calculated from the isothermal-isofield data measured with an applied magnetic field of (a) 0 T (circles), (b) 1.7 T (diamonds) and (c) 2.9 T (squares).

for quite a broad temperature range, between 180 K and 250 K, the isothermal holding experiments give similar values for the relaxation rate Z. This "plateau" is reduced by the application of the magnetic field, as it decreases M_S temperature, but not M_F.

- While the maximum values of the relative temperature rate of the resistance decrease with the applied magnetic field, the values of the relaxation rate within the "plateau" are almost independent or even slightly increase with the applied magnetic field. The maximum values of Z obtained are 12.8 for the cooling under zero field, 13.8 for the 1.7 T field cooling and 14.1 for the 2.9 T field cooling experiments.

- The intensity of isothermal effects decreases as the dwelling temperature of the isothermal isofield experiments increases from approximately 160 K to 130 K. This temperature range is well below the $\frac{\partial R}{\partial T}$ peak in the three cases. Furthermore, one can note that 160 K is approximately the apparent martensite finish temperature obtained from the resistance data, which is almost independent on the applied magnetic field. However, the relaxation rate shows relatively high values for experiments performed near 160 K. Therefore, at M_F, despite the fact that the anisothermal transformation during a continuous cooling is almost "finished", the transformation can still proceed isothermally with elevated intensity of accumulation of martensite.

All these observations seem to be closely related to the arrest of the transformation. The major differences between the temperature dependence of the relative temperature rate of the resistance and of the Z take place at the low temperatures side of the $\frac{\partial R}{\partial T}$ peak. The last two points can be better appreciated in the Figure 6.11, which compares the temperature dependence of Z for the different applied magnetic fields.

The three temperature dependences of Z are qualitatively similar on the low temperature side of the peaks. In fact, the values for the cooling under zero field experiments are even somewhat lower than the values for the 1.7 T and 2.9 T field cooling experiments, when the MT is incomplete. Note that the "-Z 1.7 T" and "-Z 2.9 T" curves almost collapse together for temperatures below 210 K, which is a behavior equivalent to the one demonstrated by the $\frac{\partial R}{\partial T}(T)$ in Figure 6.8. Therefore, for the arrested magnetostructural transformations, both $\frac{\partial R}{\partial T}(T)$ and $Z(T)$ follow a "master curve" which is independent of the applied magnetic field and, hence, of the amount of the arrested austenite.

On the other hand, the maximum of the $Z(T)$ peak, or the "plateau", also seems to be relatively independent of the amount of arrested austenite.

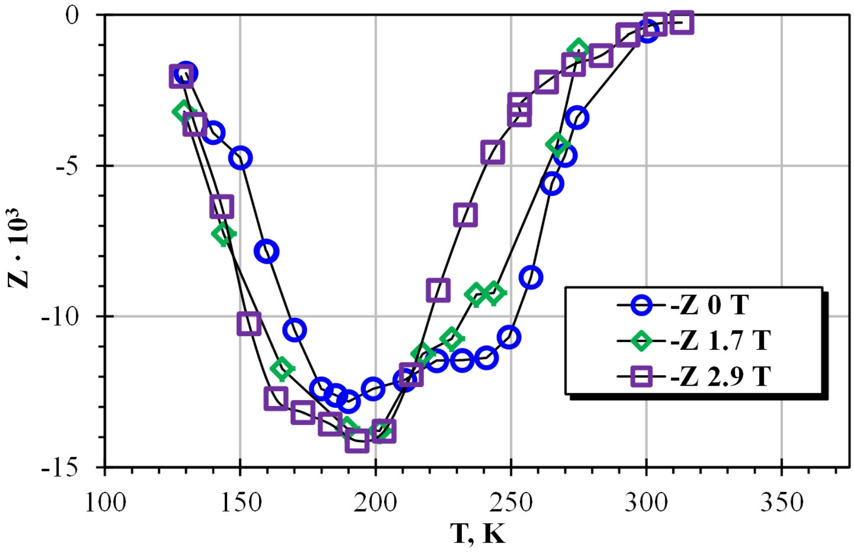

Figure 6.11: Comparison of the temperature dependence of the relaxation rate calculated from interruptions of the cooling under zero field (open circles), the 1.7 T field cooling (open diamonds) and the 2.9 T field cooling (open squares) for a sample of $Ni_{45}Mn_{36.7}In_{13.3}Co_5$ alloy annealed at 1070 K and air cooled.

This way, while the height of the $\frac{\partial R}{\partial T}$ peak decreases from about 21 K^{-1} to about 13 K^{-1} (note that in Figure 6.8b the basis of the peaks are not 0) from the cooling under zero field to the 2.9 T field cooling, the maximum of the $Z(T)$ has a very weak dependence with H, see Figure 6.11.

In the framework of the model of bistable units, $Z(T)$ is closely related with the number of units that can relax during an isothermal holding experiment $N(T)$, equation (5.25) in page 178. The results of the Section 6.1 demonstrate that the applied magnetic field affects the thermodynamic equilibrium of the phases changing the temperature dependence of $N(T)$, see Figure 6.5 and page 6.1. The decrease of the transformation temperatures, especially M_S, with H is also observed in the present case, Figure 6.10. However, the transformation is arrested by the applied magnetic field below the $\frac{\partial R}{\partial T}$ peak temperature. The arrest reduces the quantity of austenite which transforms to martensite during a continuous cycle. By contrast, the intensity of the isothermal transformation of the arrested transformation does not depend significantly on the amount of austenite that is arrested.

Therefore, the proportionality between Z and $\frac{\partial R}{\partial T}$ disappears for the arrested state because the number of units which are transforming anisothermally at certain temperature during a continuous cooling are not proportional to the number of units which can transform isothermally at the same temperature. This difference is especially notable near the M_F temperature, about 160 K, were very few material can transform during the continuous cooling, but the isothermal accumulation of resistance is high, Figure 6.9. Therefore, one should conclude that there is a part of kinetically arrested austenite which can actually transform isothermally.

The arrest of the transformation during a continuous cooling can be associated with the appearance of long incubation times in the isothermal holding experiments shown in Figure 6.9. The incubation time increases as the temperature decreases; hence, it increases with decreasing the driving force and increasing the amount of arrested austenite.

The qualitative interpretation of this regularities of the anisothermal and isothermal behavior of the arrested MT in terms of the elaborated model (Section 5.2) can be as follows. The decrease of the driving force of the MT (entropy difference) with decreasing temperatures (increasing applied field) can produce the situation when the energy barriers, impeding the progress of the MT, cannot be overcome during continuous cooling, since the driving force remains too low. Hence, the anisothermal MT is blocked, "arrested". On the other hand, the same barriers can be overcome with the assistance of thermal fluctuations in isothermal experiments, giving rise to the isothermal kinetics.

The amount of such "frozen" configurations increases with decreasing temperature and/or increasing applied field. This fact results in the opposite dependences of the anisothermal transformation rate and isothermal relaxation rate on the temperature and/or applied field. The decrease of the temperature, on the other hand, reduces the efficiency of the thermal fluctuations and requires longer waiting time, that is, the incubation time. All these features are observed in the experiments reported above.

In order to extend the investigation of the behavior of the isothermal magnetostructural transformation, the effect of removal of the applied magnetic field during isothermally dwellings was studied. The idea behind these experiments was that the removal of the applied field in the arrested state of the MT can increase dramatically the driving force of the transformation.

A new experimental protocol was developed and used. The sample was cooled under an applied magnetic field of 2.9 T at 2 K/min until the preset temperature for the isothermal holding experiment was reached and the cooling was interrupted. Next, the sample was kept under constant temperature and magnetic field for about 2400 s, like in the normal isothermal isofield experiments. After the normal isothermal dwelling, the magnetic field was removed and the new isothermal kinetics was registered again for about 2400 seconds. Figure 6.12 presents in a synthetic plot the time evolution of the resistance registered after the removal of the applied magnetic field at different dwelling temperatures for the SC sample.

Note that in the isothermal curves shown in Figure 6.12, R_0 is not the value of the resistance right after the interruption of the 2.9 T field cooling. When the applied magnetic field is removed, a jump of the resistance occurs because of the jump of the transformation driving force. Therefore, some of the austenite transforms “instantaneously” after the removal of the field, but the systems reaches quickly a new state with a fraction of metastable austenite and the isothermal transformation continues. Then, R_0 is the resistance of the sample after the resistance jump caused by the removal of H and before the new relaxation process starts.

For clarity, the data from the isothermal holding experiments shown in Figure 6.12 are separated in two panels depending on the dwelling temperature, from 128 K to 163 K in panel (a) and from 193 K to 313 K in panel (b). The accumulation of resistance during 2400 s after the removal of H and resistance jump, increases on reducing the dwelling temperature, panel (b), it reaches a maximum for the curve registered at 153 K, panel (a), and starts to decrease slightly with temperature to the curve registered at 128 K. The accumulation of resistance is high, for the time evolution curve taken at 153 K, it is more than twice the accumulation during the “normal” isothermal dwellings, Figure 6.9, and it is comparable to other isothermal transformations, Figure 6.3. In Figure 6.12, one can also observe the absence of a notable incubation time for the curves registered at low temperature, unlike in the time evolution experiments before the removal of the applied magnetic field, 6.9c. This lack of incubation time suggest that, by contrast with the isothermal holding experiments for the arrested transformation, the transformation has now very high driving force after the removal of H.

Finally, the curves shown in panel (a), registered at lower temperatures, are quite noisy. The origin of this relatively elevated noise-to-signal ratio is unknown. It may be related to the instability of the isothermal transformation in the arrested state. In addition, the removal of the field seems to produce a small temperature jump, up to 1 K, but the good temperature stability is rapidly recovered afterwards.

Figure 6.13 shows a comparison between the isothermal transformation rate Z calculated from the time evolution curves measured after removing the applied magnetic field, H, of 2.9 T, Figure 6.12, and Z obtained from the kinetics of the resistance after interruptions of the cooling under zero field and the 2.9 T field cooling, already shown in panels (a) and (c) of the Figure 6.10.

One observes in Figure 6.13 that the relaxation rate after the removal of the applied magnetic field increases with the reduction of the dwelling

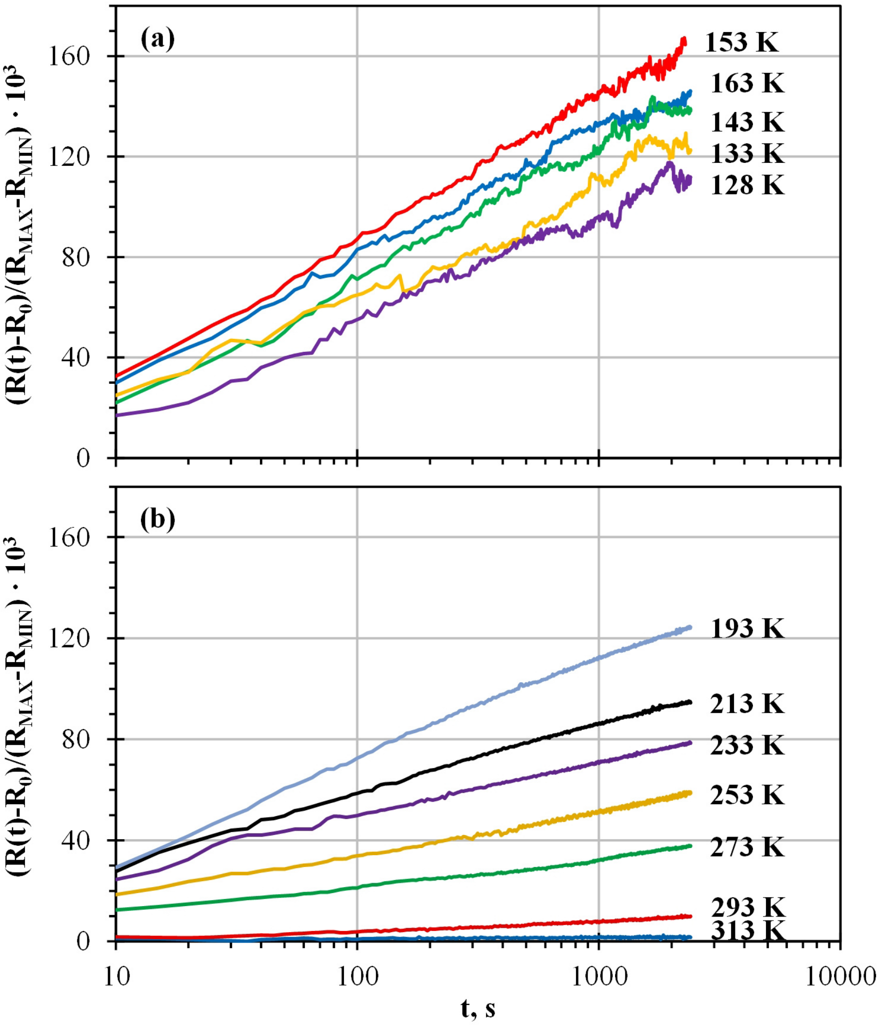

Figure 6.12: Time evolution of the resistance after the interruption of the 2.9 T field cooling and the removal of the applied magnetic field for the direct $L2_1 \rightarrow 6M$ transformation range for a sample of $Ni_{45}Mn_{36.7}In_{13.3}Co_5$ alloy annealed at 1070 K and air cooled; (a) Time evolution curves taken between 128 K and 163 K; (b) Time evolution curves taken between 193 K and 313 K.

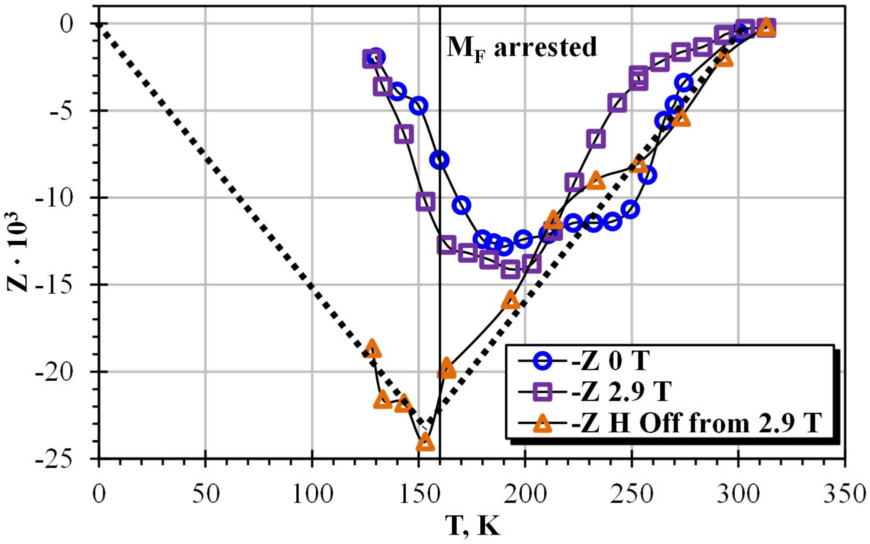

Figure 6.13: Comparison of the temperature dependence of the isothermal transformation rate Z for a sample of $Ni_{45}Mn_{36.7}In_{13.3}Co_5$ alloy annealed at 1070 K and air cooled: after interruption of 2.9 T field cooling and removal of the applied magnetic field (open triangles); after interruptions of the cooling under zero field (open circles); after interruptions of the 2.9 T field cooling (open squares). Vertical line shows the position of M_F calculated from the resistance data in continuous cooling scans. Dashed lines approximate the behavior of the "-Z H Off from 2.9 T" curve.

temperature until the point at 153 K, which is quite close to the MT finish temperature of the “master curve” in the arrested state. This strong increase of the intensity of the isothermal effects down to the apparent MT finish temperature can be accounted for by the increase of the number of “frozen” units, which are not able to transform anisothermally. The low-temperature data for $Z(T)$ after removal of the magnetic field are unfortunately incomplete since at the lowest experimentally achievable dwelling temperature, 128 K, the accumulation of resistance remains very intense. At this temperature, 128 K, the transformation during the 2.9 T field cooling, Figure 6.8a, has already reached the fully arrested state and does not proceed upon cooling. Thus, it can be assumed that the amount of the material in the metastable state, or the number of metastable units $N(T)$, remains constant below this temperature. Following equation (5.31) in page 181, one should expect that under this condition the intensity of isothermal effects will decrease linearly with the temperature.

This expected linear temperature dependence of the isothermal accumulation of martensite from the fully arrested state can be derived from the data by Pérez-Landazábal et al [64] for a sample of $Ni_{45}Mn_{36.7}In_{13.3}Co_5$ alloy annealed at 1070 K and air cooled, the same composition/heat treatment as our SC sample. They cooled the sample from 300 K under a field of 60 kOe to a preset temperature. Afterwards, the field was decreased to 40 kOe with registration of the isothermal evolution of the magnetization. This procedure was repeated for experiments at 10, 50 and 100 K. From these isothermal dwellings, the relaxation rate, Z_m, calculated as $\frac{\Delta M}{M} = Z_m ln((t + t_0)/t_0)$, gives ∼0, 0.014 and 0.028 for 10 K, 50 K and 100 K, respectively. These values of Z_m are represented in Figure 6.14, which clearly shows the linear dependence.

In the Figure 6.13, the straight dashed line between 0 K and 150 K indicates the possible temperature dependence of Z_{Hoff} from the arrested state. The values of Z_{Hoff} for the experiments performed between 128 K and 153 K seem to fit well the linear dependence. The few points between 128 K and 153 K are not enough to confirm/reject the linear temperature dependence. However, the results of Pérez-Landazábal et al [64], see Figure 6.14, clearly indicate that for the completely frozen transformation the intensity of isothermal effects depends linearly on temperature, according to the model developed in the present work.

Finally, it is important to comment that the MT has an elevated driving force after the removal of the applied magnetic field and, hence, the accumulation of martensite perfectly fits the logarithmic kinetics without any incubation time, as has been discussed above for the Figure 6.12. In other words, the arrested transformation has very low driving force and the time

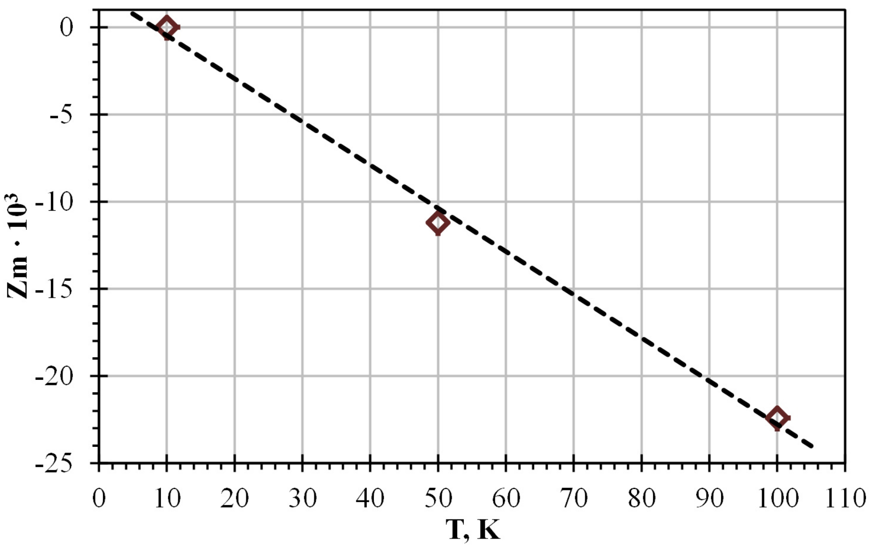

Figure 6.14: Temperature dependence of the isothermal transformation rate Z_m for a sample of $Ni_{45}Mn_{36.7}In_{13.3}Co_5$ alloy annealed at 1070 K and air cooled. The sample was cooled from 300 K to the dwelling temperature T under field of 60 kOe. The field was rapidly reduced to 40 kOe and the time evolution of the magnetization was registered. Finally, the relaxation rate, Z_m, was calculated as $\frac{\Delta M}{M} = Z_m ln((t+t_0)/t_0)$. These data were obtained by Pérez-Landazábal et al [64].

evolution of the resistance deviates from the logarithmic kinetics through the appearance of the temperature-dependent incubation time and the intensity of isothermal effects fails to be proportional to the amount of austenite which transforms anisothermally during uninterrupted cooling. However, when the field is removed and the driving force is increased, the isothermal transformation proceeds without incubation times. In addition, $Z_{Hoff}(T)$ seems to be proportional to the austenite which was previously arrested, i.e., to the amount of austenite which becomes metastable after the removal of H. Thus, basic features of the isothermal MTs both for complete and “arrested” MTs can be self-consistently accounted for by the developed phenomenological model. Fine details, like weak temperature dependence of the slopes of the isothermal kinetics in the arrested state, Figure 6.9, calls for further studies.

Chapter 7

Conclusions

In this brief final chapter the experimental results are summarized and the interpretations and conclusions are formulated which were reached in the course of the present work.

Development of experimental methods and techniques

- A new construction of the experimental setup for observations of isothermal effects in electrical resistance has been implemented in the present work. This system, designed previously, is characterized by a very low thermal inertia, since the sample with attached control thermocouple is directly cooled/heated by a flow of gaseous He. This property is crucial if isothermal kinetics has to be studied experimentally and is a necessary condition to study efficiently the incubation time. In the course of the present work, the existing electronics and cooling-heating system have been matched with a Lakeshore electromagnet, which permits obtaining high values of magnetic field up to 3 T. The final experimental arrangement has been used in initial studies of the isothermal magnetostructural transition in Ni–Co–Mn–In alloy and is planned to be used extensively in the continuation of the present work.

New experiments and experimental results

- One of the most important results of the present work is, undoubtedly, the discovery of the isothermal nature of certain martensitic transformations in the Ni–Ti system of alloys. Before this study, the martensitic transformations in the Ni–Ti system served as an example of thermoelastic, diffusionless and athermal transition.

- As a consequence of this discovery, in a continuation of the initial experiments, a systematic study of the isothermal/athermal nature of all possible transformation paths in the Ni–Ti system has been performed. In order to realize all possible transformation paths, a wide range of materials has been investigated, including Ni- and Ti-rich binary Ni–Ti alloys (from both sides of the equiatomic stoichiometric composition) subjected to different heat treatments, and ternary alloys from Ni–Ti–Fe and Ni–Ti–Cu families. It has been shown that some transformation paths in the Ni–Ti system (B2↔R, B2↔B19) can be classified as athermal, whereas all transitions involving B19' martensite demonstrate different intensity of the isothermal effects.

- It has been shown experimentally that the intensity of the isothermal effects during transitions to B19' martensite decreases with the increase of the transformation temperature, explaining the controversy in classifying the reverse transformations from the B19' phase as athermal/isothermal.

- Experiments, employing linear and non-linear ultrasonic premartensitic anelasticity, have been performed for the first time in order to confirm the results of the electrical resistance studies. These experiments yielded important additional information concerning the role of thermal fluctuations in nucleation and growth processes involved in the martensitic transformation.

- Another qualitatively new type of experiments has been performed for metamagnetic Ni–Mn–Co–In alloys. For this system of alloys, experiments were conducted for a complete temperature-induced martensitic transformation (low degree of long-range order of the samples) as well as for the incomplete one (high degree of order) which is frequently referred to as the "arrested" transition. The experimental novelty here included studying the kinetics of resistance under field and zero field conditions as well as during switching off the polarizing field. The effect of magnetic field on the kinetics of the isothermal accumulation of resistance has been studied both for the complete and "arrested" transformations.

Interpretations of the experimental results and conclusions drawn

1. The most important conclusion drawn in the present work is that, contrary to the existing doctrine, it is the stage of the growth of the

martensitic variants rather than the nucleation stage which is responsible for the isothermal nature of the transformations which do not involve atomic diffusion.

2. It has been shown that the athermal/isothermal nature of the martensitic transformation is determined by the

   a transformation hysteresis

   b transformation range.

   A correlation is found between the isothermal/athermal behavior of the transformations and the width of transformation hysteresis and the transformation range: all athermal transformations possess a narrow hysteresis (up to approximately 10 K), whereas all isothermal ones have a substantially wider hysteresis, of the order of 30 K. The only exception from this rule, found in the present work, is the isothermal B19↔B19' transformation, for which the transformation hysteresis is relatively narrow, but which possesses an extremely broad transformation range. This peculiarity is attributed to a low chemical driving force for this transformation.

3. The correlation between the width of the transformation hysteresis and its athermal/isothermal nature permitted us to ascribe these isothermal effects to the frictional forces impeding the motion of interphase boundaries, the conclusion being fully consistent with the declared isothermal nature of the growth process. Different possible origins of the friction forces have been analyzed and the conclusion has been reached that a substantial role in this friction is played by the process of creation of the lattice defects, primarily dislocations, during the transformation. This conclusion explains logically the difference in the intensity of isothermal effects during the direct and reverse transformations.

4. In the Ni–Ti system, the difference between isothermal behaviour of the transitions to/from B19' phase and athermal features of all other transformation paths is ascribed to the difference in crystallography of the phases. More specifically, this distinction of transformation paths is ascribed to the differences in the accommodation of low symmetry phases: complex one for the B19' phase and nearly perfect ones for other transformation paths.

5. A conclusion is drawn that the temperature dependence of the intensity of isothermal transformations is controlled by the amount of athermally

transforming material. The effect of temperature is reduced to a much weaker linear dependence, which is usually overwhelmed by the temperature dependence of the amount of athermally transforming material.

6. A phenomenological model, based on the Néel model of the thermal fluctuation magnetic aftereffect, is constructed. The model predicts experimentally observed logarithmic kinetics of the isothermal accumulation of martensite and also accounts for the possible existence of the saturation and incubation time. The latter is ascribed to a depletion of the activation energies distribution from the low-energy configuration side.

7. A magnetostructural transition in the Ni–Mn–Co–In alloys also demonstrates isothermal features, both for complete and arrested transformations. Whereas the complete magnetostructural transition follows closely general regularities observed in the Ni–Ti system, the arrested transformation shows significant deviations from the simple model of relaxation of bistable units. At least part of this deviation has been attributed to the strongly decreasing driving force of the transformation (low entropy difference between austenite and martensite).

Bibliography

[1] W. J. Buehler, J. W. Gilfrich, and R. C. Wiley. Effects of low temperature phase changes on the mechanical properties of alloys near composition TiNi. *Journal of Applied Physics*, 34:1473–1475, 1963.

[2] G. V. Kurdjumov. *Izv. Akad. Nauk SSSR Otd. Him. Nauk*, 2:271, 1936.

[3] A. L. Roitburd and G. V. Kurdjumov. The nature of martensitic transformations. *Materials Science and Engineering*, 39(2):141–167, 1979.

[4] V. A. Lobodyuk and Emmanuil I. Estrin. Isothermal martensitic transformations. *Physics-Uspekhi*, 48(7):713, July 2005.

[5] R. J. Salzbrenner and M. Cohen. On the thermodynamics of thermoelastic martensitic transformations. *Acta Metallurgica*, 27(5):739–748, May 1979.

[6] P. Wollants, J. R. Roos, and L. Delaey. Thermally- and stress-induced thermoelastic martensitic transformations in the reference frame of equilibrium thermodynamics. *Progress in Materials Science*, 37(3):227–288, 1993.

[7] K. F. Hane and T. W. Shield. Symmetry and microstructure in martensites. *Philosophical Magazine A*, 78(6):1215–1252, 1998.

[8] K. Otsuka and T. Saburi. *Functional Metallic Materials.* University of Tokyo Press, 1985. Chapter 3.

[9] K. Otsuka and X. Ren. Physical metallurgy of Ti–Ni-based shape memory alloys. *Progress in Materials Science*, 50(5):511–678, July 2005. Chapter 6.

[10] X. Huang and Y. Liu. Effect of annealing on the transformation behavior and superelasticity of NiTi shape memory alloy. *Scripta Materialia*, 45(2):153–160, July 2001.

[11] M. Es-Souni, M. Es-Souni, and H. F. Brandies. On the transformation behaviour, mechanical properties and biocompatibility of two NiTi-based shape memory alloys: NiTi42 and NiTi42Cu7. *Biomaterials*, 22(15):2153–2161, 2001.

[12] A. L. McKelvey and R. O. Ritchie. On the temperature dependence of the superelastic strength and the prediction of the theoretical uniaxial transformation strain in nitinol. *Philosophical Magazine A*, 80(8):1759–1768, 2000.

[13] I. Ohkata and Y. Suzuki. *Functional Metallic Materials*. University of Tokyo Press, 1985. Chapter 11.

[14] J. Van Humbeeck. Non-medical applications of shape memory alloys. *Materials Science and Engineering: A*, 273–275:134–148, 1999.

[15] Furukawa Techno Material Co. https://www.furukawa-ftm.com/english/index.htm.

[16] K. N. Melton. *Functional Metallic Materials*. University of Tokyo Press, 1985. Chapter 10.

[17] J. L. Proft and T. W. Duerig. The mechanical aspects of constrained recovery. In *Engineering Aspects of Shape Memory Alloys*, pages 115–129. Butterworth-Heinemann, 1990.

[18] D.Z. Liu, W.X. Liu, and F.Y. Gong. Engineering application of Fe-based shape memory alloy on connecting pipe line. *Journal de Physique IV*, 05(C8):1241–1246, December 1995.

[19] E. J. Graesser and F. Cozzarelli. Shape-memory alloys as new materials for aseismic isolation. *Journal of Engineering Mechanics*, 117(11):2590–2608, 1991.

[20] E. J. Graesser and F. A. Cozzarelli. A proposed three-dimensional constitutive model for shape memory alloys. *Journal of Intelligent Material Systems and Structures*, 5(1):78–89, January 1994.

[21] T Duerig, A Pelton, and D Stöckel. An overview of nitinol medical applications. *Materials Science and Engineering: A*, 273–275:149–160, 1999.

[22] B. Bertheville. Porous single-phase NiTi processed under Ca reducing vapor for use as a bone graft substitute. *Biomaterials*, 27(8):1246–1250, March 2006.

[23] Y. Fukui, T. Inamura, H. Hosoda, K. Wakashima, and S. Miyazaki. Mechanical properties of a Ti–Nb–Al shape memory alloy. *Materials Transactions*, 45(4):1077–1082, 2004.

[24] S. Miyazaki and H. Y. Kim. TiNi-Base and Ti-Base shape memory alloys. *Materials Science Forum*, 561-565:5–21, 2007.

[25] C.-M. Chan, S. Trigwell, and T. Duerig. Oxidation of an NiTi alloy. *Surface and Interface Analysis*, 15(6):349–354, June 1990.

[26] C. Trépanier, M. Tabrizian, Lh. Yahia, L. Bilodeau, and D. L. Piron. Improvement of the corrosion resistance of NiTi stents by surface treatments. *MRS Online Proceedings Library*, 459:363–368, 1996.

[27] N. B Morgan. Medical shape memory alloy applications – the market and its products. *Materials Science and Engineering: A*, 378(1–2):16–23, July 2004.

[28] L. S. Castleman, S. M. Motzkin, F. P. Alicandri, V. L. Bonawit, and A. A. Johnson. Biocompatibility of nitinol alloy as an implant material. *Journal of Biomedical Materials Research*, 10(5):695–731, September 1976.

[29] D. J. Wever, A. G. Veldhuizen, M. M. Sanders, J. M. Schakenraad, and J. R. Van Horn. Cytotoxic, allergic and genotoxic activity of a nickel-titanium alloy. *Biomaterials*, 18(16):1115–1120, 1997.

[30] J. Ryhänen, M. Kallioinen, J. Tuukkanen, J. Junila, E. Niemelä, P. Sandvik, and W. Serlo. In vivo biocompatibility evaluation of nickel-titanium shape memory metal alloy: Muscle and perineural tissue responses and encapsule membrane thickness. *Journal of Biomedical Materials Research*, 41(3):481–488, September 1998.

[31] S. Kujala, J. Ryhänen, T. Jämsä, A. Danilov, J. Saaranen, A. Pramila, and J. Tuukkanen. Bone modeling controlled by a nickel-titanium shape memory alloy intramedullary nail. *Biomaterials*, 23(12):2535–2543, June 2002.

[32] A. Suzuki, H. Kanetaka, Y. Shimizu, R. Tomizuka, H. Hosoda, S. Miyazaki, O. Okuno, K. Igarashi, and H. Mitani. Orthodontic buccal tooth movement by Nickel-free Titanium-based shape memory and superelastic alloy wire. *The Angle Orthodontist*, 76(6):1041–1046, November 2006.

[33] Johnson & Johnson Company. http://www.jnj.com/.

[34] K. Kuribayashi, K. Tsuchiya, Z. You, D. Tomus, M. Umemoto, T. Ito, and M. Sasaki. Self-deployable origami stent grafts as a biomedical application of Ni-rich TiNi shape memory alloy foil. *Materials Science and Engineering: A*, 419(12):131–137, March 2006.

[35] N. N. Thadhani and M. A. Meyers. Kinetics of isothermal martensitic transformation. *Progress in Materials Science*, 30(1):1–37, 1986.

[36] T. B. Massalski. Comments concerning some features of phase diagrams and phase transformations. *Materials Transactions*, 51(4):583–596, 2010.

[37] D. E. Laughlin, N. J. Jones, A. J. Schwartz, and T. B. Massalski. *Proceedings ICOMAT-08: Thermally Activated Martensite: Its Relationship to Non-Thermally Activated (Athermal) Martensite (pages 141–144).* Warren-dale (PA): TMS, 2009.

[38] G. V. Kurdjumov and O. P. Maksimova. *Dokl. Akad. Nauk SSSR*, 61:83–86, 1948.

[39] V. A. Lobodyuk and E. I. Estrin. *Martensitic transformations.* Moscow: Fiz-matlit, 2009.

[40] G. Ghosh and G. B. Olson. Kinetics of F.C.C. → B.C.C. heterogeneous martensitic nucleation–I. The critical driving force for athermal nucleation. *Acta Metallurgica et Materialia*, 42(10):3361–3370, October 1994.

[41] J. R. C. Guimarães and P. R. Rios. Driving force and thermal activation in martensite kinetics. *Metallurgical and Materials Transactions A*, 40(10):2264–2272, October 2009.

[42] T. Kakeshita, K. Kuroiwa, K. Shimizu, T. Ikeda, A. Yamagishi, and M. Date. A new model explainable for both the athermal and isothermal natures of martensitic transformations in Fe–Ni–Mn alloys. *Materials Transactions, JIM*, 34(5):423–428, 1993.

[43] T. Kakeshita, K. Kuroiwa, K. Shimizu, T. Ikeda, A. Yamagishi, and M. Date. Effect of magnetic fields on athermal and isothermal martensitic transformations in Fe–Ni–Mn alloys. *Materials Transactions, JIM*, 34(5):415–422, 1993.

[44] T. Kakeshita, T. Fukuda, and T. Saburi. Time-dependent nature and origin of displacive transformation. *Science and Technology of Advanced Materials*, 1(1):63, March 2000.

[45] K. Otsuka, X. Ren, and T. Takeda. Experimental test for a possible isothermal martensitic transformation in a Ti–Ni alloy. *Scripta Materialia*, 45(2):145–152, July 2001.

[46] T. Kakeshita, T. Takeguchi, T. Fukuda, and T. Saburi. Time-dependent nature of the athermal martensitic transformation in a Cu–Al–Ni shape memory alloy. *Materials Transactions, JIM*, 37(3):299–303, 1996.

[47] E. Cingolani, M. Ahlers, and J. Van Humbeeck. Stabilization and two-way shape memory effect in Cu–Al–Ni single crystals. *Metallurgical and Materials Transactions A*, 30(3):493–499, March 1999.

[48] U. Chandni, S. Kar-Narayan, A. Ghosh, H. S. Vijaya, and S. Mohan. A fluctuation-based characterization of athermal phase transitions: Application to shape memory alloys. *Acta Materialia*, 57(20):6113–6122, 2009.

[49] A. Planes, F.-J. Pérez-Reche, E. Vives, and Ll. Mañosa. Kinetics of martensitic transitions in shape-memory alloys. *Scripta Materialia*, 50(2):181–186, 2004.

[50] T. Lipe and M. A. Morris. Effect of thermally activated mechanisms on the martensitic transformation of modified Cu–Al–Ni alloys. *Acta Metallurgica et Materialia*, 43(3):1293–1303, March 1995.

[51] Q. Meng, H. Yang, Y. Liu, and T. Nam. Transformation intervals and elastic strain energies of b2-b19' martensitic transformation of NiTi. *Intermetallics*, 18(12):2431–2434, 2010.

[52] J. Van Humbeeck and A. Planes. On the interpretation of differential scanning calorimetry results for thermoelastic martensitic transformations: Athermal versus thermally activated kinetics. *Scripta Materialia*, 34(9):1357–1360, May 1996.

[53] H. Abe, M. Ishibashi, K. Ohshima, T. Suzuki, M. Wuttig, and K. Kakurai. Kinetics of the martensitic transition in In-Tl alloys. *Physical Review B*, 50(13):9020–9024, October 1994.

[54] D. J. Sordelet, M. F. Besser, R. T. Ott, B. J. Zimmerman, W. D. Porter, and B. Gleeson. Isothermal nature of martensite formation in Pt-modified β-NiAl alloys. *Acta Materialia*, 55(7):2433–2441, 2007.

[55] C. Hürrich, S. Roth, M. Pötschke, B. Rellinghaus, and L. Schultz. Isothermal martensitic transformation in polycrystalline Ni50Mn29Ga21. *Journal of Alloys and Compounds*, 494(12):40–43, 2010.

[56] R. Kainuma, Y. Imano, W. Ito, Y. Sutou, H. Morito, S. Okamoto, O. Kitakami, K. Oikawa, A. Fujita, T. Kanomata, and K. Ishida. Magnetic-field-induced shape recovery by reverse phase transformation. *Nature*, 439(7079):957–960, February 2006.

[57] R. Y. Umetsu, W. Ito, K. Ito, K. Koyama, A. Fujita, K. Oikawa, T. Kanomata, R. Kainuma, and K. Ishida. Anomaly in entropy change between parent and martensite phases in the $Ni_{50}Mn_{34}In_{16}$ heusler alloy. *Scripta Materialia*, 60(1):25–28, 2009.

[58] V. K. Sharma, M. K. Chattopadhyay, and S. B. Roy. Kinetic arrest of the first order austenite to martensite phase transition in $Ni_{50}Mn_{34}In_{16}$: dc magnetization studies. *Physical Review B*, 76(14):140401, October 2007.

[59] S. Chatterjee, S. Giri, S. Majumdar, and S. K. De. Thermomagnetic irreversibility in $Ni_2Mn_{1.36}Sn_{0.64}$ shape-memory alloy. *Physical Review B*, 77(22):224440, June 2008.

[60] S. Kustov, M. L. Corró, J. Pons, and E. Cesari. Entropy change and effect of magnetic field on martensitic transformation in a metamagnetic Ni–Co–Mn–In shape memory alloy. *Applied Physics Letters*, 94(19):191901, May 2009.

[61] W. Ito, R. Y. Umetsu, R. Kainuma, T. Kakeshita, and K. Ishida. Heat-induced and isothermal martensitic transformations from kinetically arrested parent phase in NiCoMnIn metamagnetic shape memory alloy. *Scripta Materialia*, 63(1):73–76, July 2010.

[62] S. Kustov, I. Golovin, M. L. Corró, and E. Cesari. Isothermal martensitic transformation in metamagnetic shape memory alloys. *Journal of Applied Physics*, 107(5):053525, March 2010.

[63] T. Kakeshita, J. Nam, and T. Fukuda. Kinetics of martensitic transformations in magnetic field or under hydrostatic pressure. *Science and Technology of Advanced Materials*, 12(1):015004, February 2011.

[64] J. I. Pérez-Landazábal, V. Recarte, V. Sánchez-Alarcos, C. Gómez-Polo, S. Kustov, and E. Cesari. Magnetic field induced martensitic transformation linked to the arrested austenite in a Ni–Mn–In–Co shape memory alloy. *Journal of Applied Physics*, 109(9):093515, May 2011.

[65] Y. Lee, M. Todai, T. Okuyama, T. Fukuda, T. Kakeshita, and R. Kainuma. Isothermal nature of martensitic transformation in an Ni45Co5Mn36.5In13.5 magnetic shape memory alloy. *Scripta Materialia*, 64(10):927–930, May 2011.

[66] S. Kustov, D. Salas, E. Cesari, R. Santamarta, and J. Van Humbeeck. Isothermal and athermal martensitic transformations in Ni–Ti shape memory alloys. *Acta Materialia*, 60(6–7):2578–2592, 2012.

[67] G. R. Barsch. Mobility of domain walls in proper ferroelastic martensites. *Le Journal de Physique IV*, 05(C8):C8–119–C8–124, December 1995.

[68] K. Otsuka and X. Ren. Physical metallurgy of Ti–Ni-based shape memory alloys. *Progress in Materials Science*, 50(5):511–678, July 2005. Chapter 3.

[69] A. K. Srivastava, D. Schryvers, and J. Van Humbeeck. Grain growth and precipitation in an annealed cold-rolled $Ni_{50.2}Ti_{49.8}$ alloy. *Intermetallics*, 15(12):1538–1547, 2007.

[70] M. H. Mueller and H. W. Knott. The crystal structures of Ti2Cu, Ti2Ni, Ti4Ni2O and Ti4Cu2O. *Transactions of the Metallurgical Society of AIME*, 227:674–678, 1963.

[71] Ch. Somsen, H. Zähres, J. Kästner, E. F. Wassermann, T. Kakeshita, and T. Saburi. Influence of thermal annealing on the martensitic transitions in Ni–Ti shape memory alloys. *Materials Science and Engineering: A*, 273–275:310–314, 1999.

[72] V. Zel'dovich, G. Sobyanina, and T. V. Novoselova. Martensitic transformations in TiNi alloys with Ti_3Ni_4 precipitates. *Le Journal de Physique IV*, 07(C5):C5–299–C5–304, November 1997.

[73] T. B. Massalski and H. Okamoto. *Binary alloy phase diagrams, 2nd edition, vol. 3.* Material Park, OH: ASM International, 1990.

[74] O. W. Bertacchini, Dimitris C. Lagoudas, F. T. Calkins, and J. H. Mabe. *Proceedings ICOMAT-08: Transformation Induced Cyclic Behavior and Fatigue Properties of Nickel Rich NiTi Shape Memory Alloy Actuators (pages 199–206).* Warren-dale (PA): TMS, 2009.

[75] R. C. O'Handley and S. M. Allen. *Encyclopedia of Smart Materials.* Wiley, New York, 2002.

[76] K. Ullakko, J. K. Huang, C. Kantner, R. C. O'Handley, and V. V. Kokorin. Large magnetic-field-induced strains in Ni_2MnGa single crystals. *Applied Physics Letters*, 69(13):1966–1968, September 1996.

[77] S. J. Murray, M. Marioni, S. M. Allen, R. C. O'Handley, and T. A. Lograsso. 6% magnetic-field-induced strain by twin-boundary motion in ferromagnetic Ni–Mn–Ga. *Applied Physics Letters*, 77(6):886–888, August 2000.

[78] L. Chen, F. X. Hu, J. Wang, J. Shen, J. Zhang, J. R. Sun, B. G. Shen, J. H. Yin, and L. Q. Pan. Magnetoresistance and magnetocaloric effect in metamagnetic alloys $Ni_{45}Co_5Mn_{36.5}In_{13.5}$. *Journal of Applied Physics*, 107(9):09A940, May 2010.

[79] T. Krenke, E. Duman, M. Acet, E. F. Wassermann, X. Moya, Ll. Mañosa, and A. Planes. Inverse magnetocaloric effect in ferromagnetic Ni–Mn–Sn alloys. *Nature Materials*, 4(6):450–454, June 2005.

[80] W. Ito, K. Ito, R. Y. Umetsu, R. Kainuma, K. Koyama, K. Watanabe, A. Fujita, K. Oikawa, K. Ishida, and T. Kanomata. Kinetic arrest of martensitic transformation in the NiCoMnIn metamagnetic shape memory alloy. *Applied Physics Letters*, 92(2):021908, January 2008.

[81] T. Krenke, E. Duman, M. Acet, E. F. Wassermann, X. Moya, Ll. Mañosa, A. Planes, E. Suard, and B. Ouladdiaf. Magnetic superelasticity and inverse magnetocaloric effect in Ni–Mn–In. *Physical Review B*, 75(10):104414, March 2007.

[82] K. Koyama, H. Okada, K. Watanabe, T. Kanomata, R. Kainuma, W. Ito, K. Oikawa, and K. Ishida. Observation of large magnetoresistance of magnetic heusler alloy $Ni_{50}Mn_{36}Sn_{14}$ in high magnetic fields. *Applied Physics Letters*, 89(18):182510, October 2006.

[83] J. Enkovaara, O. Heczko, A. Ayuela, and R. M. Nieminen. Coexistence of ferromagnetic and antiferromagnetic order in mn-doped Ni_2MnGa. *Physical Review B*, 67(21):212405, June 2003.

[84] E. Şaşıoğu, L. M. Sandratskii, and P. Bruno. Role of conduction electrons in mediating exchange interactions in Mn-based heusler alloys. *Physical Review B*, 77(6):064417, February 2008.

[85] G. W. H. Höhne, W. Hemminger, and H.-J. Flammersheim. *Differential Scanning Calorimetry: an introduction to practitioners.* Springer-Verlag Berlin Heidelberg, 1996. Chapter 3.

[86] H. Zheng, W. Wang, D. Wu, S. Xue, Q. Zhai, J. Frenzel, and Z. Luo. Athermal nature of the martensitic transformation in heusler alloy Ni–Mn–Sn. *Intermetallics*, 36:90–95, May 2013.

[87] S. Xue, W. Wang, D. Wu, Q. Zhai, and H. Zheng. On the explanation for the time-dependence of B2 to R martensitic transformation in $Ti_{50}Ni_{47}Fe_3$ shape memory alloy. *Materials Letters*, 72:119–121, 2012.

[88] S. H. Chang and S. K. Wu. Effect of cooling rate on transformation temperature measurements of $Ti_{50}Ni_{50}$ alloy by differential scanning calorimetry and dynamic mechanical analysis. *Materials Characterization*, 59(8):987–990, 2008.

[89] L. D. Landau and E. M. Lifshitz. *Electrodynamics of the Continuous Media.* Pergamon, Oxford, 1960.

[90] S. C. Das Gupta and B. S. Lement. Isothermal formation of martensite at subzero temperatures in a chromium steel. *Journal of Metals - Transactions of the Metallurgical Society of AIME*, 3:727–731, 1951.

[91] E. S. Machlin and M. Cohen. Isothermal mode of the martensitic transformation. *Journal of Metals - Transactions of the Metallurgical Society of AIME*, 4:489–500, 1952.

[92] G. Bertotti. *Hysteresis in Magnetism.* Academic Press San Diego, USA, 1998. Chapter 10.

[93] S. A. Golovin. Methods of mechanical spectroscopy in physical metallurgy. *Metal Science and Heat Treatment*, 44(5-6):227–231, May 2002.

[94] A. S. Nowick and B. S. Berry. Anelastic relaxation in crystalline solids: Characterization of anelastic behavior. In *Anelastic Relaxation in Crystalline Solids*, pages 1–29. Academic Press, 1972. Chapter 1.

[95] G. Fantozzi. Mechanical spectroscopy Q^{-1} 2001: 1.1 phenomenology and definitions. *Materials Science Forum*, 366-368:3–31, 2001.

[96] A. S. Nowick and B. S. Berry. Anelastic relaxation in crystalline solids: Further dislocations effects. In *Anelastic Relaxation in Crystalline Solids*, pages 411–434. Academic Press, 1972. Chapter 14.

[97] G. Gremaud, S. Kustov, and O. Bremnes. Mechanical spectroscopy Q^{-1} 2001: 9.2 ultrasonics techniques: PUCOT and ACT. *Materials Science Forum*, 366-368:652–666, 2001.

[98] S. Kustov, S. Golyandin, A. Ichino, and G. Gremaud. A new design of automated piezoelectric composite oscillator technique. *Materials Science and Engineering: A*, 442(1–2):532–537, 2006.

[99] S. L. Quimby. On the experimental determination of the viscosity of vibrating solids. *Physical Review*, 25(4):558–573, 1925.

[100] J. Marx. Use of the piezoelectric gauge for internal friction measurements. *Review of Scientific Instruments*, 22(7):503–509, July 1951.

[101] A. S. Nowick. Internal friction in metals. *Progress in Metal Physics*, 4:1–70, 1953.

[102] S. D. Devine and W. H. Robinson. Ultrasonically modulated paramagnetic resonance. In John S. Waugh, editor, *Advances in Magnetic and Optical Resonance*, volume 10, pages 53–117. Academic Press, 1982.

[103] W. H. Robinson and A Edgar. The piezoelectric method of determining mechanical damping at frequencies of 30 to 200 kHz. *IEEE Transactions on Sonics and Ultrasonics*, 21(2):98–105, April 1974.

[104] W. H. Robinson, S. H. Carpenter, and J. L. Tallon. Piezoelectric method of determining torsional mechanical damping between 40 and 120 kHz. *Journal of Applied Physics*, 45(5):1975–1981, May 1974.

[105] S. D. Devine and W. H. Robinson. Flexural composite oscillators for the measurement of anelastic and elastic properties of solids at frequencies of 1 to 10 kHz. *IEEE Transactions on Ultrasonics, Ferroelectrics, and Frequency Control*, 45(1):11–22, 1998.

[106] R. B. Schwarz. Simple system using one-crystal composite oscillator for internal friction and modulus measurements. *Review of Scientific Instruments*, 48(2):111–115, February 1977.

[107] S. Miyazaki, Y. Igo, and K. Otsuka. Effect of thermal cycling on the transformation temperatures of Ti–Ni alloys. *Acta Metallurgica*, 34(10):2045–2051, October 1986.

[108] T. M. Brill, S. Mittelbach, W. Assmus, M. Mullner, and B. Luthi. Elastic properties of NiTi. *Journal of Physics: Condensed Matter*, 3(48):9621, December 1991.

[109] S. K. Wu, H. C. Lin, and T. Y. Lin. Electrical resistivity of Ti–Ni binary and Ti–Ni–X (X = Fe, Cu) ternary shape memory alloys. *Materials Science and Engineering: A*, 438–440:536–539, November 2006.

[110] P. G. McCormick and Y. Liu. Thermodynamic analysis of the martensitic transformation in NiTi–II. effect of transformation cycling. *Acta Metallurgica et Materialia*, 42(7):2407–2413, July 1994.

[111] V. Pelosin and A. Riviere. Effect of thermal cycling on the R-phase and martensitic transformations in a ti-rich NiTi alloy. *Metallurgical and Materials Transactions A*, 29(4):1175–1180, April 1998.

[112] T. H. Nam, T. Saburi, and S. Ken'ichi. Cu-content dependence of shape memory characteristics in Ti-Ni-Cu alloys. *Materials Transactions, JIM*, 31(11):959—967, 1990.

[113] T. H. Nam, T. Saburi, Y. Nakata, and S. Ken'ichi. Shape memory characteristics and lattice deformation in Ti-Ni-Cu alloys. *Materials Transactions, JIM*, 31(12):1050—1056, 1990.

[114] A. Nespoli, E. Villa, and S. Besseghini. Characterization of the martensitic transformation in $\mathrm{Ni}_{50-x}\mathrm{Ti}_{50}\mathrm{Cu}_X$ alloys through pure thermal measurements. *Journal of Alloys and Compounds*, 509(3):644–647, 2011.

[115] S. K Wu and H. C Lin. Damping characteristics of TiNi binary and ternary shape memory alloys. *Journal of Alloys and Compounds*, 355(1–2):72–78, June 2003.

[116] I. Yoshida, D. Monma, K. Iino, T. Ono, K. Otsuka, and M. Asai. Internal friction of Ti–Ni–Cu ternary shape memory alloys. *Materials Science and Engineering: A*, 370(1–2):444–448, 2004.

[117] T. Fukuda, T. Saburi, T. Chihara, and Y. Tsuzuki. Mechanism of B2-B19-B19' transformation in shape memory Ti-Ni-Cu alloys. *Materials Transactions, JIM*, 36(10):1244—1248, 1995.

[118] T. Fukuda, S. Yoshida, and T. Kakeshita. Isothermal nature of the B2-B19' martensitic transformation in a Ti–51.2Ni (at.%) alloy. *Scripta Materialia*, 68(12):984–987, June 2013.

[119] K. Otsuka and X. Ren. Physical metallurgy of Ti–Ni-based shape memory alloys. *Progress in Materials Science*, 50(5):511–678, July 2005. Chapter 4.

[120] A. Ibarra, D. Caillard, J. San Juan, and M. L. Nó. Martensite nucleation on dislocations in Cu–Al–Ni shape memory alloys. *Applied Physics Letters*, 90(10):101907, March 2007.

[121] J. San Juan and R. B. Perez-Saez. Mechanical spectroscopy Q^{-1} 2001: 5.4 transitory effects. *Materials Science Forum*, 366-368:416–436, 2001.

[122] S. Kustov and J. Van Humbeeck. *Advances in Shape Memory Materials.* Trans Tech Publications, Zürich, Switzerland, 2008. Pages 85–109.

[123] S Golyandin, S Kustov, K Sapozhnikov, M Parlinska, R Gotthardt, J Van Humbeeck, and R De Batist. Structural anelasticity of NiTi during two-stage martensitic transformation. *Journal of Alloys and Compounds*, 310(1–2):312–317, September 2000.

[124] S. H. Chang and S. K. Wu. Inherent internal friction of B→R→B19' martensitic transformations in equiatomic TiNi shape memory alloy. *Scripta Materialia*, 55(4):311–314, 2006.

[125] S. H. Chang and S. K. Wu. Internal friction of R-phase and B19' martensite in equiatomic TiNi shape memory alloy under isothermal conditions. *Journal of Alloys and Compounds*, 437(1–2):120–126, June 2007.

[126] P. Moine, G. M. Michal, and R. Sinclair. A morphological study of "premartensitic" effects in TiNi. *Acta Metallurgica*, 30(1):109–123, 1982.

[127] Y. Murakami and D. Shindo. Changes in microstructure near the R-phase transformation in $Ti_{50}Ni_{48}Fe_2$ studied by in-situ electron microscopy. *Philosophical Magazine Letters*, 81(9):631–638, September 2001.

[128] S. Sarkar, X. Ren, and K. Otsuka. Evidence for strain glass in the ferroelastic-martensitic system $Ti_{50-X}Ni_{50+X}$. *Physical Review Letters*, 95(20):205702, November 2005.

[129] G. Gremaud. Mechanical spectroscopy Q^{-1} 2001: 3.3 dislocation - point defect interactions. *Materials Science Forum*, 366-368:178–246, 2001.

[130] S. Kustov, S. Golyandin, K. Sapozhnikov, E. Cesari, J. Van Humbeeck, and R. De Batist. Influence of martensite stabilization on the low-temperature non-linear anelasticity in Cu-Zn-Al shape memory alloys. *Acta Materialia*, 50(11):3023–3044, June 2002.

[131] S. Kustov, S. Golyandin, K. Sapozhnikov, J. Pons, E. Cesari, and J. Van Humbeeck. Effect of off-stoichiometry on the mobility of point-like defects and damping in binary Cu–Al martensites. *Acta Materialia*, 54(8):2075–2085, May 2006.

[132] G. Mazzolai. Recent progresses in the understanding of the elastic and anelastic properties of H-free, H-doped and H-contaminated NiTi based alloys. *AIP Advances*, 1(4):040701, December 2011.

[133] M. Kozuma, Y. Murakami, T. Kawano, and K. Otsuka. An isothermal martensitic transformation in a quenched Au-49.5at%Cd alloy. *Scripta Materialia*, 36(2):253–258, 1997.

[134] R. Schmidt, M. Schlereth, H. Wipf, W. Assmus, and M. Mullner. Hydrogen solubility and diffusion in the shape-memory alloy NiTi. *Journal of Physics: Condensed Matter*, 1(14):2473, April 1989.

[135] M. Grujicic, G. B. Olson, and W. S. Owen. Mobility of martensitic interfaces. *Metallurgical Transactions A*, 16(10):1713–1722, October 1985.

[136] G. B. Olson and M. Cohen. Interphase-boundary dislocations and the concept of coherency. *Acta Metallurgica*, 27(12):1907–1918, 1979.

[137] W. Benoit. Mechanical spectroscopy Q^{-1} 2001: 3.2 dislocation - lattice interactions. *Materials Science Forum*, 366-368:158–177, 2001.

[138] G. R. Barsch and J. A. Krumhansl. Twin boundaries in ferroelastic media without interface dislocations. *Physical Review Letters*, 53(11):1069–1072, September 1984.

[139] J. Zhang, C. Somsen, T. Simon, X. Ding, S. Hou, S. Ren, X. Ren, G. Eggeler, K. Otsuka, and J. Sun. Leaf-like dislocation substructures and the decrease of martensitic start temperatures: A new explanation

for functional fatigue during thermally induced martensitic transformations in coarse-grained Ni-rich Ti–Ni shape memory alloys. *Acta Materialia*, 60(5):1999–2006, March 2012.

[140] R. J. Wasilewski. Martensitic transformation and fatigue strength in TiNi. *Scripta Metallurgica*, 5(3):207–211, March 1971.

[141] A. R. Pelton, G. H. Huang, P. Moine, and R. Sinclair. Effects of thermal cycling on microstructure and properties in nitinol. *Materials Science and Engineering: A*, 532:130–138, 2012.

[142] S. Chikazumi. *Physics of Magnetism.* Oxford University Press, New York, 1997. Chapter 20.

[143] É. Trémolet, D. Gignoux, and M. Shlenker. *Magnetism Fundamentals.* Springer, Boston, USA, 2005. Chapters 3 and 6.

[144] L. Néel. Théorie du traînage magnétique des substances massives dans le domaine de Rayleigh. *Journal de Physique et le Radium*, 11(2):49–61, 1950.

[145] L. Néel. Le traînage magnétique. *Journal de Physique et le Radium*, 12(3):339–351, 1951.

[146] D. Salas, E. Cesari, J. Van Humbeeck, and S. Kustov. Isothermal B2–B19' martensitic transformation in Ti-rich Ni–Ti shape memory alloy. *Scripta Materialia*, 74:64–67, March 2014.

[147] J. I. Pérez-Landazábal, V. Recarte, J. Torrens-Serra, and E. Cesari. Relaxation effects in magnetic-field-induced martensitic transformation of an Ni–Mn–In–Co alloy. *Acta Materialia*, 71:117–125, June 2014.

[148] R. Street and J. C. Woolley. A study of magnetic viscosity. *Proceedings of the Physical Society. Section A*, 62(9):562, September 1949.

[149] A. Labarta, O. Iglesias, Ll. Balcells, and F. Badia. Magnetic relaxation in small-particle systems: T $\ln(t/\tau_0)$ scaling. *Physical Review B*, 48(14):10240–10246, October 1993.

[150] W. Ito, Y. Imano, R. Kainuma, Y. Sutou, K. Oikawa, and K. Ishida. Martensitic and magnetic transformation behaviors in Heusler-type NiMnIn and NiCoMnIn metamagnetic shape memory alloys. *Metallurgical and Materials Transactions A*, 38(4):759–766, April 2007.

[151] W. Ito, M. Nagasako, R. Y. Umetsu, R. Kainuma, T. Kanomata, and K. Ishida. Atomic ordering and magnetic properties in the $Ni_{45}Co_5Mn_{36.7}In_{13.3}$ metamagnetic shape memory alloy. *Applied Physics Letters*, 93(23):232503, December 2008.

[152] J. I. Pérez-Landazábal, V. Recarte, V. Sánchez-Alarcos, S. Kustov, D. Salas, and E. Cesari. Effect of magnetic field on the isothermal transformation of a Ni–Mn–In–Co magnetic shape memory alloy. *Intermetallics*, 28:144–148, September 2012.

[153] J. M. Barandiaran, V. A. Chernenko, E. Cesari, D. Salas, J. Gutierrez, and P. Lazpita. Magnetic field and atomic order effect on the martensitic transformation of a metamagnetic alloy. *Journal of Physics: Condensed Matter*, 25(48):484005, December 2013.

[154] E. Cesari, D. Salas, and S. Kustov. Entropy changes in ferromagnetic shape memory alloys. *Materials Science Forum*, 684:49–60, May 2011.